

Dissertation

submitted to the
Combined Faculties of the Natural Sciences and Mathematics
of the Ruperto-Carola-University of Heidelberg, Germany
for the degree of
Doctor of Natural Sciences

Put forward by

Joachim Kopp

Born in Regensburg

Oral examination: 15 April 2009

New phenomena in neutrino physics

Referees: Prof. Dr. Manfred Lindner
Prof. Dr. Hans Jürgen Pirner

Neue Phänomene in der Neutrinophysik

Thema dieser Arbeit sind zwei neue Konzepte in der Neutrinophysik: der Neutrino-Mössbauer-Effekt und Nicht-Standard-Wechselwirkungen der Neutrinos. Wir zeigen, dass rückstoßfrei emittierte und absorbierte Neutrinos (Mössbauer-Neutrinos) trotz ihres quasi-monochromatischen Energiespektrums oszillieren können. Wir untermauern diese Aussage mit Hilfe des quantenmechanischen Wellenpaket-Formalismus, und mit Hilfe einer quantenfeldtheoretischen Berechnung der kombinierten Emissions-, Propagations- und Absorptionsrate für Mössbauer-Neutrinos. Der QFT-Ansatz kommt ohne Annahmen über die Neutrino-Wellenfunktion aus, und erlaubt uns überdies eine realistische Behandlung der unterschiedlichen Mechanismen, die zu einer Verbreiterung der Emissions- und Absorptionslinien führen. Im zweiten Teil der Arbeit beschäftigen wir uns mit der Phänomenologie der Nicht-Standard-Wechselwirkungen (NSI). Wir klassifizieren die erlaubten NSI-Operatoren anhand ihrer Auswirkungen auf zukünftige Oszillationsexperimente, und zeigen numerische Resultate für die NSI-Sensitivität von Reaktor-, Superbeam- und Neutrino-fabrik-Experimenten. Wir weisen darauf hin, dass NSI Standard-Effekte imitieren können, was unter Umständen zu falschen Fit-Werten für die Oszillationsparameter führen kann. Für den Fall der Neutrino-fabrik führen wir eine detaillierte Optimierungs-Studie durch, um die optimale Myon-Energie und Detektor-Konfiguration zu bestimmen.

New phenomena in neutrino physics

In this thesis, we discuss two new concepts in neutrino physics: The neutrino Mössbauer effect and non-standard neutrino interactions. We show that neutrinos emitted and absorbed in recoil-free processes (Mössbauer neutrinos) can oscillate in spite of their near monochromaticity. We support this statement by quantum mechanical wave packet arguments and by a quantum field theoretical (QFT) calculation of the combined rate of Mössbauer neutrino emission, propagation and absorption. The QFT approach does not require any a priori assumptions on the neutrino wave function, and it allows us to include a realistic treatment of the different mechanisms leading to broadening of the emission and absorption lines. In the second part of this work, we study the phenomenology of non-standard neutrino interactions (NSI). We classify the allowed NSI operators according to their impact on future oscillation experiments and present numerical results for the NSI sensitivities of reactor, superbeam and neutrino factory experiments. We point out that NSI could mimic standard oscillation effects, and might therefore lead to incorrect fit values for the oscillation parameters. For the case of the neutrino factory, we perform a detailed optimisation study to determine the optimum muon energy and detector configuration.

Contents

1	Introduction	9
2	A mini-review on neutrino oscillation physics	11
2.1	Theory of neutrino oscillations — The standard lore	11
2.1.1	The neutrino Lagrangian	11
2.1.2	The “textbook derivation” of the neutrino oscillation probability and its shortcomings	12
2.1.3	Neutrino oscillations in matter	14
2.2	Current experimental knowledge about neutrinos	15
2.3	Future neutrino oscillation experiments	16
3	Mössbauer neutrinos	21
3.1	Feasibility of a Mössbauer neutrino experiment	22
3.2	Prospects of a Mössbauer neutrino experiment	24
3.3	Mössbauer neutrinos do oscillate	25
3.4	Mössbauer neutrino wave packets	26
3.4.1	Gaussian wave packets	26
3.4.2	Lorentzian wave packets	32
3.5	Mössbauer neutrinos in quantum field theory	34
3.5.1	The Feynman diagram	34
3.5.2	Inhomogeneous line broadening	41
3.5.3	Homogeneous line broadening	46
3.5.4	Natural line broadening	49
3.6	Discussion	55
3.7	Mössbauer neutrinos and the time-energy uncertainty relation	58
4	Non-standard neutrino interactions	61
4.1	The formalism of non-standard interactions	62
4.1.1	The effective NSI Lagrangian	62
4.1.2	Modified oscillation probabilities in the presence of NSI	63
4.1.3	Current bounds on non-standard interactions	65
4.2	Non-standard interactions in reactor and superbeam experiments	65
4.2.1	Theoretical expectations	66
4.2.2	Simulation of reactor and superbeam experiments	70
4.2.3	Discovery reach	74
4.2.4	NSI-induced offsets and discrepancies in θ_{13} fits	77

4.3	Non-standard interactions in a neutrino factory	82
4.3.1	Theoretical expectations	84
4.3.2	Simulation of a neutrino factory	84
4.3.3	Optimisation of the parent muon energy	88
4.3.4	Baseline optimisation	89
4.3.5	Summary of neutrino factory optimisation for non-standard inter- actions	91
5	Summary and conclusions	97
A	Weisskopf-Wigner approach to Mössbauer neutrinos for natural line width dominance	101
B	NSI operators with non-$(V - A)(V - A)$ Lorentz structure	111
C	The non-standard neutrino oscillation probabilities	115
C.1	The $\bar{\nu}_e \rightarrow \bar{\nu}_e$ channel	115
C.2	The $\nu_\mu \rightarrow \nu_e$ channel	116
C.3	The $\nu_\mu \rightarrow \nu_\mu$ channel	120
	List of Figures	121
	List of Tables	123
	Bibliography	125

1

Introduction

In a poem written in 1988 by Nobel Laureate Sheldon L. Glashow [1], one can find the verses

We must pity the student in his deep dark hole
Whose thesis depends on that one monopole,
Or on solar neutrinos that wriggle about
Unless they are saying our sun has gone out.

Fortunately, our central star is still shining brightly, and, for all we know, will continue to do so for several billion years. But nevertheless, neutrinos have told us a lot about the world around us: They have shed light onto new aspects in the evolution of astrophysical objects [2], and have given us ground-breaking new insights into the world of elementary particles. In particular, neutrino oscillations have been observed for atmospheric neutrinos [3–7], solar neutrinos [8–10], reactor neutrinos [11, 12] and accelerator neutrinos [13, 14], so that the existence of nonzero neutrino masses and large neutrino mixing is now firmly established. Neutrino physics has thus witnessed an era of great progress over the last decade, so that nowadays it takes little persuasion for a physics student to start working on one of the many exciting underground neutrino experiments around the world.

The great experimental discoveries in neutrino physics have been accompanied by no less vigorous progress on the theoretical side [15]. The formalism of neutrino mixing and oscillations has been developed [16] models have been constructed attempting to explain the lightness of the neutrino masses and the peculiar features of the leptonic mixing matrix [17, 18], and detailed phenomenological predictions for present and future experiments have been derived from the theory [19]. Moreover, the role of neutrinos in astrophysics has been studied, in particular their impact on supernova explosions [20] and on the evolution of the early universe [21].

With the standard lore being so well established by now, new concepts are receiving more and more interest. In this thesis, we will consider two of them: Mössbauer neutrinos and non-standard neutrino interactions. We will lay the foundations for our discussion in chapter 2 by introducing neutrino oscillations and highlighting important past and future experimental activities.

Chapter 3 will be devoted to Mössbauer neutrinos, i.e. neutrinos that are emitted and absorbed in recoil-free interactions with nuclei embedded into solid state lattices. The peculiar features of these emission and absorption processes have led to the question whether Mössbauer neutrinos can oscillate. We will give an affirmative answer to this question, and present a detailed phenomenological study of Mössbauer neutrino properties. Our calculations will show that a purely quantum mechanical (QM) description, in which the neutrino is treated as a wave packet, can capture some aspects of the problem, but is inferior to a quantum field theoretical (QFT) derivation. In QFT, it is possible to include the dynamics of the production and detection processes in the calculation, so that no ad hoc assumptions on the neutrino wave function are required. We will show how a reliable estimate for the combined rate of Mössbauer neutrino emission, oscillation and absorption can be obtained in QFT, and how the effects of different line broadening mechanisms can be described in a realistic way.

While Mössbauer neutrinos are a phenomenon totally within the Standard Model (amended by neutrino mass terms), we will go beyond that model in chapter 4 and discuss non-standard neutrino interactions. These hypothetical interactions manifest themselves as four-fermion terms in the effective Lagrangian, and thus provide a model-independent way of parameterising new physics in the neutrino sector. After introducing the NSI formalism and classifying the allowed terms, we will study their impact on future neutrino oscillation experiments in detailed numerical simulations. We will show that the unnoticed presence of NSI may lead to severely wrong fits of the standard oscillation parameters in reactor and superbeam experiments. Moreover, we will consider NSI in the context of a neutrino factory experiment, and show how such an experiment should be designed in order to provide optimal sensitivity to both standard and non-standard observables. We will summarise our results and draw some conclusions in chapter 5.

The most exciting phrase to hear in science, the one that heralds new discoveries, is not “Eureka!” but “That’s funny . . .”

Isaac Asimov

2

A mini-review on neutrino oscillation physics

In this chapter, we will set the stage for the discussion of new phenomena in neutrino physics by reviewing several important results from the past which will be relevant to the subsequent chapters. We will first introduce the formalism of neutrino oscillations in sec. 2.1 and argue why the derivation of the oscillation probability found in most textbooks is not fully satisfactory. (We will discuss improved approaches to neutrino oscillations in chapter 3.) Then, we will review the current experimental knowledge about neutrinos in sec. 2.2 and describe the future experimental program in sec. 2.3.

2.1 Theory of neutrino oscillations — The standard lore

2.1.1 The neutrino Lagrangian

From the theoretical point of view, the phenomenology of neutrino interactions and oscillations is contained in the following Lagrangian terms [22]:

$$\begin{aligned} \mathcal{L} \supset \sum_{j=1,2,3} \left[i\bar{\nu}_j \not{\partial} \nu_j - m_j \bar{\nu}_j \nu_j \right] + \frac{g}{2 \cos \theta_W} \sum_{j=1,2,3} \bar{\nu}_j \gamma^\mu \frac{1 - \gamma^5}{2} \nu_j Z_\mu^0 \\ + \frac{g}{\sqrt{2}} \sum_{j=1,2,3} \sum_{\alpha=e,\mu,\tau} \left[\bar{\ell}_\alpha \gamma^\mu \frac{1 - \gamma^5}{2} U_{\alpha j} \nu_j W_\mu^+ + h.c. \right]. \quad (2.1) \end{aligned}$$

Here, g is the weak coupling constant, θ_W is the Weinberg angle, $W_\mu^- = (W_\mu^+)^\dagger$ and Z_μ^0 are the weak gauge boson fields, ℓ_α are the three charged lepton fields, and ν_j are the three neutrino fields in the mass basis, which is defined such that the mass matrix is $\text{diag}(m_1, m_2, m_3)$. For simplicity, we have assumed only Dirac mass terms for the

neutrinos, since it can be shown that the oscillation phenomenology is the same for Dirac and Majorana neutrinos [23]. The basis of neutrino states participating in the weak gauge interactions (“flavour basis”) is rotated compared to the mass basis by the leptonic mixing matrix U :

$$\nu_\alpha = \sum_j U_{\alpha j} \nu_j. \quad (2.2)$$

U is often called PMNS (Pontecorvo-Maki-Nakagawa-Sakata) matrix in the literature. It is conventionally parameterised in terms of three mixing angles θ_{12} , θ_{13} , θ_{23} and one CP violating phase δ_{CP} :

$$U = \begin{pmatrix} c_{12}c_{13} & s_{12}c_{13} & s_{13}e^{-i\delta_{\text{CP}}} \\ -s_{12}c_{23} - c_{12}s_{13}s_{23}e^{i\delta_{\text{CP}}} & c_{12}c_{23} - s_{12}s_{13}s_{23}e^{i\delta_{\text{CP}}} & c_{13}s_{23} \\ s_{12}s_{23} - c_{12}s_{13}c_{23}e^{i\delta_{\text{CP}}} & -c_{12}s_{23} - s_{12}s_{13}c_{23}e^{i\delta_{\text{CP}}} & c_{13}c_{23} \end{pmatrix}. \quad (2.3)$$

Here, we have used, the abbreviations $s_{ij} = \sin \theta_{ij}$ and $c_{ij} = \cos \theta_{ij}$.

2.1.2 The “textbook derivation” of the neutrino oscillation probability and its shortcomings

To see why neutrino mixing leads to oscillatory flavour transition, it is assumed in most textbooks, that a neutrino source produces a plane wave neutrino state of the form

$$|\psi(0)\rangle \equiv |\nu_\alpha\rangle = \sum_j U_{\alpha j}^* |\nu_j\rangle. \quad (2.4)$$

After a time t , and at a distance L from the origin, this state has evolved into

$$|\psi(L, t)\rangle = \sum_j U_{\alpha j}^* \exp[-iE_j t + ip_j L] |\nu_j\rangle, \quad (2.5)$$

where the E_j and p_j are the energies momenta associated with the individual neutrino mass eigenstates. The oscillation probability $P_{\alpha\beta}$ for the flavour transition $\alpha \rightarrow \beta$ is given by

$$\begin{aligned} P_{\alpha\beta}(t, L) &= |\langle \nu_\beta | \psi(L, t) \rangle|^2 \\ &= \sum_{j,k} U_{\alpha j}^* U_{\beta j} U_{\alpha k} U_{\beta k}^* \exp[-i(E_j - E_k)t + i(p_j - p_k)L]. \end{aligned} \quad (2.6)$$

If one postulates that all neutrino mass eigenstates are emitted with the same energy E , and that they are ultrarelativistic, i.e.

$$\frac{\Delta m_{jk}^2}{2E} \ll E, \quad (2.7)$$

one can make the approximation

$$(E_j - E_k)t + (p_j - p_k)L = \left(\sqrt{E^2 - m_j^2} - \sqrt{E^2 - m_k^2} \right) L \simeq -\frac{\Delta m_{jk}^2}{2E} L, \quad (2.8)$$

where $\Delta m_{jk}^2 = m_j^2 - m_k^2$. The oscillation probability then becomes

$$P_{\alpha\beta}(L) \simeq \sum_{j,k} U_{\alpha j}^* U_{\beta j} U_{\alpha k} U_{\beta k}^* \exp \left[-2\pi i \frac{L}{L_{jk}^{\text{osc}}} \right], \quad (2.9)$$

with the partial oscillation lengths

$$L_{jk}^{\text{osc}} = \frac{4\pi E}{\Delta m_{jk}^2}. \quad (2.10)$$

If only two neutrino flavours with a mixing angle θ are considered, $P_{\alpha\beta}$ takes the familiar form

$$P_{\alpha\beta}(L) = \sin^2 2\theta \sin^2 \pi L / L_{jk}^{\text{osc}}. \quad (2.11)$$

Eq. (2.9) can also be obtained by considering not the spatial, but the temporal, evolution of the neutrino, assuming equal momenta instead of equal energies for the different mass eigenstates. Then, the oscillation phase becomes

$$(E_j - E_k)t + (p_j - p_k)L = \left(\sqrt{p^2 + m_j^2} - \sqrt{p^2 + m_k^2} \right) t \simeq \frac{\Delta m_{jk}^2}{2p} t \simeq \frac{\Delta m_{jk}^2}{2E} L. \quad (2.12)$$

The last equality follows from $E \simeq p$, and from the relation

$$L \simeq t, \quad (2.13)$$

which is valid for ultrarelativistic particles in classical mechanics. It needs to be stressed that neither the equal energy or equal momentum approximations, nor the restriction to only the spatial or only the temporal evolution, nor the classical relation (2.13) are generically valid [24–29]. Instead, they are approximations which work for neutrinos from most sources, because these neutrinos are ultra-relativistic, and their spatial delocalisation is small compared to their oscillation lengths, so that evolution in space and evolution in time are equivalent for them. Moreover, their energy and momentum uncertainties are sufficiently large (and of the same order of magnitude), so that energy (momentum) differences of $\mathcal{O}(\Delta m_{jk}^2/2E)$, as required in the equal momentum (equal energy) approach, are allowed at least in principle. We will see in sec. 3 that the condition of sufficient energy uncertainty is, for example, violated in the case of Mössbauer neutrinos.

In reality, both the equal energy and the equal momentum assumption would in most cases violate energy-momentum conservation at the production and detection vertices. Therefore, it is more realistic to allow for $E_j \neq E_k$ and $p_j \neq p_k$ simultaneously in eq. (2.6). Then, in the ultrarelativistic limit, $E_j \simeq E + \xi m_j^2/2E$ and $p_j \simeq E - (1 - \xi)m_j^2/2E$, where ξ

is a parameter determined by the properties of the neutrino source. Using eq. (2.13), one finds that the ξ -dependent terms in the oscillation phase cancel, so that $P_{\alpha\beta}$ again takes the form of eq. (2.9). However, the classical relation eq. (2.13) is also not valid in general. In particular, it makes sense only for localised particles and is thus in contradiction to our assumption of the neutrino state being composed of infinitely delocalised plane waves with well-defined energies E_j and momenta p_j .

These problems can be circumvented by treating the neutrino as a quantum mechanical wave packet (see refs. [25, 28, 30–33] and sec. 3.4), or, even more generally, by determining the form of the neutrino wave function from the wave functions of its interaction partners in the framework of quantum field theory (see refs. [16, 34–42] and sec. 3.5).

2.1.3 Neutrino oscillations in matter

When neutrinos travel through matter, their interactions with this matter lead to interesting modifications of the mixing and oscillation phenomenology. Of particular interest is the process of coherent forward scattering, where the contributions from a large number N of scattering centres along the neutrino trajectory add up coherently. The effect is thus enhanced by a factor of N compared to incoherent scattering. According to the Lagrangian (2.1), coherent forward scattering in ordinary matter can occur via neutral current (NC) interactions with electrons, protons and neutrons, and, for ν_e and $\bar{\nu}_e$, also via charged current (CC) interactions with electrons. For neutrino energies much smaller than the mass of the W boson, the effect of these interactions can be described by an additional potential V_{MSW} in neutrino Hamiltonian, which then reads in the flavour basis [23]

$$H = H_0 + V_{\text{MSW}}. \quad (2.14)$$

Here, $H_0 = U \text{diag}(E_1, E_2, E_3) U^\dagger$ is the vacuum Hamiltonian, and

$$V_{\text{MSW}} = \sqrt{2}G_F \begin{pmatrix} N_e + N_n/2 & & \\ & N_n/2 & \\ & & N_n/2 \end{pmatrix}. \quad (2.15)$$

As usual, G_F is the Fermi constant, N_e denotes the electron number density in the background matter, and N_n is the number density of neutrons. Note that the NC contributions from protons and electrons cancel because, in neutral matter, these particles appear in equal numbers. The index “MSW” of the potential honours Stanislav Mikheyev, Alexei Smirnov and Lincoln Wolfenstein, who were the first to discuss matter effects in neutrino oscillations [43–45].

To derive the neutrino oscillation probability in matter, the new Hamiltonian (2.14) needs to be diagonalised, yielding a new mixing matrix \tilde{U} and new energy eigenvalues $\tilde{E}_j = (p_j^2 + \tilde{m}_j^2)^{1/2}$. Here, \tilde{m}_j are the effective neutrino masses in matter. By replacing U and m_j by \tilde{U} and \tilde{m}_j in eq. (2.9), the neutrino oscillation probability in matter can easily be computed. Note that only energy differences are relevant in this computation,

so the flavour diagonal contributions to V_{MSW} cancel, and, without loss of generality, a simplified matter potential

$$V_{\text{MSW}} = \sqrt{2}G_F N_e U^\dagger \text{diag}(1, 0, 0)U \quad (2.16)$$

may be used instead of eq. (2.15).

2.2 Current experimental knowledge about neutrinos

For a long time, neutrino oscillations have been considered a rather exotic phenomenon, not believed in by many particle physicists. The reason was that the Standard Model of elementary particles did not contain right-handed neutrinos, so that the mass terms in the Lagrangian (2.1) were absent ($m_1 = m_2 = m_3 = 0$), and it is easy to see from eq. (2.9) that no oscillations are possible in this limit. It was not until 1998 that the existence of neutrino oscillations was finally established experimentally by the Super-Kamiokande experiment [3, 4] for atmospheric neutrinos. Four years later, the SNO collaboration was able to demonstrate that also the long-standing solar neutrino problem — i.e. the apparently depleted flux of electron neutrinos from the sun [10, 46–49] — is solved by neutrino oscillations [9]. Later measurements by Super-Kamiokande [5], by the reactor experiments KamLAND [11, 50] and CHOOZ [51] and by the accelerator experiments K2K [52, 53] and MINOS [14, 54] have confirmed our picture of neutrino oscillations and have provided precise values or tight constraints for most of the oscillation parameters. These results are summarised in fig. 2.1, taken from ref. [55], in which a global fit to all available neutrino oscillation data has been performed.

We see that, of the three mixing angles in (2.3), two are large:

$$\sin^2 \theta_{12} = 0.32^{+0.08}_{-0.06} \quad (3\sigma), \quad (2.17)$$

$$\sin^2 \theta_{23} = 0.50^{+0.17}_{-0.16} \quad (3\sigma), \quad (2.18)$$

while the third one is close or identical to zero:

$$\sin^2 \theta_{13} \leq 0.050 \quad (3\sigma). \quad (2.19)$$

The two mass squared differences, which determine the oscillation lengths according to eq. (2.10), have the values

$$\Delta m_{21}^2 = 7.6^{+0.7}_{-0.5} \cdot 10^{-5} \text{ eV}^2 \quad (3\sigma), \quad (2.20)$$

$$|\Delta m_{31}^2| = 2.4^{+0.3}_{-0.3} \cdot 10^{-3} \text{ eV}^2 \quad (3\sigma). \quad (2.21)$$

It is not yet known whether Δm_{31}^2 is positive (“normal mass hierarchy” $m_1 < m_2 < m_3$) or negative (“inverted mass hierarchy” $m_3 < m_1 < m_2$).¹ Also, there is no information

¹We will use the term “mass hierarchy” when referring to the sign of Δm_{31}^2 even for the case of non-hierarchical (quasi-degenerate) neutrino masses.

yet on the CP violating phase δ_{CP} . Note that the sensitivity to θ_{23} and Δm_{31}^2 comes mainly from atmospheric and accelerator neutrino experiments, while θ_{12} and Δm_{21}^2 are measured in solar neutrino experiments and in KamLAND. The limit on θ_{13} is dominated by the CHOOZ reactor experiment.

Since neutrino oscillation experiments are only sensitive to mass squared differences, they cannot provide information on the absolute neutrino masses. We know, however, from kinematical studies of the electron spectrum in nuclear β -decay [56, 57], that neutrinos are lighter than ~ 2.3 eV (95% C.L.). Cosmological observations even constrain their masses to lie below ~ 0.2 eV [58], however, due to the strong model dependence and large systematical uncertainties of cosmological data sets, this result has to be taken with a grain of salt [59]. For the case of neutrinos with Majorana mass terms, there is a bound on the level of 0.35 eV (90% C.L.) from the search for neutrinoless double beta decay [60].

Many experiments have also searched for new effects beyond the framework of three massive neutrinos with Standard Model interactions, but no evidence for such effects has been found yet. Instead, constraints have been derived on non-standard neutrino interactions [61–63], neutrino decay [64], neutrino decoherence [65], oscillations into sterile neutrinos (i.e. neutrinos not coupling to the Z boson) [66] and other “exotic” scenarios. Present and future bounds on non-standard neutrino interactions will also be one of the main topics of chapter 4 of this thesis.

2.3 Future neutrino oscillation experiments

Even though we have seen in the previous section that neutrino oscillation physics has come a long way over the last decade, better knowledge on the oscillation parameters is desirable because it might shed new light onto the origin of the flavour structure of elementary particles. Of particular interest in this context are the following questions:

- Is there CP violation in the lepton sector, and what is the value of δ_{CP} ?
- What is the value of θ_{13} ? Is it so close to zero that it might indicate the presence of a new symmetry?
- Is the mass hierarchy normal or inverted?
- Is θ_{23} exactly maximal or are there deviations?
- Are there subdominant non-standard effects?

To answer these questions, a plethora of new experiments has been proposed, and some are already under construction.

Reactor neutrino experiments

The upcoming experiments Double Chooz [67] in France and Daya Bay [68] in China aim at the detection of electron anti-neutrinos produced in a nuclear power plant at a baseline of

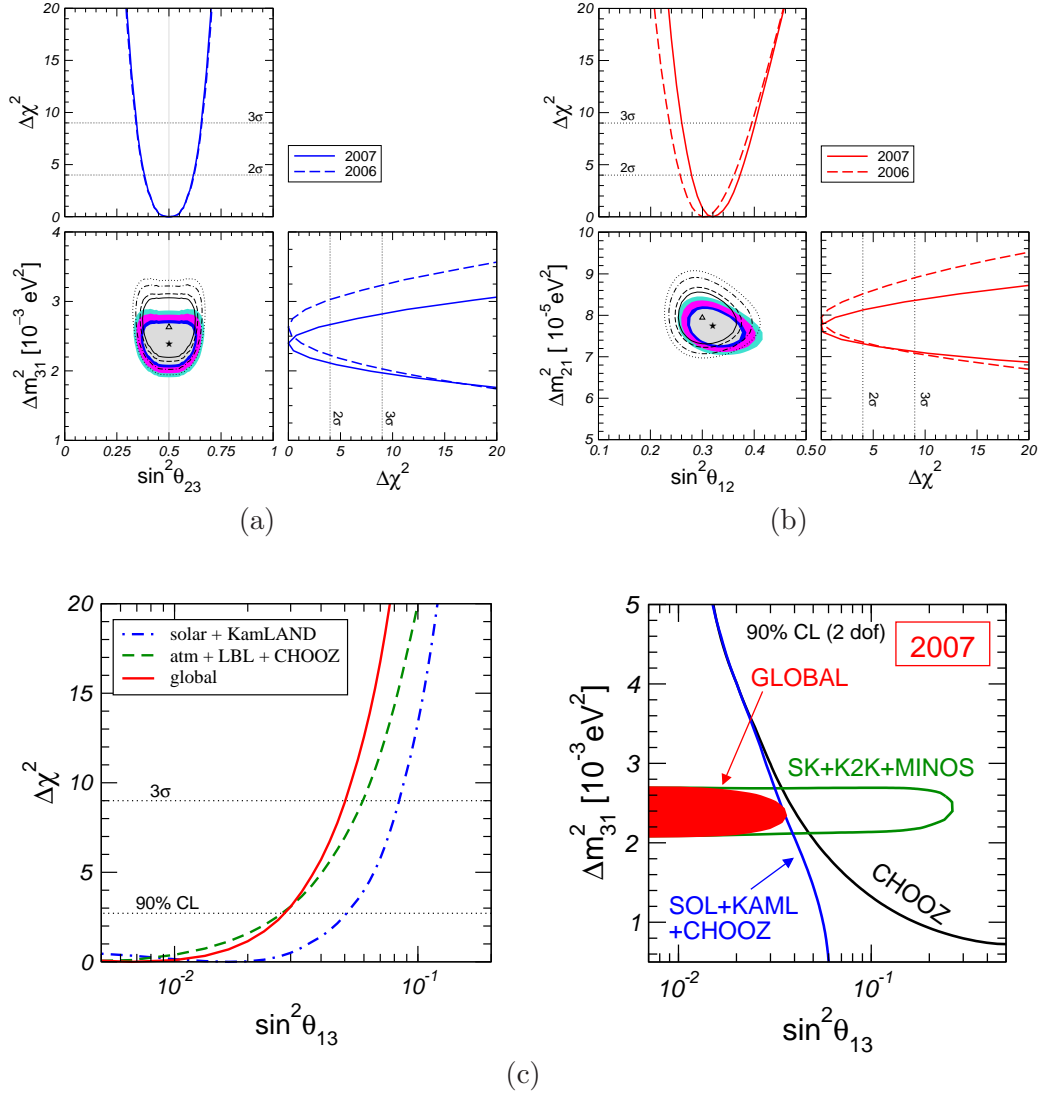


Figure 2.1: Results of a global fit to all available neutrino oscillation data. Panel (a) shows the allowed region in the $(\sin^2 \theta_{23}, \Delta m_{31}^2)$ plane at the 90%, 95%, 99% and 3 σ confidence levels, together with the projections of the χ^2 manifold onto the $\sin^2 \theta_{23}$ and Δm_{31}^2 axes. The coloured areas and solid χ^2 curves are obtained from a 2007 fit, while the black contours and dashed χ^2 curves are for an older data set from 2006, omitting the latest MINOS results. Similar plots in panel (b) show the fit results for the parameters $\sin^2 \theta_{12}$ and Δm_{21}^2 . There, the 2006 data set lacks the most recent KamLAND data. Panel (c) shows the allowed region for $\sin^2 \theta_{13}$ and its dependence on Δm_{31}^2 . Plots taken from ref. [55].

~ 1 km. For typical reactor neutrino energies of several MeV, this corresponds to the first maximum of Δm_{31}^2 -driven oscillations. Reactor neutrino experiments search for a small deficit in the $\bar{\nu}_e$ flux, which would be the signature for nonzero θ_{13} . Double Chooz is able to probe $\sin^2 2\theta_{13}$ to the level of 0.03 (90% C.L.) [67], while Daya Bay aims at a sensitivity better than $\sin^2 2\theta_{13} \simeq 0.01$ (90% C.L.) [68]. To achieve these sensitivities in spite of the large systematical errors on the reactor neutrino flux and spectrum, dedicated “near detectors” are planned to be built close to the reactor cores to measure these quantities before the neutrinos can oscillate. In order to avoid detector-related uncertainties, the near and far detectors have to be as similar as possible.

Superbeam experiments

In superbeam experiments, an intense proton beam is directed onto a target, where a large number of secondary pions and kaons is produced, which in turn decay into neutrinos. The beam consists mainly of ν_μ , with a small admixture of ν_e . At a distance of several hundred kilometres, corresponding to $L_{31}^{\text{osc}}/2$, a massive detector is placed to detect oscillations of ν_μ into ν_e , which provide a sensitivity to $\sin^2 2\theta_{13}$ similar to that of reactor experiments, and in addition may give some information on δ_{CP} and on the neutrino mass hierarchy. Moreover, the investigation of ν_μ disappearance due to oscillations into (undetectable) τ -neutrinos allows for a precision measurement of θ_{23} and Δm_{31}^2 . There are currently two superbeam experiments being developed: T2K (“Tokai to Kamioka”) [69] in Japan and NO ν A (“NuMI Off-axis ν_e Appearance Experiment”) [70] in the United States. In T2K, the neutrino beam is produced at the Japan Proton Accelerator Research Complex JPARC, and the Super-Kamiokande detector at a baseline of 295 km is used as a far detector. For NO ν A, the NuMI (Neutrinos at the Main Injector) facility at Fermilab provides the neutrino beam, and a far detector is planned to be built at a baseline of 812 km. In both experiments, dedicated near detectors are required to measure the unoscillated neutrino spectrum and thus reduce the systematical uncertainties.

Beta beams

One of the main disadvantages of superbeam experiments is the unavoidable admixture of ν_e to the ν_μ beam, which limits the detection potential for $\nu_\mu \rightarrow \nu_e$ oscillations. A flavour-pure neutrino beam could be achieved using the beta beam concept [71, 72]. The idea behind this concept is to accelerate unstable ions and circulate them in a storage ring, where they will ultimately decay and thus produce a highly boosted ν_e beam. Observation of subsequent $\nu_e \rightarrow \nu_\mu$ oscillations can be used to measure θ_{13} and δ_{CP} in the same way as in a superbeam experiment, where the time-reversed oscillation channel is employed. The sensitivity of beta beams depends strongly on the achievable luminosity and energy of the storage ring, but it is in general better than the sensitivity of superbeam experiments. Since the concept is much more advanced, no concrete beta beam experiments are planned yet, but great R&D efforts are undertaken.

The Neutrino factory

The ultimate tool to study neutrino oscillations if θ_{13} is extremely small is a neutrino factory [19, 73–75]. The realisation of such a device would require the production and storage of a beam of high-energy muons, which would then decay into neutrinos. The neutrino energy is typically very high (up to 25 or 50 GeV), so that the detector needs to be placed at a baseline of several thousand kilometres for oscillations to develop. An active R&D program towards a neutrino factory is currently being carried out in the framework of the International Design Study for the Neutrino Factory (IDS-NF) [19, 76]. Many theoretical studies show that a neutrino factory would have the potential to measure the oscillation parameters θ_{23} , Δm_{31}^2 , θ_{13} and δ_{CP} with extremely high precision, and to disentangle the correlations between them [77–81].

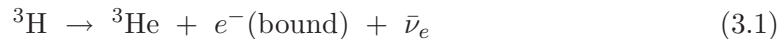
*One's first step in wisdom is to question everything
— and one's last is to come to terms with everything.*

Georg Christoph Lichtenberg

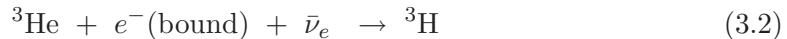
3

Mössbauer neutrinos

The idea of exploiting the Mössbauer effect in weak interactions to enhance the small neutrino cross sections has originally been devised by Visscher in 1959 [82], i.e. shortly after the famous photon Mössbauer effect had been discovered in 1958 [83]. Visscher realised that electron capture decays of nuclei bound in a crystal lattice have a nonzero probability of occurring recoillessly, i.e. without being accompanied by phonon emission or absorption. The energy which the neutrino emitted in such a process (“Mössbauer neutrino”) receives matches precisely the energy required for the inverse process of recoil-free neutrino absorption, so that a resonance phenomenon can occur, greatly enhancing the neutrino interaction cross section. More than twenty years after Visscher’s paper, Kells and Schiffer [84,85] proposed bound state beta decay [86] as an alternative production mechanism for Mössbauer neutrinos. The antineutrino emitted in this process could be absorbed resonantly by induced orbital electron capture [87]. Recently, interest in Mössbauer neutrinos from bound state beta decay has been revived by several papers by Raghavan [88–91], in which the technical feasibility of an experiment using the emission process



and the detection process



has been studied. The tritium (${}^3\text{H}$) and Helium-3 (${}^3\text{He}$) atoms were proposed to be embedded into metal crystals. The produced ${}^3\text{H}$ atoms in the detector could be counted either by observing their beta decays, or by extracting them from the crystal using mass spectroscopy. Raghavan estimated that the resonance nature of the neutrino absorption process could enhance the cross section by up to a factor of 10^{12} compared to the non-resonant capture of neutrinos of the same energy. The main reason for this huge enhancement is the small spectral line width (i.e. neutrino energy smearing) $\sim 10^{-11}$ eV [92,93] of the proposed Mössbauer source and absorber.

Achieving this value is one of the main technical challenges that any realistic experiment will face, therefore we will begin our discussion of Mössbauer neutrino experiments with some considerations on their feasibility (sec. 3.1). Afterwards, we will describe the interesting physics program that could be carried out in a Mössbauer neutrino experiment (sec. 3.2). We will see that neutrino oscillation studies are one of the main applications of Mössbauer neutrinos, and this will lead us to a discussion of their oscillation phenomenology. In particular we will address concerns that have been raised as to whether Mössbauer neutrinos, being nearly monochromatic, do oscillate at all. Bilenky et al. have argued that the answer to this questions depends on whether different neutrino mass eigenstates are assumed to be emitted with equal energies or with equal momenta [94]. We have seen in sec. 2.1 that, in general, neither of these assumptions is valid, but we will show in sec. 3.3 that Mössbauer neutrinos can be approximately described using the equal energy approach, and that oscillations are predicted in this approach. We will confirm this statement in sec. 3.3 by deriving the flavour transition probability for Mössbauer neutrinos, including coherence, localisation and resonance effects, in the quantum mechanical wave packet model mentioned at the end of sec. 2.1.2. In sec. 3.5, we will generalise our results further by using the formalism of quantum field theory to explicitly include the dynamics of the neutrino production and detection processes. In particular, we will discuss different mechanisms that can smear the neutrino energy and thus lead to line broadening. We will compare the results obtained in the different approaches in sec. 3.6. In sec. 3.7, we will address another concern raised by Bilenky et al., namely the possible inhibition of Mössbauer neutrino oscillations by the time-energy uncertainty principle [95–97]. This chapter is based on work done in collaboration with Evgeny Kh. Akhmedov and Manfred Lindner [29, 98].

3.1 Feasibility of a Mössbauer neutrino experiment

A Mössbauer neutrino experiment faces tremendous technical challenges. The first of these concerns the production of suitable crystals for the neutrino source and the neutrino detector. For a “proof-of-principle” experiment, in which the distance L between the source and the detector is only ~ 5 cm, a 1 kCi source is typically considered, while for an oscillation experiment ($L \simeq 10$ m), at least 1 MCi would be required. Metal tritides in which ^3H atoms fill interstitial sites in, e.g., a Nb lattice, might offer a possibility to engineer such strong sources. For the detector crystal, one could use an aged metal tritide, in which a sufficient number of ^3H atoms has already decayed to ^3He . The remaining ^3H would have to be removed completely, since it would mimic a neutrino signal. One option to achieve this is the replacement of tritium by deuterium [89, 99]. Afterwards, one has to ensure that no new ^3H is produced by neutron activation, implying the need for efficient shielding against cosmic radiation.

Another limiting factor for the prospects of a Mössbauer neutrino experiment will be the need to ensure sufficient overlap of the emission and absorption lines, and to avoid line broadening as far as possible. We will see in secs. 3.4 and 3.5 that the interaction

rate contains a Breit-Wigner factor of the form

$$\frac{(\gamma_S + \gamma_D)/2\pi}{(E_{S,0} - E_{D,0})^2 + \frac{(\gamma_S + \gamma_D)^2}{4}}, \quad (3.3)$$

where γ_S and γ_D are the widths of the emission and absorption lines, respectively, and $E_{S,0}$ and $E_{D,0}$ are their central energies. It is obvious from this expression that the transition rate can only be large if γ_S and γ_D are small and if the resonance condition $E_{S,0} - E_{D,0} \ll (\gamma_S + \gamma_D)/2$ is fulfilled.

The dominant contributions to γ_S , γ_D and $(E_{S,0} - E_{D,0})$ come from solid state effects, some of which are controllable to a certain degree, while others are outside the experimenter's sphere of influence. One distinguishes homogeneous effects, which influence all atoms in the solid state lattice in the same way, and inhomogeneous effects, which have a different impact on different atoms. Homogeneous effects are [92, 100]

- **Electromagnetic relaxation effects.** These are interactions of the atoms with random, fluctuating electromagnetic fields created by the spins of the neighbouring particles [92, 93]. They have been estimated to reduce the width of the Mössbauer neutrino line in the ${}^3\text{H} - {}^3\text{He}$ system from $\gamma^{\text{natural}} = 1/\tau = 1.17 \cdot 10^{-24}$ eV to at least 10^{-11} eV [100].
- **Different binding energies in the source and in the detector.** Since the source and detector crystals in a Mössbauer neutrino experiment cannot be exactly identical — one of them has to contain large amounts of tritium, while the other contains essentially none — the energy levels $E_{\text{H},S}$ and $E_{\text{He},S}$ of the ${}^3\text{H}$ and ${}^3\text{He}$ atoms in the source will be different from the corresponding energy levels $E_{\text{H},D}$ and $E_{\text{He},D}$ in the detector (see ref. [101] for a discussion of H and He energies in metal crystals). Therefore, it is very likely that also the energies of the emission and absorption lines, which are given by $E_{S,0} = E_{\text{H},S} - E_{\text{He},S}$ and $E_{D,0} = E_{\text{H},D} - E_{\text{He},D}$, respectively, will be different, so that the resonance condition might no longer be fulfilled.
- **Lattice expansion and contraction during the decay.** In classical Mössbauer experiments, the photon is emitted in a nuclear deexcitation process, which does not affect the chemical properties of the emitting atom. In particular, its effective size remains essentially unchanged. In contrast, the ${}^3\text{H}$ and ${}^3\text{He}$ atoms involved in the neutrino Mössbauer process do take up different amounts of space in the crystal, so that the decay and absorption processes (3.1) and (3.2) are accompanied by an expansion resp. contraction of the nearby lattice cells. It is very likely that a phonon is created due to this deformation, destroying the recoilless nature of the process. It has been estimated [100] that taking into account lattice deformations might reduce the fraction f of recoil-free emissions by three orders of magnitude compared to the commonly used estimate $f \sim 0.3$ [88, 89]. Since the probability for recoil-free absorption receives a similar suppression, the achievable event rate would be reduced by a factor of 10^{-6} , which might render the experiment impracticable.

- **Second order Doppler shift.** The energy of a Mössbauer neutrino emitted by a nucleus moving at a velocity v will be shifted due to the Doppler effect according to

$$E_{S,0} \rightarrow E_{S,0} \sqrt{\frac{1 \mp v}{1 \pm v}} \simeq E_{S,0} \left[1 \mp v + \frac{v^2}{2} \mp \dots \right]. \quad (3.4)$$

For a nucleus bound in crystal at rest, $\langle v \rangle = 0$, so the first order term vanishes.¹ The second order term, however, is non-negligible because $\langle v^2 \rangle \neq 0$ even in the ground state due to zero point motion. Ideally, the resulting shift of the neutrino line is identical in the source and the detector, but slightly different Debye temperatures or slightly different heat bath temperatures of the two crystals can change this, and thus bring the system out of resonance.

Inhomogeneous line broadening is mainly caused by lattice defects and impurities. The best available crystals in photon Mössbauer spectroscopy lead to inhomogeneous line widths $\gtrsim 10^{-13} - 10^{-12}$ eV [92,103]. It is doubtful whether similar values can be achieved also for the metal tritides proposed for a Mössbauer neutrino experiment. In particular, inhomogeneities in the ${}^3\text{H}/{}^3\text{He}$ distribution throughout the crystal would already perturb the regularity of the lattice. In the remainder of this chapter, we will for definiteness assume that line widths of 10^{-11} eV can be achieved, but our analytical results will remain true also if the line widths are several orders of magnitude larger.

3.2 Prospects of a Mössbauer neutrino experiment

If the difficulties discussed in the previous section could be circumvented and a Mössbauer neutrino experiment could be built, this experiment could carry out a very interesting physics program [89,100]:

- **Neutrino oscillations on a laboratory scale.** Due to the low energy of Mössbauer neutrinos, $E \simeq 18.6$ keV, the oscillation lengths are ~ 20 m for atmospheric oscillations governed by Δm_{31}^2 , and ~ 600 m for solar oscillations, governed by Δm_{21}^2 . Mössbauer neutrinos could thus be used to measure the neutrino oscillation parameters at baselines much shorter than those used in conventional neutrino oscillation experiments [104].
- **Gravitational interactions of neutrinos.** One of the first applications of the classical Mössbauer effect has been the measurement of the gravitational redshift of photons [105]. If a Mössbauer neutrino experiment could be realised, it would open up the possibility to perform a similar experiment with neutrinos, whose gravitational interactions have never been studied in the laboratory.

¹Since the typical timescale of lattice vibrations is of $\mathcal{O}(10^{-13}$ s) [102], while the neutrino emission process takes $\mathcal{O}(10^{-5}$ s) (see below), only the mean values of v and v^2 are relevant, and all fluctuations average out.

- **Solid state effects.** The extreme sensitivity of the Mössbauer resonance condition to atomic interactions inside the source and detector crystals could allow for a study of such interactions with unprecedented precision, and might thus greatly improve our understanding of solid state physics.

3.3 Mössbauer neutrinos do oscillate

Let us now address the question, raised by Bilenky et al. [94–97], whether Mössbauer neutrinos can oscillate. In sec. 2.1.2, we have discussed the “textbook derivation” of the neutrino oscillation probability, eq. (2.9). In this approach, the neutrino was treated as a plane wave, and it was assumed that all mass eigenstates forming a given flavour eigenstate are emitted with the same energy or with the same momentum. For Mössbauer neutrinos, the equal momentum approximation is certainly unrealistic because it would imply that the energies associated with different mass eigenstates have to differ by $|E_j - E_k| \sim 6 \cdot 10^{-8}$ eV for $\Delta m_{jk}^2 \sim 2.4 \cdot 10^{-3}$ eV² and $E = 18.6$ keV (cf. eq. (2.12)). This is precluded by the tiny energy uncertainty of $\mathcal{O}(10^{-11})$ eV [92,93] in a Mössbauer neutrino experiment.

On the other hand, the equal energy approximation, though invalid for conventional neutrino experiments, is justified for Mössbauer neutrinos because their energy spread is much smaller than the inverse oscillation length. There remains the question whether the *momentum* uncertainty σ_p of the Mössbauer source and detector is large enough to allow for the coherent emission and absorption of all three neutrino mass eigenstates. If this were not the case, the coherent production of different mass eigenstates would not be possible, so that no oscillations could occur. According to eq. (2.8), we have to check whether the condition

$$p_k - p_j \sim 6 \cdot 10^{-8} \text{ eV} \ll \sigma_p \quad (3.5)$$

is fulfilled. The neutrino momentum can in principle be determined by measuring the recoil momentum of the crystal in which the emitting or absorbing nucleus is embedded. The ultimate uncertainty σ_p of this measurement is related to the coordinate uncertainty σ_x of the emitting nucleus through the Heisenberg relation $\sigma_p \sigma_x \geq 1/2$. The most conservative estimate for σ_x is several cm, the size of the source and detector crystals. This would imply $\sigma_p \gtrsim 2 \cdot 10^{-5}$ eV, already fulfilling eq. (3.5). In reality, σ_x can be determined to a much better accuracy because it is in principle possible to find out which particular nuclei have participated in the Mössbauer process by destroying the crystals and checking which atom has undergone a ${}^3\text{H} \leftrightarrow {}^3\text{He}$ transition. Thus, a more realistic estimate is $\sigma_x \simeq 10^{-10}$ m and $\sigma_p \gtrsim 2 \cdot 10^3$ eV. This value certainly fulfills eq. (3.5), so that we can conclude that Mössbauer neutrinos do oscillate, with the oscillation probability being approximately given by eq. (2.9).

The above statements can also be formulated in a different way [106]. Neutrino oscillations require the quantum mechanical coherence of different mass eigenstates, therefore they can only occur if the experiment is not able to distinguish different mass eigenstates.

The mass resolution σ_{m^2} is related to the neutrino energy E and momentum p , and to the uncertainties σ_E and σ_p of these quantities by

$$\sigma_{m^2} = \sqrt{(2E\sigma_E)^2 + (2p\sigma_p)^2}, \quad (3.6)$$

where it is assumed that σ_E and σ_p are statistically independent. From the estimates $E \simeq p = 18.6$ keV, $\sigma_E \sim 10^{-11}$ eV, and $\sigma_p \sim 2$ keV, it follows that

$$\sigma_{m^2} \sim 9 \cdot 10^3 \text{ eV}^2 \gg \Delta m_{jk}^2. \quad (3.7)$$

This shows that the small energy spread of Mössbauer neutrinos does not preclude oscillations because a large momentum uncertainty persists.

3.4 Mössbauer neutrino wave packets

3.4.1 Gaussian wave packets

Although the arguments given in the previous section indicate that Mössbauer neutrinos do oscillate, and can, to some extent, be described by using the equal energy approximation, a more realistic treatment of the problem is desirable in order to avoid the imperfections of the textbook derivation, discussed at the end of sec. 2.1.2. As a first step, we will now derive the flavour transition probability in a formalism in which the neutrino is described as a superposition of wave packets rather than plane waves [25, 28, 30–33].

Following most of the literature, we first assume a Gaussian shape for the wave packets, and write the momentum space wave function for a neutrino, produced with the initial flavour α , as

$$\langle p | \nu_{\alpha S}(t) \rangle = \frac{1}{(2\pi\gamma_S^2)^{1/4}} \sum_j U_{\alpha j}^* \exp \left[-\frac{(p - p_{jS})^2}{4\gamma_S^2} \right] \exp \left[-iE_j t \right] |\nu_j\rangle. \quad (3.8)$$

Here, $|\nu_j\rangle$ are the neutrino mass eigenstates in three-dimensional flavour space, $E_j = (p^2 + m_j^2)^{1/2}$ is the energy corresponding to the momentum p , p_{jS} is the average momentum of the mass eigenstate $|\nu_j\rangle$, and γ_S is the wave packet width in momentum space. The index S indicates quantities that are determined by the properties of the neutrino source, and we will use an index D for quantities depending on the detector properties. For Mössbauer neutrinos, we estimate $\gamma_S \sim 10^{-11}$ eV, i.e. the wave packet width is given by the *energy* uncertainty of the source, and not by its much larger momentum uncertainty. This is due to the on-shellness of the propagating neutrino, which ensures, by virtue of the relativistic energy-momentum relation, that the wave packet for each individual mass eigenstate cannot have a momentum spread larger than its energy spread. (Of course, the momenta of *different* mass eigenstates will differ by much larger amounts, as discussed in sec. 3.3.)

The wave packet in eq. (3.8) is defined such that, at $t = 0$, it is located at $x = 0$. This is most easily seen from the coordinate space representation of eq. (3.8),

$$\begin{aligned} \langle x | \nu_{\alpha S}(t) \rangle &= \frac{1}{(2\pi\gamma_S^2)^{1/4}} \sum_j U_{\alpha j}^* \int \frac{dp}{(2\pi)^{1/2}} \exp \left[-\frac{(p - p_{jS})^2}{4\gamma_S^2} \right] \exp [-iE_j t + ipx] |\nu_j\rangle \\ &= \left(\frac{2\gamma_S^2}{\pi} \right)^{1/4} \sum_j U_{\alpha j}^* \exp [- (x - v_{jS} t)^2 \gamma_S^2] \exp [-iE_j t + ip_{jS} x] |\nu_j\rangle. \end{aligned} \quad (3.9)$$

To be able to evaluate the momentum integral, we have made use of the smallness of γ_S , and expanded the phase factor in the integrand to first order in p around p_{jS} :²

$$-i\sqrt{p^2 + m_j^2} t + ipx \simeq -iE_{jS} t + ip_{jS} x + i(x - v_{jS} t)(p - p_{jS}). \quad (3.10)$$

The average energy E_{jS} and the average group velocity v_{jS} of the neutrino mass eigenstate $|\nu_j\rangle$ are defined by

$$E_{jS} = \sqrt{p_{jS}^2 + m_j^2} \quad \text{and} \quad v_{jS} = \frac{p_{jS}}{\sqrt{p_{jS}^2 + m_j^2}}. \quad (3.11)$$

The amplitude for the state $|\nu_{\alpha S}\rangle$ to have evolved into another state $|\nu_{\beta D}\rangle$ after a time t and after travelling a distance L is given by

$$\mathcal{A}_{\alpha\beta}(t, L) = \int dp \langle \nu_{\beta D}(0) | p \rangle \langle p | \nu_{\alpha S}(t) \rangle \exp[ipL], \quad (3.12)$$

where the factor $\exp[ipL]$ is chosen such that the final state $\langle \nu_{\beta D}(0) | p \rangle \exp[ipL]$ is a wave packet centred at $x = L$. $|\nu_{\beta D}(0)\rangle$ does not depend on t because the time evolution of the system is already fully described by the time dependence of $|\nu_{\alpha S}(t)\rangle$. On this point, we disagree with ref. [28], where the detection operator is assumed to be not a time-independent, but only a time-averaged, quantity. Note that the central momenta p_{jD} and the width γ_D of the final state wave packet, which depend on the properties of the neutrino detector, are in general different from the corresponding parameters p_{jS} and γ_S of $|\nu_{\alpha S}\rangle$. Plugging eq. (3.8) into eq. (3.12), the transition amplitude takes the form

$$\mathcal{A}_{\alpha\beta}(t, L) = \sum_j U_{\alpha j}^* U_{\beta j} \int dp \frac{1}{(2\pi\gamma_S\gamma_D)^{1/2}} e^{-iE_j t + ipL} \exp \left[-\frac{(p - p_{jS})^2}{4\gamma_S^2} - \frac{(p - p_{jD})^2}{4\gamma_D^2} \right]. \quad (3.13)$$

To evaluate the integral over p , a momentum expansion of E_j , similar to eq. (3.10), is required. Here, however, we expand not around p_{jS} , but around the mean momentum

²This approximation neglects dispersion (wave packet spreading), which is a second-order effect [16].

$\bar{p}_j = (p_{jS} + p_{jD})/2$ in order to preserve the symmetry of eq. (3.13) under the exchange of source- and detector-related quantities. Hence, we write

$$\sqrt{p^2 + m_j^2} t \simeq \bar{E}_j t + \bar{v}_j t(p - \bar{p}_j), \quad (3.14)$$

with the definitions

$$\bar{E}_j = \sqrt{\bar{p}_j^2 + m_j^2} \quad \text{and} \quad \bar{v}_j = \frac{\bar{p}_j}{\sqrt{\bar{p}_j^2 + m_j^2}}. \quad (3.15)$$

The expansion (3.14) is a good approximation as long as $(p - \bar{p}_j)/\bar{E}_j \ll \bar{E}_j^2/m_j^2$ for all p within the peak regions of the source and detector wave packets. The momentum integral in (3.13) now gives

$$\begin{aligned} \mathcal{A}_{\alpha\beta}(t, L) = (4\pi\tilde{\gamma}^2)^{1/2} \sum_j U_{\alpha j}^* U_{\beta j} \exp \left[-\frac{(p_{jS} - p_{jD})^2}{4(\gamma_S^2 + \gamma_D^2)} - (L - \bar{v}_j t)^2 \tilde{\gamma}^2 \right] \\ \cdot \exp \left[i \frac{(L - \bar{v}_j t)(p_{jS}\gamma_D^2 + p_{jD}\gamma_S^2)}{\gamma_S^2 + \gamma_D^2} - i\bar{E}_j t + i\bar{v}_j \bar{p}_j t \right]. \end{aligned} \quad (3.16)$$

In this expression, we have introduced an effective total momentum uncertainty $\tilde{\gamma}$, given by

$$\frac{1}{\tilde{\gamma}^2} \equiv \frac{1}{\gamma_S^2} + \frac{1}{\gamma_D^2}. \quad (3.17)$$

The probability of the transition $|\nu_{\alpha S}\rangle \rightarrow |\nu_{\beta D}\rangle$ is

$$\mathcal{P}_{\alpha\beta}(L) = \mathcal{N} \int dt \mathcal{A}_{\alpha\beta}^*(t, L) \mathcal{A}_{\alpha\beta}(t, L), \quad (3.18)$$

where the time integration reflects the fact that we do not precisely know at which point in time the production and detection reactions take place. Since the formalism presented here does not automatically yield a physically meaningful normalisation for $\mathcal{P}_{\alpha\beta}(L)$, we have by hand introduced a normalisation constant \mathcal{N} , which will be chosen such that, in the case of vanishing neutrino mixing and identical initial and final states, $\mathcal{P}_{\alpha\beta}(L)$ becomes equal to unity:

$$\mathcal{P}_{\alpha\beta}(L) = \delta_{\alpha\beta} \quad \text{for } U = \mathbb{1}_3 \text{ and } |\nu_{\alpha S}\rangle \equiv |\nu_{\alpha D}\rangle. \quad (3.19)$$

Here, $\mathbb{1}_3$ is the three-dimensional unit matrix. The expected experimental event rate Γ will be proportional to $\mathcal{P}_{\alpha\beta}(L)$, but the proportionality constant can only be determined if the production and detection processes are included in the computation. For the case of Mössbauer neutrinos, we will explicitly elucidate the relation between $\mathcal{P}_{\alpha\beta}(L)$ and Γ in sec. 3.5. Note that $\mathcal{P}_{\alpha\beta}(L)$ is not an oscillation probability in the strict sense because

we will see below that $\mathcal{P}_{\alpha\beta}(L)|_{\Delta m_{jk}^2=0} \neq \delta_{\alpha\beta}$. Therefore, we will for the most part refer to it as a “transition probability” rather than an oscillation probability.

Eq. (3.18) gives, after a straightforward evaluation of the Gaussian time integral,

$$\begin{aligned} \mathcal{P}_{\alpha\beta} = \mathcal{N} \sum_{j,k} U_{\alpha j}^* U_{\alpha k} U_{\beta k}^* U_{\beta j} N_{jk} \exp \left[iL(p_{jS} - p_{kS}) \frac{\gamma_D^2}{\gamma_S^2 + \gamma_D^2} + iL(p_{jD} - p_{kD}) \frac{\gamma_S^2}{\gamma_S^2 + \gamma_D^2} \right] \\ \cdot \exp \left[-i\Delta E_{jk} L \frac{\bar{v}_j + \bar{v}_k}{\bar{v}_j^2 + \bar{v}_k^2} \right] \cdot \exp \left[-\frac{(p_{jS} - p_{jD})^2}{4(\gamma_S^2 + \gamma_D^2)} - \frac{(p_{kS} - p_{kD})^2}{4(\gamma_S^2 + \gamma_D^2)} \right. \\ \left. - \frac{\Delta E_{jk}^2}{4\bar{\gamma}^2(\bar{v}_j^2 + \bar{v}_k^2)} - \frac{L^2(\bar{v}_j - \bar{v}_k)^2 \bar{\gamma}^2}{\bar{v}_j^2 + \bar{v}_k^2} \right], \end{aligned} \quad (3.20)$$

with the abbreviations

$$\Delta E_{jk} \equiv \bar{E}_j - \bar{E}_k + \frac{\gamma_S^2 - \gamma_D^2}{\gamma_S^2 + \gamma_D^2} [\bar{v}_j(p_{jD} - p_{jS}) - \bar{v}_k(p_{kD} - p_{kS})] \quad (3.21)$$

and

$$N_{jk} = \left(\frac{\pi}{\bar{\gamma}^2(v_{jS}^2 + v_{kS}^2)} \right)^{1/2} \left(\frac{2\gamma_D^2}{\gamma_S^2 + \gamma_D^2} \right)^{1/2} \left(\frac{2\gamma_S^2}{\gamma_S^2 + \gamma_D^2} \right)^{1/2}. \quad (3.22)$$

To simplify $\mathcal{P}_{\alpha\beta}$ further, and to facilitate its physical interpretation, let us make use of the fact that, in realistic experiments, neutrinos are ultra-relativistic, i.e. $m_j \ll \bar{E}_j$. This suggests the expansion

$$p_{jS} \simeq E_{S,0} - (1 - \xi_S) \frac{m_j^2}{2E_{S,0}}, \quad p_{jD} \simeq E_{D,0} - (1 - \xi_D) \frac{m_j^2}{2E_{D,0}}, \quad (3.23)$$

from which it follows that

$$\bar{E}_j \simeq \bar{E} + \bar{\xi} \frac{m_j^2}{2\bar{E}}, \quad \bar{p}_j \simeq \bar{E} - (1 - \bar{\xi}) \frac{m_j^2}{\bar{E}}, \quad \bar{v}_j \simeq 1 - \frac{m_j^2}{2\bar{E}^2}, \quad (3.24)$$

with

$$\bar{E} \equiv \frac{1}{2}(E_{S,0} + E_{D,0}) \quad \text{and} \quad 1 - \bar{\xi} \equiv \frac{\bar{E}}{2} \left(\frac{1 - \xi_S}{E_{S,0}} + \frac{1 - \xi_D}{E_{D,0}} \right). \quad (3.25)$$

In these expressions, $E_{S,0}$ and $E_{D,0}$ are the mean energies for the case of massless neutrinos and ξ_S , ξ_D are constant parameters determined by the properties of the source and the detector, respectively. They can be calculated only in an explicit treatment of the neutrino production and detection processes. For conventional neutrino sources, ξ_S and ξ_D are of $\mathcal{O}(1)$, but for Mössbauer neutrinos, the energies associated with different neutrino mass eigenstates have to coincide within the line widths γ_S and γ_D , so that ξ_S , ξ_D and $\bar{\xi}$ must be very small in this case.

Here, we will consider two special cases of eq. (3.24): The first one, $E_{S,0} = E_{D,0} = \bar{E}$, applies to oscillation experiments with conventional neutrino detectors, whose sensitivity is essentially uniform over a wide range of neutrino energies, so that there is no reason to expect $E_{S,0} \neq E_{D,0}$. The situation is different in Mössbauer neutrino experiments, where the resonance behaviour limits the sensitivity to a narrow energy interval. Unless the setup is perfectly tuned into resonance, we must therefore assume $E_{S,0} \neq E_{D,0}$. On the other hand, we will use the equal energy assumption $E_{jS} = E_{S,0}$, $E_{jD} = E_{D,0}$ (which implies $\xi_S = \xi_D = 0$ and $\tilde{\xi} = -(E_{S,0} - E_{D,0})^2/4E_{S,0}E_{D,0}$) for Mössbauer neutrinos.

In the first case, $E_{S,0} = E_{D,0} = \bar{E}$, the transition probability takes the form

$$\mathcal{P}_{\alpha\beta} = \sum_{j,k} U_{\alpha j}^* U_{\alpha k} U_{\beta k}^* U_{\beta j} \exp \left[-2\pi i \frac{L}{L_{jk}^{\text{osc}}} - \left(\frac{L}{L_{jk}^{\text{coh}}} \right)^2 - \frac{\pi^2}{2} \tilde{\xi}^2 \left(\frac{1}{\tilde{\gamma} L_{jk}^{\text{osc}}} \right)^2 - \frac{[(\xi_S - \xi_D)(m_j^2 + m_k^2)]^2}{32\bar{E}^2(\gamma_S^2 + \gamma_D^2)} \right], \quad (3.26)$$

with the oscillation and coherence lengths

$$L_{jk}^{\text{osc}} = \frac{4\pi\bar{E}}{\Delta m_{jk}^2} \quad \text{and} \quad L_{jk}^{\text{coh}} = \frac{2\sqrt{2}\bar{E}^2}{\tilde{\gamma}|\Delta m_{jk}^2|}, \quad (3.27)$$

and the quantity $\tilde{\xi}$ being defined by

$$\frac{\tilde{\xi}^2}{\tilde{\gamma}^2} \equiv \frac{\xi_S^2}{\gamma_S^2} + \frac{\xi_D^2}{\gamma_D^2}. \quad (3.28)$$

In eq. (3.26), we have neglected the dependence of the prefactor N_{jk} on the neutrino masses, and have implemented eq. (3.19) by choosing $\mathcal{N} = 1/N_{jk}$.

We see that the first term in the exponent of (3.26) is the standard oscillation phase. The second term suppresses oscillations in the j - k -sector if $L \gg L_{jk}^{\text{coh}}$. In this case, the wave packets corresponding to the mass eigenstates ν_j and ν_k separate before reaching the detector because of their different group velocities. Note, however, that L_{jk}^{coh} depends on the momentum uncertainties of both, the source and the detector. This means that a measurement with small momentum uncertainty $\gamma_D \ll \gamma_S$, i.e. large spatial uncertainty $\sigma_{xD} = 1/2\gamma_D \gg \sigma_{xS} = 1/2\gamma_S$, can restore coherence even if the wave packets have separated by more than their spatial width σ_{xS} .

The third term in eq. (3.26) implements a localisation condition of the form

$$\frac{\tilde{\xi}}{\tilde{\gamma} L_{jk}^{\text{osc}}} \stackrel{!}{\ll} 1, \quad (3.29)$$

For neutrinos from conventional sources with $\tilde{\xi} \sim \mathcal{O}(1)$, oscillations are thus suppressed if the effective spatial extent of the wave packets, $\sigma_x \equiv 1/2\tilde{\gamma}$ (which takes into account the coherence properties of the source and the detector), is larger than the oscillation

length. If $\tilde{\xi} \ll 1$, as for Mössbauer neutrinos, this condition is relaxed. In the derivation of eq. (3.26), one contribution to the localisation exponent arises from the term proportional to $\Delta E_{jk}^2/\tilde{\gamma}^2$ in the last line of (3.20). This term suppresses interference between different neutrino mass eigenstates if their phase difference at the detector site changes significantly during the time it takes to absorb the neutrino wave packet. In this case, oscillations are effectively averaged out. Another contribution to the condition (3.29) comes from the terms proportional to $(p_{jS} - p_{jD})^2/(\gamma_S^2 + \gamma_D^2)$ and $(p_{kS} - p_{kD})^2/(\gamma_S^2 + \gamma_D^2)$ in (3.20). They enforce sufficient overlap of the neutrino wave packets with the wave packets describing the detection process. This requirement corresponds to the approximate conservation of the average momentum for each mass eigenstate. If the overlap is better for some neutrino mass eigenstates than for others, flavour mixing is effectively reduced, and the associated suppression of oscillations is described by a localisation exponential.

The last term in the exponent of (3.26) also arises from the requirement of approximate conservation of the average momenta. However, unlike the localisation term, it does not only depend on Δm_{jk}^2 , but also on the absolute scale of the neutrino masses. It suppresses the transition probability if p_{jS} and p_{jD} differ by more than $(\gamma_S^2 + \gamma_D^2)^{1/2}$. For small γ_S and γ_D , one might call this constraint a resonance condition. While the oscillation, coherence and localisation terms in (3.26) agree with those found by other authors (see e.g. [25, 28]), we are not aware of previous discussions of the resonance term in the context of the quantum mechanical wave packet formalism. In quantum field theoretical descriptions of neutrino oscillations, a term proportional to $(m_j^2 + m_k^2)^2$ is found [16, 107], but its precise form is not the same as that of the resonance term in eq. (3.26). For example, it does not vanish if the properties of the source and the detector, and thus ξ_S and ξ_D , are identical. We attribute this to the fact that in our formalism it is implicitly assumed that all mass eigenstate components of $|\nu_{\alpha S}\rangle$ are emitted with equal probabilities, and all components of $|\nu_{\beta D}\rangle$ are absorbed with equal probabilities. In reality, this will generally not be the case due to the kinematics of the production and detection processes, which are correctly described only in QFT models of neutrino oscillations. In that sense, the resonance term in (3.26) should be considered incomplete.

In terrestrial experiments using atmospheric neutrinos, reactor neutrinos or accelerator neutrinos, the coherence, localisation and resonance terms in (3.26) are negligible, but for astrophysical neutrinos, decoherence is important.

Eq. (3.26) is different from the corresponding result derived in ref. [28] using the density matrix formalism. In particular, the author of [28] does not obtain any overlap or resonance condition because he does not assume full time-independence of the detection operator (see discussion below eq. (3.12)), and treats the neutrino density matrix as a matrix in flavour space, but only as a function of x in coordinate space.

Let us now consider the second limiting case of eq. (3.24), $E_{jS} = E_{S,0}$ and $E_{jD} = E_{D,0}$. Under this assumption, inserting the approximations (3.23) and (3.24) into eq. (3.20)

yields

$$\begin{aligned}
 \mathcal{P}_{\alpha\beta} = & \sum_{j,k} U_{\alpha j}^* U_{\alpha k} U_{\beta k}^* U_{\beta j} \exp \left[-i \frac{\Delta m_{jk}^2 L}{2\bar{E}} \left(1 + \frac{E_{S,0} - E_{D,0}}{2\bar{E}} \frac{\gamma_S^2 - \gamma_D^2}{\gamma_S^2 + \gamma_D^2} \right) \right] \\
 & \cdot \exp \left[-\frac{\tilde{\gamma}^2 (\Delta m_{jk}^2)^2 L^2}{8\bar{E}^4} - \frac{(E_{S,0} - E_{D,0})^2}{2(\gamma_S^2 + \gamma_D^2)} \left(1 + \frac{m_j^2 + m_k^2}{2E_{S,0}E_{D,0}} + \frac{(m_j^4 + m_k^4)\bar{E}^2}{2E_{S,0}^3 E_{D,0}^3} \right) \right. \\
 & \quad \left. - \frac{(E_{S,0} - E_{D,0})^4}{8\tilde{\gamma}^2 (\gamma_S^2 + \gamma_D^2)^2} \left(\frac{\Delta m_{jk}^2}{2\bar{E}} \right)^2 \left(\frac{E_{D,0}\gamma_D^2 + E_{S,0}\gamma_S^2}{E_{S,0}E_{D,0}\bar{E}} \right)^2 \right]. \quad (3.30)
 \end{aligned}$$

To obtain this expression, the second order terms in the expansions (3.23) have to be taken into account for consistency. For $E_{jS} = E_{S,0}$, $E_{jD} = E_{D,0}$, they have the form $-m_j^4/8E_{S,0}^3$ and $-m_j^4/8E_{D,0}^3$, respectively. Many of the terms in eq. (3.30) are subdominant for realistic assumptions on the parameters ($L \sim L_{jk}^{\text{osc}}$, $E_{S,0} - E_{D,0} \lesssim \tilde{\gamma}$), and can be neglected. This leads to

$$\mathcal{P}_{\alpha\beta} = \sum_{j,k} U_{\alpha j}^* U_{\alpha k} U_{\beta k}^* U_{\beta j} \exp \left[-2\pi i \frac{L}{L_{jk}^{\text{osc}}} - \left(\frac{L}{L_{jk}^{\text{coh}}} \right)^2 - \frac{(E_{S,0} - E_{D,0})^2}{2(\gamma_S^2 + \gamma_D^2)} \right]. \quad (3.31)$$

We encounter the same oscillation and decoherence factors as in eq. (3.26), but, as expected, the $\tilde{\xi}$ -dependent localisation and resonance terms are absent. Instead, a new resonance term appears, which depends on $E_{S,0} - E_{D,0}$ rather than $(\xi_S - \xi_D)m_j^2/2\bar{E}$. Note that, for Mössbauer neutrinos, $\gamma_S \sim \gamma_D \sim \tilde{\gamma} \sim 10^{-11}$ eV implies that the coherence lengths L_{jk}^{coh} are of order 10^{13} km, so that wave packet decoherence is completely irrelevant.

3.4.2 Lorentzian wave packets

Even though the formalism of Gaussian wave packets is widely used in the literature, it does not always provide a realistic description of physics. For example, we expect the emission and absorption lines for Mössbauer neutrinos to have a Lorentzian shape, like the emission and absorption lines encountered in Mössbauer experiments with photons [102, 103]. Also the momentum uncertainty of neutrinos emitted in decays of free particles is described by Lorentzian rather than Gaussian wave packets. Therefore, let us re-derive the flavour transition probability using Lorentzian wave packets of the form

$$\langle p | \nu_{\alpha S}(t) \rangle = \sum_j U_{\alpha j}^* \frac{\sqrt{\gamma_S/2\pi}}{p - p_{jS} + i\gamma_S/2} \exp[-iE_j t] |\nu_j\rangle. \quad (3.32)$$

This leads to

$$\begin{aligned} \mathcal{A}_{\alpha\beta}(t, L) = & \sum_j U_{\alpha j}^* U_{\beta j} \frac{-i\gamma_S}{p_{jS} - p_{jD} - i(\gamma_S + \gamma_D)/2} \exp \left[-i\bar{E}_j t + i\bar{v}_j \bar{p}_j t \right] \\ & \cdot \left\{ \exp \left[\left(ip_{jS} + \frac{\gamma_S}{2} \right) (L - \bar{v}_j t) \right] \theta(\bar{v}_j t - L) + \exp \left[\left(ip_{jD} - \frac{\gamma_D}{2} \right) (L - \bar{v}_j t) \right] \theta(-\bar{v}_j t + L) \right\}, \end{aligned} \quad (3.33)$$

where θ denotes the Heaviside step function. Calculation of the transition probability according to eq. (3.18) requires splitting the time integral into three separate integrals with integration domains $(-\infty, L/\bar{v}_k]$, $(L/\bar{v}_k, L/\bar{v}_j)$ and $[L/\bar{v}_j, \infty)$ for $m_j > m_k$, or $(-\infty, L/\bar{v}_j]$, $[L/\bar{v}_j, L/\bar{v}_k]$ and $[L/\bar{v}_k, \infty)$ for $m_j < m_k$. Here, we will only show how to evaluate one of these integrals, since the others are similar. Consider

$$\begin{aligned} J_{jk} = & \int_{L/\bar{v}_k}^{L/\bar{v}_j} dt \exp \left[-i(\bar{E}_j - \bar{E}_k)t + i(\bar{v}_j \bar{p}_j - \bar{v}_k \bar{p}_k)t - i(\bar{v}_j p_{jD} - \bar{v}_k p_{kS})t \right. \\ & \left. + \frac{1}{2}(\gamma_D \bar{v}_j - \gamma_S \bar{v}_k)t + i(p_{jD} - p_{kS})L - \frac{1}{2}(\gamma_D - \gamma_S)L \right] \end{aligned} \quad (3.34)$$

for $m_j > m_k$. After using the relativistic approximation (3.24), neglecting terms containing the small product $\Delta m_{jk}^2(E_{S,0} - E_{D,0})/\bar{E}^2$ and, in the denominator, also neglecting terms of order $\tilde{\gamma}m_j^2/\bar{E}^2$, we obtain

$$J_{jk} = \frac{A_{jk}^{(S)} - A_{jk}^{(D)}}{\frac{1}{2}(\gamma_D - \gamma_S) + i(E_{S,0} - E_{D,0}) - i\tilde{\xi}\Delta m_{jk}^2/2\bar{E}} \quad (3.35)$$

with the oscillation and coherence terms abbreviated as

$$\begin{aligned} A_{jk}^{(S,D)} = & \exp \left[-i\frac{\Delta m_{jk}^2 L}{2\bar{E}} - \frac{|\Delta m_{jk}^2| \gamma_{S,D} L}{4\bar{E}^2} \right] \\ \equiv & \exp \left[-2\pi i \frac{L}{L_{jk}^{\text{osc}}} - \frac{L}{L_{S,D,jk}^{\text{coh}}} \right]. \end{aligned} \quad (3.36)$$

The full expression for $\mathcal{P}_{\alpha\beta}(L)$ (normalised according to (3.19)) is

$$\begin{aligned} \mathcal{P}_{\alpha\beta}(L) = & \frac{\gamma_S + \gamma_D}{4} \sum_{j,k} U_{\alpha j}^* U_{\alpha k} U_{\beta k}^* U_{\beta j} \gamma_S \gamma_D \\ & \cdot \left[E_{S,0} - E_{D,0} - m_j^2 \left(\frac{1 - \xi_S}{2E_{S,0}} - \frac{1 - \xi_D}{2E_{D,0}} \right) - \frac{i(\gamma_S + \gamma_D)}{2} \right]^{-1} \\ & \cdot \left[E_{S,0} - E_{D,0} - m_k^2 \left(\frac{1 - \xi_S}{2E_{S,0}} - \frac{1 - \xi_D}{2E_{D,0}} \right) + \frac{i(\gamma_S + \gamma_D)}{2} \right]^{-1} \\ & \cdot \left\{ \frac{A_{jk}^{(S)}}{\gamma_S + i\xi_S \frac{\Delta m_{jk}^2}{2E_{S,0}}} + \frac{A_{jk}^{(D)}}{\gamma_D - i\xi_D \frac{\Delta m_{jk}^2}{2E_{D,0}}} + \frac{A_{jk}^{(S)} - A_{jk}^{(D)}}{\frac{1}{2}(\gamma_D - \gamma_S) \pm i(E_{S,0} - E_{D,0}) - i\tilde{\xi} \frac{\Delta m_{jk}^2}{2\bar{E}}} \right\}. \end{aligned} \quad (3.37)$$

In the last term, the upper sign applies to the case $\Delta m_{jk}^2 > 0$, while the lower one applies to $\Delta m_{jk}^2 < 0$. It is straightforward to approximate eq. (3.37) further by considering again the special cases $E_{S,0} = E_{D,0}$ and $E_{jS} = E_{S,0}$, $E_{jD} = E_{D,0}$. We are particularly interested in the second of these, which is relevant to Mössbauer neutrinos. It leads to

$$\mathcal{P}_{\alpha\beta}(L) = \sum_{j,k} U_{\alpha j}^* U_{\alpha k} U_{\beta k}^* U_{\beta j} \frac{(\gamma_S + \gamma_D)/4}{(E_{S,0} - E_{D,0})^2 + \frac{1}{4}(\gamma_S + \gamma_D)^2} \cdot \left\{ \frac{\gamma_S + \gamma_D}{2} (A_{jk}^{(S)} + A_{jk}^{(D)}) - \frac{1}{2} \frac{(A_{jk}^{(S)} - A_{jk}^{(D)}) [(E_{S,0} - E_{D,0})(\gamma_S - \gamma_D) \pm i \frac{(\gamma_S + \gamma_D)^2}{2}]}{E_{S,0} - E_{D,0} \pm i \frac{\gamma_S - \gamma_D}{2}} \right\}. \quad (3.38)$$

We see that, like in the case of Gaussian wave packets (eq. (3.31)), oscillation, decoherence and resonance terms emerge. However, the exponents in the coherence terms are now linear rather than quadratic in L , and the resonance term has a Breit-Wigner form, as for the classical Mössbauer effect.

Even though we will confirm in eq. (3.80) that (3.38) provides a realistic description of Mössbauer neutrinos, the derivation presented here has several shortcomings. In particular, the shapes, widths and central energies of the wave packets had to be put in by hand, and it is not straightforward to verify that the estimates we have used for them were appropriate. Moreover, it is not clear whether γ_S , γ_D , $E_{S,0}$, $E_{D,0}$, ξ_S and ξ_D are sufficient to describe all features of the source and the detector that are relevant to the oscillation phenomenology. To avoid these shortcomings of the quantum mechanical formalism, we have to employ quantum field theory, which allows us to explicitly include the neutrino production and detection processes in the calculation. This will be the subject of the next section.

3.5 Mössbauer neutrinos in quantum field theory

3.5.1 The Feynman diagram

The quantum field theoretical approach to neutrino oscillations, in which the neutrino is treated as an intermediate state, has been developed in [16, 34–42, 107] for conventional neutrino sources, and we will now adapt it to the case of Mössbauer neutrinos. Our aim is to compute the amplitude for the combined process of neutrino production in bound state tritium decay, neutrino propagation and oscillation, and neutrino absorption by induced electron capture on ^3He . This process is depicted schematically in the Feynman diagram shown in fig. 3.1. We assume the external ^3H and ^3He atoms to be confined by quantum mechanical harmonic oscillator potentials to reflect the fact that they are bound in crystal lattices. Typical values for the harmonic oscillator frequencies are of the order of the Debye temperature $\Theta_D \sim 600 \text{ K} \simeq 0.05 \text{ eV}$ of the respective crystals [89, 92]. Even though this simple model does not account for the details of the solid state binding forces, it is known to correctly reproduce the main features of the conventional Mössbauer

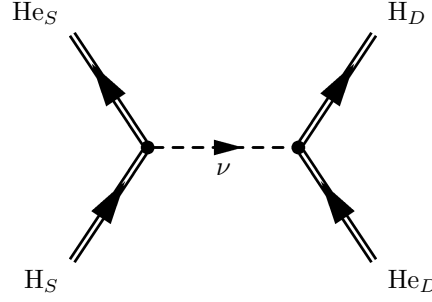


Figure 3.1: Feynman diagram for neutrino emission, propagation and absorption in the ${}^3\text{H} - {}^3\text{He}$ system.

effect [108]. Since we are interested mainly in the oscillation physics rather than in the exact overall rate of the Mössbauer processes, it is also sufficient for our purposes. As we consider only recoil-free neutrino emission and absorption, we can neglect thermal excitations and assume the parent and daughter nuclei in the source and detector to be in the ground states of their respective harmonic oscillator potentials. Their normalised wave functions thus have the form

$$\psi_{A,B,0}(\mathbf{x}, t) = \left[\frac{m_A \omega_{A,B}}{\pi} \right]^{\frac{3}{4}} \exp \left[-\frac{1}{2} m_A \omega_{A,B} |\mathbf{x} - \mathbf{x}_B|^2 \right] e^{-iE_{A,B}t}, \quad (3.39)$$

where the index $A = \{\text{H}, \text{He}\}$ distinguishes the two types of atoms and $B = \{S, D\}$ distinguishes between quantities related to the source and to the detector, respectively. The masses of the tritium and ${}^3\text{He}$ atoms are denoted by m_{H} and m_{He} , and the coordinates of the lattice sites at which the atoms are localised in the source and in the detector are \mathbf{x}_S and \mathbf{x}_D . The quantities $\omega_{A,B}$ are the harmonic oscillator frequencies, which are in general different for ${}^3\text{H}$ and ${}^3\text{He}$ because of the different chemical properties of these atoms. Moreover, they are different in the source and the detector because of the different ${}^3\text{H}$ and ${}^3\text{He}$ abundances in the two crystals. The energies $E_{A,B}$ of the external particles are not exactly fixed due to the line broadening mechanisms discussed in sec. 3.1, but follow narrow distribution functions, which are centred around $E_{A,B,0} = m_A + \frac{1}{2}\omega_{A,B}$. For the differences of these mean energies of tritium and helium atoms in the source and detector we will use the notation

$$E_{S,0} = E_{\text{H},S,0} - E_{\text{He},S,0}, \quad E_{D,0} = E_{\text{H},D,0} - E_{\text{He},D,0}. \quad (3.40)$$

These quantities correspond to the central values of the neutrino emission and absorption lines.

Factorisation approach: Production and detection as separate processes

As a prelude to our calculation of the combined overall rate of neutrino production, propagation and detection, let us first compute the neutrino production rate and the

detection cross section separately. This factorisation approach is very instructive, and it will allow us later to identify the unique features of the combined treatment.

Neutrino production and absorption in a Mössbauer neutrino experiment are governed by the Hamiltonians

$$H_S^+ = \int d^3x \frac{1}{\sqrt{2}} G_F \cos \theta_c \langle {}^3\text{He} | J^\mu | {}^3\text{H} \rangle \bar{\psi}_{e,S} \gamma_\mu (1 - \gamma^5) \psi_\nu \quad (3.41)$$

and

$$H_D^- = \int d^3x \frac{1}{\sqrt{2}} G_F \cos \theta_c \langle {}^3\text{H} | J^\mu | {}^3\text{He} \rangle \bar{\psi}_\nu \gamma_\mu (1 - \gamma^5) \psi_{e,D}, \quad (3.42)$$

respectively. H_S^+ describes tritium decay in the source, while H_D^- describes $\bar{\nu}_e$ capture in the detector. Here, G_F is the Fermi constant, θ_c is the Cabibbo angle, $\psi_{e,S}$, $\psi_{e,D}$, and ψ_ν are the field operators for the electron and the neutrino, respectively, and $\langle {}^3\text{He} | J^\mu | {}^3\text{H} \rangle$, $\langle {}^3\text{H} | J^\mu | {}^3\text{He} \rangle$ are the hadronic currents.

If we assume for the moment that the four-momentum $p_\nu = (E_\nu, \mathbf{p}_\nu)$ of the neutrinos from the production process (3.1) is fixed, i.e. no line broadening is effective, the amplitude of recoilless neutrino production is

$$\begin{aligned} i\mathcal{A} = & \int d^3x dt \left(\frac{m_{\text{H}} \omega_{\text{H},S}}{\pi} \right)^{\frac{3}{4}} \exp \left[-\frac{1}{2} m_{\text{H}} \omega_{\text{H},S} |\mathbf{x}|^2 \right] e^{-iE_{\text{H},S,0}t} \\ & \cdot \left(\frac{m_{\text{He}} \omega_{\text{He},S}}{\pi} \right)^{\frac{3}{4}} \exp \left[-\frac{1}{2} m_{\text{He}} \omega_{\text{He},S} |\mathbf{x}|^2 \right] e^{iE_{\text{He},S,0}t} e^{iE_\nu t - i\mathbf{p}_\nu \cdot \mathbf{x}} \\ & \cdot \frac{G_F \cos \theta_c}{\sqrt{2}} \psi_e(R) \int \Psi_{Z=2,S}(\mathbf{r})^* \Psi_{Z=1,S}(\mathbf{r}) d^3r \\ & \cdot \bar{u}_{\text{He}} \left(M_V \delta_0^\mu - \frac{1}{\sqrt{3}} g_A M_A \gamma^i \gamma^5 \delta_i^\mu \right) u_{\text{H}} \bar{u}_e \gamma_\mu (1 - \gamma^5) v_\nu(p_\nu). \end{aligned} \quad (3.43)$$

Here, u_{H} , u_{He} , u_e and $v_\nu(p_\nu)$ are the spinors of the ${}^3\text{H}$ and ${}^3\text{He}$ atoms, the electron and the neutrino, respectively. The atoms and the electron are non-relativistic, so the momentum-dependence of their spinors can be neglected. On the other hand, the neutrino is ultra-relativistic, so its mass can be set to zero in $v_\nu(p_\nu)$. In the hadronic current, M_V and M_A denote the vector and axial-vector (or Fermi and Gamow-Teller) nuclear matrix elements and $g_A \simeq 1.25$ is the axial-vector coupling constant. For the allowed beta transition ${}^3\text{H} \rightarrow {}^3\text{He}$, $M_V = 1$ and $M_A \approx \sqrt{3}$ [109, 110]. The quantity $\psi_e(R)$ is the value of the anti-symmetrised atomic wave function of ${}^3\text{He}$ at the surface of the nucleus. The integral in the third line of eq. (3.43) gives the overlap of the electronic $1s$ wave functions of ${}^3\text{H}$ and ${}^3\text{He}$, and thus accounts for the fact that the spectator electron, which is initially in the $1s$ atomic state of ${}^3\text{H}$, ends up in the $1s$ state of ${}^3\text{He}$.

After evaluating the integrals over \mathbf{x} and t in eq. (3.43), we can easily compute the rate for Mössbauer neutrino emission using Fermi's Golden Rule. We find

$$\Gamma_p = \Gamma_0 X_S, \quad (3.44)$$

with

$$\Gamma_0 = \frac{G_F^2 \cos^2 \theta_c}{\pi} |\psi_e(R)|^2 m_e^2 (|M_V|^2 + g_A^2 |M_A|^2) \left(\frac{E_{S,0}}{m_e} \right)^2 \kappa_S \quad (3.45)$$

and

$$\kappa_S = \left| \int \Psi_{Z=2,S}(\mathbf{r})^* \Psi_{Z=1,S}(\mathbf{r}) d^3 r \right|^2. \quad (3.46)$$

The factor X_S in eq. (3.44) is defined as

$$X_S = 8 \left(\eta_S + \frac{1}{\eta_S} \right)^{-3} \exp \left[-\frac{\mathbf{p}_\nu^2}{\sigma_{pS}^2} \right] \equiv Y_S \exp \left[-\frac{\mathbf{p}_\nu^2}{\sigma_{pS}^2} \right], \quad (3.47)$$

where $|\mathbf{p}_\nu| = (E_{S,0}^2 - m^2)^{1/2}$ is the neutrino momentum³, and we have introduced the notation

$$\eta_S = \sqrt{\frac{m_H \omega_{H,S}}{m_{He} \omega_{He,S}}}, \quad \sigma_{pS}^2 = m_H \omega_{H,S} + m_{He} \omega_{He,S}. \quad (3.48)$$

The factor $\exp[-\mathbf{p}_\nu^2/\sigma_{pS}^2]$ is the well-known Lamb-Mössbauer factor or recoil-free fraction [88, 102, 108], which gives the relative probability of recoil-free emission compared to the total emission probability. We see that recoilless emission is suppressed if the neutrino momentum $|\mathbf{p}_\nu|$ is larger than the effective momentum uncertainty σ_{pS} of the emitting atom, because in that case, the recoil energy is likely to lead to a phonon excitation.

From eq. (3.44) and our assumption of monochromatic emission, it follows that the energy spectrum $\rho(E)$ of the emitted Mössbauer neutrinos is

$$\rho(E) = \Gamma_0 X_S \delta(E - E_{S,0}). \quad (3.49)$$

In a similar way as the production rate, we can also derive the detection cross section

$$\sigma(E) = B_0 X_D \delta(E - E_{D,0}), \quad (3.50)$$

with

$$B_0 = 4\pi G_F^2 \cos^2 \theta_c |\psi_e(R)|^2 (|M_V|^2 + g_A^2 |M_A|^2) \kappa_D, \quad (3.51)$$

$$X_D = 8 \left(\eta_D + \frac{1}{\eta_D} \right)^{-3} \exp \left[-\frac{\mathbf{p}_\nu^2}{\sigma_{pD}^2} \right] \equiv Y_D \exp \left[-\frac{\mathbf{p}_\nu^2}{\sigma_{pD}^2} \right], \quad (3.52)$$

$$\eta_D = \sqrt{\frac{m_H \omega_{H,D}}{m_{He} \omega_{He,D}}}, \quad (3.53)$$

$$\sigma_{pD}^2 = m_H \omega_{H,D} + m_{He} \omega_{He,D}. \quad (3.54)$$

³Since in this calculation we ignore neutrino oscillations, we also neglect the neutrino mass differences.

The factor κ_D is defined in analogy to eq. (3.46). In the approximation of hydrogen-like atomic wave functions, one has $\kappa_S = \kappa_D = 512/729 \simeq 0.7$.

The Mössbauer neutrino production rate Γ_p and detection cross section $\sigma(E)$ differ from the corresponding results previously obtained for unbound parent and daughter nuclei (refs. [86] and [87]) by the factors X_S and X_D . Note that in the limit $m_H \omega_{H,S} = m_{He} \omega_{He,S}$, $m_H \omega_{H,D} = m_{He} \omega_{He,D}$, these factors reduce to a numerical constant times the Lamb-Mössbauer factor.

Assuming factorisation of the production and detection probabilities, and neglecting neutrino oscillations, we can combine eqs. (3.44) and (3.50) to obtain the detection rate

$$\Gamma = \frac{1}{4\pi L^2} \int_0^\infty \rho(E) \sigma(E) dE = \frac{\Gamma_0 B_0}{4\pi L^2} X_S X_D \delta(E_{S,0} - E_{D,0}). \quad (3.55)$$

The geometric factor $1/(4\pi L^2)$, which is valid only for isotropic emission (i.e. for an unpolarised source), describes the attenuation of the flux over the baseline L . We see that Γ is infinite when the Mössbauer resonance condition $E_{S,0} = E_{D,0}$ is exactly satisfied and zero otherwise, which is a consequence of our assumption of infinitely sharp emission and absorption lines. This assumption is certainly unphysical, and a realistic calculation should take into account the finite linewidth effects. Therefore, let us introduce Lorentzian broadening factors of width γ_S and γ_D , respectively, in $\rho(E)$ and $\sigma(E)$, so that these quantities become

$$\rho(E) = \Gamma_0 X_S \frac{\gamma_S/2\pi}{(E - E_{S,0})^2 + \gamma_S^2/4}, \quad \sigma(E) = B_0 X_D \frac{\gamma_D/2\pi}{(E - E_{D,0})^2 + \gamma_D^2/4}. \quad (3.56)$$

Then,

$$\Gamma \simeq \frac{\Gamma_0 B_0}{4\pi L^2} X_S X_D \frac{(\gamma_S + \gamma_D)/2\pi}{(E_{S,0} - E_{D,0})^2 + (\gamma_S + \gamma_D)^2/4}. \quad (3.57)$$

This shows that the Mössbauer resonance is strong if

$$(E_{S,0} - E_{D,0})^2 \ll (\gamma_S + \gamma_D)^2/4. \quad (3.58)$$

In that case, the neutrino detection cross section is enhanced by a factor of order $(\alpha Z m_e)^3/[p_e E_e(\gamma_S + \gamma_D)]$ compared to cross sections of non-resonant capture reactions $\bar{\nu}_e + A \rightarrow A' + e^+$ for neutrinos of the same energy (assuming the recoil-free fraction to be of order 1). For $\gamma_S + \gamma_D \sim 10^{-11}$ eV the enhancement factor can be as large as 10^{12} .

Combined approach: Production, propagation and detection as a single processes

We now turn to the treatment of Mössbauer neutrino production, propagation and absorption as one single process. Initially, we will neglect line broadening. We derive the transition amplitude by applying the coordinate space Feynman rules to the diagram in

fig. 3.1, using the bound state wave functions $\psi_{A,B,0}(\mathbf{x}, t)$ from eq. (3.39) for the external tritium and helium atoms. This leads to

$$\begin{aligned}
 i\mathcal{A} = & \int d^3x_1 dt_1 \int d^3x_2 dt_2 \left(\frac{m_H \omega_{H,S}}{\pi} \right)^{\frac{3}{4}} \exp \left[-\frac{1}{2} m_H \omega_{H,S} |\mathbf{x}_1 - \mathbf{x}_S|^2 \right] e^{-iE_{H,S}t_1} \\
 & \cdot \left(\frac{m_{\text{He}} \omega_{\text{He},S}}{\pi} \right)^{\frac{3}{4}} \exp \left[-\frac{1}{2} m_{\text{He}} \omega_{\text{He},S} |\mathbf{x}_1 - \mathbf{x}_S|^2 \right] e^{+iE_{\text{He},S}t_1} \\
 & \cdot \left(\frac{m_{\text{He}} \omega_{\text{He},D}}{\pi} \right)^{\frac{3}{4}} \exp \left[-\frac{1}{2} m_{\text{He}} \omega_{\text{He},D} |\mathbf{x}_2 - \mathbf{x}_D|^2 \right] e^{-iE_{\text{He},D}t_2} \\
 & \cdot \left(\frac{m_H \omega_{H,D}}{\pi} \right)^{\frac{3}{4}} \exp \left[-\frac{1}{2} m_H \omega_{H,D} |\mathbf{x}_2 - \mathbf{x}_D|^2 \right] e^{+iE_{H,D}t_2} \\
 & \cdot \sum_j \mathcal{M}_S^\mu \mathcal{M}_D^{\nu*} |U_{ej}|^2 \int \frac{d^4p}{(2\pi)^4} \exp \left[-ip_0(t_2 - t_1) + i\mathbf{p}(\mathbf{x}_2 - \mathbf{x}_1) \right] \\
 & \cdot \bar{u}_{e,S} \gamma_\mu (1 - \gamma^5) \frac{i(\not{p} + m_j)}{p_0^2 - \mathbf{p}^2 - m_j^2 + i\epsilon} (1 + \gamma^5) \gamma_\nu u_{e,D}. \tag{3.59}
 \end{aligned}$$

In this expression, the Dirac spinors of the external particles are $u_{A,B}$, with $A = \{e, H, \text{He}\}$ and $B = \{S, D\}$. They are all non-relativistic, so we can neglect their momentum dependence. The matrix elements \mathcal{M}_S^μ and \mathcal{M}_D^μ are given by

$$\mathcal{M}_{S,D}^\mu = \frac{G_F \cos \theta_c}{\sqrt{2}} \psi_e(R) \bar{u}_{\text{He}}(M_V \delta_0^\mu - g_A M_A \gamma^i \gamma^5 \delta_i^\mu / \sqrt{3}) u_H \kappa_{S,D}^{1/2}. \tag{3.60}$$

They encode the information on the bound state tritium beta decay and on the inverse process, the induced orbital electron capture taking place in the detector.

The integrations over t_1 and t_2 in eq. (3.59) yield energy-conserving δ -functions at the neutrino production and detection vertices. The spatial integrals are Gaussian and can be evaluated after making the transformations $\mathbf{x}_1 \rightarrow \mathbf{x}_1 + \mathbf{x}_S$ and $\mathbf{x}_2 \rightarrow \mathbf{x}_2 + \mathbf{x}_D$. We obtain

$$\begin{aligned}
 i\mathcal{A} = & \mathcal{N} \int \frac{d^4p}{(2\pi)^4} 2\pi\delta(p_0 - E_S) 2\pi\delta(p_0 - E_D) \exp \left[-\frac{\mathbf{p}^2}{2\sigma_p^2} \right] \\
 & \cdot \sum_j \mathcal{M}_S^\mu \mathcal{M}_D^{\nu*} |U_{ej}|^2 \bar{u}_{e,S} \gamma_\mu (1 - \gamma^5) \frac{i(\not{p} + m_j) e^{i\mathbf{p}\mathbf{L}}}{p_0^2 - \mathbf{p}^2 - m_j^2 + i\epsilon} (1 + \gamma^5) \gamma_\nu u_{e,D}, \tag{3.61}
 \end{aligned}$$

where we have used the notation

$$E_S = E_{H,S} - E_{\text{He},S}, \quad E_D = E_{H,D} - E_{\text{He},D}, \tag{3.62}$$

and introduced the baseline vector $\mathbf{L} = \mathbf{x}_D - \mathbf{x}_S$. The quantity σ_p , which is given by

$$\frac{1}{\sigma_p^2} = \frac{1}{\sigma_{pS}^2} + \frac{1}{\sigma_{pD}^2} = \frac{1}{m_H \omega_{H,S} + m_{\text{He}} \omega_{\text{He},S}} + \frac{1}{m_H \omega_{H,D} + m_{\text{He}} \omega_{\text{He},D}}, \tag{3.63}$$

can be interpreted as an effective momentum uncertainty of the neutrino. In eq. (3.61), we have absorbed the normalisation factors from the wave functions (3.39) and those coming from the integrals over \mathbf{x}_1 and \mathbf{x}_2 into a constant

$$\mathcal{N} = \left(\frac{m_H \omega_{H,S}}{\pi} \right)^{\frac{3}{4}} \left(\frac{m_{He} \omega_{He,S}}{\pi} \right)^{\frac{3}{4}} \left(\frac{m_{He} \omega_{He,D}}{\pi} \right)^{\frac{3}{4}} \left(\frac{m_H \omega_{H,D}}{\pi} \right)^{\frac{3}{4}} \cdot \left(\frac{2\pi}{m_H \omega_{H,S} + m_{He} \omega_{He,S}} \right)^{\frac{3}{2}} \left(\frac{2\pi}{m_H \omega_{H,D} + m_{He} \omega_{He,D}} \right)^{\frac{3}{2}}. \quad (3.64)$$

We now use one of the δ -functions in eq. (3.61) to perform the integration over p_0 , the timelike component of the neutrino momentum, thus fixing p_0 at the value $p_0 = E_S = E_D$. To compute the remaining integral over the three-momentum \mathbf{p} , we use a theorem by Grimus and Stockinger [38], which states the following: Let $\psi(\mathbf{p})$ be a three times continuously differentiable function on \mathbb{R}^3 , such that ψ itself and all its first and second derivatives decrease at least as $1/|\mathbf{p}|^2$ for $|\mathbf{p}| \rightarrow \infty$. Then, for any real number $A > 0$,

$$\int d^3p \frac{\psi(\mathbf{p}) e^{i\mathbf{p}\mathbf{L}}}{A - \mathbf{p}^2 + i\epsilon} \xrightarrow{|\mathbf{L}| \rightarrow \infty} -\frac{2\pi^2}{L} \psi(\sqrt{A}\frac{\mathbf{L}}{L}) e^{i\sqrt{A}L} + \mathcal{O}(L^{-\frac{3}{2}}). \quad (3.65)$$

It is easy to check that the validity conditions are fulfilled in our case, so that, to leading order in $1/L$, we have

$$i\mathcal{A} = \frac{-i}{2L} \mathcal{N} \delta(E_S - E_D) \sum_j \exp \left[-\frac{E_S^2 - m_j^2}{2\sigma_p^2} \right] \mathcal{M}_S^\mu \mathcal{M}_D^{\nu*} |U_{ej}|^2 e^{i\sqrt{E_S^2 - m_j^2}L} \cdot \bar{u}_{e,S} \gamma_\mu (1 - \gamma^5) (\not{p}_j + m_j) (1 + \gamma^5) \gamma_\nu u_{e,D}. \quad (3.66)$$

Here, $p_j = (E_S, [E_S^2 - m_j^2]^{1/2} \mathbf{L}/L)$ is the on-shell 4-momentum of the neutrino mass eigenstate j . The Grimus-Stockinger theorem ensures that for $L \gg E_S^{-1}$, the intermediate-state neutrino is essentially on mass shell, and its momentum points from the neutrino source to the detector. In a Mössbauer neutrino experiment, $E_S \sim 18.6$ keV, so $L \gg 10^{-11}$ m is already sufficient to ensure on-shellness.

From (3.66), one can compute the transition probability \mathcal{P} by summing $|\mathcal{A}|^2$ over the spins of the final states and averaging over the initial-state spins. Note that no integration over final-state momenta is necessary because we consider transitions into discrete states. The transition rate is $\Gamma = d\mathcal{P}/dT$, where T is the total running time of the experiment. As we shall see below, in the case of inhomogeneous line broadening, $\mathcal{P} \propto T$ for large T , so that Γ is independent of T in that limit. The same is true for homogeneous line broadening, except for the special case of the line width being dominated by natural broadening; there, the dependence on T is more complicated (see sec. 3.5.4).

3.5.2 Inhomogeneous line broadening

Computation of Γ

As we have seen in sec. 3.1, one of the limiting factors in a Mössbauer neutrino experiment is inhomogeneous line broadening due to lattice defects, impurities, etc. Because of these effects, the ground state energies for different individual ^3H or ^3He atoms are slightly different. To account for this in our computation, we have to sum the probabilities of the process for all possible energies of the external particles, weighted with the probability distributions of these energies. In other words, we are going to fold the probability or total rate of the process with the energy distributions of the tritium and helium atoms in the source and detector, $\rho_{\text{He},S}(E_{\text{He},S})$, $\rho_{\text{H},D}(E_{\text{H},D})$, $\rho_{\text{H},S}(E_{\text{H},S})$ and $\rho_{\text{He},D}(E_{\text{He},D})$. We have to compute

$$\mathcal{P} = \int_0^\infty dE_{\text{H},S} dE_{\text{He},S} dE_{\text{He},D} dE_{\text{H},D} \cdot \rho_{\text{H},S}(E_{\text{H},S}) \rho_{\text{He},D}(E_{\text{He},D}) \rho_{\text{He},S}(E_{\text{He},S}) \rho_{\text{H},D}(E_{\text{H},D}) \overline{|\mathcal{A}|^2}, \quad (3.67)$$

where $\overline{|\mathcal{A}|^2}$ denotes the squared modulus of the amplitude, averaged over initial spins and summed over final spins. Using the standard trace techniques to evaluate these spin sums and neglecting the momenta of the non-relativistic external particles, one finds

$$\begin{aligned} \mathcal{P} = & T \frac{G_F^4 \cos^4 \theta_c}{\pi L^2} |\psi_e(R)|^4 E_{S,0}^2 (|M_V|^2 + g_A^2 |M_A|^2)^2 Y_S Y_D \kappa_S \kappa_D \\ & \cdot \int_0^\infty dE_{\text{H},S} dE_{\text{He},S} dE_{\text{He},D} dE_{\text{H},D} \rho_{\text{H},S}(E_{\text{H},S}) \rho_{\text{He},D}(E_{\text{He},D}) \rho_{\text{He},S}(E_{\text{He},S}) \rho_{\text{H},D}(E_{\text{H},D}) \\ & \cdot \delta(E_S - E_D) \sum_{j,k} |U_{ej}|^2 |U_{ek}|^2 \exp \left[-\frac{2E_S^2 - m_j^2 - m_k^2}{2\sigma_p^2} \right] e^{i(\sqrt{E_S^2 - m_j^2} - \sqrt{E_S^2 - m_k^2})L}, \end{aligned} \quad (3.68)$$

where Y_S and Y_D have been defined in eqs. (3.47) and (3.52), respectively. Note that we have rewritten the squared δ -function appearing in $\overline{|\mathcal{A}|^2}$ according to the standard formula [111, 112]

$$[\delta(E_S - E_D)]^2 \simeq \frac{1}{2\pi} \delta(E_S - E_D) \int_{-T/2}^{T/2} dt e^{i(E_S - E_D)t} = \frac{T}{2\pi} \delta(E_S - E_D), \quad (3.69)$$

which holds for $T \gg (E_S - E_D)^{-1}$.⁴ The overall process rate Γ is then obtained from eq. (3.68) by dividing by T . Using the definitions of Γ_0 and B_0 given in eqs. (3.45) and

⁴The expression $\delta(E_S - E_D)$ here should be understood as a δ -like function of very small width. For $|E_S - E_D| \sim 10^{-11}$ eV, the condition $T \gg (E_S - E_D)^{-1}$ would require $T \gg 10^{-4}$ s, which should be very well satisfied in any realistic experiment.

(3.51), one finds

$$\begin{aligned}
 \Gamma = & \frac{\Gamma_0 B_0}{4\pi L^2} Y_S Y_D \int_0^\infty dE_{H,S} dE_{He,S} dE_{He,D} dE_{H,D} \\
 & \cdot \delta(E_S - E_D) \rho_{H,S}(E_{H,S}) \rho_{He,D}(E_{He,D}) \rho_{He,S}(E_{He,S}) \rho_{H,D}(E_{H,D}) \\
 & \cdot \sum_{j,k} |U_{ej}|^2 |U_{ek}|^2 \exp \left[-\frac{2E_S^2 - m_j^2 - m_k^2}{2\sigma_p^2} \right] \exp \left[-i \frac{\Delta m_{jk}^2 L}{2E_S} \right]. \quad (3.70)
 \end{aligned}$$

In this expression, we have used the approximation of ultra-relativistic (or nearly mass-degenerate) neutrinos,

$$\frac{\Delta m_{jk}^2}{2E_S} \ll E_S, \quad (3.71)$$

so that the complex exponential reduces to the standard oscillation phase. Note that (3.71) is a good approximation only if the energy distributions $\rho_{A,B}$ are such that only values of E_S much larger than the neutrino mass contribute significantly to Γ . This is indeed the case, because inhomogeneous line broadening effects are very well described by [103]

$$\rho_{A,B}(E_{A,B}) = \frac{\gamma_{A,B}/2\pi}{(E_{A,B} - E_{A,B,0})^2 + \gamma_{A,B}^2/4}, \quad (3.72)$$

with $A = \{H, He\}$, $B = \{S, D\}$, $E_{A,B,0} = m_A + \frac{1}{2}\omega_{A,B}$, and $\gamma_S \sim \gamma_D \sim 10^{-11}$ eV (see sec. 3.1). We see that the widths of the $\rho_{A,B}$ are much smaller than their peak energies $E_{A,B,0}$, and that these peak energies, as well as the differences $E_{H,S,0} - E_{He,S,0}$ and $E_{H,S,0} - E_{He,S,0}$ that determine the neutrino energies are much larger than the neutrino masses.

After inserting (3.72) into (3.70), we simplify the energy integrals by making use of the identity

$$\begin{aligned}
 & \int_{-\infty}^\infty dE_a dE_b \frac{\gamma_a/2\pi}{(E_a - E_{a,0})^2 + \frac{\gamma_a^2}{4}} \frac{\gamma_b/2\pi}{(E_b - E_{b,0})^2 + \frac{\gamma_b^2}{4}} f(E_a - E_b) \\
 & = \int_{-\infty}^\infty d(E_a - E_b) \frac{(\gamma_a + \gamma_b)/2\pi}{[(E_a - E_b) - (E_{a,0} - E_{b,0})]^2 + \frac{(\gamma_a + \gamma_b)^2}{4}} f(E_a - E_b), \quad (3.73)
 \end{aligned}$$

which holds for any function $f(E)$ for which the integrals on the left and right hand sides exist. Applying this identity requires extending the domain of the $E_{A,B}$ integrals from the physical region $[\max_j(m_j), \infty)$ to the whole real axis, $(-\infty, \infty)$. This is possible due to the small widths of the Lorentzians $\rho_{A,B}(E_{A,B})$, which ensure that the unphysical contributions are strongly suppressed, the error introduced by the extension of the integration interval being of order $\gamma_{S(D)}/E_{S(D),0} \sim 10^{-15}$. Of the two energy integrals remaining

after (3.73) has been applied in (3.70), one is trivial due to the factor $\delta(E_S - E_D)$, so that the expression for Γ becomes

$$\Gamma = \frac{\Gamma_0 B_0}{4\pi L^2} Y_S Y_D \int_{-\infty}^{\infty} dE \frac{\gamma_S/2\pi}{(E - E_{S,0})^2 + \gamma_S^2/4} \frac{\gamma_D/2\pi}{(E - E_{D,0})^2 + \gamma_D^2/4} \cdot \sum_{j,k} |U_{ej}|^2 |U_{ek}|^2 \exp \left[-\frac{2E^2 - m_j^2 - m_k^2}{2\sigma_p^2} \right] \exp \left[-i \frac{\Delta m_{jk}^2 L}{2E} \right]. \quad (3.74)$$

In the next step, we pull the real exponential in the second line, which we will interpret below as the analogue of the Lamb-Mössbauer factor, out of the integral, replacing it by its value at

$$\bar{E} = (E_{S,0} + E_{D,0})/2. \quad (3.75)$$

This is justified by the observation that $\gamma_S, \gamma_D \sim 10^{-11}$ eV $\ll \sigma_p \sim 10$ keV, so that the exponent is nearly constant over the region where the integrand is sizeable. We are thus left with the task to compute the expression

$$I_{jk} \equiv \int_{-\infty}^{\infty} dE \frac{\gamma_S/2\pi}{(E - E_{S,0})^2 + \gamma_S^2/4} \frac{\gamma_D/2\pi}{(E - E_{D,0})^2 + \gamma_D^2/4} \exp \left[-i \frac{\Delta m_{jk}^2 L}{2E} \right], \quad (3.76)$$

which can be done by integration in the complex plane. The integrand has four complex poles, two above the real axis and two below, and an essential singularity at $E = 0$ (see fig. 3.2). To circumvent the essential singularity, we choose the integration contour as depicted in fig. 3.2: It consists of the real axis with a small interval $[-\varepsilon, \varepsilon]$ cut out, supplemented by a half-circle of radius ε around the point $E = 0$ and closed by a half-circle of large radius. The contribution of the small half-circle vanishes when its radius goes to zero provided that we avoid the point $E = 0$ from above when $\Delta m_{jk}^2 > 0$ and from below when $\Delta m_{jk}^2 < 0$. Thus, we close the integration contour in the upper half-plane for $\Delta m_{jk}^2 > 0$ and in the lower half-plane for $\Delta m_{jk}^2 < 0$. The contribution from the large half-circle vanishes when its radius tends to infinity because the product of two Lorentzians goes to zero as $|E|^{-4}$ for $|E| \rightarrow \infty$, while the exponential becomes unity in this limit. Application of the residue theorem yields now

$$\begin{aligned} I_{jk} &= \frac{1}{2\pi} \frac{1}{E_{S,0} - E_{D,0} \pm i \frac{\gamma_S - \gamma_D}{2}} \left\{ \frac{\gamma_D A_{jk}^{(S)}}{E_{S,0} - E_{D,0} \pm i \frac{\gamma_S + \gamma_D}{2}} + \frac{\gamma_S A_{jk}^{(D)}}{E_{S,0} - E_{D,0} \mp i \frac{\gamma_S + \gamma_D}{2}} \right\} \\ &= \frac{1}{2\pi} \frac{1}{(E_{S,0} - E_{D,0})^2 + \frac{(\gamma_S + \gamma_D)^2}{4}} \left\{ \frac{\gamma_S + \gamma_D}{2} (A_{jk}^{(S)} + A_{jk}^{(D)}) \right. \\ &\quad \left. - \frac{1}{2} (A_{jk}^{(S)} - A_{jk}^{(D)}) [(E_{S,0} - E_{D,0})(\gamma_S - \gamma_D) \pm i \frac{(\gamma_S + \gamma_D)^2}{2}] \right\}, \quad (3.77) \end{aligned}$$

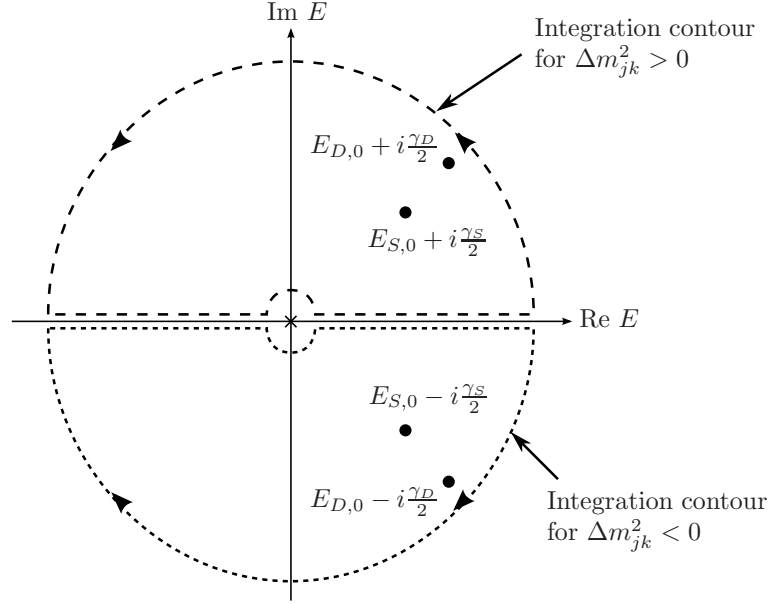


Figure 3.2: Integration contours in the complex E plane, used in the evaluation of (3.76).

where the upper (lower) signs correspond to $\Delta m_{jk}^2 > 0$ ($\Delta m_{jk}^2 < 0$). Here, we have introduced the abbreviation

$$\begin{aligned} A_{jk}^{(B)} &= \exp \left[-i \frac{\Delta m_{jk}^2}{2(E_{B,0} \pm i \frac{\gamma_B}{2})} L \right] \\ &\simeq \exp \left[-2\pi i \frac{L}{L_{B,jk}^{\text{osc}}} \right] \exp \left[-\frac{L}{L_{B,jk}^{\text{coh}}} \right], \end{aligned} \quad (3.78)$$

for $B = \{S, D\}$. The oscillation and coherence lengths are

$$L_{B,jk}^{\text{osc}} = \frac{4\pi E_{B,0}}{\Delta m_{jk}^2} \simeq \frac{4\pi \bar{E}}{\Delta m_{jk}^2} \quad \text{and} \quad L_{B,jk}^{\text{coh}} = \frac{4E_{B,0}^2}{\gamma_B |\Delta m_{jk}^2|} \simeq \frac{4\bar{E}^2}{\gamma_B |\Delta m_{jk}^2|}, \quad (3.79)$$

in analogy to eqs. (2.10) and (3.27). Note that the $A_{jk}^{(B)}$, as defined here, coincide with the quantities of the same name introduced in sec. 3.4.2 only after replacing $E_{B,0}$ by \bar{E} in the expressions for the oscillation and coherence lengths. However, the discrepancy of $\mathcal{O}(\Delta m_{jk}^2 (E_{S,0} - E_{D,0}) / \bar{E}^2)$ is smaller than the accuracy of the approximations made in sec. 3.4.2, and should therefore be neglected. Inserting I_{jk} from eq. (3.77) into eq. (3.74), we obtain our final expression for the decay rate in the case of inhomogeneous line

broadening,

$$\Gamma = \frac{\Gamma_0 B_0}{4\pi L^2} Y_S Y_D \frac{1}{2\pi} \sum_{j,k} |U_{ej}|^2 |U_{ek}|^2 \exp \left[-\frac{2\bar{E}^2 - m_j^2 - m_k^2}{2\sigma_p^2} \right] \frac{1}{(E_{S,0} - E_{D,0})^2 + \frac{(\gamma_S + \gamma_D)^2}{4}} \cdot \left\{ \frac{\gamma_S + \gamma_D}{2} (A_{jk}^{(S)} + A_{jk}^{(D)}) - \frac{1}{2} \frac{(A_{jk}^{(S)} - A_{jk}^{(D)}) [(E_{S,0} - E_{D,0})(\gamma_S - \gamma_D) \pm i \frac{(\gamma_S + \gamma_D)^2}{2}]}{E_{S,0} - E_{D,0} \pm i \frac{\gamma_S - \gamma_D}{2}} \right\}, \quad (3.80)$$

It is interesting to observe that this expression depends not on the individual energies and widths of all external states separately, but only on the resulting average neutrino energies $E_{B,0} = E_{H,B,0} - E_{He,B,0}$ and on $\gamma_B = \gamma_{H,B} + \gamma_{He,B}$.

Discussion

Eq. (3.80), contains an exponential suppression factor $\exp[-(2\bar{E}^2 - m_j^2 - m_k^2)/2\sigma_p^2]$, which is an analogue of the Lamb-Mössbauer factor (or recoil-free fraction) that we have already encountered in eqs. (3.47) and (3.52). For Mössbauer neutrinos, this factor depends on the neutrino masses, and is thus different for different mass eigenstates. If two mass eigenstates ν_j and ν_k do not satisfy the relation $|\Delta m_{jk}^2| \lesssim 2\sigma_p^2$, the emission and absorption of the lighter mass eigenstate is suppressed compared to the emission and absorption of the heavier one. This can be viewed as a reduced mixing of the two states, which in turn leads to a suppression of oscillations. To reflect this point directly in our formulas, we will henceforth write

$$\exp \left[-\frac{2\bar{E}^2 - m_j^2 - m_k^2}{2\sigma_p^2} \right] = \exp \left[-\frac{(p_{jk}^{\min})^2}{\sigma_p^2} \right] \exp \left[-\frac{|\Delta m_{jk}^2|}{2\sigma_p^2} \right], \quad (3.81)$$

where

$$(p_{jk}^{\min})^2 = \bar{E}^2 - \max(m_j^2, m_k^2), \quad (3.82)$$

i.e. p_{jk}^{\min} is the smaller of the two momenta of the mass eigenstates ν_j and ν_k . We will call the exponential depending on p_{jk}^{\min} a generalised Lamb-Mössbauer factor because it describes the suppression of the emission rate and the absorption cross section. The exponential depending on $|\Delta m_{jk}^2|$ can be viewed as a localisation term because the condition $|\Delta m_{jk}^2| \lesssim 2\sigma_p^2$ can be reformulated as $L_{jk}^{\text{osc}} \gtrsim 8\pi\bar{E}\sigma_x/\sigma_p$, where $\sigma_x = 1/2\sigma_p$. Since the generalised Lamb-Mössbauer factor (the first factor in eq. (3.81)) enforces $\bar{E} \lesssim \sigma_p$, this inequality is certainly fulfilled if $|L_{jk}^{\text{osc}}| \gtrsim 2\pi\sigma_x$ holds. The latter, stronger, localisation condition is the one obtained in other external wave packet calculations [16, 36, 39].

Another interesting observation that can be made from eq. (3.80) is that Γ factorises into the no-oscillation rate (3.57) computed at the resonance ($E_{S,0} = E_{D,0}$), multiplied with the transition probability (3.38) derived in the quantum mechanical formalism under the assumption of Lorentzian neutrino wave packets. This observation also provides the a posteriori justification for the assumptions and approximations we have made in sec. 3.4.

If the localisation condition $|\Delta m_{jk}^2| \ll 2\sigma_p^2$ is satisfied for all j and k , as it is expected to be the case in realistic experiments, one can pull the generalised Lamb-Mössbauer factor out of the sum in eq. (3.80) and replace the localisation exponentials by unity, which yields

$$\Gamma \simeq \frac{\Gamma_0 B_0}{4\pi L^2} Y_S Y_D \exp \left[-\frac{E_{S,0}^2 - m_0^2}{\sigma_p^2} \right] \sum_{j,k} |U_{ej}|^2 |U_{ek}|^2 I_{jk}. \quad (3.83)$$

Here, m_0 is an average neutrino mass and I_{jk} is given by eq. (3.77).

To describe experimental results, it is often sufficient to use a two-flavour version of eq. (3.80), parameterising oscillations in terms of only one mixing angle θ and one mass squared difference Δm^2 . In particular, a hypothetical Mössbauer neutrino experiment studying oscillations driven by θ_{13} would operate at a baseline $L \simeq 10$ m, at which the solar mass squared difference Δm_{21}^2 is inessential. For longer baselines around $L \simeq 300$ m, which are suitable for studying oscillations driven by Δm_{21}^2 and θ_{12} , the subdominant oscillations governed by Δm_{31}^2 and θ_{13} are in the averaging regime, leading to an effective two-flavour oscillation probability.

For $L \ll L^{\text{coh}}$, which is easily fulfilled in terrestrial experiments because $L_{S,D}^{\text{coh}} = 4\bar{E}^2/\Delta m^2 \gamma_{S,D} \sim 10^{13}$ km, the two-flavour approximation to (3.83) becomes

$$\begin{aligned} \Gamma \simeq \frac{\Gamma_0 B_0}{4\pi L^2} Y_S Y_D \exp \left[-\frac{E_{S,0}^2 - m_0^2}{\sigma_p^2} \right] & \frac{(\gamma_S + \gamma_D)/2\pi}{(E_{S,0} - E_{D,0})^2 + \frac{(\gamma_S + \gamma_D)^2}{4}} \\ & \cdot \left\{ 1 - \sin^2 2\theta \sin^2 \left(\pi \frac{L}{L^{\text{osc}}} \right) \right\}, \end{aligned} \quad (3.84)$$

which is just the no-oscillation rate (3.57), multiplied with the standard two-flavour $\bar{\nu}_e$ survival probability.

3.5.3 Homogeneous line broadening

In sec. 3.1 we have emphasised the importance of homogeneous line broadening, caused by fluctuating electromagnetic fields in the solid state crystal. By definition, it affects all emitters or absorbers equally, and thus cannot be implemented in our calculation of Γ by averaging the unperturbed transition probability over the energy distributions of the participating particles, as in the case of inhomogeneous broadening. Instead, one has to modify already the expression for the amplitude. Since the homogeneous broadening effects are stochastic, a proper averaging procedure, adequate to the broadening mechanism, has then to be employed. For the conventional Mössbauer effect with long-lived nuclei, a number of models of homogeneous broadening has been investigated in [93, 113–116]. In all the considered cases, a Lorentzian shape has been obtained for the emission and absorption lines. The same models can also be used for the neutrino Mössbauer effect; therefore, we expect that for most homogeneous broadening mechanisms, the form of the Mössbauer resonance will also be Lorentzian, i.e. the expression for the

transition rate will coincide with eq. (3.80). To show this explicitly, we will use the homogeneous line broadening model from ref. [114], and insert time-dependent modulation factors of the form

$$f_{A,B}(t) = \exp \left[-i \int_0^t dt' [E_{A,B}(t') - E_{A,B,0}] t' \right], \quad (3.85)$$

with $A = \text{H, He}$ and $B = S, D$, into the external particle wave functions. These modulation factors describe the integrated effect of small phase shifts, caused by fluctuations of the ${}^3\text{H}$ and ${}^3\text{He}$ energy levels $E_{A,B}$ around their mean values $E_{A,B,0}$. Note that this model describes only the contribution of solid-state effects to homogeneous line broadening, but not broadening due to the natural line width. The latter effect (which is completely negligible in the ${}^3\text{H} - {}^3\text{He}$ system) will be treated separately in the next section. The transition amplitude (3.59), including the modulation factors (3.85), is

$$\begin{aligned} i\mathcal{A} = & \int d^3x_1 dt_1 \int d^3x_2 dt_2 \left(\frac{m_{\text{H}}\omega_{\text{H},S}}{\pi} \right)^{\frac{3}{4}} \exp \left[-\frac{1}{2} m_{\text{H}}\omega_{\text{H},S} |\mathbf{x}_1 - \mathbf{x}_S|^2 \right] f_{\text{H},S}(t_1) e^{-iE_{\text{H},S}t_1} \\ & \cdot \left(\frac{m_{\text{He}}\omega_{\text{He},S}}{\pi} \right)^{\frac{3}{4}} \exp \left[-\frac{1}{2} m_{\text{He}}\omega_{\text{He},S} |\mathbf{x}_1 - \mathbf{x}_S|^2 \right] f_{\text{He},S}^*(t_1) e^{+iE_{\text{He},S}t_1} \\ & \cdot \left(\frac{m_{\text{He}}\omega_{\text{He},D}}{\pi} \right)^{\frac{3}{4}} \exp \left[-\frac{1}{2} m_{\text{He}}\omega_{\text{He},D} |\mathbf{x}_2 - \mathbf{x}_D|^2 \right] f_{\text{He},D}(t_2) e^{-iE_{\text{He},D}t_2} \\ & \cdot \left(\frac{m_{\text{H}}\omega_{\text{H},D}}{\pi} \right)^{\frac{3}{4}} \exp \left[-\frac{1}{2} m_{\text{H}}\omega_{\text{H},D} |\mathbf{x}_2 - \mathbf{x}_D|^2 \right] f_{\text{H},D}^*(t_2) e^{+iE_{\text{H},D}t_2} \\ & \cdot \sum_j \mathcal{M}_S^\mu \mathcal{M}_D^{\nu*} |U_{ej}|^2 \int \frac{d^4p}{(2\pi)^4} \exp [-ip_0(t_2 - t_1) + i\mathbf{p}(\mathbf{x}_2 - \mathbf{x}_1)] \\ & \cdot \bar{u}_{e,S} \gamma_\mu (1 - \gamma^5) \frac{i(\not{p} + m_j)}{p_0^2 - \mathbf{p}^2 - m_j^2 + i\epsilon} (1 + \gamma^5) \gamma_\nu u_{e,D}. \end{aligned} \quad (3.86)$$

with the notation from sec. 3.5.1. The spatial integrals in this expression are the same as those encountered in (3.59) and yield a factor $\exp[-\mathbf{p}^2/2\sigma_p^2] \exp[i\mathbf{p}\mathbf{L}]$, as in eq. (3.61). To evaluate the three-momentum integral over \mathbf{p} , we again employ the Grimus-Stockinger theorem and find

$$\begin{aligned} i\mathcal{A} = & \frac{-i}{8\pi^2 L} \mathcal{N} \sum_j \mathcal{M}_S^\mu \mathcal{M}_D^{\nu*} |U_{ej}|^2 \int_{-\infty}^{\infty} dt_1 dt_2 f_{\text{H},S}(t_1) f_{\text{He},S}^*(t_1) f_{\text{He},D}(t_2) f_{\text{H},D}^*(t_2) \\ & \cdot \int_{-\infty}^{\infty} dp_0 \exp \left[-\frac{p_0^2 - m_j^2}{2\sigma_p^2} \right] e^{i\sqrt{p_0^2 - m_j^2} L} e^{-i(E_{S,0} - p_0)t_1 + i(E_{D,0} - p_0)t_2} \\ & \cdot \bar{u}_{e,S} \gamma_\mu (1 - \gamma^5) (\not{p}_j + m_j) (1 + \gamma^5) \gamma_\nu u_{e,D} \end{aligned} \quad (3.87)$$

Since we do not know the exact form of the modulation factors $f_{A,B}(t)$, we cannot evaluate the time integrals at this stage. However, ultimately, we are only interested in

the transition rate Γ , which is proportional to $\langle \mathcal{A} \mathcal{A}^* \rangle$, the statistical average of $\mathcal{A} \mathcal{A}^*$ over all possible ${}^3\text{H}$ and ${}^3\text{He}$ states in the source and the detector. This expression can be simplified using statistical arguments. In particular, when evaluating it, we encounter the quantity

$$B_S(t_1, \tilde{t}_1) \equiv \left\langle f_{\text{H},S}(t_1) f_{\text{He},S}^*(t_1) f_{\text{H},S}^*(\tilde{t}_1) f_{\text{He},S}(\tilde{t}_1) \right\rangle = \left\langle \exp \left[-i \int_{\tilde{t}_1}^{t_1} dt' \Delta E_S(t') \right] \right\rangle, \quad (3.88)$$

and a similar term from the detector-related modulation factors. Here, t_1 and \tilde{t}_1 are the time variables appearing in the expressions for \mathcal{A} and \mathcal{A}^* , respectively. To shorten the notation, we have defined $\Delta E_S(t') \equiv E_S(t') - E_{S,0}(t') = [E_{\text{H},S}(t') - E_{\text{He},S}(t')] - [E_{\text{H},S,0}(t') - E_{\text{He},S,0}(t')]$, which gives the deviation of the energy of the neutrino emission line from its mean value at time t' . Following [114], we assume $\Delta E_S(t')$ to be a Gaussian random variable centred around zero:

$$\langle \Delta E_S(t') \rangle = 0. \quad (3.89)$$

Moreover, we assume fluctuations at different points in time to be uncorrelated (Markovian approximation), which implies

$$\langle \Delta E_S(t') \Delta E_S(t'') \rangle = \gamma_S \delta(t' - t''). \quad (3.90)$$

This is a good approximation if the correlation time of the fluctuations is much smaller than all other time scales appearing in the problem, in particular the tritium life time and the running time of the experiment. The constant γ_S will turn out to be the width of the neutrino emission line. Proceeding along the lines of refs. [114, 117], we expand (3.88) into a Taylor series and obtain

$$B_S(t_1, \tilde{t}_1) = \sum_{n=0}^{\infty} \frac{(-i)^n}{n!} \int_{\tilde{t}_1}^{t_1} dt^{(1)} \dots dt^{(n)} \langle \Delta E_S(t^{(1)}) \dots \Delta E_S(t^{(n)}) \rangle. \quad (3.91)$$

One can now use the assumption that $\Delta E_S(t^{(i)})$ is normally distributed around zero to show that the n -point correlation functions on the right hand side can, for even n , be rewritten by splitting them into products of two-point functions (which can be evaluated by using (3.90)) and summing over all $(n-1)(n-3)\dots 3 \cdot 1 = n!/2^{n/2}(n/2)!$ distinct combinations of such two-point functions. For odd n , the n -point correlation functions can be transformed into products of $(n-1)/2$ two-point functions and a one-point function, which is zero by virtue of eq. (3.89). Therefore, $B_S(t_1, \tilde{t}_1)$ takes the form

$$\begin{aligned} B_S(t_1, \tilde{t}_1) &= \sum_{n=0}^{\infty} \frac{(-\gamma_S/2)^n}{n!} \prod_{i=1}^n \int_{\tilde{t}_1}^{t_1} dt^{(2i)} dt^{(2i-1)} \delta(t^{(2i)} - t^{(2i-1)}) \\ &= \exp \left[-\frac{1}{2} \gamma_S |t_1 - \tilde{t}_1| \right]. \end{aligned} \quad (3.92)$$

Using

$$\begin{aligned} & \int_{-\infty}^{\infty} dt_1 d\tilde{t}_1 dt_2 d\tilde{t}_2 \exp \left[-\frac{1}{2}\gamma_S |t_1 - \tilde{t}_1| - i(E_{S,0} - p_0)t_1 + (E_{S,0} - \tilde{p}_0)\tilde{t}_1 \right] \\ & \quad \cdot \exp \left[-\frac{1}{2}\gamma_D |t_2 - \tilde{t}_2| + i(E_{D,0} - p_0)t_2 - (E_{D,0} - \tilde{p}_0)\tilde{t}_2 \right] \\ & = (2\pi)^4 [\delta(p_0 - \tilde{p}_0)]^2 \frac{\gamma_S/2\pi}{(E_{S,0} - p_0)^2 + \gamma_S^2/4} \frac{\gamma_D/2\pi}{(E_{D,0} - p_0)^2 + \gamma_D^2/4}, \end{aligned} \quad (3.93)$$

the expression for $\langle \mathcal{A}\mathcal{A}^* \rangle$ now becomes

$$\begin{aligned} \langle \mathcal{A}\mathcal{A}^* \rangle &= \frac{\mathcal{N}^2}{64\pi^4 L^2} \sum_{j,k} \mathcal{M}_S^\mu \mathcal{M}_D^{\nu*} \mathcal{M}_S^{\rho*} \mathcal{M}_D^\sigma |U_{ej}|^2 |U_{ek}|^2 \int_{-\infty}^{\infty} dp_0 d\tilde{p}_0 \exp \left[-\frac{2p_0^2 - m_j^2 - m_k^2}{2\sigma_p^2} \right] \\ & \quad \cdot (2\pi)^4 [\delta(p_0 - \tilde{p}_0)]^2 \frac{\gamma_S/2\pi}{(E_{S,0} - p_0)^2 + \gamma_S^2/4} \frac{\gamma_D/2\pi}{(E_{D,0} - p_0)^2 + \gamma_D^2/4} e^{i(\sqrt{p_0^2 - m_j^2} - \sqrt{p_0^2 - m_k^2})L} \\ & \quad \cdot \bar{u}_{e,S} \gamma_\mu (1 - \gamma^5)(\not{p}_j + m_j)(1 + \gamma^5)\gamma_\nu u_{e,D} \bar{u}_{e,D} \gamma_\sigma (1 - \gamma^5)(\not{p}_j + m_k)(1 + \gamma^5)\gamma_\rho u_{e,D}. \end{aligned} \quad (3.94)$$

We can rewrite the squared δ -function as $T/2\pi \cdot \delta(p_0 - \tilde{p}_0)$, and use the remaining δ -factor to evaluate the \tilde{p}_0 integral. We are left with the p_0 integration, which receives its main contribution from the region where $|E_S - p_0| \lesssim \gamma_S$ and $|E_D - p_0| \lesssim \gamma_D$ due to the Lorentzians on the right hand side of eq. (3.94). Since $\gamma_{S,D} \ll \sigma_p$ and $\gamma_{S,D} \ll \bar{E}$, the spinorial factors as well as the real exponential that will lead to the generalised Lamb-Mössbauer factor and to the localisation term are almost constant over this region and may be replaced by their values at $\bar{E} = (E_S + E_D)/2$. If we finally expand the oscillation phase in $\Delta m_{jk}^2/p_0^2$, we see that the p_0 integral is identical to the expression I_{jk} which we have encountered in the previous section (eqs. (3.76) and (3.77)). Therefore, the transition rate Γ for the case of homogeneous line broadening is

$$\begin{aligned} \Gamma &= \frac{\Gamma_0 B_0}{4\pi L^2} Y_S Y_D \frac{1}{2\pi} \sum_{j,k} |U_{ej}|^2 |U_{ek}|^2 \exp \left[-\frac{2\bar{E}^2 - m_j^2 - m_k^2}{2\sigma_p^2} \right] \frac{1}{(E_{S,0} - E_{D,0})^2 + \frac{(\gamma_S + \gamma_D)^2}{4}} \\ & \quad \cdot \left[\frac{\gamma_S + \gamma_D}{2} (A_{jk}^{(S)} + A_{jk}^{(D)}) - \frac{1}{2} \frac{(A_{jk}^{(S)} - A_{jk}^{(D)}) [(E_{S,0} - E_{D,0})(\gamma_S - \gamma_D) \pm i \frac{(\gamma_S + \gamma_D)^2}{2}]}{E_{S,0} - E_{D,0} \pm i \frac{\gamma_S - \gamma_D}{2}} \right], \end{aligned} \quad (3.95)$$

and thus coincides with the expression for the case of inhomogeneous line broadening, eq. (3.80), as expected.

3.5.4 Natural line broadening

Although the line width in the Mössbauer neutrino experiment proposed by Raghavan, using a tritium source and a ^3He absorber, will be limited by homogeneous and inhomogeneous solid state effects, it is interesting to ask how the situation would change in a

hypothetical experiment in which these effects could be eliminated so that line broadening would be dominated by the natural line width.

In such a case, we have to modify eq. (3.59) by including exponential decay factors in the ${}^3\text{H}$ wave functions. For tritium in the source, this factor has the form $\exp(-\gamma t/2)$, describing a decay starting at $t = 0$, the time at which the experiment starts.⁵ For the tritium which is produced in the detector, the decay factor is $\exp(-\gamma(T - t_2)/2)$, where t_2 is the time at which the neutrino is absorbed and T is the time at which the number of produced ${}^3\text{H}$ atoms is counted. Note that γ here is the total decay width of tritium, not the partial width for bound state beta decay. Since we are taking into account the finite lifetime of tritium, we also have to restrict the domain of all time integrations in \mathcal{A} to the interval $[0, T]$ instead of $(-\infty, \infty)$. We thus have to compute

$$\begin{aligned}
 i\mathcal{A} = & \int d^3x_1 \int_0^T dt_1 \int d^3x_2 \int_0^T dt_2 \left(\frac{m_{\text{H}\omega_{\text{H},S}}}{\pi} \right)^{\frac{3}{4}} \exp \left[-\frac{1}{2} m_{\text{H}\omega_{\text{H},S}} |\mathbf{x}_1 - \mathbf{x}_S|^2 \right] e^{-iE_{\text{H},S,0}t_1 - \frac{1}{2}\gamma t_1} \\
 & \cdot \left(\frac{m_{\text{He}\omega_{\text{He},S}}}{\pi} \right)^{\frac{3}{4}} \exp \left[-\frac{1}{2} m_{\text{He}\omega_{\text{He},S}} |\mathbf{x}_1 - \mathbf{x}_S|^2 \right] e^{+iE_{\text{He},S,0}t_1} \\
 & \cdot \left(\frac{m_{\text{He}\omega_{\text{He},D}}}{\pi} \right)^{\frac{3}{4}} \exp \left[-\frac{1}{2} m_{\text{He}\omega_{\text{He},D}} |\mathbf{x}_2 - \mathbf{x}_D|^2 \right] e^{-iE_{\text{He},D,0}t_2} \\
 & \cdot \left(\frac{m_{\text{H}\omega_{\text{H},D}}}{\pi} \right)^{\frac{3}{4}} \exp \left[-\frac{1}{2} m_{\text{H}\omega_{\text{H},D}} |\mathbf{x}_2 - \mathbf{x}_D|^2 \right] e^{+iE_{\text{H},D,0}t_2 - \frac{1}{2}\gamma(T-t_2)} \\
 & \cdot \sum_j \mathcal{M}_S^\mu \mathcal{M}_D^{\nu*} |U_{ej}|^2 \int \frac{d^4p}{(2\pi)^4} e^{-ip_0(t_2-t_1) + i\mathbf{p}(\mathbf{x}_2-\mathbf{x}_1)} \\
 & \cdot \bar{u}_{e,S} \gamma_\mu (1 - \gamma^5) \frac{i(\not{p} + m_j)}{p_0^2 - \mathbf{p}^2 - m_j^2 + i\epsilon} (1 + \gamma^5) \gamma_\nu u_{e,D}.
 \end{aligned} \tag{3.96}$$

The arguments leading to this expression for \mathcal{A} can also be put into a rigorous form by using the Weisskopf-Wigner approximation [39, 119–121]. We will show this in appendix A.

Computation of Γ

In the same way as before, we can evaluate the spatial and three-momentum integrals in eq. (3.96). The time integrals can also be evaluated straightforwardly, and give approximate energy conserving factors for the production and detection vertices. Energy conservation is not exact here because of the non-zero width of the tritium states and

⁵It is assumed that, at $t = 0$, the number of ${}^3\text{H}$ atoms in the source is known. In reality, this is true to a good approximation if the source is fabricated in a time interval that is short compared to the tritium lifetime $\gamma^{-1} = 17.79$ years [118].

because of the finite measurement time T . We find

$$\begin{aligned}
 i\mathcal{A} = & \frac{-i}{8\pi^2 L} \mathcal{N} \sum_j \mathcal{M}_S^\mu \mathcal{M}_D^{\nu*} |U_{ej}|^2 \int_{-\infty}^{\infty} dp_0 \bar{u}_{e,S} \gamma_\mu (1 - \gamma^5) (\not{p}_j + m_j) (1 + \gamma^5) \gamma_\nu u_{e,D} \\
 & \cdot e^{-\gamma T/2} \frac{e^{-i(E_S - p_0)T - \gamma T/2} - 1}{p_0 - E_S + i\gamma/2} \frac{e^{i(E_D - p_0)T + \gamma T/2} - 1}{p_0 - E_D + i\gamma/2} \exp \left[-\frac{p_0^2 - m_j^2}{2\sigma_p^2} \right] e^{i\sqrt{p_0^2 - m_j^2} L},
 \end{aligned} \tag{3.97}$$

where the 4-vector p_j is defined as $p_j = (p_0, (p_0^2 - m_j^2)^{1/2} \mathbf{L}/L)$. The spinorial factors and the exponential depending on σ_p^2 can be approximated by their values $\bar{E} = (E_S + E_D)/2$ because $\gamma \ll \sigma_p$ ensures that they are almost constant in the region $|p_0 - E_S| \lesssim \gamma$ and $|p_0 - E_D| \lesssim \gamma$, from which the main contribution to the integral comes. The fact that this region is very narrow also allows us to expand the oscillation phase around \bar{E} ,

$$i\sqrt{p_0^2 - m_j^2} L \simeq i\sqrt{\bar{E}^2 - m_j^2} L + i\frac{L}{v_j} (p_0 - \bar{E}). \tag{3.98}$$

Here, an effective neutrino velocity has been defined by

$$v_j = (\bar{E}^2 - m_j^2)^{1/2} / \bar{E}. \tag{3.99}$$

The integral over p_0 can be evaluated by complex contour integration. The denominator has poles at $p_0 = E_S - i\gamma/2$ and $p_0 = E_D - i\gamma/2$ (see fig. 3.3), while the p_0 -dependent terms in the numerator are

$$\begin{aligned}
 & \left(e^{-i(E_S - p_0)T - \gamma T/2} - 1 \right) \left(e^{i(E_D - p_0)T + \gamma T/2} - 1 \right) e^{i(p_0 - \bar{E}) \frac{L}{v_j}} \\
 & = \underbrace{e^{ip_0 \frac{L}{v_j}} e^{-i(E_S - E_D)T - \bar{E} \frac{L}{v_j}}}_{(A)} - \underbrace{e^{ip_0(T + \frac{L}{v_j})} e^{-iE_S T - i\bar{E} \frac{L}{v_j} - \gamma T/2}}_{(B)} \\
 & \quad - \underbrace{e^{-ip_0(T - \frac{L}{v_j})} e^{iE_D T - i\bar{E} \frac{L}{v_j} + \gamma T/2}}_{(C)} + \underbrace{e^{i\frac{L}{v_j} p_0} e^{-i\bar{E} \frac{L}{v_j}}}_{(D)}.
 \end{aligned} \tag{3.100}$$

We close the integration contour by adding to the real axis a half-circle of infinite radius. For the terms labelled (A), (B) and (D), this half-circle has to lie in the upper half-plane, while for (C) it has to lie in the upper half-plane for $T < L/v_j$ and in the lower half-plane for $T > L/v_j$. As the integrand is holomorphic for $\text{Im}(p_0) \geq 0$, the integral can be non-zero only in this last case. The residue theorem then yields

$$\begin{aligned}
 i\mathcal{A} = & \frac{\mathcal{N}}{4\pi L} \sum_j \theta(T - L/v_j) \mathcal{M}_S^\mu \mathcal{M}_D^{\nu*} |U_{ej}|^2 \bar{u}_{e,S} \gamma_\mu (1 - \gamma^5) (\not{p}_j + m_j) (1 + \gamma^5) \gamma_\nu u_{e,D} \\
 & \cdot \exp \left[-\frac{\bar{E}^2 - m_j^2}{2\sigma_p^2} \right] e^{i\sqrt{\bar{E}^2 - m_j^2} L} \frac{e^{-\frac{1}{2}\gamma(T - \frac{L}{v_j})} e^{-\frac{i}{2}(E_S - E_D)T}}{E_S - E_D} \\
 & \cdot \left\{ \exp \left[-\frac{i}{2}(E_S - E_D)(T - \frac{L}{v_j}) \right] - \exp \left[\frac{i}{2}(E_S - E_D)(T - \frac{L}{v_j}) \right] \right\},
 \end{aligned} \tag{3.101}$$

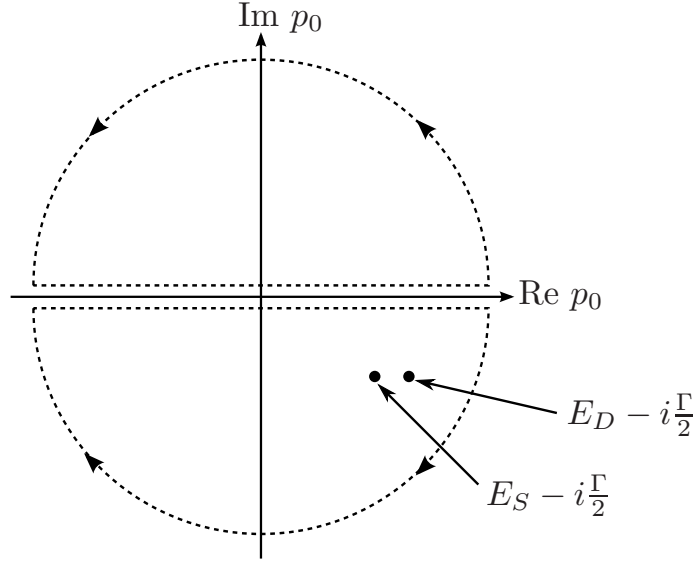


Figure 3.3: Integration contours in the complex p_0 plane, used in the evaluation of (3.97).

where now $\bar{p}_j = (\bar{E}, (\bar{E}^2 - m_j^2)^{1/2} \mathbf{L}/L)$, and $\theta(x)$ is the Heaviside step function. The total probability for finding a tritium atom at the lattice site \mathbf{x}_D in the detector after a time T is

$$\mathcal{P} = \overline{|\mathcal{A}|^2}, \quad (3.102)$$

where the bar indicates the average over initial spins and the sum over final spins. Apart from these spin sums, no integration over the energy distributions of the initial and final state nuclei is necessary as long as only natural line broadening is taken into account, because we are dealing with transitions between discrete energy eigenstates. A straightforward evaluation of (3.102) yields

$$\begin{aligned} \mathcal{P} = & \frac{\Gamma_0 B_0}{4\pi L^2} Y_S Y_D \frac{2}{\pi} \sum_{j,k} \theta(T_{jk}) |U_{ej}|^2 |U_{ek}|^2 \\ & \cdot \exp \left[-\frac{(p_{jk}^{\min})^2}{\sigma_p^2} \right] \exp \left[-\frac{|\Delta m_{jk}^2|}{2\sigma_p^2} \right] e^{i(\sqrt{\bar{E}^2 - m_j^2} - \sqrt{\bar{E}^2 - m_k^2})L} \\ & \cdot e^{-\gamma T_{jk}} e^{-L/L_{jk}^{\text{coh}}} \frac{\sin \left[\frac{1}{2}(E_{S,0} - E_{D,0})(T - \frac{L}{v_j}) \right] \sin \left[\frac{1}{2}(E_{S,0} - E_{D,0})(T - \frac{L}{v_k}) \right]}{(E_{S,0} - E_{D,0})^2}. \end{aligned} \quad (3.103)$$

Note that we have parameterised the generalised Lamb-Mössbauer factor and the localisation exponential according to eq. (3.81). Moreover, we have defined the quantity

$$T_{jk} = \min \left(T - \frac{L}{v_j}, T - \frac{L}{v_k} \right), \quad (3.104)$$

corresponding to the total running time of the experiment, minus the time of flight of the heavier of the two mass eigenstates ν_j and ν_k . The appearance of the Heaviside factor $\theta(T_{jk})$ in eq. (3.103) is related to the nonzero neutrino time of flight between the source and the detector and to the fact that the interference between the j th and k th mass components leading to oscillations is only possible if both have already arrived at the detector. As in secs. 3.5.2 and 3.5.3, decoherence exponentials appear containing the characteristic coherence lengths

$$\frac{1}{L_{jk}^{\text{coh}}} = \gamma \left| \frac{1}{v_j} - \frac{1}{v_k} \right|. \quad (3.105)$$

In the approximation of ultra-relativistic (or nearly mass-degenerate) neutrinos, this becomes

$$L_{jk}^{\text{coh}} = \frac{4\bar{E}^2}{\gamma |\Delta m_{jk}^2|}, \quad (3.106)$$

and is thus analogous to eqs. (3.27) and (3.79).

Discussion

While the first two lines of eq. (3.103) contain the standard oscillation terms, the generalised Lamb-Mössbauer factor and some numerical factors, the expression in the third line is unique to Mössbauer neutrinos in the regime of natural linewidth dominance. To interpret this part of the probability, it is helpful to consider the approximation of massless neutrinos. In this limit, $v_j = 1$ for all j , and thus $L_{jk}^{\text{coh}} = \infty$. If we neglect the time of flight L/v_j compared to the total running time of the experiment T , we find that \mathcal{P} is proportional to

$$e^{-\gamma T} \frac{\sin^2[(E_{S,0} - E_{D,0})\frac{T}{2}]}{(E_{S,0} - E_{D,0})^2}. \quad (3.107)$$

The factor $\exp(-\gamma t)$ accounts for the depletion of ${}^3\text{H}$ in the source and for the decay of the produced ${}^3\text{H}$ in the detector.

It is easy to see that for $\gamma = 0$ and $T \rightarrow \infty$, eq. (3.70) is recovered, except for the omitted folding with the energy distributions of the initial and final state nuclei. In particular, we see that, in this limit, due to the emerging δ -function, the Mössbauer effect can only occur if the resonance energies $E_{S,0}$ and $E_{D,0}$ match exactly. For finite T , in contrast, the matching need not be exact because then, the time-energy uncertainty

relation permits a certain detuning as long as $|E_{S,0} - E_{D,0}| \lesssim 1/T$. Note that the allowed detuning of $E_{S,0}$ and $E_{D,0}$ does *not* depend on γ , but only on T . This means that the natural linewidth is not a fundamental limitation to the energy resolution of a Mössbauer neutrino experiment. Even though this observation may seem counterintuitive, there is a well-known, and experimentally verified, analogue to this in quantum optics [122], called subnatural spectroscopy. Consider an experiment, in which an atom is instantaneously excited from its ground state into an unstable state $|b\rangle$ by a strong laser pulse at $t = 0$. Moreover, the atom is continuously exposed to electromagnetic radiation with a photon energy E , which can eventually excite it further into another unstable state $|a\rangle$. If, after a time τ , the number of atoms in state $|a\rangle$ is measured, it turns out that the result is proportional to $1/[(E - \Delta E)^2 + (\gamma_a - \gamma_b)^2/4]$ rather than to the naively expected $1/[(E - \Delta E)^2 + (\gamma_a + \gamma_b)^2/4]$. Here ΔE is the energy difference between the two excited states, and γ_a, γ_b are their respective widths. In our case, the state $|b\rangle$ corresponds to a ${}^3\text{H}$ atom in the source and a ${}^3\text{He}$ atom in the detector, while $|a\rangle$ corresponds to a ${}^3\text{He}$ atom in the source and a ${}^3\text{H}$ atom in the detector. The initial excitation of the state $|b\rangle$ corresponds to producing the tritium source and starting the Mössbauer neutrino experiment, and the transition from $|b\rangle$ to $|a\rangle$ corresponds to the production, propagation and absorption of a neutrino. Since the tritium lifetime in the source and detector is the same, $\gamma_a - \gamma_b$ vanishes for Mössbauer neutrinos⁶, so that γ does not have any impact on the achievable energy resolution, in accordance with eq. (3.107). The analogy with subnatural spectroscopy shows that this is only true because the source is produced at one specific point in time, namely $t = 0$ (or, rather, during a time interval that is short compared to the tritium lifetime). If tritium were continuously replenished in the source, an additional integration of \mathcal{P} over the production time would be required, and this would yield proportionality to $1/[(E_{S,0} - E_{D,0})^2 + \gamma^2]$, in full analogy with the corresponding result in quantum optics [122].

If the resonance condition enforced by eq. (3.107) is well fulfilled, i.e. $|E_{S,0} - E_{D,0}| \ll 1/T$, the T -dependence of \mathcal{P} can be approximated by

$$T^2 e^{-\gamma T} / 4. \quad (3.108)$$

This behaviour can be understood already from a classical argument. The number of ${}^3\text{H}$ atoms in the detector N_D obeys the differential equation

$$\dot{N}_D = -\dot{N}_S N_0 P_{ee} \frac{\sigma(T)}{4\pi L^2} - \gamma N_D, \quad (3.109)$$

where, N_S is the number of ${}^3\text{H}$ atoms in the source and N_0 is the number of ${}^3\text{He}$ atoms in the detector, which we treat as constant (this is justified if the number of ${}^3\text{H}$ atoms produced in the detector is small compared to the initial number of ${}^3\text{He}$). By P_{ee} , we denote the $\bar{\nu}_e$ survival probability, and $\sigma(T)$ is the absorption cross section. The

⁶Tiny deviations of $\gamma_a - \gamma_b$ from zero are possible because the different ${}^3\text{H}$ and ${}^3\text{He}$ abundances in the source and the detector influence electromagnetic interactions in the respective crystals differently, and may thus lead to small differences between γ_a and γ_b .

latter depends on T because, due to the Heisenberg principle, the accuracy to which the resonance condition has to be fulfilled is given by T^{-1} . If we describe this limitation by assuming the emission and absorption lines to be Lorentzians of width $1/T$, we find that for $|E_{S,0} - E_{D,0}| \ll T^{-1}$ the overlap integral is proportional to T , so that we can write $\sigma = s_0 T$, with s_0 a constant. Using furthermore the fact that $N_S = N_{S,0} \exp(-\gamma T)$, the solution of eq. (3.109) is found as

$$N_D = \frac{N_{S,0} N_0 \gamma P_{ee} s_0}{8\pi L^2} T^2 e^{-\gamma T}. \quad (3.110)$$

Thus, the classical argument predicts for N_D precisely the T -dependence given by (3.108).

3.6 Discussion

To summarise our results on oscillations of Mössbauer neutrinos, let us compare the different approaches we have discussed. In sec. 3.3, we have argued that the equal energy approximation used in the plane wave (or “textbook”) derivation of the oscillation formula (see sec. 2.1.2), is justified for Mössbauer neutrinos, even though it is inconsistent for most other neutrino sources. The survival probability of Mössbauer $\bar{\nu}_e$ is thus approximately given by eq. (2.9). If the neutrino is more realistically treated as a wave packet, this expression gets modified into (3.31) for Gaussian wave packets and into (3.38) for Lorentzian wave packets. These formulas still have the disadvantage that a priori assumptions on the neutrino energies and momenta, as well as on the shape and width of the wave packets had to be made in their derivation. For example, we had to assume the central energies of the wave packets corresponding to different neutrino mass eigenstates to be equal in a Mössbauer neutrino experiment. Moreover, eqs. (3.31) and (3.38) had to be normalised by hand. These problems are circumvented in the quantum field theoretical formalism, which we have used in sec. 3.5 to derive expressions for the combined rate of Mössbauer neutrino production, propagation and absorption. In the case of an experiment dominated by inhomogeneous line broadening, we have obtained eq. (3.80), and we have shown in eq. (3.95), that this expression remains valid also if homogeneous broadening (other than the natural line width) is dominant. For practical purposes, it will usually be sufficient to use the approximate formula (3.84) instead of (3.80). In the hypothetical case of line broadening dominated by the natural line width, we have found that the probability for finding a tritium atom at a specific lattice site in the detector crystal after a running time T , is given by (3.103). In all our QFT derivations, the kinematical properties of the neutrino were automatically determined from the wave functions of the emitting and absorbing nuclei, for which we have used a well-established approximation from the theory of the classical Mössbauer effect.

The most important features of the expressions obtained in different approaches, namely the oscillation, coherence, localisation and resonance terms, are summarised in table 3.1. We see that, in all cases, Mössbauer neutrinos are predicted to oscillate. However, the oscillation terms from eqs. (3.38) (QM for Lorentzian wave packets) and

(3.80) (QFT for non-natural line broadening) match only if one assumes the Mössbauer resonance condition $E_{S,0} = E_{D,0} = \bar{E}$ to be well fulfilled. Even though this mismatch between QM and QFT is irrelevant for practical purposes, it shows that the QM formalism is imperfect.

Coherence terms are obtained in all approaches except the plane wave formalism, but their precise form is not always the same: In QFT, the exponent is linear in L/L^{coh} , while in QM, it is linear if the neutrino is described by a Lorentzian wave packet, and quadratic in the Gaussian case (the linear form of the decoherence exponents in the case of a Lorentzian neutrino energy distribution has been previously pointed out in [39]). This indicates that, for Mössbauer neutrinos, the correct QM limit of QFT is the Lorentzian wave packet formalism. Indeed, the coherence terms from eqs. (3.38) and (3.80) agree within the approximations made in the QM derivation. The predicted coherence lengths are determined by the momentum space width of the neutrino wave packets in QM, and by the energy uncertainties of the source and the detector in QFT. In realistic terrestrial experiments, the coherence lengths are always far too large to be of any practical relevance.

A localisation condition for Mössbauer neutrinos is found only in QFT, where it emerges as a result of the slightly different Lamb-Mössbauer terms (recoil-free fractions) for different mass eigenstates, which can be viewed as a suppression of neutrino mixing (cf. eq. (3.81)). For the realistic estimate $\sigma_p \gtrsim 2 \cdot 10^3$ eV (cf. sec. 3.3), this suppression is not effective. We have seen in eq. (3.30) that, for conventional neutrino sources, also the QM formalism yields a localisation term. However, the discussion below (3.29) shows that the physical origin of this term is different from the origin of the Lamb-Mössbauer term. It suppresses oscillations if conservation of the average momentum cannot be fulfilled for all mass eigenstates simultaneously, or if the oscillation phase changes significantly over timescales comparable to the duration of the detection process. We have not found a localisation term in eq. (3.38) because we have used $\xi_S = \xi_D \simeq 0$ there. It is important to keep in mind that this relation is an assumption in our QM computation, while in QFT, it emerges naturally.

The QM formalism using Lorentzian wave packets, as well as the QFT approach, are able to reproduce the Breit-Wigner shaped Mössbauer resonance factor expected for realistic experiments. In the hypothetical case of an experiment dominated by natural line broadening, however, we have found this factor to be absent. Instead, the required overlap between the emission and absorption lines is in this case determined by the inverse of the running time of the experiment, i.e. by the time-energy uncertainty relation. We have interpreted the absence of a Breit-Wigner factor in the case of natural line width dominance by drawing an analogy to subnatural spectroscopy in quantum optics.

Let us finally stress that the QFT results including the production and detection processes do not only give reliable predictions for the oscillation phenomenology, but can also be used to derive approximate estimates for the total event rate expected in a Mössbauer neutrino experiment. In principal, similar estimates can also be obtained by combining the no-oscillation rate derived in the beginning of sec. 3.5 with the flavour transition probability derived in the quantum mechanical wave packet approach. Even

	Equation	Oscillation	Coherence	Localisation	Resonance
Plane waves	(2.9)	$\exp\left[-i\frac{\Delta m_{jk}^2 L}{2E}\right]$			
QM (Gaussian)	(3.31)	$\exp\left[-i\frac{\Delta m_{jk}^2 L}{2E}\right]$	$\exp\left[-\left(\frac{\tilde{\gamma}\Delta m_{jk}^2 L}{2\sqrt{2}\bar{E}^2}\right)^2\right]$		$\exp\left[-\frac{(E_{S,0}-E_{D,0})^2}{2(\gamma_S^2+\gamma_D^2)}\right]$
QM (Lorentzian)	(3.38)	$\exp\left[-i\frac{\Delta m_{jk}^2 L}{2E}\right]$	$\exp\left[-\frac{\gamma_{S,D} \Delta m_{jk}^2 L}{4E^2}\right]$		$\frac{(\gamma_S+\gamma_D)/2\pi}{(E_{S,0}-E_{D,0})^2+(\gamma_S+\gamma_D)^2/4}$
QFT (inhom. broadening)	(3.80)	$\exp\left[-i\frac{\Delta m_{jk}^2 L}{2E_{S,D,0}}\right]$	$\exp\left[-\frac{\gamma_{S,D} \Delta m_{jk}^2 L}{4E_{S,D,0}^2}\right]$	$\exp\left[-\frac{ \Delta m_{jk}^2 }{2\sigma_p^2}\right]$	$\frac{(\gamma_S+\gamma_D)/2\pi}{(E_{S,0}-E_{D,0})^2+(\gamma_S+\gamma_D)^2/4}$
QFT (hom. broadening)	(3.95)	$\exp\left[-i\frac{\Delta m_{jk}^2 L}{2E_{S,D,0}}\right]$	$\exp\left[-\frac{\gamma_{S,D} \Delta m_{jk}^2 L}{4E_{S,D,0}^2}\right]$	$\exp\left[-\frac{ \Delta m_{jk}^2 }{2\sigma_p^2}\right]$	$\frac{(\gamma_S+\gamma_D)/2\pi}{(E_{S,0}-E_{D,0})^2+(\gamma_S+\gamma_D)^2/4}$
QFT (natural broadening)	(3.103)	$\exp\left[-i\frac{\Delta m_{jk}^2 L}{2E}\right]$	$\exp\left[-\frac{\gamma \Delta m_{jk}^2 L}{4E^2}\right]$	$\exp\left[-\frac{ \Delta m_{jk}^2 }{2\sigma_p^2}\right]$	$\frac{\sin^2(E_{S,0}-E_{D,0})T/2}{(E_{S,0}-E_{D,0})^2}$

Table 3.1: The oscillation, coherence, localisation and resonance terms obtained for Mössbauer neutrinos in the plane wave approach (sec. 3.3), in the quantum mechanical calculations for Gaussian and Lorentzian neutrino wave packets (sec. 3.4), and in the QFT formalism for inhomogeneous (sec. 3.5.2), homogeneous (sec. 3.5.3) and natural line broadening (sec. 3.5.4), respectively. The notation is as follows: Δm_{jk}^2 are the neutrino mass squared differences, L is the baseline, $E_{S,0}$ and $E_{D,0}$ are the resonance energies of the source and the detector, $\bar{E} = (E_{S,0} + E_{D,0})/2$ is the average of the resonance energies, γ_S and γ_D are the widths of the emission and absorption lines, the quantity $\tilde{\gamma}$ appearing in the second line is an effective total line width defined by $\tilde{\gamma}^{-2} = \gamma_S^{-2} + \gamma_D^{-2}$, γ is the natural line width of ${}^3\text{H}$ and σ_p is the effective momentum uncertainty defined in eq. (3.63).

though eqs. (3.38) and (3.80) show that such a factorised treatment is possible, great care has to be taken that the assumptions made in the QFT treatment of the production and detection processes, and those made in the QM treatment of the propagation, are consistent. Moreover, it has to be ensured that the transition probability obtained in QM is properly normalised by hand since the appropriate prefactor does not emerge automatically.

3.7 Mössbauer neutrinos and the time-energy uncertainty relation

In the preceding sections, we have studied in detail the conditions under which Mössbauer can oscillate. We have found that all mechanisms that might suppress oscillations are not effective in realistic experiments. In particular, decoherence and localisation conditions are well fulfilled in all imaginable scenarios.

Our conclusion has been supported by Cohen, Glashow and Ligeti [123], but disagrees with that of Bilenky, Feilitzsch and Potzel. In [94–97], these authors argue that the question whether Mössbauer neutrinos do oscillate should depend on whether neutrino oscillation are a stationary or a non-stationary phenomenon. Here, stationarity means that the neutrino flavour is different at different points in space, but does not evolve in time. In contrast, non-stationarity means that the neutrino flavour changes also in time. Bilenky et al. consider these two approaches to be fundamentally different mechanisms that can only be distinguished by an experiment. They argue that, for non-stationary evolution, the time-energy uncertainty relation forbids oscillations of Mössbauer neutrinos. In the stationary case, they consider the time-energy uncertainty relation to be not applicable.

We disagree with this point of view [29]. The time-energy uncertainty relation is based on fundamental principles of quantum theory, and must therefore be applicable to all physical systems. As for the distinction between evolution in time and evolution in space, we do not regard these options as different mechanisms, but rather as different approximations to the true behaviour of oscillating neutrinos. This true behaviour must be fully derivable within the standard quantum field theory for any given experiment.

In the following, we will first discuss the arguments from [96] concerning the time-energy uncertainty relation, because we find them very instructive, even though we consider the way in which they are applied in [96] to be erroneous. We will then explain why we come to the conclusion that time-energy uncertainty does not prevent oscillations of Mössbauer neutrinos.

The authors of [96] base their arguments on the Mandelstam-Tamm relation (see, for example, ref. [124]):

$$\Delta E \Delta O \geq \frac{1}{2} \left| \frac{d}{dt} \overline{O}(t) \right|, \quad (3.111)$$

which is a consequence of the Cauchy-Schwarz inequality. Here, O is an arbitrary quantum mechanical operator, and $\overline{O}(t) = \langle \psi(t) | O | \psi(t) \rangle$ is its expectation value in a QFT Fock state $|\psi(t)\rangle$. Bilenky et al. choose O as the projection operator onto the neutrino flavour ν_α , i.e. $O \equiv |\nu_\alpha\rangle\langle\nu_\alpha|$. With this choice, they derive the uncertainty relation

$$\Delta E \geq \frac{1}{2} \frac{|\frac{d}{dt}P(t)|}{\sqrt{P(t) - P^2(t)}}. \quad (3.112)$$

where $P(t) = |\langle \nu_\alpha | \Psi(t) \rangle|^2$, with $\Psi(t)$ being a neutrino state. In [96], $P(t)$ is interpreted as the ν_α survival probability, and, using this interpretation, it is then argued that eq. (3.112) cannot be fulfilled for the tiny energy uncertainty $\Delta E \sim 10^{-11}$ of Mössbauer neutrinos.

In our opinion, the interpretation of $P(t)$ as the ν_α survival probability is incorrect. It would be correct if the neutrino flavour were really measured by an operator of the form $|\nu_\alpha\rangle\langle\nu_\alpha|$, acting only in flavour space and leaving the spatial degrees of freedom of the neutrino untouched. A realistic neutrino detector, however, is spatially localised, so its action must depend on the coordinate. An idealised pointlike detector localised at \mathbf{x} would be described by the operator $O_{\mathbf{x}} \equiv |\nu_\alpha\rangle\langle\nu_\alpha| \otimes |\mathbf{x}\rangle\langle\mathbf{x}|$. Then, eq. (3.112) would turn into

$$\Delta E \geq \frac{1}{2} \frac{|\frac{d}{dt}P(\mathbf{x}, t)|}{\sqrt{P(\mathbf{x}, t) - P^2(\mathbf{x}, t)}}, \quad (3.113)$$

with $P(\mathbf{x}, t) = |\langle \mathbf{x} | \nu_\alpha | \Psi(t) \rangle|^2$ now being indeed a survival probability in the conventional sense. Following [32] and our derivation from sec. 3.4, we write $P(\mathbf{x}, t)$ as⁷

$$P(\mathbf{x}, t) = \sum_{j,k} |U_{\alpha j}|^2 |U_{\alpha k}|^2 e^{-2i\phi(\mathbf{x}, t)} g(\mathbf{x} - \mathbf{v}_j t) g(\mathbf{x} - \mathbf{v}_k t)^*, \quad (3.114)$$

Here, ϕ is the oscillation phase, given by

$$2\phi(\mathbf{x}, t) = (E_j - E_k)t - (\mathbf{p}_j - \mathbf{p}_k)\mathbf{x}, \quad (3.115)$$

and $g(\mathbf{x} - \mathbf{v}_j t)$ are the wave packet shape factors depending on the group velocities v_j of the neutrino mass eigenstates and on the width and shape of the wave packets. They contain the decoherence and localisation terms, but since we have shown that these are irrelevant in realistic Mössbauer neutrino experiments, we will set $g(\mathbf{x} - \mathbf{v}_j t)$ equal to unity in the following. Then, the probability $P(\mathbf{x}, t)$ takes the standard form

$$P(\mathbf{x}, t) = 1 - \sin^2 2\theta \sin^2 \phi(\mathbf{x}, t), \quad (3.116)$$

where we have additionally gone to the two-flavour approximation, and have introduced the two-flavour mixing angle θ . Substituting eq. (3.116) into eq. (3.113), one readily finds

$$\Delta E \geq |E_1 - E_2| \frac{\sin 2\theta \cos \phi(\mathbf{x}, t)}{\sqrt{1 - \sin^2 2\theta \sin^2 \phi(\mathbf{x}, t)}}. \quad (3.117)$$

⁷This equation is valid in the limit of no wave packet spreading, which is a very good approximation for neutrinos.

It is sufficient to consider the case $\sin^2 2\theta = 1$, because the right hand side has a maximum as a function of θ then. Phrased differently, (3.117) is certainly fulfilled if it is fulfilled for $\sin^2 2\theta = 1$. In this case, the inequality (3.117) amounts to

$$\Delta E \geq |E_1 - E_2|. \quad (3.118)$$

It expresses the requirement that the energy uncertainty of the neutrino state must be larger than the difference of the energies of different mass eigenstates composing the given flavour state ν_α . This condition has to be fulfilled in any oscillation experiment, and will certainly be satisfied in Mössbauer neutrino experiments where, due to the large momentum uncertainty of the emitted neutrino state, the energy difference $|E_1 - E_2|$ can be vanishingly small without violating the energy-momentum relation of relativistic neutrinos.

*“When you have eliminated all which is impossible,
then whatever remains, however improbable, must be the truth.”*

Sherlock Holmes

4

Non-standard neutrino interactions

Great efforts are currently undertaken to gain a better understanding of neutrino masses and mixing angles, and to measure generic three-flavour effects such as leptonic CP violation in new oscillation experiments (see chapter 2). However, true to the motto “today’s signal is tomorrow’s background”, physicists are going even farther and consider possible subdominant effects, originating from new physics beyond the standard model. Under discussion are neutrino decay, neutrino decoherence, Lorentz violation, and in particular non-standard neutrino interactions (NSI), which will be the subject of this chapter.

NSI have been discussed by many authors, first as an *alternative* to standard oscillations [43, 125–127], and later as a possible additional feature. Most studies use a model-independent formalism [127–131], but NSI have also been investigated in the context of concrete models [127, 132–138]. Their phenomenology has been studied in the context of solar neutrinos [43, 126, 127, 139–143], reactor neutrinos [144], atmospheric neutrinos [145–150], conventional and upgraded neutrino beams [148, 150–158], neutrino factories [130, 152, 159–169], beta beams [170], supernova neutrinos [171, 172], cosmological relic neutrinos [173], high energy astrophysical neutrinos [174], e^+e^- colliders [175], neutrino-electron scattering [176, 177] and neutrino-nucleus scattering [177, 178]. Reviews of the current experimental bounds on NSI can be found in refs. [61, 63]

In the following sections, we will first introduce the effective field theory formalism used to describe NSI, and briefly discuss current constraints on the respective higher dimensional operators (sec. 4.1). Afterwards, we will investigate the impact that NSI can have on future neutrino oscillation experiments. In sec. 4.2, we will focus on reactor and superbeam setups and study the NSI discovery potential of these experiments. Moreover, we will show that large NSI can mimic standard effects, and, for example, may lead to wrong fits of θ_{13} . Sec. 4.3 will be devoted to neutrino factories, for which we will determine the optimal muon energy and detector configuration, aiming at excellent sensitivity to both standard and non-standard observables.

4.1 The formalism of non-standard interactions

4.1.1 The effective NSI Lagrangian

In the standard model, charged current (CC) and neutral current (NC) neutrino interactions originate from the Lagrangian operators (see eq. (2.1))

$$\mathcal{L}_{\text{CC}} = \frac{g}{\sqrt{2}} \left[\bar{\ell}_\alpha \gamma^\mu \frac{1 - \gamma_5}{2} \nu_\alpha W_\mu^+ + \text{h.c.} \right] \quad (4.1)$$

and

$$\mathcal{L}_{\text{NC}} = \frac{g}{2 \cos \theta_W} \bar{\nu}_\alpha \gamma^\mu \frac{1 - \gamma_5}{2} \nu_\alpha Z_\mu^0. \quad (4.2)$$

Here, g is the weak coupling constant, θ_W is the Weinberg angle, ν_α is the neutrino field of flavour α , and ℓ_α is the corresponding charged lepton field. At energies much below the W boson mass M_W , it is more convenient to describe neutrino interactions with the effective dimension 6 operators

$$\mathcal{L}_{\text{CC}}^{\text{eff}} = \frac{G_F}{\sqrt{2}} [\bar{\nu}_\alpha \gamma^\rho (1 - \gamma_5) \ell_\alpha] [\bar{f} \gamma_\rho (1 - \gamma_5) f'] + \text{h.c.}, \quad (4.3)$$

and

$$\mathcal{L}_{\text{NC}}^{\text{eff}} = \frac{G_F}{\sqrt{2}} [\bar{\nu}_\alpha \gamma^\rho (1 - \gamma_5) \nu_\alpha] [\bar{f} \gamma_\rho (g_V^f - g_A^f \gamma_5) f], \quad (4.4)$$

where $G_F = \sqrt{2}g^2/8M_W^2$ is the Fermi constant. The fermions f and f' in the expression for $\mathcal{L}_{\text{CC}}^{\text{eff}}$ are the members of an arbitrary weak doublet, while the field f appearing in $\mathcal{L}_{\text{NC}}^{\text{eff}}$ can also be an iso-singlet. The constants g_V^f and g_A^f are the vector and axial vector couplings of f [22].

If new high energy phenomena beyond the standard weak interactions exist, it is very likely that their low-energy fingerprint will also have the form of effective dimension 6 operators. Since there is only a limited set of such operators, they provide a convenient, model independent approach to new physics phenomena in low-energy neutrino experiments. Here, we consider mostly operators with $(V - A)(V - A)$ Lorentz structure, and refer the reader to appendix B for a discussion of more general NSI operators. Moreover, we neglect NSI involving right handed neutrinos because these are always doubly suppressed in the formulas for the interaction rates: To produce and detect a right handed neutrino, either two NSI couplings or one NSI coupling and one neutrino helicity flip are required. Operators fulfilling these restrictions must have a form similar to eqs. (4.3) and (4.4), and can be written as

$$\begin{aligned} \mathcal{L}_{\text{NSI}} = & \frac{G_F}{\sqrt{2}} \sum_{f, f'} \varepsilon_{\alpha\beta}^{\text{CC}, f, f'} [\bar{\nu}_\alpha \gamma^\rho (1 - \gamma_5) \ell_\beta] [\bar{f} \gamma_\rho (1 - \gamma_5) f'] + \text{h.c.} \\ & + \frac{G_F}{\sqrt{2}} \sum_f \varepsilon_{\alpha\beta}^{\text{NC}, f} [\bar{\nu}_\alpha \gamma^\rho (1 - \gamma_5) \nu_\beta] [\bar{f} \gamma_\rho (1 - \gamma_5) f] + \text{h.c.} \end{aligned} \quad (4.5)$$

The dimensionless parameters $\varepsilon_{\alpha\beta}^{\text{CC},f,f'}$ and $\varepsilon_{\alpha\beta}^{\text{NC},f}$ (to which we will sometimes collectively refer as “the ε parameters”) give the strength of the non-standard interactions relative to G_F . The $\varepsilon_{\alpha\beta}^{\text{CC},f,f'}$ are arbitrary complex 3×3 matrices, while the $\varepsilon_{\alpha\beta}^{\text{NC},f}$ have to be hermitian. Note that, for certain choices of f , f' and ℓ_β , not all ε parameters are independent. For example, $\varepsilon_{\alpha\beta}^{\text{CC},\ell_\rho,\nu_\sigma}$ is identical to $(\varepsilon_{\sigma\rho}^{\text{CC},\ell_\beta,\nu_\alpha})^*$, and $\varepsilon_{\alpha\beta}^{\text{CC},\ell_\beta,\nu_\sigma}$ is related to $\varepsilon_{\alpha\sigma}^{\text{NC},\ell_\beta}$ by virtue of the Fierz identity.

The numerical value of $G_F|\varepsilon|$ is, for all ε parameters, related to the scale of new physics M_{NSI} in the same way as G_F is related to M_W [160]:

$$G_F|\varepsilon| \sim \frac{g^2}{M_{\text{NSI}}^2} \quad (4.6)$$

or, equivalently,

$$|\varepsilon| \sim \frac{M_W^2}{M_{\text{NSI}}^2}, \quad (4.7)$$

This estimate is obtained under the assumption that the NSI are mediated by new heavy particles with masses of order M_{NSI} , and that the coupling constants of these particles at high energies are similar to the weak gauge coupling g . For $M_{\text{NSI}} \sim 1$ TeV, eq. (4.7) would yield $|\varepsilon| \sim 0.006$.

4.1.2 Modified oscillation probabilities in the presence of NSI

We will now describe in general how NSI can be incorporated into the calculation of neutrino oscillation probabilities. It is sufficient here to consider the oscillation formula obtained from the “textbook derivation”, eq. (2.9), because one can easily argue that the additional terms appearing in wave packet models, are irrelevant in terrestrial long-baseline neutrino oscillation experiments on which we will focus here. It will be convenient to rewrite eq. (2.9) in matrix form:

$$P(\nu_\alpha \nu_\beta) = |\langle \nu_\beta | e^{-iHL} | \nu_\alpha \rangle|^2, \quad (4.8)$$

where

$$H = U \begin{pmatrix} 0 & & \\ & \Delta m_{21}^2/2E & \\ & & \Delta m_{31}^2/2E \end{pmatrix} U^\dagger + V_{\text{MSW}}, \quad (4.9)$$

In this expression, E is the neutrino energy, U is the leptonic mixing matrix (2.3), and V_{MSW} is the MSW potential in the flavour basis, given by eq. (2.16). Note that H is not a Hamiltonian in the usual sense because (2.6) shows that the oscillation phase receives contributions not only from the energies of different neutrino mass eigenstates, but also from their momenta. Only if the equal momentum approximation is used — which is

not justified here even though it gives the correct result — H can rightly be called a Hamiltonian.

If non-standard interactions are present, a neutrino source will not produce a pure flavour neutrino eigenstate $|\nu_\alpha\rangle$, but rather a state

$$|\nu_\alpha^s\rangle = |\nu_\alpha\rangle + \sum_{\beta=e,\mu,\tau} \varepsilon_{\alpha\beta}^s |\nu_\beta\rangle. \quad (4.10)$$

For reactor, beta beam and superbeam sources, $\varepsilon_{\alpha\beta}^s = \varepsilon_{\beta\alpha}^{\text{CC},d,u}$, and the charged lepton flavour α can be e (reactor, beta beam, superbeam) and μ (superbeam). In a neutrino factory, ε^s will receive contributions from $\varepsilon_{\alpha\mu}^{\text{CC},e,\nu_e}$ and $\varepsilon_{\alpha e}^{\text{CC},\mu,\nu_\mu}$ (note that these operators are not independent). Similarly, the detector projects the neutrino wave function not onto the standard weak eigenstates, but onto the combinations

$$\langle\nu_\beta^d| = \langle\nu_\beta| + \sum_{\alpha=e,\mu,\tau} \varepsilon_{\alpha\beta}^d \langle\nu_\alpha|. \quad (4.11)$$

For neutrino-nucleon interactions, which will be the dominant processes in most future neutrino detectors, $\varepsilon_{\alpha\beta}^d = \varepsilon_{\alpha\beta}^{\text{CC},d,u}$. Note that in $\varepsilon_{\alpha\beta}^s$, the first index corresponds to the flavour of the charged lepton, and the second one to that of the neutrino, while in $\varepsilon_{\alpha\beta}^d$, the order is reversed. We have chosen this convention to be consistent with the literature.

The matrices $(1 + \varepsilon^s)$ and $(1 + \varepsilon^d)$ need not be unitary, i.e. $|\nu_\alpha^s\rangle$ and $|\nu_\alpha^d\rangle$ are not required to form complete orthonormal sets of basis vectors in the Hilbert space, and in general we will have

$$\sum_{\alpha=e,\mu,\tau} |\nu_\alpha^s\rangle\langle\nu_\alpha^s| \neq 1, \quad \sum_{\beta=e,\mu,\tau} |\nu_\beta^d\rangle\langle\nu_\beta^d| \neq 1, \quad (4.12)$$

$$\langle\nu_\alpha^s|\nu_\beta^s\rangle \neq \delta_{\alpha\beta}, \quad \langle\nu_\alpha^d|\nu_\beta^d\rangle \neq \delta_{\alpha\beta}. \quad (4.13)$$

The oscillation probability in the presence of NSI is

$$\begin{aligned} P(\nu_\alpha^s \rightarrow \nu_\beta^d) &= |\langle\nu_\beta^d|e^{-i\tilde{H}L}|\nu_\alpha^s\rangle|^2 \\ &= |(1 + \varepsilon^d)_{\gamma\beta} (e^{-i\tilde{H}L})_{\gamma\delta} (1 + \varepsilon^s)_{\alpha\delta}|^2 \\ &= \left| \left[(1 + \varepsilon^d)^T e^{-i\tilde{H}L} (1 + \varepsilon^s)^T \right]_{\beta\alpha} \right|^2, \end{aligned} \quad (4.14)$$

where $\tilde{H} = U \text{diag}(0, \Delta m_{21}^2/2E, \Delta m_{31}^2/2E) U^\dagger + \tilde{V}_{\text{MSW}}$. The modified matter potential is

$$\tilde{V}_{\text{MSW}} = \sqrt{2}G_F N_e \begin{pmatrix} 1 + \varepsilon_{ee}^m & \varepsilon_{e\mu}^m & \varepsilon_{e\tau}^m \\ \varepsilon_{e\mu}^{m*} & \varepsilon_{\mu\mu}^m & \varepsilon_{\mu\tau}^m \\ \varepsilon_{e\tau}^{m*} & \varepsilon_{\mu\tau}^{m*} & \varepsilon_{\tau\tau}^m \end{pmatrix}, \quad (4.15)$$

with the non-standard entries given by

$$\varepsilon_{\alpha\beta}^m = \varepsilon_{\alpha\beta}^{\text{NC},e} + 3\varepsilon_{\alpha\beta}^{\text{NC},u} + 3\varepsilon_{\alpha\beta}^{\text{NC},d}. \quad (4.16)$$

Parameter	Bound	Reference
ε_{ee}^m	3.0	[61]
$\varepsilon_{e\mu}^m$	0.0023	[61]
$\varepsilon_{e\tau}^m$	1.5	[61]
$\varepsilon_{\mu\mu}^m$	0.045	[61]
$\varepsilon_{\mu\tau}^m$	0.038	[62]
$\varepsilon_{\tau\tau}^m$	0.12	[62]

Table 4.1: Current 90% C.L. bounds on non-standard matter effects.

The last relation follows from the fact that the numbers of protons, neutrons, and electrons are similar in the Earth matter, and that each nucleon contains three valence quarks. Eq. (4.14) shows that non-standard effects in neutrino oscillation experiments interfere with the standard effects, and are therefore suppressed by only one power of the respective ε parameter. In most other experiments searching for new physics (e.g. rare decay experiments), the non-standard operators contribute incoherently, implying a suppression by at least two powers of the respective small coupling constants.

Note that, due to the non-unitarity of $(1+\varepsilon^s)$ and $(1+\varepsilon^d)$, one should, strictly speaking, not call $P(\nu_\alpha^s \rightarrow \nu_\beta^d)$ a probability because it is not normalised to unity. For lack of a better term, and since the normalisation of $P(\nu_\alpha^s \rightarrow \nu_\beta^d)$ is not relevant to our discussion, we will nevertheless continue to refer to it as the oscillation probability.

4.1.3 Current bounds on non-standard interactions

At present, the best bounds on the NSI parameter space are obtained by combining the data from oscillation and non-oscillation experiments. For NSI in the source and in the detector, a model-independent constraint $\varepsilon^{s,d} \lesssim 0.1$ can be derived from the fact that larger values of ε^s or ε^d would violate universality in lepton and pion decays [160]. Note, however, that model-dependent bounds are typically much stronger, as one may expect from the relation (4.7) between $\varepsilon^{s,d}$ and the new physics scale M_{NSI} , and from the fact that most models require $M_{\text{NSI}} \gg M_W$. Significantly stronger bounds are also obtained if it is assumed that non-standard neutrino interactions occur only in conjunction with their $SU(2)_L$ counterparts in the charged lepton sector. For non-standard matter effects, parameterised in terms of $\varepsilon_{\alpha\beta}^m$, the current bounds are summarised in table 4.1. For a short recent review on these bounds, see ref. [63].

4.2 Non-standard interactions in reactor and superbeam experiments

Let us now study in detail the impact of non-standard interactions on reactor and superbeam experiments. In these experiments, the main neutrino production processes

$N \rightarrow N' + e^- + \bar{\nu}_e$ (reactor) and $\pi \rightarrow \mu + \nu_\mu$ (superbeam), as well as the detection process $\nu_\alpha + N \rightarrow N' + \ell_\alpha$, all involve the same quark-lepton coupling, and are therefore affected by the same types of NSI. This implies that the effective coupling constants $\varepsilon_{\alpha\beta}^s$ and $\varepsilon_{\alpha\beta}^d$ are the same in reactor and superbeam experiments, and that moreover

$$\varepsilon_{\alpha\beta}^s = (\varepsilon_{\beta\alpha}^d)^* \quad (4.17)$$

holds. This constraint can only be circumvented if non- $(V-)(V-A)$ NSI are present (see appendix B), or if different detection processes, such as ν - e scattering are used. To be as general as possible, we will in the following discuss both, the case where eq. (4.17) is taken into account and the case of independent ε^s and ε^d . Another advantage of this approach is that analytical and numerical results are usually more transparent if ε^s and ε^d are treated as independent matrices.

4.2.1 Theoretical expectations

Let us first formulate our theoretical expectations for the impact of non-standard interactions on reactor and superbeam experiments. We will numerically verify these expectations in the subsequent sections.

On the one hand, the appearance of non-standard terms in the oscillation probabilities may be beneficial because it might provide the means to discover new physics in oscillation experiments. On the other hand, correlations between standard and non-standard parameters may also spoil the sensitivity to either of them [163, 179]. A particularly dangerous situation arises when data that has been affected by NSI is used in a standard oscillation fit, assuming absence of NSI. In this case, the fit values for the standard parameters may be severely wrong.

Consider figs. 4.1 – 4.3, in which we depict the possible transition chains that a neutrino can follow before its detection. Solid lines represent transitions that are unsuppressed, dotted lines indicate suppression by standard three-flavour effects (proportional to θ_{13} or $\Delta m_{21}^2/\Delta m_{31}^2$), and dashed lines stand for processes that are suppressed by the indicated NSI couplings. The blue lines correspond to standard oscillations, while transition chains involving black paths are only accessible in the presence of NSI. To find the orders of magnitude of the leading terms in a particular oscillation channel, one has to take the following steps:

1. Find all paths in figs. 4.1 – 4.3 that contribute to the considered oscillation channel.
2. For each path, the order of the corresponding term in the transition amplitude is given by the product of all suppression factors along the path.
3. The suppression factors of the leading terms in the transition *probability* are obtained by forming pairwise products of the contributions to the amplitude.

In the following discussion, we will for simplicity set $\Delta m_{21}^2/\Delta m_{31}^2 = 0$, but one should keep in mind that each term proportional to θ_{13} is accompanied by a similar term proportional to $\Delta m_{21}^2/\Delta m_{31}^2$. We will use the symbol ε (without any indices) to improve the

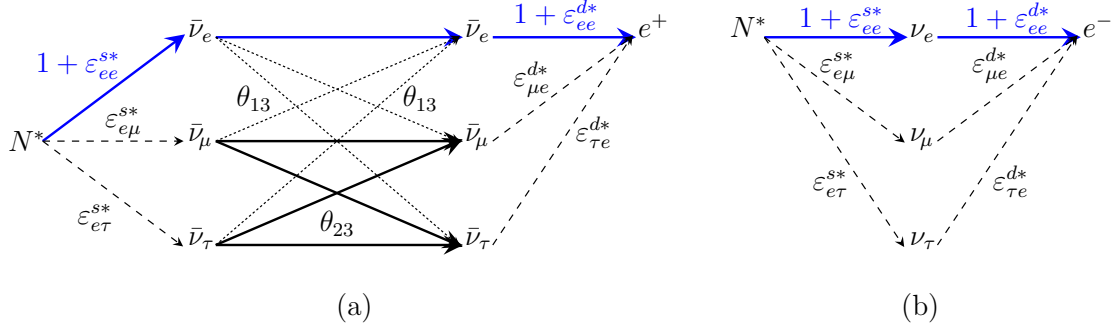


Figure 4.1: Impact of ε^s and ε^d on the event rate in the far detector (a) and the near detector (b) of a reactor $\bar{\nu}_e$ disappearance experiment. Solid lines indicate unsuppressed processes, dotted lines indicate processes that are suppressed by standard three-flavour effects proportional to θ_{13} (we assume $\Delta m_{21}^2/\Delta m_{31}^2 = 0$ for simplicity), and dashed lines represent transitions that are suppressed by the indicated NSI coupling constants. The path that is followed in the absence of NSI is drawn in blue.

readability in cases where it is obvious to which entries of ε^s , ε^d or ε^m we are referring. One should interpret ε as denoting the generic magnitude of the NSI couplings, estimated according to (4.7).

For the reactor, we can read off from fig. 4.1 that, as long as exactly one entry of ε^s , ε^d or ε^m is nonzero, only terms proportional to ε_{ee}^s , $\varepsilon_{e\mu}^s$, $\varepsilon_{e\tau}^s$, ε_{ee}^d , $\varepsilon_{\mu e}^d$ or $\varepsilon_{\tau e}^d$ can appear in the oscillation probability. The effect of ε_{ee}^s and ε_{ee}^d on the event rate is of $\mathcal{O}(\varepsilon)$ and might thus even be larger than the standard oscillation term, which is of order $s_{13}^2 \equiv \sin^2 \theta_{13}$. However, ε_{ee}^s and ε_{ee}^d affect the near detector in the same way as the far detector, and can therefore be detected only if the absolute reactor neutrino flux is known with sufficient precision. On the other hand, this type of NSI cannot spoil the θ_{13} sensitivity of the experiment, because the latter depends only on the *relative* counting rates in both detectors.

The terms proportional to $\varepsilon_{e\mu}^s$, $\varepsilon_{e\tau}^s$, $\varepsilon_{\mu e}^d$ and $\varepsilon_{\tau e}^d$, contribute to the oscillation probability at $\mathcal{O}(\varepsilon s_{13})$, and can therefore be comparable to the standard term if $\varepsilon \sim \theta_{13}$. They do not affect the near detector as long as only one of them is present. If eq. (4.17) is taken into account, both detectors will receive additional $\mathcal{O}(\varepsilon^2)$ contributions.

These considerations are summarised in the first two columns of table 4.2, and are also confirmed by a direct calculation of the oscillation probability, expanded in θ_{13} , $\Delta m_{21}^2/\Delta m_{31}^2$ and ε (see appendix C and ref. [165]).

For a superbeam experiment, fig. 4.2 shows that the $\nu_\mu \rightarrow \nu_e$ appearance signal is affected by NSI couplings to muons in the source ($\varepsilon_{\mu e}^s$, $\varepsilon_{\mu\mu}^s$, $\varepsilon_{\mu\tau}^s$) and by couplings to electrons in the detector (ε_{ee}^d , $\varepsilon_{\mu e}^d$, $\varepsilon_{\tau e}^d$). The terms proportional to $\varepsilon_{\mu\mu}^s$, $\varepsilon_{\mu\tau}^s$ and ε_{ee}^d contribute to the oscillation probability only at the level of εs_{13}^2 , which is small compared to the s_{13}^2 suppression of the standard oscillation probability. Therefore, the dominating NSI parameters in the superbeam appearance channel are $\varepsilon_{\mu e}^s$, $\varepsilon_{\mu e}^d$, and $\varepsilon_{\tau e}^d$. These

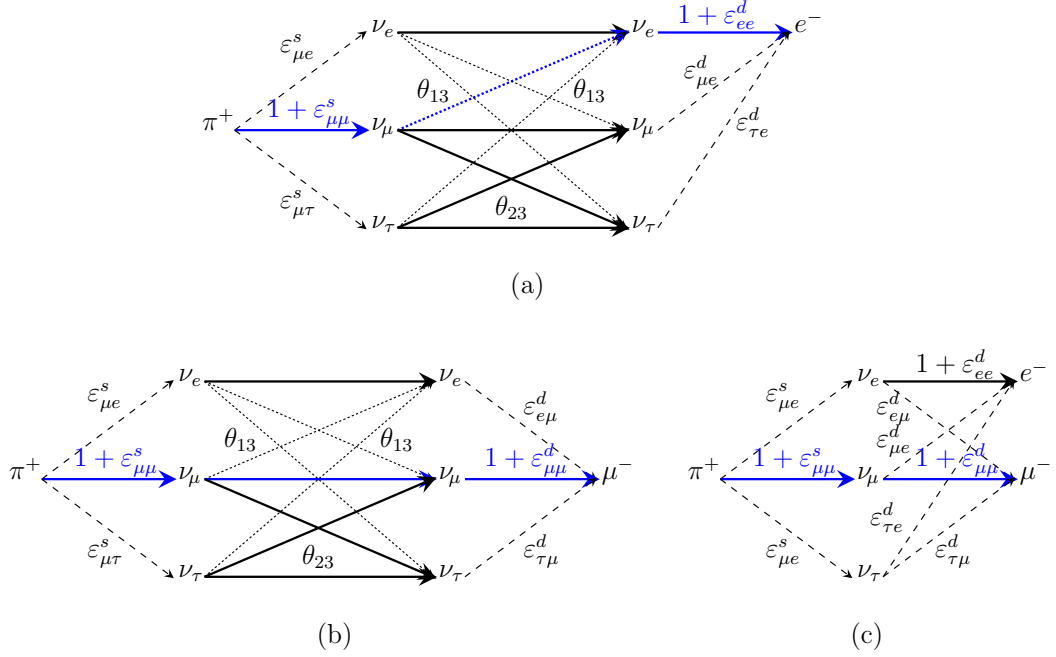


Figure 4.2: Impact of ε^s and ε^d on the event rate in a superbeam experiment for the appearance channel (a), the disappearance channel (b), and in the near detector (c). The meaning of the line styles and colours is the same as in fig. 4.1.

parameters affect the $\nu_\mu \rightarrow \nu_e$ oscillation probability at $\mathcal{O}(\varepsilon s_{13})$.

There are also contributions to the ν_e event sample coming from the intrinsic ν_e contamination of the beam via the $\nu_e \rightarrow \nu_e$ channel. The suppression factors of the corresponding terms are the same as those found for the $\bar{\nu}_e \rightarrow \bar{\nu}_e$ channel in the reactor experiment, but should now be multiplied with the fraction ξ of ν_e in the beam.

An indirect perturbation of the ν_e appearance signal can arise for nonzero $\varepsilon_{\mu\mu}^d$, because the corresponding term in the near detector mimics a modified initial ν_μ flux. This could cause an $\mathcal{O}(\varepsilon)$ miscalibration of this flux, so that the $\nu_\mu \rightarrow \nu_e$ oscillation probability, deduced from the ratio of the ν_e rate in the far detector to the ν_μ rate in the near detector, would be off by a term of $\mathcal{O}(\varepsilon s_{13}^2)$. The important point is here that $\varepsilon_{\mu\mu}^d$ *mimics* a modified ν_μ flux, while, for example, NSI proportional to $\varepsilon_{\mu\mu}^s$ do really modify this flux and therefore would lead to a harmless rescaling of the event rate in *both* detectors. In fact, $\varepsilon_{\mu\mu}^s$ is indistinguishable from a systematic misunderstanding of the beam source unless its modulus is very large.

Note that also ε_{ee}^s , $\varepsilon_{\mu e}^s$, ε_{ee}^d and $\varepsilon_{\mu e}^d$ would affect the near detector by modifying the ν_e signal. If this effect is detected and successfully disentangled from the systematical uncertainties in the intrinsic ν_e background, it could actually help to detect the presence of the NSI. On the other hand, if nonzero $\varepsilon_{\mu e}^d$ remains undetected, it will lead to the wrong conclusion that the fraction of ν_e in the beam is $\xi + |\varepsilon_{\mu e}^d|^2$ instead of ξ . If the far

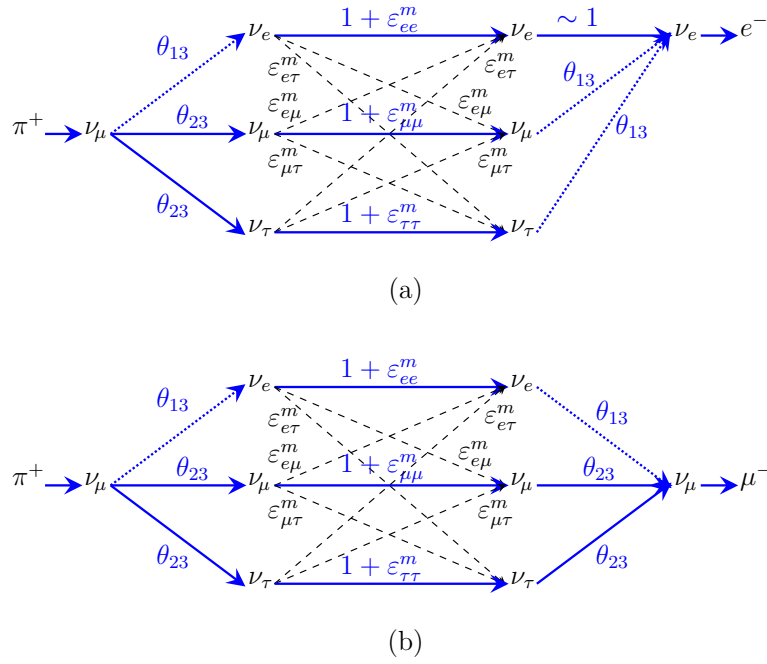


Figure 4.3: Impact of ε^m on the event rate in the superbeam appearance channel (a) and in the disappearance channel (b). The meaning of the line styles and colours is the same as in fig. 4.1.

detector then measures a ν_e appearance signal, the reconstructed oscillation probability will be of order $\sin^2 2\theta_{13} - |\varepsilon_{\mu e}^d|^2$ instead of $\sin^2 2\theta_{13}$, which will in turn lead to a wrong fit value for θ_{13} . A similar effect does *not* occur for nonzero $\varepsilon_{\mu e}^s$ because in that case, the intrinsic background is really modified.

In the superbeam disappearance channel, the relevant NSI operators are those which induce new couplings of neutrinos and muons. Terms proportional to $\varepsilon_{\mu\mu}^s$, $\varepsilon_{\mu\tau}^s$, $\varepsilon_{\mu\mu}^d$ and $\varepsilon_{\tau\mu}^d$ contribute to the oscillation probability at $\mathcal{O}(\varepsilon)$, while those proportional to $\varepsilon_{\mu e}^s$ and $\varepsilon_{e\mu}^d$ are suppressed by εs_{13} .

If the baseline of the superbeam experiment is large enough (several 100 km for typical superbeam energies of $E \sim$ several GeV), standard and non-standard matter effects will become important. In the appearance channel, the lowest order non-standard effects are those proportional to $\varepsilon_{e\mu}^m$ and $\varepsilon_{e\tau}^m$. We have seen in sec. 4.1.3 that $\varepsilon_{e\mu}^m$ is already strongly constrained experimentally to the level of $2.3 \cdot 10^{-3}$ [61, 63], but for $\varepsilon_{e\tau}^m$, the current bound is much weaker ($\varepsilon_{e\tau}^m \lesssim 1.5$), so the corresponding terms could in principle contribute significantly in the superbeam appearance channel [130, 156]. All other non-standard matter effects are suppressed by an additional power of θ_{13} and can therefore be neglected.¹ It is interesting to observe that the contribution of ε_{ee}^m , which is just a rescaling of the standard MSW potential, is not a leading order effect. This fact has been discussed in more detail in ref. [180].

The dominant matter effect in the disappearance channel is $\varepsilon_{\mu\tau}^m$, which contributes at $\mathcal{O}(\varepsilon)$ to the oscillation probability. From fig. 4.3, one might expect $\varepsilon_{\mu\mu}^m$ and $\varepsilon_{\tau\tau}^m$ to be as relevant as $\varepsilon_{\mu\tau}^m$, but when one actually calculated the oscillation probability, it turns out that the corresponding terms are always accompanied by an additional small factor $\cos 2\theta_{23}$ (see eq. (C.8)).

Let us emphasise that the arguments given in this section did not account for the complex phases of the NSI parameters and of the standard leptonic mixing matrix. A direct calculation of the approximate oscillation probabilities (cf. appendix C and ref. [157]), as well as numerical simulations (see below), show that unfavourable combinations of these phases may suppress non-standard effects, even if the moduli of the corresponding coupling constants are large.

4.2.2 Simulation of reactor and superbeam experiments

In order to fully assess the consequences of non-standard interactions for realistic reactor and superbeam experiments, we have performed numerical simulations using the GLoBES (General Long Baseline Experiment Simulator) software [181, 182]. GLoBES provides a full three-flavour treatment of the oscillation physics, and can compute and analyse the expected event spectra for many different types of neutrino experiments. Building on earlier work by Patrick Huber, Manfred Lindner and Walter Winter, we have extended the software to include the ability to study non-standard neutrino oscillation physics,

¹This might change if an experiment were performed at energies close to the MSW resonance because then, the matter enhancement could compensate for the smallness of θ_{13} .

4.2 NON-STANDARD INTERACTIONS IN REACTOR AND SUPERBEAM EXPERIMENTS

NSI	Reactor		Superbeam			
	far $\bar{\nu}_e$	near $\bar{\nu}_e$	far ν_e	far ν_μ	near ν_e	near ν_μ
None	1	1	$s_{13}^2 + \xi$	1	ξ	1
ε_{ee}^s	ε	ε	$\xi \varepsilon$		$\xi \varepsilon$	
$\varepsilon_{e\mu}^s$	εs_{13}		$\xi \varepsilon s_{13}$			
$\varepsilon_{e\tau}^s$	εs_{13}		$\xi \varepsilon s_{13}$			
$\varepsilon_{\mu e}^s$			$\varepsilon s_{13} + \varepsilon^2$	εs_{13}	ε^2	
$\varepsilon_{\mu\mu}^s$			εs_{13}^2	ε		ε
$\varepsilon_{\mu\tau}^s$			εs_{13}^2	ε		
ε_{ee}^d	ε	ε	$\varepsilon s_{13}^2 + \xi \varepsilon$		$\xi \varepsilon$	
$\varepsilon_{e\mu}^d$				εs_{13}		
$\varepsilon_{\mu e}^d$	εs_{13}		$\varepsilon s_{13} + \varepsilon^2$		ε^2	
$\varepsilon_{\mu\mu}^d$				ε		ε
$\varepsilon_{\tau e}^d$	εs_{13}		$\varepsilon s_{13} + \varepsilon^2$			
$\varepsilon_{\tau\mu}^d$				ε		
$\varepsilon_{ee}^s = \varepsilon_{ee}^{d*}$	ε	ε	$\varepsilon s_{13}^2 + \xi \varepsilon$		$\xi \varepsilon$	
$\varepsilon_{e\mu}^s = \varepsilon_{\mu e}^{d*}$	$\varepsilon s_{13} + \varepsilon^2$	ε^2	$\varepsilon s_{13} + \varepsilon^2$		ε^2	
$\varepsilon_{e\tau}^s = \varepsilon_{\tau e}^{d*}$	$\varepsilon s_{13} + \varepsilon^2$	ε^2	$\varepsilon s_{13} + \varepsilon^2$		$\xi \varepsilon^2$	
$\varepsilon_{\mu e}^s = \varepsilon_{e\mu}^{d*}$			$\varepsilon s_{13} + \varepsilon^2$	$\varepsilon s_{13} + \varepsilon^2$	ε^2	ε^2
$\varepsilon_{\mu\mu}^s = \varepsilon_{\mu\mu}^{d*}$			εs_{13}^2	ε		ε
$\varepsilon_{\mu\tau}^s = \varepsilon_{\tau\mu}^{d*}$			εs_{13}^2	ε		ε^2
ε_{ee}^m			εs_{13}^2	εs_{13}^2		
$\varepsilon_{e\mu}^m$			$\varepsilon s_{13} + \varepsilon^2$	εs_{13}		
$\varepsilon_{e\tau}^m$			$\varepsilon s_{13} + \varepsilon^2$	εs_{13}		
$\varepsilon_{\mu\mu}^m$			εs_{13}^2	$\varepsilon c_{2 \times 23}^a$		
$\varepsilon_{\mu\tau}^m$			εs_{13}^2	ε		
$\varepsilon_{\tau\tau}^m$			εs_{13}^2	$\varepsilon c_{2 \times 23}^a$		

^aThe factor $\cos 2\theta_{23}$ cannot be derived from fig. 4.3, but only from the computation of $P(\nu_\mu^s \rightarrow \nu_\mu^d)$ (see appendix C and ref. [157]).

Table 4.2: Classification of non-standard interactions according to their expected impact on the event rates in reactor and superbeam experiments. For each NSI parameter, only the leading order effects are shown. The notation is $s_{13} \equiv \sin \theta_{13}$, $c_{2 \times 23} \equiv \cos 2\theta_{23}$, and ξ is the small percentage of ν_e in the beam. In the suppression factors, we have denoted the magnitude of the respective entries of ε^s , ε^d and ε^m simply by ε (without any indices) to increase the readability.

to provide a more realistic treatment of systematical uncertainties and to offer better numerical efficiency [182, 183]. For the present study, we have simulated the following experiments:

- **T2K** (Tokai to Kamioka): Our simulation of T2K [69] is based on [184], where most experimental parameters are taken from the T2K letter of intent [185], and the systematical uncertainties are based on [186]. We include a separate 1.0 kt water Čerenkov near detector with otherwise similar properties as the far detector **Super-Kamiokande**, and with similar systematical uncertainties. To model the interplay of the two detectors, we introduce a common 10% uncertainty on the neutrino flux, and a common 20% error on the number of background events in the ν_e appearance channel. In the absence of non-standard interactions, these correlated uncertainties would cancel completely because the total neutrino flux and the background contribution are calibrated by the near detector, but if $\varepsilon^{s,d} \neq 0$, this calibration can be wrong, and there may be an observable effect. The neutrino interaction cross sections in our simulation are taken from [187, 188]. We assume 3 years of neutrino running and 3 years of anti-neutrino running, each with a beam power of 0.77 MW. The fiducial far detector mass is 22.5 kt, and the baseline is 295 km. We consider ν_e appearance events as well as the ν_μ disappearance signal. The background for the disappearance channel is made up of neutral current events, while for the appearance measurement, neutral current events, misidentified muons, and the intrinsic beam backgrounds can contribute.
- **NO ν A** (NuMI Off-axis ν_e Appearance Experiment): To simulate the NO ν A experiment, we follow ref. [70] for the ν_e appearance signal, while the simulation of the ν_μ disappearance channel is based on [189]. We assume 3 years of neutrino running and 3 years of anti-neutrino running with a beam power of 1.12 MW. The far detector mass is 25 kt, and the baseline is 812 km, with an average matter density of 2.8 g/cm³ along the trajectory. The near detector has a mass of 0.0204 kt, and is located 1 km away from the target. Again, we introduce, in addition to the uncorrelated systematical errors from [70, 189], a correlated 10% uncertainty on the total neutrino flux, and a correlated 20% error on the ν_e background.
- **Double Chooz**: For the simulation of Double Chooz [67], we use the same parameters as in [190]. In particular, we simulate two 10.16 t detectors at baselines of 0.1 km and 1.05 km, respectively. As systematical uncertainties, we introduce a 2.8% flux normalisation error, which is correlated between the near and far detectors, uncorrelated 0.6% fiducial mass errors for both detectors, uncorrelated 0.5% energy calibration uncertainties, and an independent 0.5% error in each energy bin of the spectrum. These bin-to-bin errors parameterise in a conservative way background events with an unknown energy spectrum. The cross sections for inverse beta decay in our simulation are taken from [191].
- **DC-200**: As a model for a generic next-generation reactor experiment, we consider a setup with the same parameters and systematical errors as Double Chooz,

but with a 200 t far detector. Such a setup, which we call DC-200 here, corresponds, for example, to the hypothetical **Triple Chooz** upgrade of the **Double Chooz** experiment [190]. Such an upgrade would increase the sensitivity to the energy dependence of neutrino oscillations, which is a more robust observable with respect to systematic uncertainties than the total event rate.

Unless indicated otherwise, we compute event rates assuming the following “true” values for the standard oscillation parameters [55]:

$$\begin{aligned} \sin^2 2\theta_{12}^{\text{true}} &= 0.87, & (\Delta m_{21}^2)^{\text{true}} &= 7.6 \cdot 10^{-5} \text{ eV}^2, \\ \sin^2 2\theta_{23}^{\text{true}} &= 1.0, & (\Delta m_{31}^2)^{\text{true}} &= 2.4 \cdot 10^{-3} \text{ eV}^2, \\ \sin^2 2\theta_{13}^{\text{true}} &= 0.001, & \delta_{\text{CP}}^{\text{true}} &= 3\pi/2. \end{aligned} \quad (4.18)$$

Moreover, we assume the “true” mass hierarchy to be normal, i.e. $\Delta m_{31}^2 > 0$. To analyse the simulated data, we follow the statistical procedure described in the appendix of [184], and define the following χ^2 function²

$$\chi^2 = \min_{\boldsymbol{\lambda}} \left[\sum_j^{\text{channel}} \sum_i^{\text{bin}} \frac{|N_{ij}(\boldsymbol{\lambda}^{\text{true}}, \boldsymbol{\varepsilon}^{\text{true}}, \mathbf{a} = 0) - N_{ij}(\boldsymbol{\lambda}, \boldsymbol{\varepsilon}, \mathbf{a})|^2}{N_{ij}(\boldsymbol{\lambda}^{\text{true}}, \boldsymbol{\varepsilon}^{\text{true}}, \mathbf{a} = 0)} + \chi_{\text{pull}}^2(\boldsymbol{\lambda}) + \chi_{\text{pull}}^2(\mathbf{a}) \right], \quad (4.19)$$

where N_{ij} denotes the number of events in the i -th energy bin for oscillation channel j , the vector $\boldsymbol{\lambda} = (\theta_{12}, \theta_{13}, \theta_{23}, \delta_{\text{CP}}, \Delta m_{21}^2, \Delta m_{31}^2)$ contains the standard oscillation parameters, $\boldsymbol{\varepsilon}$ is the vector of non-standard parameters, and \mathbf{a} represents the systematical biases. The pull terms $\chi_{\text{pull}}^2(\boldsymbol{\lambda})$ and $\chi_{\text{pull}}^2(\mathbf{a})$ implement external input on the parameters and have the form

$$\chi_{\text{pull}}^2(\mathbf{x}) = \sum_i \frac{(x_i - x_i^{\text{true}})^2}{\sigma_{x_i}^2}, \quad (4.20)$$

where x_i are the components of the vector \mathbf{x} , and σ_{x_i} is the externally given uncertainty of x_i . We assume θ_{12} and Δm_{21}^2 to be known to within 5% from solar and reactor experiments [55]. When analysing **Double Chooz** or **DC-200** alone, we additionally assume a 10% uncertainty on θ_{23} and a 5% error on Δm_{31}^2 . Beam experiments are themselves sensitive to θ_{23} and Δm_{31}^2 , so we omit these priors if **T2K** or **NO ν A** is included in the simulation. In the fit, we minimise χ^2 over all systematical biases and all standard oscillation parameters unless indicated otherwise. As a first step in the minimisation procedure, we perform a rough scan of the χ^2 manifold over the θ_{13} – δ_{CP} plane in order to find the approximate positions of all local minima. These are then refined using the local minimisation algorithm provided by **GLOBES**. In this way, we ensure that all

²In the implementation of superbeam experiments, we actually assume the events to follow the Poisson distribution. However, for illustrative purposes, it is sufficient to consider the more compact approximate Gaussian expression here.

degenerate solutions are properly taken into account. In the initial scan, we neglect systematical uncertainties, correlations with the solar parameters and, except in the simulations leading to figs. 4.6 – 4.9, also correlations with Δm_{31}^2 and θ_{23} . We perform separate scans for the normal and inverted mass hierarchies.

4.2.3 Discovery reach

In this section, we study the prospects for detecting NSI in future reactor and superbeam experiments. We define the discovery reach (or discovery potential) of an experiment for some NSI parameter ε as the minimum value the true $|\varepsilon|$ must have in order to be distinguishable from the $\varepsilon = 0$ case at a given confidence level. To compute the discovery reach, we simulate the event spectra for different “true” values of ε and then perform fits in which ε is kept fixed at zero. In fig. 4.4, we show the NSI discovery reach of T2K, Double Chooz and of a combined analysis of these experiments. We have computed results for all NSI parameters which, according to table 4.2, might potentially be detectable, and we consider scenarios both with and without the constraint (4.17), $\varepsilon_{\alpha\beta}^s = (\varepsilon_{\alpha\beta}^d)^*$.

Our first observation is that the discovery reach crucially depends on the values nature has chosen for the complex phases δ_{CP} and $\arg(\varepsilon_{\alpha\beta}^{s,d,m})$.³ For favourable combinations of these phases (light portions of bars), much smaller non-standard effects may be detected than for unfavourable combinations (dark portions of bars).

Reactor

By comparing fig. 4.4 with table 4.2, one can see that our expectations for the relative importance of different NSI parameters are mostly confirmed. In particular, the figure shows that reactor experiments are sensitive only to non-standard CC interactions of neutrinos and electrons, i.e. to the parameters ε_{ee}^s , $\varepsilon_{e\mu}^s$, $\varepsilon_{e\tau}^s$, ε_{ee}^d , $\varepsilon_{\mu e}^d$ and $\varepsilon_{\tau e}^d$. As discussed in sec. 4.2.1, the discovery potential for ε_{ee}^s and ε_{ee}^d can never be better than the uncertainty in the reactor neutrino flux and spectrum, which is on the per cent level. It can, however, be much worse if $\arg(\varepsilon_{ee}^{s,d}) \sim \pi/2$, $3\pi/2$ because then, the lowest order contribution to $P(\bar{\nu}_e^s \rightarrow \bar{\nu}_e^d)$ vanishes (cf. eq. (C.2)).

The phase dependence that it visible for the parameters $\varepsilon_{e\mu}^s$, $\varepsilon_{e\tau}^s$, $\varepsilon_{\mu e}^d$ and $\varepsilon_{\tau e}^d$ disappears when the combinations $\varepsilon_{e\mu}^s = (\varepsilon_{\mu e}^d)^*$ and $\varepsilon_{e\tau}^s = (\varepsilon_{\tau e}^d)^*$ are considered. We interpret this feature with the help of the analytical expression for $P(\bar{\nu}_e^s \rightarrow \bar{\nu}_e^d)$ from eq. (C.2): In general, the main sensitivity to NSI parameters comes from terms having an energy dependence different from that of the standard oscillation probability. In (C.2), this is the case for terms containing a factor $\sin(\Delta m_{31}^2 L/2E)$. For $\varepsilon_{e\mu}^s = (\varepsilon_{\mu e}^d)^*$ and $\varepsilon_{e\tau}^s = (\varepsilon_{\tau e}^d)^*$, however, all such terms cancel, and therefore, spectral information can no longer be used to disentangle standard and non-standard effects. On the other hand, the second order expansion of the $\bar{\nu}_e$ survival probability at $L = 0$, given in eq. (C.3), shows that the near

³The impact of the true δ_{CP} is not directly evident from fig. 4.4, which has been computed for fixed $\delta_{\text{CP}}^{\text{true}} = 3\pi/2$. It can, however, be seen from the equations given in appendix C, in which most terms depend on sums or differences of δ_{CP} and the non-standard phases.

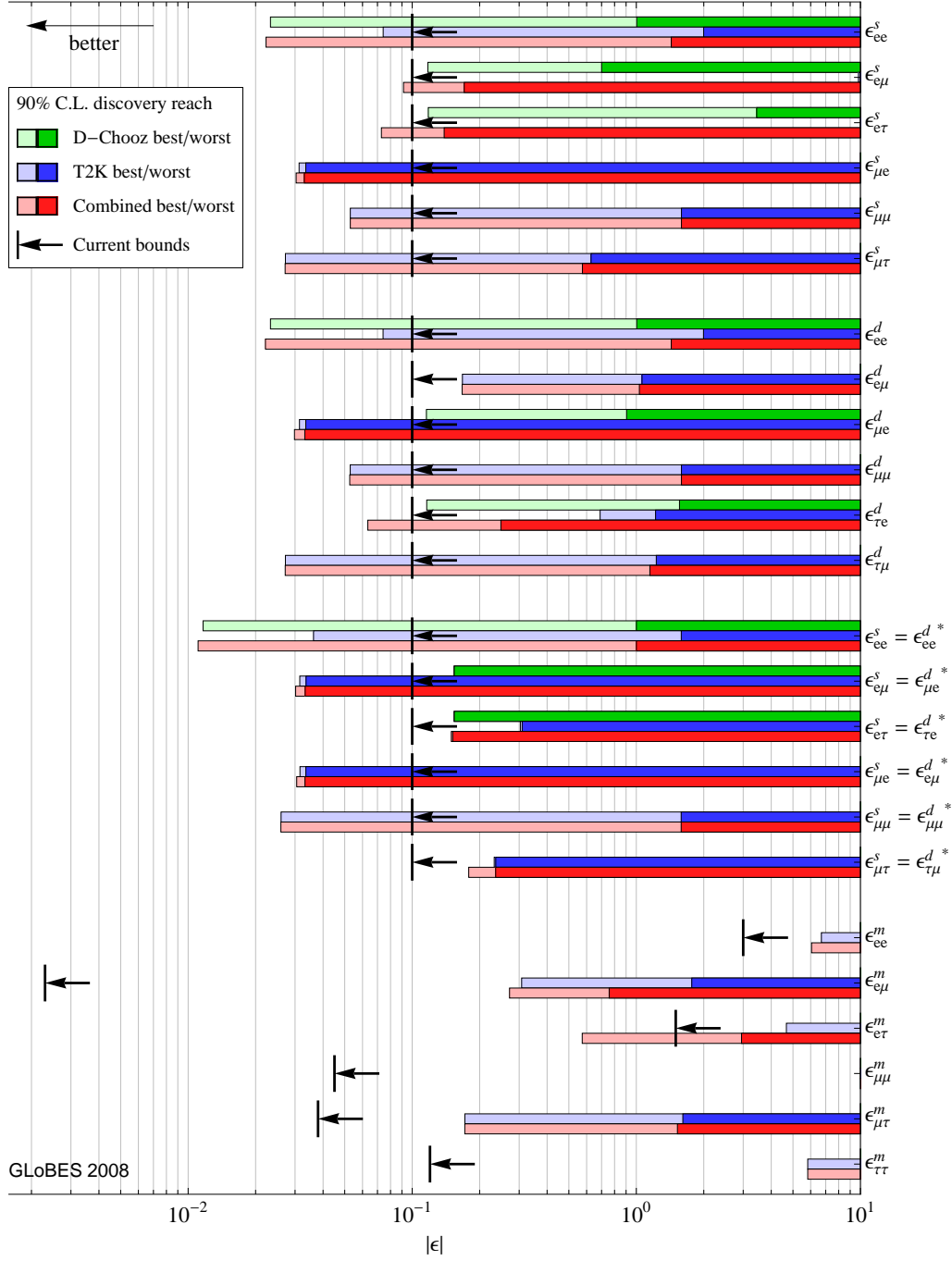


Figure 4.4: 90% C.L. NSI discovery reaches of Double Chooz (green bars), T2K (blue bars), and of a combined analysis of these experiments (red bars). Parameter values covered by the dark portions of the bars can be discovered independently of the complex phases, while values covered by the light portions are accessible only if nature has chosen favourable values for the phases.

detector is sensitive to the combinations $\varepsilon_{e\mu}^s = (\varepsilon_{\mu e}^d)^*$ and $\varepsilon_{e\tau}^s = (\varepsilon_{\tau e}^d)^*$, even though it is insensitive to each parameter on its own. We conclude that the discovery reaches for $\varepsilon_{e\mu}^s$, $\varepsilon_{e\tau}^s$, $\varepsilon_{\mu e}^d$ and $\varepsilon_{\tau e}^d$, treated as independent parameters, are dominated by phase-dependent spectral distortions seen in the far detector, while the discovery reaches for $\varepsilon_{e\mu}^s = (\varepsilon_{\mu e}^d)^*$ and $\varepsilon_{e\tau}^s = (\varepsilon_{\tau e}^d)^*$ come mainly from phase-independent terms in the near detector.

Superbeam

The superbeam has some sensitivity to all shown NSI parameters except $\varepsilon_{e\mu}^s$ and $\varepsilon_{e\tau}^s$. For most parameters, however, the discovery potential is competitive with current bounds only for very special values of the complex phases. Unaffected by the phases are only the discovery potentials for $\varepsilon_{\mu e}^s$, $\varepsilon_{\mu e}^d$, and for the combinations $\varepsilon_{e\mu}^s = (\varepsilon_{\mu e}^d)^*$, $\varepsilon_{e\tau}^s = (\varepsilon_{\tau e}^d)^*$, $\varepsilon_{\mu e}^s = (\varepsilon_{e\mu}^d)^*$ and $\varepsilon_{\mu\tau}^s = (\varepsilon_{\tau\mu}^d)^*$. In all of these cases, the sensitivity is dominated by $\mathcal{O}(\varepsilon^2)$ effects causing a modified ν_e or ν_μ flux in the near detector. Also the relatively good sensitivity to ε_{ee}^s and ε_{ee}^d is due to near detector effects. Of the other discovery reaches, those for $\varepsilon_{\tau e}^d$, $\varepsilon_{e\mu}^m$ and $\varepsilon_{e\tau}^m$ come from the appearance channel, while those for $\varepsilon_{\mu\mu}^s$, $\varepsilon_{\mu\tau}^s$, $\varepsilon_{\mu\mu}^d$, $\varepsilon_{\tau\tau}^d$ and $\varepsilon_{\mu\tau}^m$ are dominated by the disappearance channel.

A careful inspection of the superbeam discovery reaches shows that, in several places, our expectations from table 4.2 are contradicted by the simulation. For example, we would have expected the discovery reach for the parameter combination $\varepsilon_{\mu\tau}^s = (\varepsilon_{\tau\mu}^d)^*$ to be similar to or better than the discovery reaches for $\varepsilon_{\mu\tau}^s$ and $\varepsilon_{\tau\mu}^d$ treated as independent parameters. The reason why this is not the case can be deduced from eq. (C.7) or eq. (C.8). These expressions show that, of the terms proportional to $\varepsilon_{\mu\tau}^s$ and $\varepsilon_{\tau\mu}^d$, those having a non-standard energy dependence $\sim \sin(\Delta m_{31}^2 L/2E)$, cancel in the case $\varepsilon_{\mu\tau}^s = (\varepsilon_{\tau\mu}^d)^*$.

It is also interesting to observe that the discovery reach of the superbeam for $\varepsilon_{e\mu}^m$ is more than an order of magnitude better than the discovery reach for $\varepsilon_{e\tau}^m$ even though the corresponding terms in eq. (C.6) are identical up to effects of $\mathcal{O}(\theta_{23} - \pi/4)$, and up to signs. It turns out that an intricate interplay of these signs causes the contributions proportional to $\varepsilon_{e\tau}^m$ to be always smaller. In sec. 4.3, we will see that, in a neutrino factory experiment, the sensitivities to $\varepsilon_{e\mu}^m$ and $\varepsilon_{e\tau}^m$ are more similar than in the superbeam case.

Combined analysis

Comparing the discovery reaches achievable in T2K and Double Chooz separately to the potential of a combined analysis, we find that for most parameters, the combined analysis is dominated either by the reactor experiment or by the superbeam, and that the contribution from the other experiment is negligible. For $\varepsilon_{\tau e}^d$ and $\varepsilon_{e\tau}^m$, however, the discovery prospects in the combined approach are much better than in the single experiment fits. We will see in the next section that this can be explained by the fact that the χ^2 of a standard oscillation fit to a single set of experimental data is very small in the presence of $\varepsilon_{\tau e}^d$ or $\varepsilon_{e\tau}^m$, but that there is a large discrepancy between the fitted

parameter values obtained in the reactor and superbeam experiments, respectively. It is this discrepancy, which effectively enhances the sensitivity of the combined analysis.

In conclusion, we have seen that reactor and superbeam experiments have some discovery potential for non-standard interactions, but only if the NSI couplings are very large and if, moreover, the complex phases are favourable. Next-generation neutrino oscillation experiments will certainly not be able to probe the parameter region $\varepsilon_{\alpha\beta}^{s,d,m} < 0.01$, in which new effects might be expected, according to the estimate (4.7), if there is new physics at the TeV scale.

4.2.4 NSI-induced offsets and discrepancies in θ_{13} fits

In sec. 4.2.1, we have already mentioned that non-standard interactions can spoil the fits of the standard oscillation parameters in reactor and superbeam experiments if they are not taken into account properly. Let us now study this in more detail: In fig. 4.5, we show two extreme examples. Assuming only the NSI parameters $\varepsilon_{e\tau}^m = 0.5 e^{-i\pi/2}$ (upper plots) or $\varepsilon_{e\tau}^s = \varepsilon_{\tau e}^d = 0.05$ (lower plots) to be non-zero, we have simulated the expected event spectra in T2K, Double Chooz, NO ν A and DC-200, and have then performed a fit of θ_{13} and δ_{CP} , naively neglecting the non-standard effects. According to the discussion from sec. 4.2.1, we expect only the superbeam experiments to be affected by $\varepsilon_{e\tau}^m$, while nonvanishing $\varepsilon_{e\tau}^s$ and $\varepsilon_{\tau e}^d$ should also have an impact on the reactor experiments. Indeed, fig. 4.5 confirms this expectation. The upper plots show that the reactor experiments give the correct best fit value for θ_{13} (vertical black lines) in the case $\varepsilon_{e\tau}^m = 0.5 e^{-i\pi/2}$, while the superbeam fits are severely wrong if the non-standard effects are neglected in the analysis. For the parameter values we have chosen, the discrepancy is so large that the standard oscillation fit of T2K and NO ν A data would erroneously rule out the true θ_{13} at the 90% confidence level. NO ν A would even yield a θ_{13} value above the CHOOZ bound and a fake hint to the mass hierarchy. This example shows that reactor and superbeam experiments, though seemingly redundant in the standard oscillation case, may be highly complementary if non-standard interactions are present. In particular, a discrepancy between their respective θ_{13} fits may indicate the presence of NSI that would remain undetected if only one experiment were performed.

The second example shown in fig. 4.5 (lower plots) is more dangerous because there, the reactor and the superbeam experiments both rule out the true θ_{13} at 90%, while agreeing very well among each other on a false value. This common offset renders a detection of the mistake impossible unless complementary data sets from other experiments are available.

Of course, the NSI parameters used in fig. 4.5 were specifically selected in such a way that the discrepancies and offsets in the θ_{13} fits were most apparent. In particular, the chosen moduli of $\varepsilon_{e\tau}^m$ resp. $\varepsilon_{e\tau}^s = \varepsilon_{\tau e}^{d*}$ are close to the current upper limits, and we are not aware of any realistic model that could yield such large NSI. Therefore, let us now turn to a more systematic analysis of the possible impact of NSI on the θ_{13} fits in reactor and superbeam experiments. In figs. 4.6 – 4.8, we take the role of the devil’s advocate and

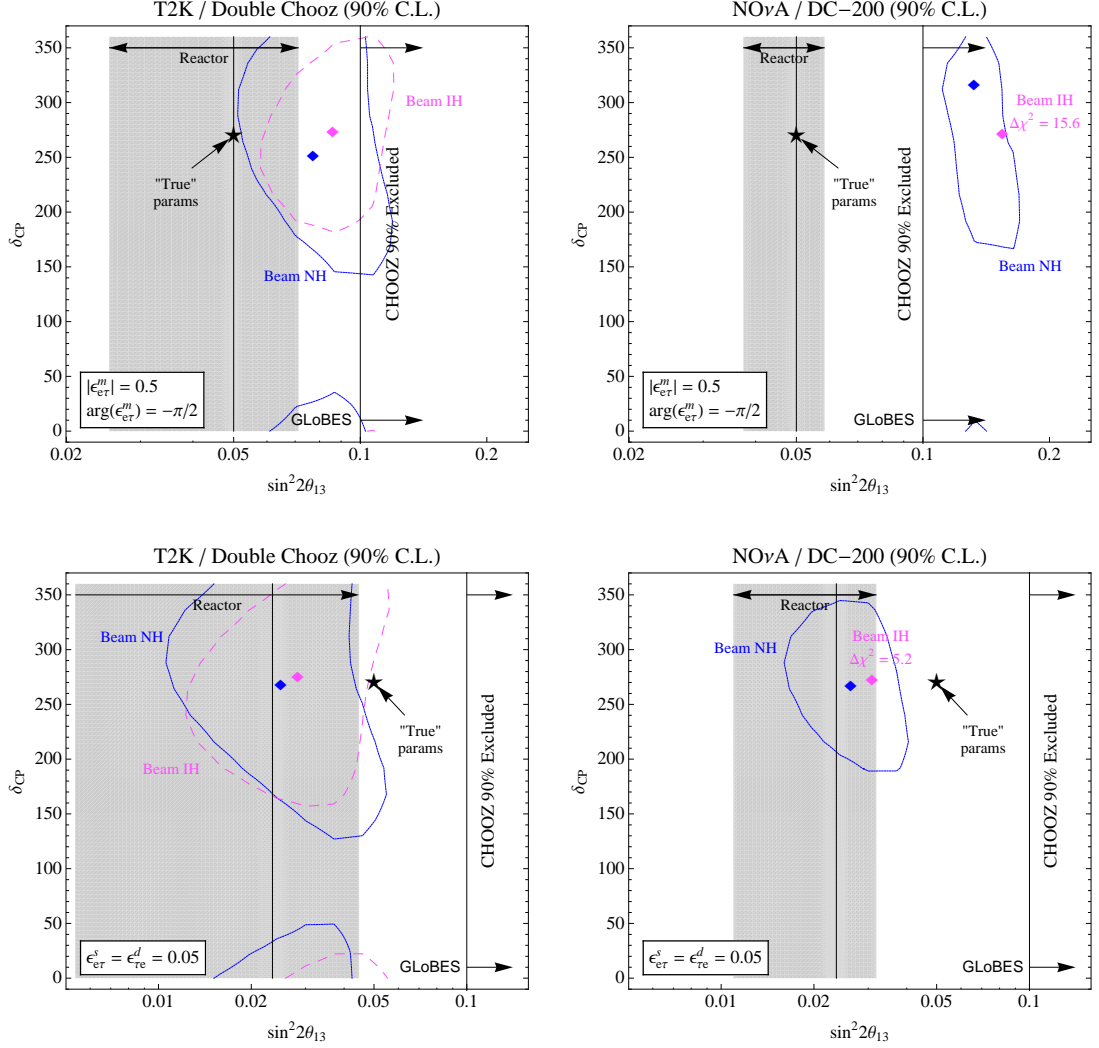


Figure 4.5: Two extreme examples for the consequences of neglecting non-standard interactions when fitting θ_{13} and δ_{CP} to the data of reactor and superbeam experiments. The left hand plots compare T2K and Double Chooz, while the right hand ones show results for NOvA and DC-200. The gray shading represents the 90% confidence region from the reactor experiment, and the vertical black line shows the corresponding best fit θ_{13} value. The 90% contours from the superbeam are shown as solid blue lines for a normal hierarchy fit, and as dashed pink lines for an inverted hierarchy fit. The coloured diamonds represent the corresponding best fit points. In our χ^2 analysis, we have assumed 2 degrees of freedom in the beam experiments, and one degree of freedom in the reactor setups. For $\epsilon_{er}^m = 0.5e^{-i\pi/2}$ (upper panels), a discrepancy arises between the results of the two experiments, while for $\epsilon_{er}^s = \epsilon_{er}^d = 0.05$ (lower panels), they agree with each other, but the fit value for θ_{13} is offset from the “true” value.

show by which amount standard oscillation fits of θ_{13} to data taken in the presence of NSI can maximally fail. In each panel, one of the $|\varepsilon_{\alpha\beta}^{s,d,m}|$ parameters was assumed to saturate its current upper bound, while all other NSI were assumed to vanish. For different values of the phases $\arg(\varepsilon_{\alpha\beta}^{s,d,m})$, we have simulated the expected T2K and Double Chooz data, and have then fitted θ_{13} to it, neglecting NSI in the fit. The points and error bars in the figures show the results of these fits, with the colour indicating the minimum χ^2 , i.e. the quality of the fit in each case. Dark blue means perfect agreement of the standard fit with the non-standard data, while points drawn in grey indicate that standard oscillations are correctly ruled out at more than 3σ . Fig. 4.6 is for $(V-A)(V-A)$ charged current NSI, respecting the constraint $\varepsilon_{\alpha\beta}^s = (\varepsilon_{\alpha\beta}^d)^*$, while fig. 4.7 is for the more general case where ε^s and ε^d are treated as independent matrices, and fig. 4.8 is for non-standard matter effects, parameterised by $\varepsilon_{\alpha\beta}^m$. Note that, as in the previous section, we do not show plots for CC NSI couplings to τ leptons, because we have argued in sec. 4.2.1 (table 4.2) that these do not affect reactor and superbeam experiments. We also omit all NC NSI except those proportional to $\varepsilon_{e\tau}^m$ because they have turned out to leave the θ_{13} fits essentially unaffected ($\varepsilon_{ee}^m, \varepsilon_{\mu\mu}^m, \varepsilon_{\mu\tau}^m, \varepsilon_{\tau\tau}^m$) or are already strongly constrained ($\varepsilon_{e\mu}^m$). For ε^s and ε^d we only show results for T2K and Double Chooz, but we have checked that the corresponding plots for NO ν A and DC-200 are similar, with somewhat smaller error bars. For $\varepsilon_{e\tau}^m$, we show results for both combinations of experiments because the sensitivity to matter effects is much better in NO ν A than in T2K due to the longer baseline.

By comparing figs. 4.6 – 4.8 with table 4.2, we can easily check, that our expectations for the impact of the different NSI parameters on the $\nu_\mu \rightarrow \nu_e$ channel, and thus on the θ_{13} fits, are confirmed. A particularly interesting situation arises for $\varepsilon_{\tau e}^d$, because this parameter has a sizeable effect on both, the reactor experiment and the superbeam. It is especially dangerous, because it induces a similar offset in both fits, and also gives a low χ^2 in both of them. This means that one would find perfectly consistent values for θ_{13} , which might, however, be far away from the true value. Other NSI parameters, in particular $\varepsilon_{e\tau}^m$, may lead to seemingly conflicting results, represented in our plots by best fit points far from the diagonal. Note that, in some cases, NO ν A and T2K might even erroneously report a θ_{13} value above the CHOOZ bound.

Let us now drop the assumption that only one non-standard parameter is non-zero. Since it is impossible to visualise the emerging high-dimensional parameter space, we resort to the scatter plots shown in fig. 4.9. Each point in these plots was computed by choosing a random set of NSI parameters and then determining the impact of this parameter combination on the θ_{13} fits in the same way as above. Only $(V-A)(V-A)$ operators were considered, i.e. $\varepsilon_{\alpha\beta}^s = (\varepsilon_{\beta\alpha}^d)^*$ was assumed (see eq. (4.17)). The moduli of the $\varepsilon_{\alpha\beta}^{s,m}$ were randomly chosen on a logarithmic scale between 10^{-5} and the respective current upper limits from sec. 4.1.3. The phases are distributed linearly between 0 and 2π . We see that there are again points representing a clear discrepancy between the standard oscillation θ_{13} fits of the reactor and superbeam experiments, and others which correspond to a common offset of the fit value. The colour coding shows that, for some fraction of the parameter space, the non-standard effect can actually be discovered, as

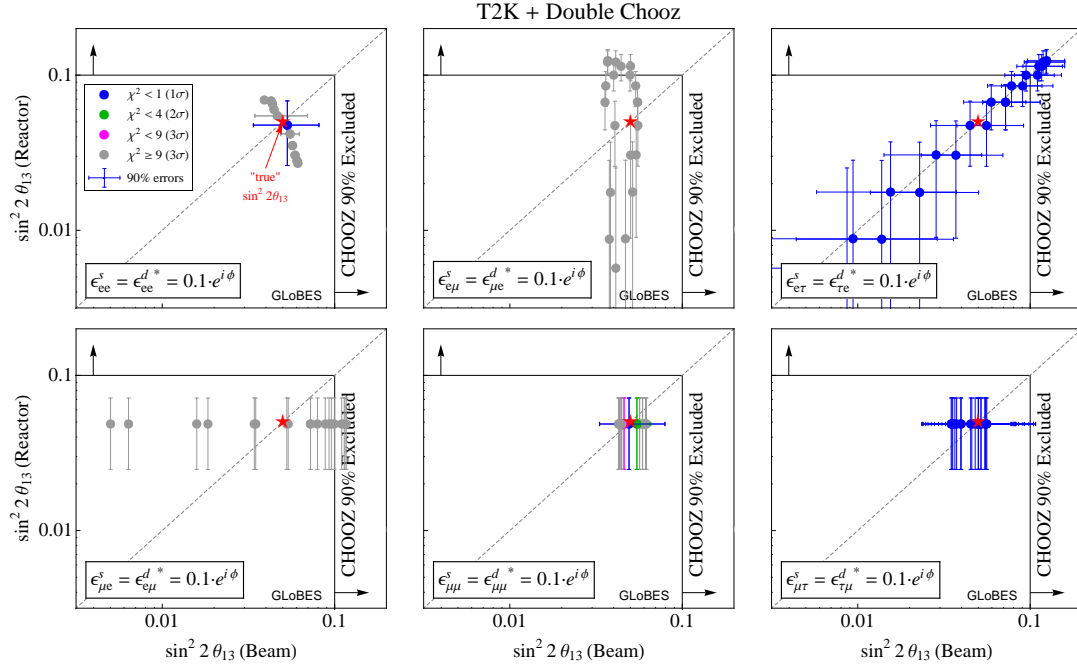


Figure 4.6: Impact of $(V-A)(V-A)$ type charged current NSI (fulfilling $\varepsilon_{\alpha\beta}^s = (\varepsilon_{\beta\alpha}^d)^*$) on naive standard oscillation fits in T2K and Double Chooz. For each NSI parameter, $|\varepsilon|$ was chosen at the current upper limit, and $\arg(\varepsilon)$ was varied in the interval $[0, 2\pi]$. The colour of the dots indicates the resulting χ^2 values in a fit assuming $\varepsilon = 0$, and the error bars indicate the 90% confidence intervals obtained for θ_{13} . The red star shows the assumed “true” θ_{13} .

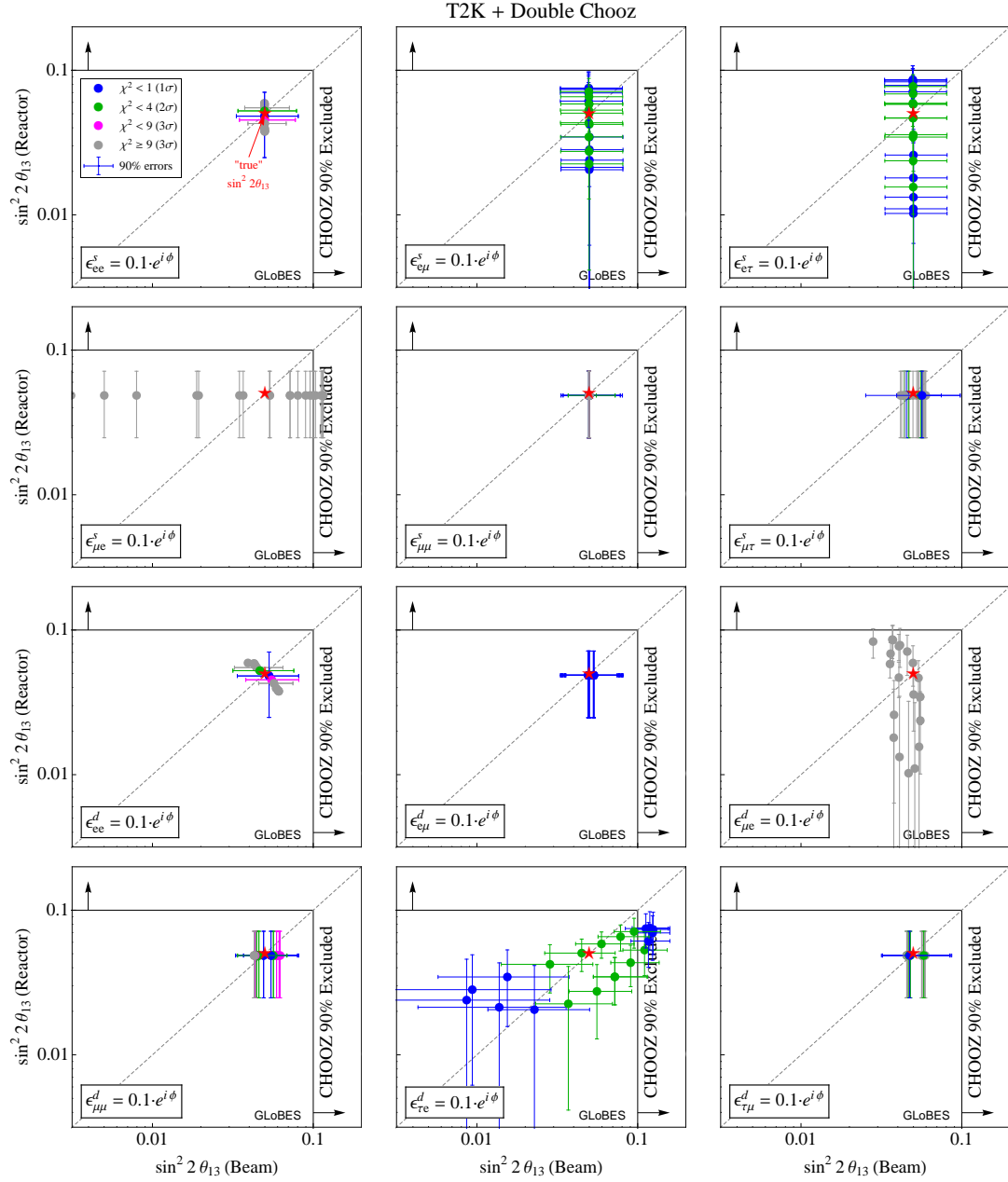


Figure 4.7: Impact of arbitrary charged current non-standard interactions (ϵ^s and ϵ^d treated as independent matrices) on naive standard oscillation fits in T2K and Double Chooz. Plots similar to fig. 4.6.

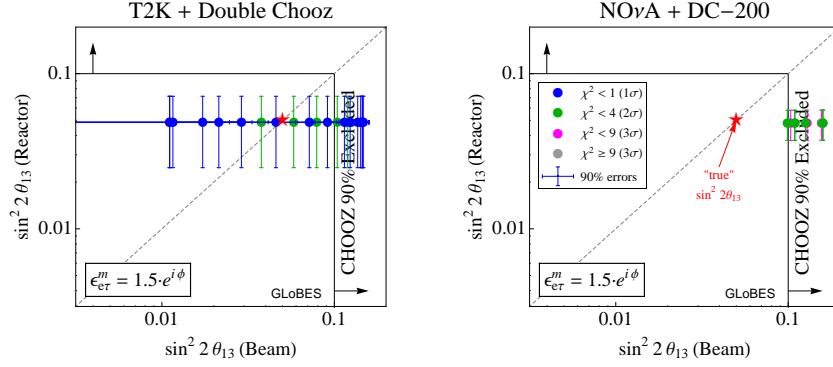


Figure 4.8: Impact of non-standard matter effects proportional to $\varepsilon_{e\tau}^m$ on naive standard oscillation fits in T2K, Double Chooz, NO ν A and DC-200. Plots similar to fig. 4.6.

one should expect from fig. 4.4. It is interesting to observe that there are some points for which the reactor fit lies above the CHOOZ bound. This indicates that already with the presently available data, the corresponding combination of NSI parameters and $\theta_{13}^{\text{true}}$ could be excluded. Let us, however, also emphasise that the majority of our random NSI scenarios leads to fit points very close to the “true” value.

4.3 Non-standard interactions in a neutrino factory

Depending on the findings of upcoming reactor and superbeam neutrino oscillation experiments, the further route in precision neutrino physics may very well lead to the construction of a neutrino factory. As we have mentioned in sec. 2.3, such a device has an extremely good sensitivity to the standard oscillation parameters θ_{23} , Δm_{31}^2 , θ_{13} and δ_{CP} . It is therefore natural to ask how sensitive it is to non-standard effects, such as NSI. This question has been addressed previously by many authors [130, 161–168, 179], and it has been shown that a neutrino factory can, for favourable values of the complex phases, probe some of the ε parameters to the level of 10^{-3} [165], which corresponds to a new physics scale $M_{\text{NSI}} \sim 2.5$ TeV according to the estimate (4.7). If no NSI are detected, the sensitivity limits for some NSI couplings can be improved to less than $10^{-2} - 10^{-1}$, i.e. M_{NSI} of the order of several hundred GeV [165, 167].

Here, we are going to study the optimisation of a neutrino factory experiment for constraining non-standard interactions. In particular we will determine the optimum parent muon energy and optimal detector baselines. We will only consider non-standard matter effects, parameterised by $\varepsilon_{\alpha\beta}^m$, because these effects can be probed *only* by a neutrino factory with its long baseline and high neutrino energy. Moreover, we expect that, in the long run, limits on most charged current effects will be more efficiently improved by other experiments, such as short baseline neutrino scattering experiments, experiments on charged lepton flavour violation, or the LHC. Also a neutrino factory near

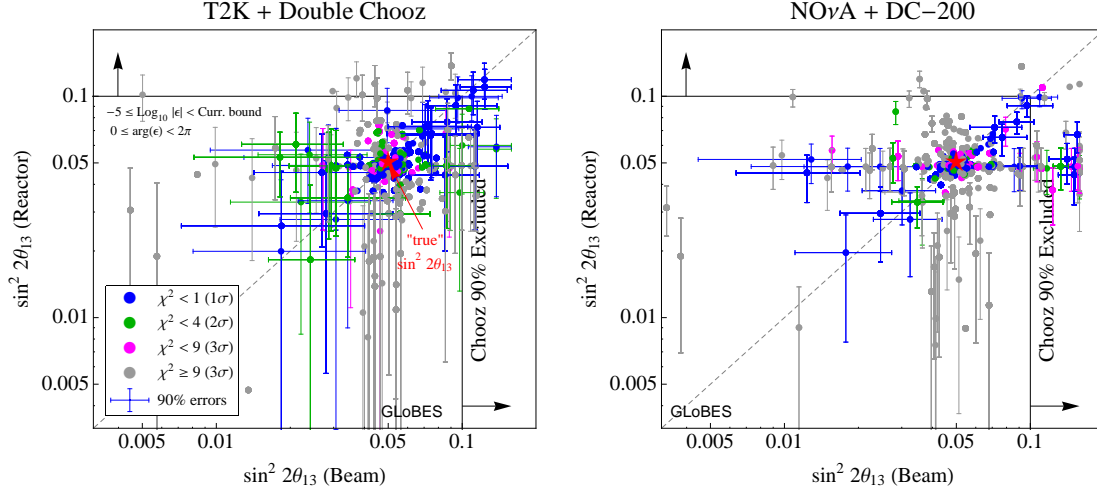


Figure 4.9: Possible outcomes of naive standard oscillation fits to reactor and superbeam data taken in the presence of combinations of several NSI. For each plot, 3000 random sets of NSI parameters were generated, with the moduli of the $\varepsilon_{\alpha\beta}^{s,m}$ being distributed logarithmically between 10^{-5} and their current upper bounds, and the phases distributed linearly between 0 and 2π . Only $(V-A)(V-A)$ operators are considered, i.e. $\varepsilon_{\alpha\beta}^s = (\varepsilon_{\beta\alpha}^d)^*$ is assumed. The colour of the dots indicates the minimum χ^2 obtained in fits assuming no NSI, and the error bars indicate the 90% confidence intervals for θ_{13} deduced from these fits. In order to improve the clarity of the plots, we show error bars only for fit points far from the “true” value. The figure shows that large NSI could induce ostensible discrepancies between reactor and superbeam data (off-diagonal points), or common offsets (close-to-diagonal points far from the “true” value), which would lead to consistent, but wrong results.

NSI	Neutrino factory		
	$\nu_e \rightarrow \nu_\mu$ ("golden")	$\nu_\mu \rightarrow \nu_\mu$ ("disappearance")	$\nu_e \rightarrow \nu_\tau$ ("silver")
None	s_{13}^2	1	s_{13}^2
ε_{ee}^m	εs_{13}^2	εs_{13}^2	εs_{13}^2
$\varepsilon_{e\mu}^m$	$\varepsilon s_{13} + \varepsilon^2$	εs_{13}	$\varepsilon s_{13} + \varepsilon^2$
$\varepsilon_{e\tau}^m$	$\varepsilon s_{13} + \varepsilon^2$	εs_{13}	$\varepsilon s_{13} + \varepsilon^2$
$\varepsilon_{\mu\mu}^m$	εs_{13}^2	ε	εs_{13}^2
$\varepsilon_{\mu\tau}^m$	εs_{13}^2	ε	εs_{13}^2
$\varepsilon_{\tau\tau}^m$	εs_{13}^2	ε	εs_{13}^2

Table 4.3: Classification of non-standard interactions according to their expected impact on the oscillation probability for the different oscillation channels observable in a neutrino factory. For each NSI coupling, only the leading order effect is shown.

detector can contribute significantly, but the optimisation of this detector will be mainly a technological problem, and is therefore far beyond the scope of our more theoretical study.

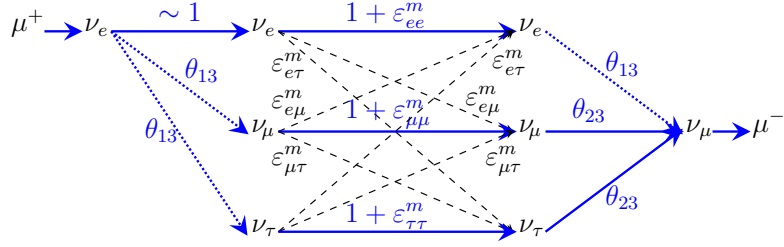
4.3.1 Theoretical expectations

As in sec. 4.2, let us begin by formulating our theoretical expectations for the impact of different non-standard terms on the neutrino factory experiment. By considering fig. 4.10 and table 4.3, we see that the dominant effect in the “golden channel” $\nu_e \rightarrow \nu_\mu$ and in the “silver channel” $\nu_e \rightarrow \nu_\tau$ comes from terms proportional to $\varepsilon_{e\mu}^m$ and $\varepsilon_{e\tau}^m$, while the disappearance channel is most strongly affected by NSI in the μ - τ sector, i.e. by terms proportional to $\varepsilon_{\mu\mu}^m$, $\varepsilon_{\mu\tau}^m$ or $\varepsilon_{\tau\tau}^m$.

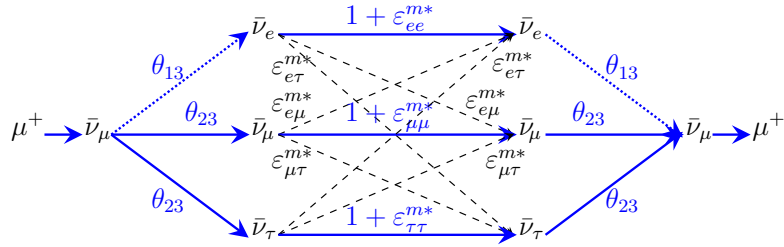
It would, however, be premature to draw conclusions on the NSI sensitivities of a neutrino factory from the suppression factors listed in table 4.3. In particular, we will see below that correlations between different parameters can greatly reduce the achievable sensitivities. Moreover, at long baselines, also subdominant effects can lead to appreciable shifts of the oscillation phase. Finally, the MSW enhancement can partly compensate for the smallness of θ_{13} .

4.3.2 Simulation of a neutrino factory

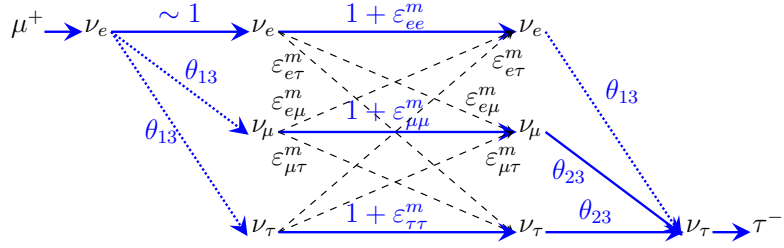
The starting point for our optimisation study will be the neutrino factory setup considered by the International Design Study for the Neutrino Factory (IDS-NF) [19, 76]. Within the International Scoping Study of a Future Neutrino Factory and Superbeam Facility [19, 81], this setup has been optimised for the measurement of $\sin^2 2\theta_{13}$, the neutrino mass hierarchy and leptonic CP violation in the case of standard three-flavour oscillations. For these performance indicators, the optimum configuration was deter-



(a)



(b)



(c)

Figure 4.10: Impact of ϵ^m on the event rate in the neutrino factory golden channel (a), in the disappearance channel (b) and in the silver channel (c). Note the similarity of (b) to fig. 4.3b. The meaning of the colours and line styles is the same as in figs. 4.1 – 4.3.

mined to be a 25 GeV muon storage ring, capable of delivering $2.5 \cdot 10^{21}$ useful muon decays (i.e. muons decaying in that section of the ring which is pointing towards the detector) and $2.5 \cdot 10^{21}$ useful antimuon decays during its total operating time. The IDS-NF setup involves two identical 50 kt magnetised iron detectors, one of them at a baseline $L_1 \sim 3\,000 - 5\,000$ km, and the other at $L_2 \sim 7\,000 - 8\,000$ km (i.e. close to the “magic baseline” [192]). For definiteness, we choose $L_1 = 4\,000$ km and $L_2 = 7\,500$ km. In addition, the IDS-NF neutrino factory features a 10 kt emulsion cloud chamber (“silver channel detector”), placed at the shorter baseline L_1 , to detect ν_τ interactions. In this work, we will also consider a hypothetical, improved silver channel detector dubbed “Silver*”, which features five times the signal and three times the background of the detector proposed by the IDS-NF. This corresponds to a situation where hadronic τ decays can be reconstructed and used in the analysis [81]. In some cases, we will also omit the silver channel detector altogether because we will show that it does not significantly improve the sensitivity of the experiment, neither to standard physics nor to NSI. In our simulations, the detector resolutions, efficiencies and systematical errors follow [76, 193]. As discussed above, we exclude the near detector from our optimisation study, and therefore do not simulate it explicitly. However, we include its capability of normalising the unoscillated neutrino flux by assuming appropriately small values for the systematical uncertainties on that flux. In summary, we include the following oscillation channels:

1. $\nu_e \rightarrow \nu_\mu$ at 4 000 km (ν_μ appearance, “golden” channel)
2. $\bar{\nu}_e \rightarrow \bar{\nu}_\mu$ at 4 000 km ($\bar{\nu}_\mu$ appearance, “golden” channel)
3. $\nu_e \rightarrow \nu_\mu$ at 7 500 km (ν_μ appearance, “golden” channel)
4. $\bar{\nu}_e \rightarrow \bar{\nu}_\mu$ at 7 500 km ($\bar{\nu}_\mu$ appearance, “golden” channel)
5. $\nu_\mu + \bar{\nu}_e \rightarrow \nu_\mu + \bar{\nu}_\mu$ at 4 000 km (ν_μ disappearance)
6. $\bar{\nu}_\mu + \nu_e \rightarrow \bar{\nu}_\mu + \nu_\mu$ at 4 000 km ($\bar{\nu}_\mu$ disappearance)
7. $\nu_\mu + \bar{\nu}_e \rightarrow \nu_\mu + \bar{\nu}_\mu$ at 7 500 km (ν_μ disappearance)
8. $\bar{\nu}_\mu + \nu_e \rightarrow \bar{\nu}_\mu + \nu_\mu$ at 7 500 km ($\bar{\nu}_\mu$ disappearance)
9. $\nu_e \rightarrow \nu_\tau$ at 4 000 km (ν_τ appearance, “silver” channel)

Note that we do not require charge identification in the disappearance channel (i.e. we add the ν_μ and $\bar{\nu}_\mu$ event rates) because it has been demonstrated in [81] that the better efficiencies and better energy threshold in this case lead to a better performance. The “wrong sign muon” contribution from $\nu_e \rightarrow \nu_\mu$ oscillations is small anyway if θ_{13} is small. We do not consider the $\bar{\nu}_e \rightarrow \bar{\nu}_\tau$ channel because we are not aware of any efficiency and background estimates for $\bar{\nu}_\tau$ detection. For ν_τ interactions, the detector performance is based on the experience from the OPERA experiment [193, 194], which, however, was so far exposed only to a neutrino beam, but never to anti-neutrinos.

As in sec. 4.2, all numerical simulations have been performed using **GLOBES** [181,182], with the experiment description files being based on refs. [76,81,184,187,188]. The matter density profile along the neutrino trajectory is approximated by a single layer of constant density for neutrinos that do not cross the core of the Earth, and by three layers of constant density for core-crossing neutrinos (baseline $L > 10\,673$ km). The density within each layer is computed by averaging the PREM profile (Preliminary Reference Earth Model) [195] along the neutrino trajectory. Using appropriate pull terms in eq. (4.19), we allow for a 5% systematical bias on the matter density [196,197], and we assume this bias to be the same for detectors operated at the same baseline, but uncorrelated between different baselines. For the “true” standard oscillation parameters with the exception of θ_{13} , and for their external errors, we assume the same values as in the superbeam case (see eq. (4.18)) unless stated otherwise. For θ_{13} , we use the smaller value $\sin^2 2\theta_{13}^{\text{true}} = 0.001$ because small θ_{13} constitutes the strongest physics case for a neutrino factory. To analyse the simulated data, we proceed in the same way as in sec. 4.2. In those cases where NSI parameters are marginalised over in the fit, we include these parameters also in the initial scan of the χ^2 manifold (in addition to θ_{13} and δ_{CP}) in order to ensure that all non-standard degeneracies are found. As in sec. 4.2, the preliminary scan is performed without taking into account systematical uncertainties and correlations with the solar parameters. Correlations with θ_{23} and Δm_{31}^2 are included only when computing θ_{13} sensitivities.

To quantitatively assess the physics potential of the neutrino factory, we define the following performance indicators

- **Sensitivity to $\sin^2 2\theta_{13}$ (5σ):** This is the bound that the neutrino factory can set on $\sin^2 2\theta_{13}$ if the true value is zero. In other words, it is the maximum $\sin^2 2\theta_{13}$ that is still able to provide an acceptable fit to data taken at $\sin^2 2\theta_{13}^{\text{true}} = 0$.
- **Sensitivity to normal mass hierarchy (5σ) for $\delta_{\text{CP}}^{\text{true}} = 3\pi/2$:** This is defined as the largest $\sin^2 2\theta_{13}^{\text{true}}$ for which a 5σ determination of the mass hierarchy is no longer possible if the true mass hierarchy is to be normal. The choice of $\delta_{\text{CP}}^{\text{true}} = 3\pi/2$ corresponds to a conservative assumption because at most other values of the CP phase, degeneracies have a weaker impact.
- **Sensitivity to maximal CP violation $\delta_{\text{CP}}^{\text{true}} = 3\pi/2$ (5σ):** This performance indicator gives the largest $\sin^2 2\theta_{13}^{\text{true}}$ for which $\delta_{\text{CP}}^{\text{true}} = 3\pi/2$ can no longer be distinguished from the CP conserving cases $\delta_{\text{CP}} = 0, \pi$.
- **Sensitivity to $|\varepsilon_{e\tau}^m|$ (3σ):** In analogy to the $\sin^2 2\theta_{13}$ sensitivity defined above, the sensitivity to $|\varepsilon_{e\tau}^m|$ is the bound that the experiment can set on $|\varepsilon_{e\tau}^m|$ provided that the true value is zero. In the fit, the phase of $\varepsilon_{e\tau}^m$ as well as all standard oscillation parameters and systematical biases are marginalised over, but the other NSI parameters are kept fixed at zero. The last simplification, which greatly reduces the numerical effort, is justified for the following reasons:

- Correlations between $\varepsilon_{e\tau}^m$ and ε_{ee}^m are equivalent to correlations with the matter density, which are implemented in our simulations anyway.
- Correlations between $\varepsilon_{e\tau}^m$ and $\varepsilon_{e\mu}^m$ are unimportant due to the strong constraint $\varepsilon_{e\mu}^m \lesssim 0.0023$.
- Correlations between $\varepsilon_{e\tau}^m$ and the μ - τ sector ($\varepsilon_{\mu\mu}^m$, $\varepsilon_{\mu\tau}^m$, $\varepsilon_{\tau\tau}^m$) are absent because $\varepsilon_{e\tau}^m$ affects mainly the appearance channel, while $\varepsilon_{\mu\mu}^m$, $\varepsilon_{\mu\tau}^m$ and $\varepsilon_{\tau\tau}^m$ are most relevant in the disappearance channel (cf. table 4.3). For the $\varepsilon_{e\tau}^m$ - $\varepsilon_{\tau\tau}^m$ correlation, this has explicitly been demonstrated numerically in [167].
- **Sensitivity to $|\varepsilon_{\mu\tau}^m|$ (3σ):** This is defined in the same way as the $|\varepsilon_{e\tau}^m|$ sensitivity; again, we do not marginalise over NSI parameters (except for $\arg(\varepsilon_{\mu\tau}^m)$), because the above arguments show that correlations with ε_{ee}^m , $\varepsilon_{e\mu}^m$ and $\varepsilon_{e\tau}^m$ are negligible, and we have checked numerically that this is also true for correlations with $\varepsilon_{\mu\mu}^m$ and $\varepsilon_{\tau\tau}^m$.
- **Sensitivity to $|\varepsilon_{\tau\tau}^m|$ (3σ):** The definition is again analogous to the definition of the other NSI sensitivities, but here, correlations between $\varepsilon_{\mu\mu}^m$ and $\varepsilon_{\tau\tau}^m$ have to be taken into account, because eq. (C.8) shows that, to leading order, the neutrino factory is sensitive only to the combination $\varepsilon_{\mu\mu}^m - \varepsilon_{\tau\tau}^m$. All other correlations are, as before, irrelevant.

We do not consider the sensitivity to ε_{ee}^m because this parameter is directly correlated with the matter density [167], the sensitivity to which has been studied in great detail in the literature [198–200]. We also neglect the sensitivity to $\varepsilon_{e\mu}^m$, which is already strongly constrained, and the sensitivity to $\varepsilon_{\mu\mu}^m$, which will be similar to the $\varepsilon_{\tau\tau}^m$ sensitivity due to the strong correlation between these two parameters.

4.3.3 Optimisation of the parent muon energy

The first important parameter of a neutrino factory is the energy E_μ of the parent muons, which also determines the maximum neutrino energy. In fig. 4.11, we show the dependence of the 3σ sensitivity to $|\varepsilon_{e\tau}^m|$, $|\varepsilon_{\mu\tau}^m|$ and $|\varepsilon_{\tau\tau}^m|$ as a function of E_μ , with all other experimental parameters (baselines, efficiencies, etc.) fixed at the values proposed in [19]. We show results for two different combinations of $\sin^2 2\theta_{13}$ and δ_{CP} , both with and without inclusion of the Silver resp. Silver* detector at $L_{\text{Silver}} = 4000$ km. The plots reveal that, for $E_\mu \gtrsim 25$ GeV, the NSI sensitivity becomes almost independent of E_μ . The reason for this is that above the matter resonance oscillations are suppressed, so no improvement of the sensitivity is expected from that region. On the other hand, E_μ should not be lower than the 25 GeV proposed in the IDS-NF setup, because this would lead to a severe loss of sensitivity. A comparison of the two panels of fig. 4.11 shows that there is virtually no dependence of the NSI sensitivity on $\sin^2 2\theta_{13}$ and δ_{CP} . The plots also show that the sensitivities to $|\varepsilon_{\mu\tau}^m|$ and $|\varepsilon_{\tau\tau}^m|$ do not benefit at all from the inclusion of a silver channel detector, and that the improvement in the sensitivity to $|\varepsilon_{e\tau}^m|$ is rather small, and only visible at high energies. We have checked that this conclusion holds also

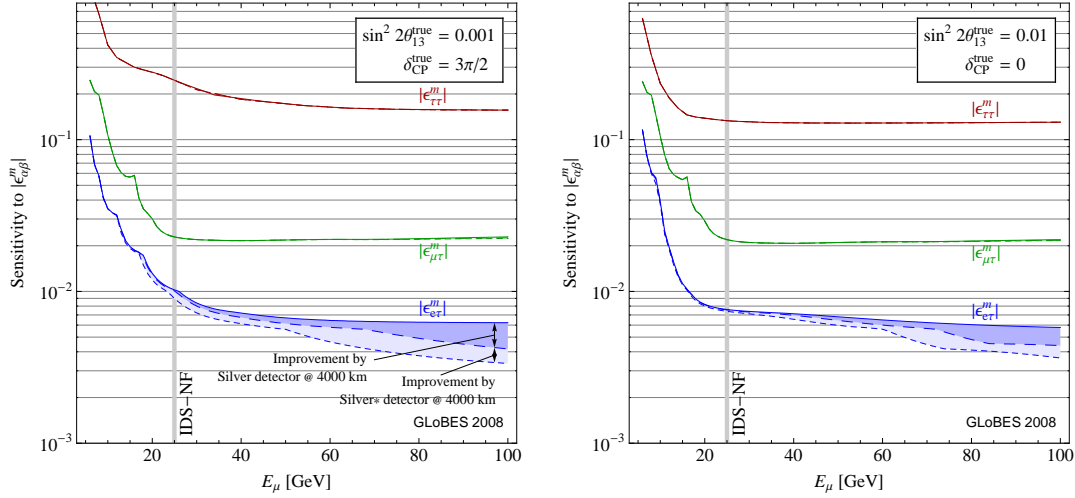


Figure 4.11: NSI sensitivity (3σ) of a neutrino factory as a function of the parent muon energy E_μ for two different combination of $\theta_{13}^{\text{true}}$ and $\delta_{\text{CP}}^{\text{true}}$. Two 50 kt magnetised iron detectors were simulated at baselines of 4000 km and 7500 km, respectively, and for the long- and short-dashed curves also a Silver resp. Silver* detector was added at 4000 km.

when the silver channel detector is placed at a different baseline. In fact, ref [167] shows that $L_{\text{Silver}} \sim 4000$ km was already the optimal choice.

4.3.4 Baseline optimisation

Let us now determine the optimum baselines L_1 and L_2 for the two golden channel detectors included in the IDS-NF setup. To this end, we study the behaviour of the performance indicators introduced in sec. 4.3.2 as functions of L_1 and L_2 . All other experimental parameters are fixed at the values chosen for the IDS-NF setup. The silver channel detector is omitted in this section because we have checked that it does not improve the results significantly.

In fig. 4.12, we analyse the dependence of the standard oscillation performance indicators ($\sin^2 2\theta_{13}$ sensitivity, sensitivity to the normal mass hierarchy, sensitivity to maximal CP violation $\delta_{\text{CP}}^{\text{true}} = 3\pi/2$) on L_1 and L_2 . The indicated threshold values have been chosen in such a way that the resulting contours enclose approximately equal areas. The lower right panel shows the overall optimum region, which is obtained as the intersection of the optimum regions from the other three panels. We have computed results both for a standard fit, in which all NSI parameters are kept fixed at zero (shaded regions), and for an extended fit, in which $|\varepsilon_{e\tau}^m|$ and $\arg(\varepsilon_{e\tau}^m)$ are marginalised over (dotted contours).

Both for the standard and for the non-standard fit, we find that the sensitivity to $\sin^2 2\theta_{13}$ is best if one of the two baselines is close to the “magic baseline” [192], because there, parameter degeneracies can most easily be resolved. This is in agreement with

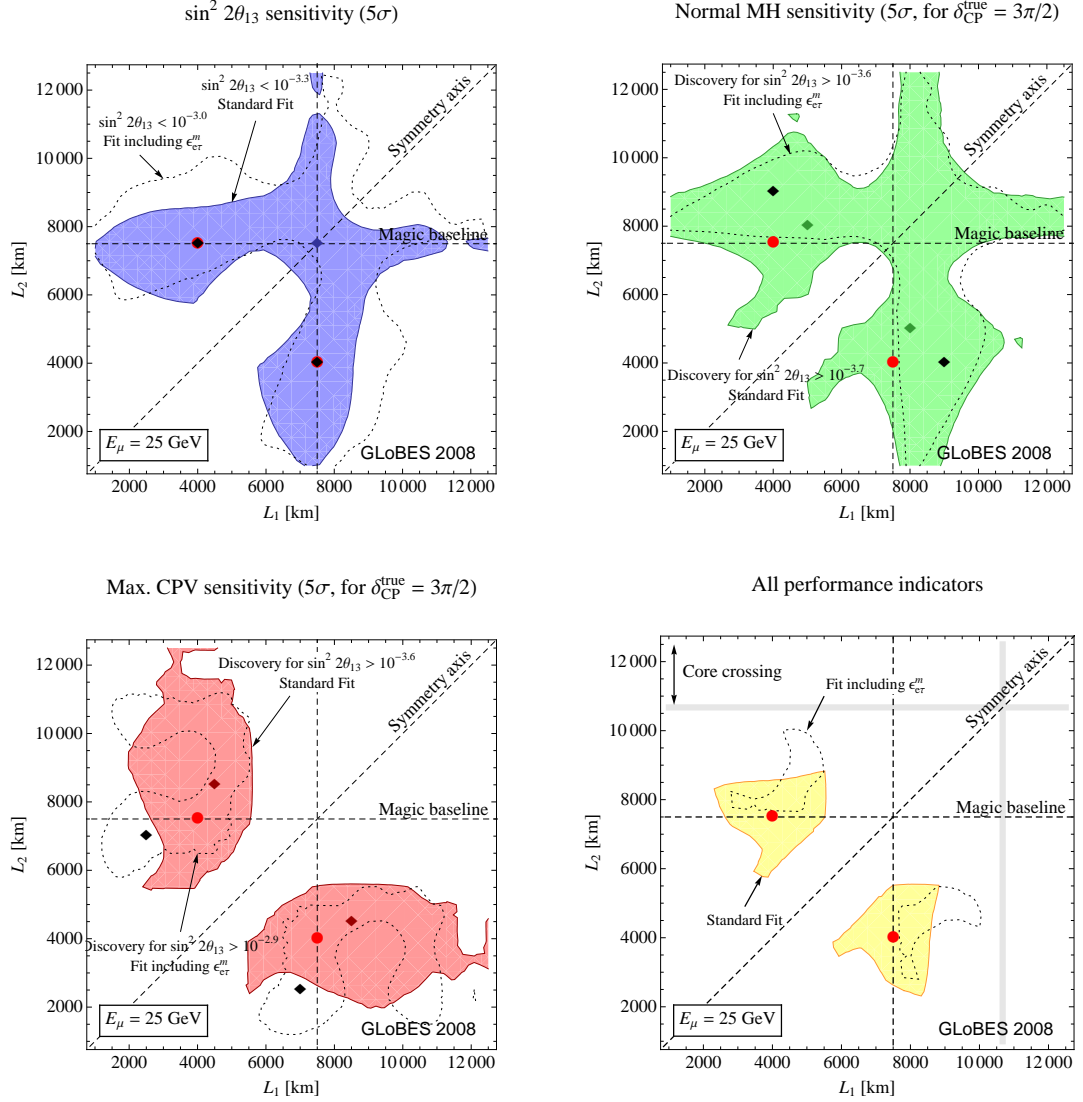


Figure 4.12: Baseline optimisation for a neutrino factory with two golden channel detectors with respect to standard oscillation performance indicators. The shaded regions indicate those combinations of L_1 and L_2 for which the 5σ sensitivity to $\sin^2 2\theta_{13}$ is better than $10^{-3.3}$ (upper left panel), a 5σ discovery of the normal mass hierarchy (MH) is possible for all $\sin^2 2\theta_{13} \geq 10^{-3.7}$ (upper right panel), and a 5σ discovery of maximal CP violation $\delta_{\text{CP}}^{\text{true}} = 3\pi/2$ is possible for all $\sin^2 2\theta_{13} \geq 10^{-3.6}$ (lower left panel). The intersection of these regions is depicted in orange in the lower right panel. We also show the optimum regions for a fit which includes marginalisation over ϵ_{er}^m , with the true ϵ_{er}^m assumed to vanish (dotted contours). The diamonds mark the setups with the best sensitivities (coloured for the standard fit, black for the fit including ϵ_{er}^m), and the red circles represent the IDS-NF setup with $L_1 = 4000$ km and $L_2 = 7500$ km.

fig. 1 from ref. [192], which is similar to the upper left panel of our fig. 4.12. Similarly, also the sensitivity to the normal mass hierarchy is best if either L_1 or L_2 is “magic”. For good sensitivity to maximal CP violation, it is crucial that one baseline be short (2 000 – 5 000 km) because in this region, the dependence of the oscillation probability on δ_{CP} is strongest (this can be seen from the third and fourth lines of eq. (C.6)). On the other hand, the second baseline should be larger in order to resolve degeneracies. In particular, scenarios with $L_1 = L_2$ are undesirable if CP violation is to be measured. Combining the above considerations, the lower right panel of fig 4.12 shows that the IDS-NF setup with $L_1 = 4\,000$ km, $L_2 = 7\,500$ km (marked by the red circle) provides close to optimum sensitivity to all three standard physics observables studied here. This conclusion holds independent of whether $\varepsilon_{e\tau}^m$ is included in the fit or not. Thus, even though marginalisation over NSI parameters can reduce the sensitivity of a neutrino factory [163, 179], the optimisation of L_1 and L_2 remains unaffected. We have checked that this is also true if one of the other $\varepsilon_{\alpha\beta}^m$ is marginalised over. The parameters $\varepsilon_{\mu\mu}^m$, $\varepsilon_{\mu\tau}^m$ or $\varepsilon_{\tau\tau}^m$ do not affect the sensitivities to $\sin^2 2\theta_{13}$, the normal mass hierarchy and maximal CP violation at all because they are subdominant in the appearance channel, on which these performance indicators mainly depend. The effect of including $\varepsilon_{e\mu}^m$ in the fit is qualitatively similar to the effect of including $\varepsilon_{e\tau}^m$.

Next, we address the question whether the the combination $L_1 = 4\,000$ km, $L_2 = 7\,500$ km is also optimal with respect to the non-standard performance indicators. Therefore, we plot in fig. 4.13 the 3σ sensitivities to $|\varepsilon_{e\tau}^m|$ (upper row), $|\varepsilon_{\mu\tau}^m|$ (middle row) and $|\varepsilon_{\tau\tau}^m|$ (bottom row) as functions of L_1 and L_2 . The left column of plots is for a parent muon energy $E_\mu = 25$ GeV (as in the IDS-NF setup), while the right column is for $E_\mu = 50$ GeV. We see that the sensitivity to $|\varepsilon_{e\tau}^m|$ is close to optimal at $L_1 = 4\,000$ km, $L_2 = 7\,500$ km at $E_\mu = 25$ GeV, while for larger E_μ , longer baselines are preferable. For $|\varepsilon_{\mu\tau}^m|$ and $|\varepsilon_{\tau\tau}^m|$, the baselines should always be as long as possible. However, the decrease in sensitivity at $L_1 = 4\,000$ km, $L_2 = 7\,500$ km compared to the optimum value is not dramatic, so we conclude that the IDS-NF baselines are satisfactory also for constraining non-standard interactions.

4.3.5 Summary of neutrino factory optimisation for non-standard interactions

In summary, we have found the following (see also table 4.4 and fig. 4.14):

- The neutrino factory has excellent and highly competitive sensitivity to standard oscillation observables (θ_{13} , mass hierarchy, CP violation), as well as to the NSI parameters $\varepsilon_{e\tau}^m$ and $\varepsilon_{\mu\tau}^m$. The sensitivity to $\varepsilon_{\mu\mu}^m$ and $\varepsilon_{\tau\tau}^m$ is limited by the mutual correlation of these two parameters. The bound on $\varepsilon_{e\mu}^m$ is already strong, and can therefore not be improved significantly by the neutrino factory. The sensitivity to ε_{ee}^m is competitive, but is limited by the correlation with the matter density uncertainty.
- The optimal muon energy is $E_\mu = 25$ GeV. Lower energies would greatly reduce

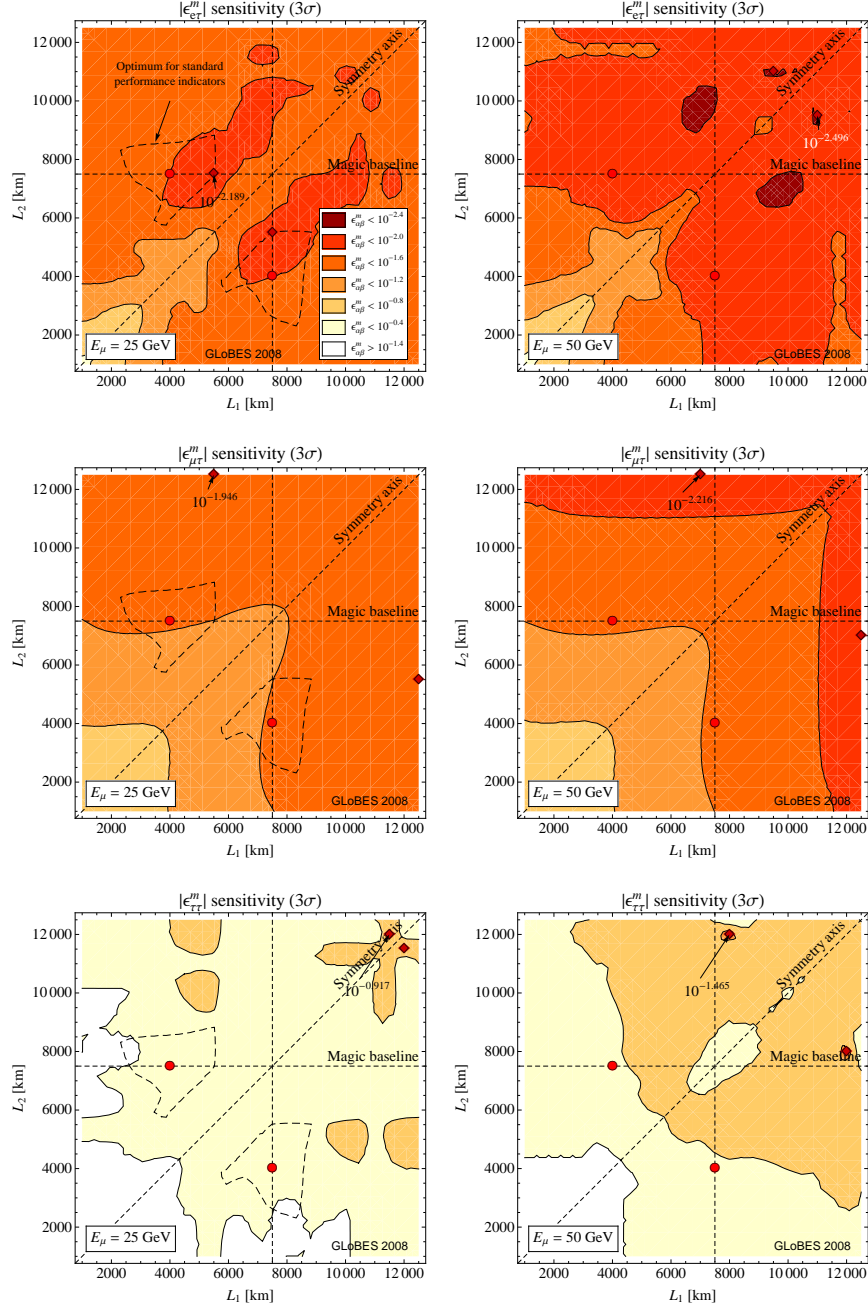


Figure 4.13: Sensitivities to $|\varepsilon_{e\tau}^m|$ (upper row), $|\varepsilon_{\mu\tau}^m|$ (middle row) and $|\varepsilon_{\tau\tau}^m|$ (bottom row) as functions of L_1 and L_2 in a neutrino factory with two golden channel detectors and with $E_\mu = 25$ GeV (left column) or $E_\mu = 50$ GeV (right column). The dashed contour is the optimum region for standard performance indicators, taken from the lower right panel of fig. 4.12. The dark diamonds represent the optimum points in each plot, and the red circles mark the IDS-NF scenario $L_1 = 4000$ km, $L_2 = 7500$ km.

the sensitivity, while higher energies are hardly beneficial.

- The optimum baseline combination is $L_1 = 4\,000$ km, $L_2 = 7\,500$ km, as proposed by the IDS-NF. Longer baselines would be favourable if strong emphasis were put on the sensitivities to $\varepsilon_{\mu\tau}^m$ and $\varepsilon_{\tau\tau}^m$, even at the cost of greatly reduced standard oscillation sensitivities.
- The silver channel detector does not help to improve the sensitivity of the neutrino factory, neither to standard oscillation observables, nor to ε^m .

One may ask whether other types of new physics could constitute a physics case for ν_τ detection at long baselines. One possibility are effects that directly influence ν_τ interactions, e.g. charged current NSI proportional to $\varepsilon_{\tau\tau}^d$. Non-standard effects in *oscillation* physics, however, will always contribute also to the much more easily accessible golden or disappearance channel because of strong μ - τ mixing. Recently, it has been shown that the $\nu_\mu \rightarrow \nu_\tau$ channel can help to resolve degeneracies in sterile neutrino models [169]. Another scenario that might justify the construction of a silver channel detector at a long baseline are unitarity studies. To test the unitarity of the leptonic mixing matrix, one could either measure the oscillation probabilities for several channels separately, and then form their sum, or one could study neutral current events. In the former case, the weakest link will most likely not be ν_τ detection, but ν_e detection, which is extremely difficult in a magnetised iron calorimeter, and has uncertainties on the level of a few per cent. This is comparable to the uncertainties of neutral currents events [201], so it is easier to use the latter for studying unitarity in neutrino oscillations. These considerations show that our conclusions regarding the silver channel detector apply not only to neutral current NSI, but also to many other new physics scenarios.

Performance indicator	90% C.L.	3σ C.L.	5σ C.L.
Standard oscillation physics			
$\sin^2 2\theta_{13}$	$4.8 \cdot 10^{-5}$	$1.41 \cdot 10^{-4}$	$3.56 \cdot 10^{-4}$
Normal hierarchy (for $\delta_{\text{CP}} = 3\pi/2$)	$2.01 \cdot 10^{-5}$	$5.82 \cdot 10^{-5}$	$1.31 \cdot 10^{-4}$
Max. CP violation ($\delta_{\text{CP}} = 3\pi/2$, NH)	$1.65 \cdot 10^{-5}$	$5.41 \cdot 10^{-5}$	$1.45 \cdot 10^{-4}$
Standard oscillation physics (fit including $\varepsilon_{e\tau}^m$)			
$\sin^2 2\theta_{13}$	$9.68 \cdot 10^{-5}$	$2.31 \cdot 10^{-4}$	$5.64 \cdot 10^{-4}$
Normal hierarchy (for $\delta_{\text{CP}} = 3\pi/2$)	$4.45 \cdot 10^{-5}$	$1.13 \cdot 10^{-4}$	$2.83 \cdot 10^{-4}$
Max. CP violation ($\delta_{\text{CP}} = 3\pi/2$, NH)	$5.52 \cdot 10^{-5}$	$1.63 \cdot 10^{-4}$	$7.09 \cdot 10^{-4}$
Sensitivities to non-standard interactions			
ε_{ee}^m	$[-1.3 \cdot 10^{-1},$ $1.19 \cdot 10^{-1}]$	$[-1.79,$ $2.17 \cdot 10^{-1}]$	$[-1.85,$ $3.72 \cdot 10^{-1}]$
$\varepsilon_{\mu\mu}^m$	$[-1.19 \cdot 10^{-1},$ $1.3 \cdot 10^{-1}]$	$[-2.17 \cdot 10^{-1},$ $2.42 \cdot 10^{-1}]$	$[-3.72 \cdot 10^{-1},$ $3.62 \cdot 10^{-1}]$
$\varepsilon_{\tau\tau}^m$	$[-1.22 \cdot 10^{-1},$ $1.33 \cdot 10^{-1}]$	$[-2.21 \cdot 10^{-1},$ $2.47 \cdot 10^{-1}]$	$[-3.76 \cdot 10^{-1},$ $3.65 \cdot 10^{-1}]$
$ \varepsilon_{e\mu}^m $	$3.37 \cdot 10^{-3}$	$5.67 \cdot 10^{-3}$	$7.72 \cdot 10^{-3}$
$ \varepsilon_{e\tau}^m $	$5.65 \cdot 10^{-3}$	$1.02 \cdot 10^{-2}$	$1.79 \cdot 10^{-2}$
$ \varepsilon_{\mu\tau}^m $	$1.81 \cdot 10^{-2}$	$2.29 \cdot 10^{-2}$	$3.37 \cdot 10^{-2}$

Table 4.4: Summary of the sensitivity of a neutrino factory ($L_1 = 4000$ km, $L_2 = 7500$ km, $E_\mu = 25$ GeV) to standard and non-standard observables. For the real diagonal entries of ε^m , we give the positive and negative limits separately. The true parameter values were assumed to be $\sin^2 2\theta_{13}^{\text{true}} = 0.001$ and $\delta_{\text{CP}}^{\text{true}} = 3\pi/2$. Note that especially the sensitivity to ε_{ee}^m depends on this choice.

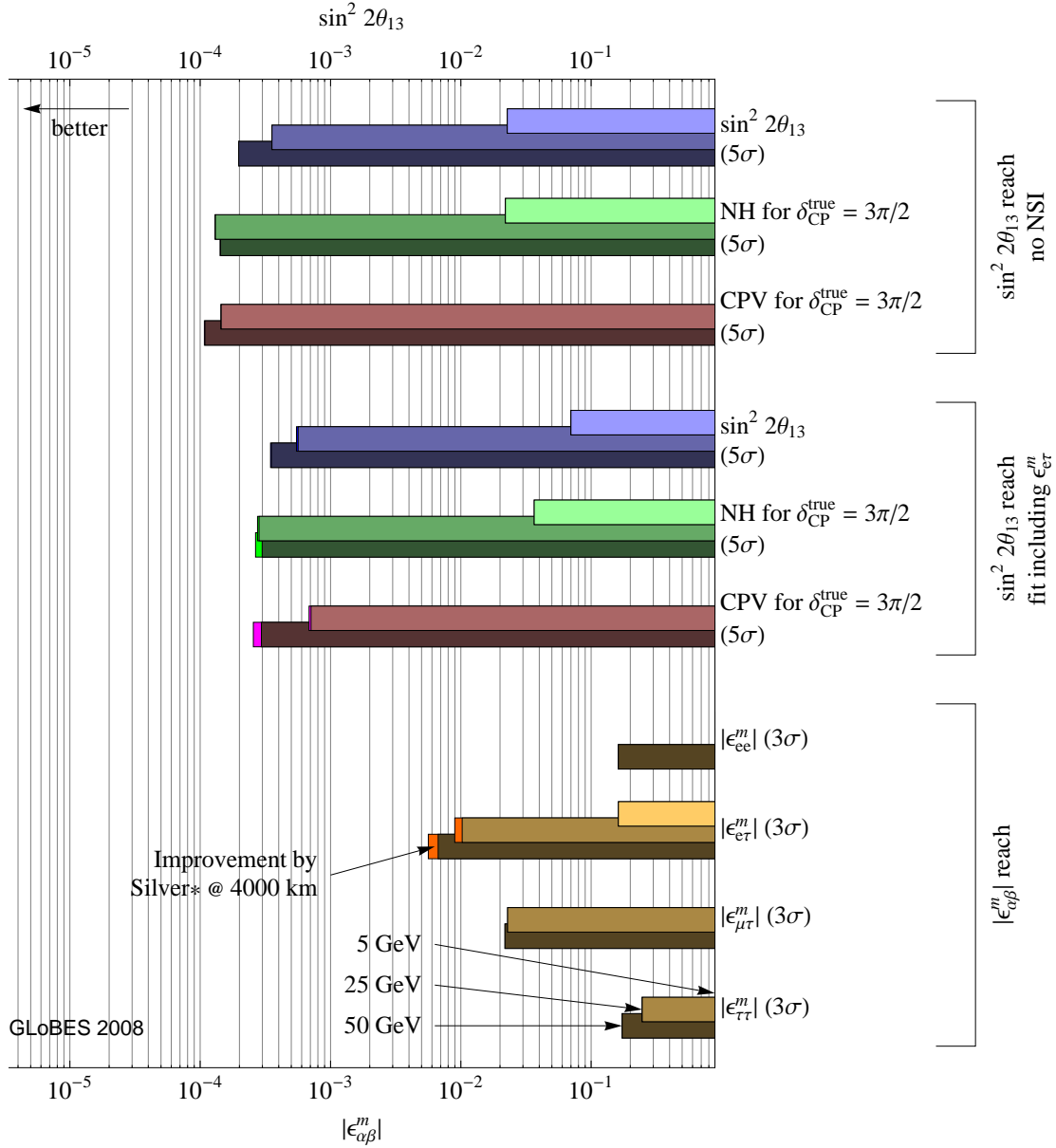


Figure 4.14: Summary of the neutrino factory performance with and without the presence of non-standard interactions. The IDS-NF setup with $L_1 = 4\,000$ km, $L_2 = 7\,500$ km was used, and the “true” parameter values $\sin^2 2\theta_{13}^{\text{true}} = 0.001$ and $\delta_{CP}^{\text{true}} = 3\pi/2$ were assumed. The plot shows that sensitivities are poor at $E_\mu = 5$ GeV (light bars), but increase dramatically at $E_\mu = 25$ GeV (medium light bars). The benefit from increasing E_μ further to 50 GeV (dark bars) is only marginal, as is the benefit from including a silver channel detector.

A conclusion is the place where you got tired of thinking.

Martin H. Fischer

5

Summary and conclusions

In this work, we have discussed two interesting new topics from neutrino physics: Mössbauer neutrinos and non-standard neutrino interactions (NSI).

After giving a brief introduction to the theoretical and experimental status of neutrino physics, we have described the Mössbauer neutrino experiment proposed by Raghavan [88, 89]. We have discussed the many technological challenges that this experiment would face, and have then turned to the interesting theoretical aspects of Mössbauer neutrinos. We have argued that, in spite of their near monochromaticity, Mössbauer neutrinos can oscillate because the momentum uncertainties of the source and of the detector are large enough to allow for the coherent production of different mass eigenstates. We have substantiated our arguments by detailed quantum mechanical and quantum field theoretical calculations. In QM, we have computed the flavour transition probability, first treating the neutrino as a Gaussian wave packet, and then as a Lorentzian wave packet. These results are applicable also to non-Mössbauer neutrino experiments if the parameters of the wave packets are chosen appropriately. We have then proceeded to the computation of the total rate of Mössbauer neutrino production, propagation and absorption in QFT, not making any assumptions on the wave function of the intermediate state neutrino, and using a well-established approximation for the wave functions of the external particles. We have paid special attention to a realistic description of inhomogeneous and homogeneous line broadening, and have shown that the expression for the transition rate is the same in both cases. Our approach yields the standard oscillation phase, a Breit-Wigner-like resonance term and the Lamb-Mössbauer factor, which describes the relative probability of recoil-free emissions and absorptions, compared to the total emission and absorption probability. Moreover, we have obtained terms enforcing localisation and coherence conditions, which are, however, easily fulfilled in realistic experiments. Our results show that, for Mössbauer neutrinos, the correct QM limit of QFT is provided by the formalism of Lorentzian wave packets. Finally, we have argued why the time energy uncertainty relation does not prevent oscillations of Mössbauer

neutrinos, contrary to a concern that has recently been raised by Bilenky et al. [96].

In the second part of this thesis, we have studied non-standard neutrino interactions. We have distinguished between charged current NSI, which affect the neutrino production and detection processes, and neutral current NSI, which are most relevant as non-standard matter effects in neutrino propagation over long distances. We have argued that the NSI formalism provides a convenient, model independent way of parameterising many types of new physics in the neutrino sector, and have classified the NSI operators according to their impact on upcoming reactor and superbeam experiments (table 4.2). We have performed numerical simulations using the GLoBES software [181, 182] to assess the NSI discovery reach of these experiments. We have found that NSI can only be detected if the corresponding coupling constants are close to their current upper bounds, which is, however, unlikely from the model-building point of view. However, if large NSI should exist, reactor and superbeam experiments could nicely complement one another because they are sensitive to different NSI operators. In some cases, a combined analysis is necessary for optimal sensitivity. Unfortunately, NSI may also have the effect of mimicking standard oscillations, which could lead to incorrect fit results for the standard oscillation parameters if NSI are not accounted for in the fit. Particularly dangerous are situations where the analyses of reactor and superbeam experiments are misguided in the same way (common offsets), while in the case where only one of them is misguided, or they are misguided in different ways, the arising discrepancies between their respective fits could reveal the presence of NSI.

We have then turned to a study of NSI in the context of a neutrino factory. We have considered non-standard matter effects induced by neutral current NSI, and have shown how a neutrino factory should be optimised in order to provide optimal sensitivity to both standard and non-standard observables. We have found that the setup considered by the International Design Study for the Neutrino Factory (IDS-NF), with a parent muon energy of 25 GeV and two 50 kt magnetised iron detectors at baselines $L_1 \sim 4\,000$ km and $L_2 \sim 7\,500$ km, is close to optimal. For some NSI operators, the sensitivity would increase if even larger baselines were chosen, but this increase does not countervail the simultaneous decrease of the sensitivity to standard oscillation observables such as θ_{13} , the neutrino mass hierarchy and CP violation. The IDS-NF setup can probe some NSI couplings even if they are a factor of $10^{-3} - 10^{-2}$ smaller than the standard weak couplings, and might thus be sensitive to TeV-scale new physics (cf. eq. (4.7)).

Both our discussion of Mössbauer neutrinos and our work on NSI show that neutrino physics is still an exciting subject. The theory of oscillations provides deep insights into the basics of quantum mechanics, and future experiments could have the potential to discover interesting new effects from beyond the Standard Model. Coming back to the verses with which we have prefaced this thesis, we can conclude that students working in neutrino physics certainly need not be pitied.

Acknowledgments

It is a pleasure to thank all those who have accompanied me on the long route to the completion of this work. First of all, I wish to express my deep gratitude to Prof. Dr. Manfred Lindner, who accepted me as a doctoral student in his group at the Max Planck Institute for Nuclear Physics, supervised me during the many interesting projects we carried out together, but nevertheless left me enough freedom to pursue own ideas as well. Moreover, he made it possible for me to attend international summer schools, workshops and conferences, to present my work and to meet colleagues from other institutions.

Physical research is most efficient and most fun when it is carried out in collaboration. I would therefore like to thank all those with whom I have worked together as a doctoral student: Evgeny Akhmedov and Manfred Lindner for the very fruitful collaboration on Mössbauer neutrinos, Patrick Huber, Alexander Merle, Manfred Lindner, Toshihiko Ota, Mark Rolinec, Joe Sato and Walter Winter for our joint works on future neutrino experiments and on non-standard neutrino interactions, Hendrik Kienert, Manfred Lindner and Alexander Merle for a very interesting project on the GSI anomaly, and Manfred Lindner, Viviana Niro and Tom Underwood for innumerable inspiring discussions on physics beyond the Standard Model.

I am especially grateful to Evgeny Akhmedov, Patrick Huber, Alexander Merle and Toshihiko Ota for proofreading parts of this manuscript and for making many useful comments.

Moreover, I am obliged to all my colleagues from the Division on Particle and Astroparticle Physics, as well as our many foreign guests, for the many stimulating discussions we had on all kinds of physical and non-physical topics, and for many joint undertakings. In particular, I would like to mention my fellow theorists Adisorn Adulpravitchai, Evgeny Akhmedov, Fedor Bezrukov, Alexander Blum, Mathias Garny, Claudia Hagedorn, Andreas Hohenegger, Martin Holthausen, Alexander Kartavtsev, Alexander Merle, Markus Michael Müller, Viviana Niro, Toshihiko Ota, Werner Rodejohann, Michael Schmidt, Thomas Schwetz-Mangold, Tom Underwood, and especially my office mate Hendrik Kienert: Working together on our shared whiteboard, we were able to gain many deep insights into fundamental physics, but also into sociopolitical subjects like the language barriers between different parts of Germany, the optimal way to communicate with extraterrestrial life forms and a method to extend our days to 25 hours. Last but not least, Anja Berneiser, the heart and soul of our division, deserves special acknowledgment for keeping everything running, for helping me and my colleagues out of many bureaucratic and logistic dilemmas and for always having a plate full of sweets in her office. All this made working at the MPI for Nuclear Physics an extremely inspiring and enjoyable experience for me.

Even though a theoretical physicist does not need a lot of sophisticated machinery and instrumentation to be happy, a working computer, a comfortable office and a continuous replenishment of office supplies are indispensable. Therefore, I would like to thank all those people, who kept the working environment at the MPI up and running, especially our system administrators Fedor Bezrukov, Andreas Hohenegger, Alexander Kartavtsev, Frank Köck, Markus Michael Müller and Michael Schmidt, and our secretary Anja Berneiser.

I am deeply indebted to my parents Herbert and Karin Kopp, and to my girlfriend Maria, for their continuous support, for believing in me and my work, and for tolerating my many “night shifts” during the more busy phases of this project. All this would not have been possible without you!

Finally, I would like to thank the Studienstiftung des Deutschen Volkes for financial and intellectual support during the years of my studies and during my time as a doctoral student.

A

Weisskopf-Wigner approach to Mössbauer neutrinos for natural line width dominance

In this appendix, we will show how the transition amplitude for a Mössbauer neutrino experiment dominated by the natural line width, eq. (3.96), can be derived from first principles using the Weisskopf-Wigner approach [39, 119–121]. In particular, our aim is to substantiate the arguments dictating the form of the exponential decay factors.

We write the Hamiltonian of the system as $H = H_0 + e^{iH_0t}H_1e^{-iH_0t}$, where H_1 is the interaction-representation weak interaction Hamiltonian and H_0 is the remainder. Even though this decomposition of H is similar to the decomposition used in perturbation theory, we will not treat H_1 as a perturbation because this would not allow us to adequately describe the depletion of unstable states over time, which we are ultimately interested in. An arbitrary state $|\psi(t)\rangle$ can be written as $|\psi(t)\rangle = \sum_j c_j(t)|\phi_j\rangle$, where $|\phi_j\rangle$ are the eigenstates of H_0 . The Schrödinger equation then gives the evolution equations for the coefficients $c_j(t)$:

$$i\dot{c}_j(t) = \sum_k \langle \phi_j | H_1 | \phi_k \rangle c_k(t). \quad (\text{A.1})$$

For our purposes it will be convenient to slightly modify the notation and classify the different states according to their particle content, as shown in table A.1. ${}^3\text{H}$ and ${}^3\text{He}$ denote the two types of atoms in the experiment, and the index S or D shows whether the respective particle is initially localised at the source or at the detector. For those states for which we have written the electron participating in the reaction and the ${}^3\text{He}^+$ ions separately, we imply that the electron may be either free or in an atomic bound state, while for the other states only bound electrons are considered. The upper index (i) stands for the initial state, the indices (1) through (6) denote intermediate states, and (f) stands for the final state, after the decay of the source particle, the absorption of

	Particles		Energy	Coefficient	State vector
Initial state	${}^3\text{H}_S$	${}^3\text{He}_D$	$E^{(i)}$	$c^{(i)}$	$ \phi^{(i)}\rangle$
Intermediate states	${}^3\text{He}_S^+, \bar{\nu}_S, e_S^-$	${}^3\text{He}_D$	$E_j^{(1)}$	$c_j^{(1)}$	$ \phi_j^{(1)}\rangle$
	${}^3\text{H}_S$	${}^3\text{H}_D, \nu_D$	$E_k^{(2)}$	$c_k^{(2)}$	$ \phi_k^{(2)}\rangle$
	${}^3\text{He}_S^+, \bar{\nu}_S, e_S^-$	${}^3\text{H}_D, \nu_D$	$E_{jk}^{(3)}$	$c_{jk}^{(3)}$	$ \phi_{jk}^{(3)}\rangle$
	${}^3\text{He}_S$	${}^3\text{H}_D$	$E^{(4)}$	$c^{(4)}$	$ \phi^{(4)}\rangle$
	${}^3\text{H}_S$	${}^3\text{He}_D^+, \bar{\nu}_D, e_D^-, \nu_D$	$E_{kl}^{(5)}$	$c_{kl}^{(5)}$	$ \phi_{kl}^{(5)}\rangle$
	${}^3\text{He}_S^+, \bar{\nu}_S, e_S^-$	${}^3\text{He}_D^+, \bar{\nu}_D, e_D^-, \nu_D$	$E_{jkl}^{(6)}$	$c_{jkl}^{(6)}$	$ \phi_{jkl}^{(6)}\rangle$
Final state	${}^3\text{He}_S$	${}^3\text{He}_D^+, \bar{\nu}_D, e_D^-$	$E_l^{(f)}$	$c_l^{(f)}$	$ \phi_l^{(f)}\rangle$

Table A.1: Classification of the states appearing in a Mössbauer neutrino experiment.

the emitted neutrino in the detector and the decay of the produced tritium. The lower indices stand for the various quantum numbers of the particles; for example, j encodes the momenta and the spins of $\bar{\nu}_S$ and e_S^- , and the information whether e_S^- is bound or free.

The interaction Hamiltonians governing the evolution of the system is $H_1 = H_S^+ + H_D^- + \tilde{H}_D^+ + \text{h.c.}$, where

$$H_S^+ = \int d^3x \frac{1}{\sqrt{2}} G_F \cos \theta_c \langle {}^3\text{He} | J^\mu | {}^3\text{H} \rangle \bar{\psi}_{e,S} \gamma_\mu (1 - \gamma^5) \psi_\nu, \quad (\text{A.2})$$

$$H_D^- = \int d^3x \frac{1}{\sqrt{2}} G_F \cos \theta_c \langle {}^3\text{H} | J^\mu | {}^3\text{He} \rangle \bar{\psi}_\nu \gamma_\mu (1 - \gamma^5) \psi_{e,D}, \quad (\text{A.3})$$

$$\tilde{H}_D^+ = \int d^3x \frac{1}{\sqrt{2}} G_F \cos \theta_c \langle {}^3\text{He} | J^\mu | {}^3\text{H} \rangle \bar{\psi}_{e,S} \gamma_\mu (1 - \gamma^5) \psi_\nu. \quad (\text{A.4})$$

As in sec. 3.5, the operators H_S^+ and H_D^- describe tritium decay in the source and $\bar{\nu}_e$ capture in the detector, respectively, while \tilde{H}_D^+ describes the decays of the produced tritium nuclei in the detector. We denote the Hermitian conjugates of these operators by H_S^-, H_D^+ and \tilde{H}_D^- , respectively. Although the Hamiltonians (A.2) – (A.4) are related by $H_S^+ = H_D^+ = \tilde{H}_D^+$, we treat them as distinct operators throughout this appendix to keep our derivation more transparent and more general. For the transition matrix elements, the following identities hold:

$$\begin{aligned} \langle \phi^{(i)} | H_S^- | \phi_j^{(1)} \rangle &= \langle \phi_k^{(2)} | H_S^- | \phi_{jk}^{(3)} \rangle = \langle \phi_{kl}^{(5)} | H_S^- | \phi_{jkl}^{(6)} \rangle, \\ \langle \phi^{(i)} | H_D^+ | \phi_k^{(2)} \rangle &= \langle \phi_j^{(1)} | H_D^+ | \phi_{jk}^{(3)} \rangle, \\ \langle \phi^{(4)} | \tilde{H}_D^- | \phi_l^{(f)} \rangle &= \langle \phi_k^{(2)} | \tilde{H}_D^- | \phi_{kl}^{(5)} \rangle = \langle \phi_{jk}^{(3)} | \tilde{H}_D^- | \phi_{jkl}^{(6)} \rangle, \end{aligned} \quad (\text{A.5})$$

and similarly,

$$\begin{aligned}
E^{(i)} - E_j^{(1)} &= E_k^{(2)} - E_{jk}^{(3)} = E_{kl}^{(5)} - E_{jkl}^{(6)}, \\
E^{(i)} - E_k^{(2)} &= E_j^{(1)} - E_{jk}^{(3)}, \\
E^{(4)} - E_l^{(f)} &= E_k^{(2)} - E_{kl}^{(5)} = E_{jk}^{(3)} - E_{jkl}^{(6)}.
\end{aligned} \tag{A.6}$$

These relations follow from the fact that the corresponding transitions differ only in the spectator particles. The evolution equations for the system are (cf. eq. (A.1)):

$$i\dot{c}^{(i)} = \sum_j \langle \phi^{(i)} | H_S^- | \phi_j^{(1)} \rangle c_j^{(1)} + \sum_k \langle \phi^{(i)} | H_D^+ | \phi_k^{(2)} \rangle c_k^{(2)}, \tag{A.7}$$

$$i\dot{c}_j^{(1)} = \langle \phi_j^{(1)} | H_S^+ | \phi^{(i)} \rangle c^{(i)} + \sum_k \langle \phi_j^{(1)} | H_D^+ | \phi_{jk}^{(3)} \rangle c_{jk}^{(3)} + \langle \phi_j^{(1)} | H_D^+ | \phi^{(4)} \rangle c^{(4)}, \tag{A.8}$$

$$\begin{aligned}
i\dot{c}_k^{(2)} &= \langle \phi_k^{(2)} | H_D^- | \phi^{(i)} \rangle c^{(i)} + \sum_j \langle \phi_k^{(2)} | H_S^- | \phi_{jk}^{(3)} \rangle c_{jk}^{(3)} + \sum_l \langle \phi_k^{(2)} | \tilde{H}_D^- | \phi_{kl}^{(5)} \rangle c_{kl}^{(5)} \\
&\quad + \langle \phi_k^{(2)} | H_S^- | \phi^{(4)} \rangle c^{(4)},
\end{aligned} \tag{A.9}$$

$$i\dot{c}_{jk}^{(3)} = \langle \phi_{jk}^{(3)} | H_D^- | \phi_j^{(1)} \rangle c_j^{(1)} + \langle \phi_{jk}^{(3)} | H_S^+ | \phi_k^{(2)} \rangle c_k^{(2)} + \sum_l \langle \phi_{jk}^{(3)} | \tilde{H}_D^- | \phi_{jkl}^{(6)} \rangle c_{jkl}^{(6)}, \tag{A.10}$$

$$i\dot{c}^{(4)} = \sum_j \langle \phi^{(4)} | H_D^-(t_1) | \phi_j^{(1)} \rangle c_j^{(1)} + \sum_k \langle \phi^{(4)} | H_S^+ | \phi_k^{(2)} \rangle c_k^{(2)} + \sum_l \langle \phi^{(4)} | \tilde{H}_D^- | \phi_l^{(f)} \rangle c_l^{(f)}, \tag{A.11}$$

$$i\dot{c}_{kl}^{(5)} = \langle \phi_{kl}^{(5)} | \tilde{H}_D^+ | \phi_k^{(2)} \rangle c_k^{(2)} + \sum_j \langle \phi_{kl}^{(5)} | H_S^- | \phi_{jkl}^{(6)} \rangle c_{jkl}^{(6)} + \langle \phi_{kl}^{(5)} | H_S^- | \phi_l^{(f)} \rangle c_l^{(f)}, \tag{A.12}$$

$$i\dot{c}_{jkl}^{(6)} = \langle \phi_{jkl}^{(6)} | H_S^+ | \phi_{kl}^{(5)} \rangle c_{kl}^{(5)} + \langle \phi_{jkl}^{(6)} | \tilde{H}_D^+ | \phi_{jk}^{(3)} \rangle c_{jk}^{(3)}, \tag{A.13}$$

$$i\dot{c}_l^{(f)} = \sum_k \langle \phi^{(f)} | H_S^+ | \phi_{kl}^{(5)} \rangle c_{kl}^{(5)} + \langle \phi_l^{(f)} | \tilde{H}_D^+ | \phi^{(4)} \rangle c^{(4)}. \tag{A.14}$$

We treat all processes that occur within the source or within the detector non-perturbatively, while first-order perturbation theory is used for processes that require the propagation of a neutrino between the source and the detector. This second kind of transitions is suppressed due to the smallness of the solid angle at which the detector is seen from the source. Consequently, we include only the respective forward reactions (i.e. those proceeding downward in the scheme of table A.1), but neglect in the following the feedback terms printed in grey in the equations for $c_j^{(1)}$, $c_k^{(2)}$, and $c_{kl}^{(5)}$. The feedback of $|\phi_l^{(f)}\rangle$ to $|\phi^{(4)}\rangle$ is included because the production of both states from the initial state requires a single neutrino propagation between the source and the detector. The sums in eqs. (A.7) – (A.14) symbolically denote the summation over the relevant discrete indices and integration over the continuous variables. The initial conditions for the equation

system (A.7) – (A.14) are given by $c^{(i)}(0) = 1$, with all other coefficients vanishing at $t = 0$.

Our ultimate goal is to solve the set of evolution equations for $c^{(4)}(t)$, which determines the ${}^3\text{H}$ abundance in the detector at time t . It is convenient to first consider the closed subsystem formed by eqs. (A.7), (A.8), (A.9), (A.10), (A.12) and (A.13), and to solve it from the bottom upwards. We start by integrating eq. (A.13) to obtain an expression for $c_{jkl}^{(6)}$, which we then insert into eq. (A.12), the equation for $\dot{c}_{kl}^{(5)}$. We obtain

$$\begin{aligned} i\dot{c}_{kl}^{(5)}(t) &= \langle \phi_{kl}^{(5)} | \tilde{H}_D^+(t) | \phi_k^{(2)} \rangle c_k^{(2)}(t) \\ &\quad - i \sum_j \int_0^t dt_1 \langle \phi_{kl}^{(5)} | H_S^-(t) | \phi_{jkl}^{(6)} \rangle \langle \phi_{jkl}^{(6)} | H_S^+(t_1) | \phi_{kl}^{(5)} \rangle c_{kl}^{(5)}(t_1) \\ &\quad - i \sum_j \int_0^t dt_1 \langle \phi_{kl}^{(5)} | H_S^-(t) | \phi_{jkl}^{(6)} \rangle \langle \phi_{jkl}^{(6)} | \tilde{H}_D^+(t_1) | \phi_{jk}^{(3)} \rangle c_{jk}^{(3)}(t_1). \end{aligned} \quad (\text{A.15})$$

Consider first the second term, which describes the effect that decay into $|\phi_{jkl}^{(6)}\rangle$ has on $|\phi_{kl}^{(5)}\rangle$. Following the Weisskopf-Wigner procedure as described in [121], we split the quantum numbers indexed by j into the energy $E^{(6)}$ and the remaining parameters β . Denoting the density of states (the number of states per unit energy interval) by $\rho(E^{(6)}, \beta)$, we can make the replacements

$$|\phi_{jkl}^{(6)}\rangle \rightarrow |\phi_{kl}^{(6)}; E^{(6)}, \beta\rangle, \quad \sum_j \rightarrow \sum_\beta \int dE^{(6)} \rho(E^{(6)}, \beta) \quad (\text{A.16})$$

in the second term of eq. (A.15). This yields

$$-i \int dE^{(6)} K(E^{(6)}) \int_0^t dt_1 e^{i(E_{kl}^{(5)} - E^{(6)})(t-t_1)} c_{kl}^{(5)}(t_1). \quad (\text{A.17})$$

Here we have explicitly written down the time dependence of the matrix elements and introduced the quantity

$$K(E^{(6)}) = \sum_\beta \left| \langle \phi_{kl}^{(5)} | H_S^-(0) | \phi_{kl}^{(6)}; E^{(6)}, \beta \rangle \right|^2 \rho(E^{(6)}, \beta), \quad (\text{A.18})$$

which is a smooth (non-oscillating) function of energy. More specifically, $K(E^{(6)})$ represents a broad bump with a width of $\mathcal{O}(m_W)$, so that a non-negligible contribution to the energy integral in (A.17) can only arise if $t - t_1 \lesssim 1/m_W$. Otherwise, the integrand is fast oscillating and the integral is strongly suppressed. Therefore, we can replace the coefficient $c_{kl}^{(5)}(t_1)$ by its value at $t_1 = t$, if we assume that $c_{kl}^{(5)}(t_1)$ is approximately constant over time intervals of order $1/m_W$. (This assumption will be justified a posteriori

by inspection of the obtained expression for $c_{kl}^{(5)}(t)$. For $t \gg 1/m_W$, we thus obtain

$$\begin{aligned} & -i c_{kl}^{(5)}(t) \int dE^{(6)} K(E^{(6)}) \int_0^t dt_1 e^{i(E_{kl}^{(5)} - E^{(6)})(t-t_1)} \\ & \simeq -i c_{kl}^{(5)}(t) \int dE^{(6)} \left[\pi \delta(E_{kl}^{(5)} - E^{(6)}) + iP \left(\frac{1}{E_{kl}^{(5)} - E^{(6)}} \right) \right] K(E^{(6)}) \\ & = -i \left(\frac{\gamma}{2} + i\delta E \right) c_{kl}^{(5)}(t), \end{aligned} \quad (\text{A.19})$$

where

$$\gamma = 2\pi K(E_{kl}^{(5)}), \quad \delta E = P \int dE^{(6)} \frac{K(E^{(6)})}{E_{kl}^{(5)} - E^{(6)}}, \quad (\text{A.20})$$

and P denotes the principal value. As follows from the definition of the function $K(E)$ in eq. (A.18) and Fermi's golden rule, γ is just the decay width of ${}^3\text{H}$ in the source. The quantity δE is the mass renormalisation of the particles forming $|\phi_{kl}^{(5)}\rangle$. From now on, we will omit δE and similar quantities that will arise in subsequent formulas, assuming that they are already included in the definition of the physical masses of the involved particles. The formal solution to eq. (A.15) is

$$\begin{aligned} c_{kl}^{(5)}(t) = & -i \int_0^t dt_1 \langle \phi_{kl}^{(5)} | \tilde{H}_D^+(t_1) | \phi_k^{(2)} \rangle e^{-\frac{1}{2}\gamma(t-t_1)} c_k^{(2)}(t_1) \\ & + (-i)^2 \sum_j \int_0^t dt_1 \int_0^{t_1} dt_2 \langle \phi_{kl}^{(5)} | H_S^-(t_1) | \phi_{jk}^{(6)} \rangle \langle \phi_{jk}^{(6)} | \tilde{H}_D^+(t_2) | \phi_{jk}^{(3)} \rangle e^{-\frac{1}{2}\gamma(t-t_1)} c_{jk}^{(3)}(t_2). \end{aligned} \quad (\text{A.21})$$

By a similar argument, we obtain from eq. (A.10):

$$\begin{aligned} i\dot{c}_{jk}^{(3)}(t) = & \langle \phi_{jk}^{(3)} | H_D^-(t) | \phi_j^{(1)} \rangle c_j^{(1)}(t) + \langle \phi_{jk}^{(3)} | H_S^+(t) | \phi_k^{(2)} \rangle c_k^{(2)}(t) - i\tilde{\gamma} c_{jk}^{(3)}(t) \\ & - i \sum_l \int_0^t dt_1 \langle \phi_{jk}^{(3)} | \tilde{H}_D^-(t) | \phi_{jkl}^{(6)} \rangle \langle \phi_{jkl}^{(6)} | H_S^+(t_1) | \phi_{kl}^{(5)} \rangle c_{kl}^{(5)}(t_1), \end{aligned} \quad (\text{A.22})$$

where the decay width of ${}^3\text{H}$ in the detector, $\tilde{\gamma}$, has been defined in analogy with eq. (A.20). We will now show that the last term of eq. (A.22) can be neglected. To this end, we insert in it the expression for $c_{kl}^{(5)}(t)$ from (A.21), which yields

$$\begin{aligned} & (-i)^2 \sum_l \int_0^t dt_1 \int_0^{t_1} dt_2 |\langle \phi_k^{(2)} | \tilde{H}_D^-(0) | \phi_{kl}^{(5)} \rangle|^2 \langle \phi_{jkl}^{(6)} | H_S^+(t_1) | \phi_{kl}^{(5)} \rangle \\ & \quad \cdot e^{i(E_k^{(2)} - E_{kl}^{(5)})(t-t_2)} e^{-\frac{1}{2}\gamma(t_1-t_2)} c_k^{(2)}(t_2) \\ & + (-i)^3 \sum_l \int_0^t dt_1 \int_0^{t_1} dt_2 \int_0^{t_2} dt_3 |\langle \phi_k^{(2)} | \tilde{H}_D^-(0) | \phi_{kl}^{(5)} \rangle|^2 \langle \phi_{jkl}^{(6)} | H_S^+(t_1) | \phi_{kl}^{(5)} \rangle \\ & \quad \cdot \sum_{j'} \langle \phi_{kl}^{(5)} | H_S^-(t_2) | \phi_{j'kl}^{(6)} \rangle e^{i(E_k^{(2)} - E_{kl}^{(5)})(t-t_3)} c_{j'k}^{(3)}(t_3). \end{aligned} \quad (\text{A.23})$$

Here we have used the identities (A.5) and (A.6). We will argue that the first term of (A.23) can be neglected; a similar argument can then also be used to justify the neglect of the second term. Splitting the index l into $E^{(5)}$ and $\tilde{\beta}$ in analogy with eq. (A.16), we obtain

$$(-i)^2 \int dE^{(5)} \tilde{K}(E^{(5)}) \int_0^t dt_1 \int_0^{t_1} dt_2 \langle \phi_{jkl}^{(6)} | H_S^+(t_1) | \phi_{kl}^{(5)} \rangle e^{i(E_k^{(2)} - E^{(5)})(t-t_2)} e^{-\frac{1}{2}\gamma(t_1-t_2)} c_k^{(2)}(t_2), \quad (\text{A.24})$$

with $\tilde{K}(E^{(5)})$ defined analogously to $K(E^{(6)})$. As in eq. (A.17), the energy integral is non-negligible only if $t - t_2 \lesssim 1/m_W$. We see immediately that here, this condition also implies $t - t_1 \lesssim 1/m_W$. Consequently, we may pull out of the integral those terms which remain approximately constant over time intervals of $\mathcal{O}(1/m_W)$. This gives

$$\begin{aligned} & (-i)^2 \langle \phi_{jkl}^{(6)} | H_S^+(t) | \phi_{kl}^{(5)} \rangle c_k^{(2)}(t) \int dE^{(5)} \tilde{K}(E^{(5)}) \int_0^t dt_1 \int_0^{t_1} dt_2 e^{i(E_k^{(2)} - E^{(5)})(t-t_2)} \\ & \sim (-i)^2 \langle \phi_{jkl}^{(6)} | H_S^+(t) | \phi_{kl}^{(5)} \rangle c_k^{(2)}(t) \frac{1}{m_W} \int dE^{(5)} \left[\pi \delta(E_k^{(2)} - E^{(5)}) \right. \\ & \quad \left. + iP \left(\frac{1}{E_k^{(2)} - E^{(5)}} \right) \right] \tilde{K}(E^{(5)}) \\ & \sim \mathcal{O}\left(\frac{\tilde{\gamma}}{m_W}\right), \end{aligned} \quad (\text{A.25})$$

which is negligible compared to the other terms contributing to $\dot{c}_{jk}^{(3)}(t)$ (cf. eq. (A.22)). This result already suggests the general rule that the only transitions which may contribute sizeably to the evolution equations are those corresponding to the direct production of the states (i.e. production with a minimum number of intermediate steps), and those corresponding to direct feedback from a daughter state into its immediate parent state, e.g. from $|\phi_{jkl}^{(6)}\rangle$ into $|\phi_{jk}^{(3)}\rangle$. All terms corresponding to more complicated interaction chains are negligible. One can now solve eq. (A.22) for $c_{jk}^{(3)}$:

$$\begin{aligned} c_{jk}^{(3)}(t) = & -i \int_0^t dt_1 \langle \phi_{jk}^{(3)} | H_D^-(t_1) | \phi_j^{(1)} \rangle e^{-\frac{1}{2}\tilde{\gamma}(t-t_1)} c_j^{(1)}(t_1) \\ & - i \int_0^t dt_1 \langle \phi_{jk}^{(3)} | H_S^+(t_1) | \phi_k^{(2)} \rangle e^{-\frac{1}{2}\tilde{\gamma}(t-t_1)} c_k^{(2)}(t_1). \end{aligned} \quad (\text{A.26})$$

Next, we plug our expressions for $c_{jk}^{(3)}$ and $c_{kl}^{(5)}$ (eqs. (A.26) and (A.21)) into eq. (A.9):

$$\begin{aligned} i\dot{c}_k^{(2)}(t) = & \langle \phi_k^{(2)} | H_D^-(t) | \phi^{(i)} \rangle c^{(i)}(t) - i\frac{\gamma}{2} c_k^{(2)}(t) - i\frac{\tilde{\gamma}}{2} c_{jk}^{(2)}(t) \\ & - i \sum_j \int_0^t dt_1 \langle \phi_k^{(2)} | H_S^-(t) | \phi_{jk}^{(3)} \rangle \langle \phi_{jk}^{(3)} | H_D^-(t_1) | \phi_j^{(1)} \rangle e^{-\frac{1}{2}\tilde{\gamma}(t-t_1)} c_j^{(1)}(t_1). \end{aligned} \quad (\text{A.27})$$

We have omitted a term, which contains the product of $\langle \phi_k^{(2)} | \tilde{H}_D^- | \phi_{kl}^{(5)} \rangle$, $\langle \phi_{kl}^{(5)} | H_S^- | \phi_{jkl}^{(6)} \rangle$ and $\langle \phi_{jkl}^{(6)} | \tilde{H}_D^+ | \phi_{jk}^{(3)} \rangle$, and thus describes the transition chain $|\phi_{jk}^{(3)}\rangle \rightarrow |\phi_{jkl}^{(6)}\rangle \rightarrow |\phi_{kl}^{(5)}\rangle \rightarrow |\phi_k^{(2)}\rangle$, because this term can be shown to be $\mathcal{O}(\tilde{\gamma}/m_W)$ by an argument similar to the one we have used in eq. (A.25). The formal solution to eq. (A.27) is

$$c_k^{(2)}(t) = -i \int_0^t dt_1 \langle \phi_k^{(2)} | H_D^-(t_1) | \phi^{(i)} \rangle e^{-\frac{1}{2}\gamma(t-t_1) - \frac{1}{2}\tilde{\gamma}(t-t_1)} c^{(i)}(t_1) \quad (\text{A.28})$$

$$+ (-i)^2 \sum_j \int_0^t dt_1 \int_0^{t_1} dt_2 \langle \phi_k^{(2)} | H_S^-(t_1) | \phi_{jk}^{(3)} \rangle \langle \phi_{jk}^{(3)} | H_D^-(t_2) | \phi_j^{(1)} \rangle e^{-\frac{1}{2}\gamma(t-t_1) - \frac{1}{2}\tilde{\gamma}(t-t_2)} c_j^{(1)}(t_2).$$

We now proceed to eq. (A.8), which becomes, after plugging in (A.26):

$$i\dot{c}_j^{(1)}(t) = \langle \phi_j^{(1)} | H_S^+(t) | \phi^{(i)} \rangle c^{(i)}(t) - i \sum_k \int_0^t dt_1 \langle \phi_j^{(1)} | H_D^+(t) | \phi_{jk}^{(3)} \rangle \langle \phi_{jk}^{(3)} | H_D^-(t_1) | \phi_j^{(1)} \rangle e^{-\frac{1}{2}\tilde{\gamma}(t-t_1)} c_j^{(1)}(t_1). \quad (\text{A.29})$$

The contributions coming from $c_k^{(2)}$ through the transition chain $|\phi_k^{(2)}\rangle \rightarrow |\phi_{jk}^{(3)}\rangle \rightarrow |\phi_j^{(1)}\rangle$ are again omitted for being $\mathcal{O}(\tilde{\gamma}/m_W)$. The term containing the product of $\langle \phi_j^{(1)} | H_D^+(t) | \phi_{jk}^{(3)} \rangle$ and $\langle \phi_{jk}^{(3)} | H_D^-(t_1) | \phi_j^{(1)} \rangle$ describes the direct feedback from $|\phi_{jk}^{(3)}\rangle$ to $|\phi_j^{(1)}\rangle$, but since the transition $|\phi_j^{(1)}\rangle \rightarrow |\phi_{jk}^{(3)}\rangle$ does not occur spontaneously, the corresponding decay width is zero. Indeed, when applying the Weisskopf-Wigner procedure, we see that the resulting δ -function under the energy integral is zero for all allowed energies. Thus, the second term in eq. (A.29) is negligible, and the equation is solved by

$$c_j^{(1)}(t) = -i \int_0^t dt_1 \langle \phi_j^{(1)} | H_S^+(t_1) | \phi^{(i)} \rangle c^{(i)}(t_1). \quad (\text{A.30})$$

We can insert this expression, together with $c_k^{(2)}(t)$ from eq. (A.28), into the equation for $c^{(i)}(t)$, and find

$$c^{(i)}(t) = e^{-\frac{1}{2}\gamma t}, \quad (\text{A.31})$$

up to a term suppressed by $\tilde{\gamma}/m_W$. The closed-form expressions for $c_j^{(1)}(t)$, $c_k^{(2)}(t)$, $c_{jk}^{(3)}(t)$, $c_{kl}^{(5)}(t)$, and $c_{jkl}^{(6)}(t)$ are then

$$c_j^{(1)}(t) = -i \int_0^t dt_1 \langle \phi_j^{(1)} | H_S^+(t_1) | \phi^{(i)} \rangle e^{-\frac{1}{2}\gamma t_1}, \quad (\text{A.32})$$

$$c_k^{(2)}(t) = -i \int_0^t dt_1 \langle \phi_k^{(2)} | H_D^-(t_1) | \phi^{(i)} \rangle e^{-\frac{1}{2}\gamma t - \frac{1}{2}\tilde{\gamma}(t-t_1)}, \quad (\text{A.33})$$

$$c_{jk}^{(3)}(t) = (-i)^2 \left[\int_0^t dt_1 \langle \phi_j^{(1)} | H_S^+(t_1) | \phi^{(i)} \rangle e^{-\frac{1}{2}\gamma t_1} \right] \left[\int_0^t dt_1 \langle \phi_k^{(2)} | H_D^-(t_1) | \phi^{(i)} \rangle e^{-\frac{1}{2}\tilde{\gamma}(t-t_1)} \right], \quad (\text{A.34})$$

$$c_{kl}^{(5)}(t) = (-i)^2 \int_0^t dt_1 \int_0^{t_1} dt_2 \langle \phi_{kl}^{(5)} | \tilde{H}_D^+(t_1) | \phi_k^{(2)} \rangle \langle \phi_k^{(2)} | H_D^-(t_2) | \phi^{(i)} \rangle e^{-\frac{1}{2}\gamma t - \frac{1}{2}\tilde{\gamma}(t_1-t_2)}, \quad (\text{A.35})$$

$$c_{jkl}^{(6)}(t) = (-i)^3 \left[\int_0^t dt_1 \langle \phi_j^{(1)} | H_S^+(t_1) | \phi^{(i)} \rangle e^{-\frac{1}{2}\gamma t_1} \right] \cdot \left[\int_0^t dt_1 \int_0^{t_1} dt_2 \langle \phi_{kl}^{(5)} | \tilde{H}_D^+(t_1) | \phi_k^{(2)} \rangle \langle \phi_k^{(2)} | H_D^-(t_2) | \phi^{(i)} \rangle e^{-\frac{1}{2}\tilde{\gamma}(t_1-t_2)} \right]. \quad (\text{A.36})$$

In the formulas for $c_{jk}^{(3)}(t)$ and $c_{jkl}^{(6)}(t)$, we have used the identity

$$\int_0^t dt_1 \int_0^{t_1} dt_2 = \int_0^t dt_2 \int_{t_2}^t dt_1. \quad (\text{A.37})$$

Eqs. (A.31) – (A.36) show that all coefficients are slowly varying over time intervals of order $1/m_W$, which provides the a posteriori justification for pulling them out of the time integrals when applying the Weisskopf-Wigner procedure.

We have now all the ingredients required to solve for $c^{(4)}(t)$. We insert our expressions for $c_j^{(1)}(t)$ and $c_k^{(2)}(t)$ (eqs. (A.32) and (A.33)), as well as eq. (A.14) into eq. (A.11), neglect the $\mathcal{O}(\tilde{\gamma}/m_W)$ contribution from the reaction chain $|\phi_{kl}^{(5)}\rangle \rightarrow |\phi_l^{(f)}\rangle \rightarrow |\phi^{(4)}\rangle$, and apply the completeness relations

$$\sum_j |\phi_j^{(1)}\rangle \langle \phi_j^{(1)}| = 1, \quad \sum_k |\phi_k^{(2)}\rangle \langle \phi_k^{(2)}| = 1 \quad (\text{A.38})$$

to dispose of the sums over j and k and of the intermediate bra- and ket-vectors in the products of matrix elements. This leads us to the main result of this appendix,

$$c^{(4)}(t) = (-i)^2 \int_0^t dt_1 \int_0^{t_1} dt_2 \langle \phi^{(4)} | \left[H_D^-(t_1) e^{-\frac{1}{2}\tilde{\gamma}(t-t_1)} H_S^+(t_2) e^{-\frac{1}{2}\gamma t_2} + H_S^+(t_1) e^{-\frac{1}{2}\gamma t_1} H_D^-(t_2) e^{-\frac{1}{2}\tilde{\gamma}(t-t_2)} \right] | \phi^{(i)} \rangle. \quad (\text{A.39})$$

We see that $c^{(4)}(t)$ is given by the time-ordered product of the two interaction Hamiltonians, supplemented by the classically expected exponential decay factors. After inserting the appropriate expressions for H_S^+ and H_D^- , finally setting $\tilde{\gamma} = \gamma$ and applying the Feynman rules, eq. (A.39) leads directly to eq. (3.96) of sec. 3.5.4.

For completeness, we also give the expression for $c_l^{(f)}(t)$:

$$c_l^{(f)}(t) = (-i)^3 \int_0^t dt_1 \int_0^{t_1} dt_2 \int_0^{t_2} dt_3 \langle \phi_l^{(f)} | \left[\tilde{H}_D^+(t_1) H_D^-(t_2) e^{-\frac{1}{2}\tilde{\gamma}(t_1-t_2)} H_S^+(t_3) e^{-\frac{1}{2}\gamma t_3} + \tilde{H}_D^+(t_1) H_S^+(t_2) e^{-\frac{1}{2}\gamma t_2} H_D^-(t_3) e^{-\frac{1}{2}\tilde{\gamma}(t_1-t_3)} + H_S^+(t_1) e^{-\frac{1}{2}\gamma t_1} \tilde{H}_D^+(t_2) H_D^-(t_3) e^{-\frac{1}{2}\tilde{\gamma}(t_2-t_3)} \right] | \phi^{(i)} \rangle. \quad (\text{A.40})$$

Note that an alternative way of solving eqs. (A.7) – (A.14) is to exploit the fact that, in the closed system formed by eqs. (A.7), (A.8), (A.9), (A.10), (A.12), and (A.13), the processes in the source and those in the detector can be separated by using a product ansatz for the coefficients c . Once this subsystem is solved, $c^{(4)}$ and $c_i^{(f)}$ can be computed as above.

B

NSI operators with non- $(V - A)(V - A)$ Lorentz structure

In the following, we will extend the NSI formalism introduced in the beginning of chapter 4 by including operators with non- $(V - A)(V - A)$ Lorentz structure. Neglecting again the doubly suppressed NSI couplings of right handed neutrinos, the generalisation of eq. (4.5) to non- $(V - A)(V - A)$ operators is

$$\begin{aligned} \mathcal{L}_{V\pm A} = & \frac{G_F}{\sqrt{2}} \sum_{f,f'} \varepsilon_{\alpha\beta}^{\text{CC},f,f',V\pm A} [\bar{\nu}_\alpha \gamma^\rho (1 - \gamma^5) \ell_\beta] [\bar{f} \gamma_\rho (1 \pm \gamma^5) f'] + \text{h.c.} \\ & + \frac{G_F}{\sqrt{2}} \sum_{f,f''} \varepsilon_{\alpha\beta}^{\text{NC},f,f'',V\pm A} [\bar{\nu}_\alpha \gamma^\rho (1 - \gamma^5) \nu_\beta] [\bar{f} \gamma_\rho (1 \pm \gamma^5) f''] + \text{h.c.}, \end{aligned} \quad (\text{B.1})$$

$$\mathcal{L}_{S\pm P} = \frac{G_F}{\sqrt{2}} \sum_{f,f'} \varepsilon_{\alpha\beta}^{\text{CC},f,f',S\pm P} [\bar{\nu}_\alpha (1 + \gamma^5) \ell_\beta] [\bar{f} (1 \pm \gamma^5) f'] + \text{h.c.}, \quad (\text{B.2})$$

$$\mathcal{L}_T = \frac{G_F}{\sqrt{2}} \sum_{f,f'} \varepsilon_{\alpha\beta}^{\text{CC},f,f',T} [\bar{\nu}_\alpha \sigma^{\rho\tau} \ell_\beta] [\bar{f} \sigma_{\rho\tau} f'] + \text{h.c.} \quad (\text{B.3})$$

For CC interactions, f and f' must have electric charges differing by one unit, while for NC interactions, f and f'' must have equal electric charges.

To estimate which NSI operators are most relevant to realistic experiments, we assume that the dominant non-standard processes are those which can interfere coherently with standard oscillations. Indeed, non-coherent contributions to the oscillation probabilities are always small because they are suppressed by at least two powers of the small ε parameters. Interference is only possible if all interactions partners of the neutrino in the source and in the detector are the same for the interfering standard and non-standard processes. Applied to reactor, superbeam, beta beam and neutrino factory experiments, this implies the following constraints, which are also summarised in table B.1.

1. Neutrino production in nuclear decays (reactor and beta beam experiments) or meson decays (superbeam experiments) receives the strongest NSI contributions from terms proportional to $\varepsilon_{\alpha\beta}^{\text{CC},f,f'}$, with $f = d$ and $f' = u$. The lepton ℓ_β should be a muon for NSI contributions to standard oscillation channels involving an initial ν_μ (superbeam appearance channel $\nu_\mu \rightarrow \nu_e$, superbeam disappearance channel $\nu_\mu \rightarrow \nu_\mu$), and an electron for contributions to oscillation channels involving an initial ν_e (reactor and beta beam experiments, ν_e contamination in superbeams).
2. In a neutrino factory, both NC and CC NSI can modify the production rate at first order in ε . However, since NC and CC operators are related by Fierz identities, they represent merely two different ways of expressing the same non-standard physics. In the CC representation, interference of standard and non-standard amplitudes is possible if $f = \mu$, $f' = \nu_\mu$, $\ell_\beta = e$ or $f = e$, $f' = \nu_e$, $\ell_\beta = \mu$. In the NC representation, the condition is $f = e$, $f'' = \mu$ (or vice-versa), and either ν_α or ν_β corresponding to the unobserved neutrino.
3. The predominant neutrino detection processes in most experiments are CC interactions with nuclei, which are sensitive to $\varepsilon_{\alpha\beta}^{\text{CC},f,f'}$ with $f = d$, $f' = u$. The less relevant CC neutrino-electron interactions are affected by $(\varepsilon_{\alpha\beta}^{\text{CC},f,f'})^*$ with $f = e$, $f' = \nu_e$. In both cases, the flavour of the charged lepton ℓ_β has to be the same as for the corresponding standard interaction. For NSI in NC neutrino interactions, the interference conditions allows only terms proportional to $\varepsilon_{\alpha\beta}^{\text{NC},f,f'',V\pm A}$, with $f = f'' \in \{u, d, e\}$ and with the outgoing neutrino having the same flavour as in the interfering standard process.
4. In most processes, there is still room for non- $(V - A)(V - A)$ contributions, but some of these are already strongly constrained. For example, the relative magnitude of scalar or tensor coupling constants in nuclear beta decay cannot be larger than several per mille [202], so that these interactions cannot contribute significantly in reactor experiments, and only marginally in advanced beta beam experiments.¹ Pseudoscalar interactions are irrelevant to nuclear beta decay because hadronic currents of the form $\bar{d}\gamma^5 u$ vanish if d and u are non-relativistic spinors [202].
The same constraints as for beta decay apply also to the inverse beta decay process, which is the detection reaction in reactor experiments.
5. Neutrino production in superbeam sources cannot be modified by tensor interactions because the decay operator must have a parity-odd component in order to couple to pions or kaons. On the other hand, $(S + P)(S \pm P)$ type terms are even *enhanced* by a factor of [203, 204]

$$\omega = \frac{m_\pi}{m_\mu} \frac{m_\pi}{m_u + m_d} \sim 20. \quad (\text{B.4})$$

¹ A beta beam can, under favourable circumstances, discover $\sin^2 2\theta_{13}$ values below 10^{-3} [72]; therefore, non-standard terms of the same order of magnitude can affect the results of such an experiment.

The importance of this so-called chiral enhancement for superbeam neutrino experiments has been pointed out in [153]. For the dominant decay $\pi \rightarrow \mu + \nu_\mu$, there exist limits on the helicity of the produced muon [205, 206], which ensure that, in spite of the enhancement, $(S + P)(S \pm P)$ type NSI cannot affect the neutrino oscillation amplitude by more than a few per cent.

For the subdominant decay $K \rightarrow e + \nu_e + \pi^0$, which yields the main contribution to the intrinsic background of superbeam experiments, we are not aware of any such limits, so that we have to allow for chirally enhanced $(S + P)(S \pm P)$ type NSI in this channel.

6. In a neutrino factory, CC $(V - A)(V + A)$, $(S + P)(S + P)$ and TT interactions are irrelevant because the requirement of interference between standard and non-standard amplitudes can only be fulfilled if both produced neutrinos are left-handed. Moreover, CC $(S + P)(S - P)$ operators may be neglected because they would correspond to decays of right-handed muons into right-handed electrons, on which strong bounds exist [206, 207]. If we use the Fierz identity to write the NSI contributions to neutrino production in a neutrino factory in terms of NC operators, these bounds imply that NC $(V - A)(V + A)$ terms are negligible.
7. High energy detection processes receive the most sizeable NSI contributions from $(V - A)(V - A)$ interactions. For all other Lorentz structures, the interference condition requires a chirally suppressed helicity flip on at least one external leg of the NSI vertex. This chiral suppression rules out $(V - A)(V + A)$ and $(S + P)(S + P)$ contributions to CC ν - e scattering, because for these processes, a neutrino helicity flip would be required. In CC $(S + P)(S \pm P)$ and TT type interactions with nucleons or electrons, and in NC $(V - A)(V + A)$ type interactions with electrons, a helicity flip has to occur on a charged lepton line, so these interactions are suppressed by m_ℓ/E , where m_ℓ is the mass of the charged lepton. This factor is small for $\ell = e, \mu$ and E in the several GeV range, while for $\ell = \tau$, it is of $\mathcal{O}(1)$. In CC and NC $(V - A)(V + A)$ interactions with nucleons, a helicity flip is only required in the hadronic part of the vertex, so the corresponding amplitudes are suppressed by m_n/E for quasi-elastic scattering and by m_q/E for deep-inelastic scattering. Here, m_n is the nucleon mass, and m_q is the effective quark mass at the scale of the neutrino energy. For typical superbeam energies in the GeV range (i.e. in the transition regime between quasi-elastic and deep-inelastic scattering), the suppression is not very pronounced.
8. Non-standard neutral current effects in the propagation process (non-standard matter effects) require $f = f'' \in \{e, u, d\}$ in eq. (4.4). For the computation of the coherent forward scattering amplitude, the factor $\bar{f}\gamma_\rho(1 \pm \gamma^5)f$ has to be averaged over the neutrino trajectory, which yields, for unpolarised matter at rest, the fermion density $N_f = \bar{f}\gamma^0 f$. Since N_f is independent of the axial current, terms with $(V - A)(V - A)$ and $(V - A)(V + A)$ Lorentz structures are equally important, and cannot be distinguished by a neutrino oscillation experiment.

Charged current NSI in the production process					
	Reactor	Beta beam	Superbeam ($\pi \rightarrow \mu + \nu_\mu$)	Superbeam ($K \rightarrow e + \nu_e + \pi^0$)	ν -fact
f	d	d	d	d	μ / e
f'	u	u	u	u	ν_μ / ν_e
ℓ_β	e	e	μ	e	e / μ
$V - A$	✓	✓	✓	✓	✓
$V + A$	✓	✓	✓	✓	no RH ν
$S - P$	constrained	(✓)	✓	✓ (enhanced)	constrained
$S + P$	constrained	(✓)	✓	✓ (enhanced)	no RH ν
T	constrained	(✓)	no P -odd part	no P -odd part	no RH ν

Charged current NSI in the detection process				
	Low energy (Reactor exp.)	High energy $\nu + N \rightarrow N' + \ell$		High energy $\nu + e \rightarrow \nu_e + \ell'$
f	d	d	d	e
f'	u	u	u	ν_e
ℓ_β	e	e, μ	τ	e, μ, τ
$V - A$	✓	✓	✓	✓
$V + A$	✓	✓ (mild supp.)	✓ (mild supp.)	no RH ν
$S - P$	constrained	chiral supp.	✓ (mild supp.)	chiral supp.
$S + P$	constrained	chiral supp.	✓ (mild supp.)	no RH ν
T	constrained	chiral supp.	✓ (mild supp.)	chiral supp.

Neutral current NSI				
	ν -fact	Matter effects	Detection	
f	e / μ	u, d, e	u, d	e
f''	μ / e	u, d, e	u, d	e
$V - A$	✓	✓	✓	✓
$V + A$	constrained	✓	✓ (mild supp.)	chiral supp.

Table B.1: Classification of the terms in eqs. (B.1) – (B.3) according to their relevance in future experiments.

C

The non-standard neutrino oscillation probabilities

In this appendix, we collect approximate formulas for the neutrino oscillation probabilities including NSI for the most relevant oscillation channels. These formulas were originally derived by Ota [157] (their standard oscillation limits were known before, see e.g. [208]). The expansion parameters are θ_{13} , $\Delta m_{21}^2/\Delta m_{31}^2$ and the moduli of the NSI ε parameters. We use the notation $s_{ij} = \sin \theta_{ij}$, $c_{ij} = \cos \theta_{ij}$, $s_{2\times ij} = \sin 2\theta_{ij}$, and $c_{2\times ij} = \cos 2\theta_{ij}$ for the sines and cosines of the vacuum mixing angles, and

$$\tilde{s}_{13} \equiv \frac{\Delta m_{31}^2}{\Delta m_{31}^2 - a_{\text{CC}}} s_{13} + \mathcal{O}(s_{13}^2), \quad (\text{C.1})$$

with $a_{\text{CC}} = 2\sqrt{2}G_F N_e E$, for the sine of the (13)-mixing angle in matter. The ε parameters are written as $\varepsilon_{\alpha\beta}^{s,m,d} = |\varepsilon_{\alpha\beta}^{s,m,d}| \exp(i\phi_{\alpha\beta}^{s,m,d})$.

C.1 The $\bar{\nu}_e \rightarrow \bar{\nu}_e$ channel

The approximate expression for the $\bar{\nu}_e$ survival probability, relevant to reactor neutrino experiments, is

$$\begin{aligned} P(\bar{\nu}_e^s \rightarrow \bar{\nu}_e^d)^{\text{vac}} = & 1 - 4s_{13}^2 \sin^2 \frac{\Delta m_{31}^2 L}{4E} \\ & + 2|\varepsilon_{ee}^s| \cos \phi_{ee}^s + 2|\varepsilon_{ee}^d| \cos \phi_{ee}^d \\ & - 4|\varepsilon_{e\mu}^s| s_{13} s_{23} \cos(\delta_{\text{CP}} - \phi_{e\mu}^s) \sin^2 \frac{\Delta m_{31}^2 L}{4E} \\ & + 2|\varepsilon_{e\mu}^s| s_{13} s_{23} \sin(\delta_{\text{CP}} - \phi_{e\mu}^s) \sin \frac{\Delta m_{31}^2 L}{2E} \end{aligned}$$

$$\begin{aligned}
 & -4|\varepsilon_{e\tau}^s|s_{13}c_{23}\cos(\delta_{\text{CP}}-\phi_{e\tau}^s)\sin^2\frac{\Delta m_{31}^2L}{4E} \\
 & +2|\varepsilon_{e\tau}^s|s_{13}c_{23}\sin(\delta_{\text{CP}}-\phi_{e\tau}^s)\sin\frac{\Delta m_{31}^2L}{2E} \\
 & -4|\varepsilon_{\mu e}^d|s_{13}s_{23}\cos(\delta_{\text{CP}}+\phi_{\mu e}^d)\sin^2\frac{\Delta m_{31}^2L}{4E} \\
 & -2|\varepsilon_{\mu e}^d|s_{13}s_{23}\sin(\delta_{\text{CP}}+\phi_{\mu e}^d)\sin\frac{\Delta m_{31}^2L}{2E} \\
 & -4|\varepsilon_{\tau e}^d|s_{13}c_{23}\cos(\delta_{\text{CP}}+\phi_{\tau e}^d)\sin^2\frac{\Delta m_{31}^2L}{4E} \\
 & -2|\varepsilon_{\tau e}^d|s_{13}c_{23}\sin(\delta_{\text{CP}}+\phi_{\tau e}^d)\sin\frac{\Delta m_{31}^2L}{2E} \\
 & +\mathcal{O}\left(\frac{\Delta m_{21}^2}{\Delta m_{31}^2}\right)+\mathcal{O}(\varepsilon s_{13}^2)+\mathcal{O}(s_{13}^3)+\mathcal{O}(\varepsilon^2), \tag{C.2}
 \end{aligned}$$

where we have neglected terms suppressed by $\Delta m_{21}^2/\Delta m_{31}^2$, as well as matter effects, since both are irrelevant to reactor experiments. It is straightforward to obtain the standard oscillation probability from eq. (C.2) by setting all ε parameters to zero.

For the near detector of a reactor neutrino experiment ($L \simeq 0$), the $\bar{\nu}_e$ event rate is proportional to

$$\begin{aligned}
 P(\bar{\nu}_e^s \rightarrow \bar{\nu}_e^d)^{\text{ND}} &= 1 + 2|\epsilon_{ee}^s|\cos\phi_{ee}^s + 2|\epsilon_{ee}^d|\cos\phi_{ee}^d + |\epsilon_{ee}^s|^2 + |\epsilon_{ee}^d|^2 \\
 & + 2|\epsilon_{ee}^s||\epsilon_{ee}^d|[\cos(\phi_{ee}^s + \phi_{ee}^d) + \cos(\phi_{ee}^s - \phi_{ee}^d)] \\
 & + 2|\epsilon_{e\mu}^s||\epsilon_{\mu e}^d|\cos(\phi_{\mu e}^s + \phi_{e\mu}^d) \\
 & + 2|\epsilon_{e\tau}^s||\epsilon_{\tau e}^d|\cos(\phi_{\tau e}^s + \phi_{e\tau}^d) \\
 & + \mathcal{O}\left(\frac{\Delta m_{31}^2L}{4E}\right) + \mathcal{O}(\varepsilon^3), \tag{C.3}
 \end{aligned}$$

where we have included also second order terms in the NSI coupling constants.

C.2 The $\nu_\mu \rightarrow \nu_e$ channel

For the $\nu_\mu \rightarrow \nu_e$ channel, we include also terms linear in $\Delta m_{21}^2/\Delta m_{31}^2$ and find

$$\begin{aligned}
 P(\nu_\mu^s \rightarrow \nu_e^d)^{\text{vac}} &= 4s_{13}^2s_{23}^2\sin^2\frac{\Delta m_{31}^2L}{4E} \\
 & + \left(\frac{\Delta m_{21}^2}{\Delta m_{31}^2}\right)^2 c_{23}^2s_{2\times 12}^2\left(\frac{\Delta m_{31}^2L}{4E}\right)^2 \\
 & + \frac{\Delta m_{21}^2}{\Delta m_{31}^2}s_{13}s_{2\times 12}s_{2\times 23}\cos\delta_{\text{CP}}\frac{\Delta m_{31}^2L}{4E}\sin\frac{\Delta m_{31}^2L}{2E} \\
 & - 2\frac{\Delta m_{21}^2}{\Delta m_{31}^2}s_{13}s_{2\times 12}s_{2\times 23}\sin\delta_{\text{CP}}\frac{\Delta m_{31}^2L}{4E}\sin^2\frac{\Delta m_{31}^2L}{4E}
 \end{aligned}$$

$$\begin{aligned}
 & -4|\epsilon_{\mu e}^s|s_{13}s_{23}\cos(\phi_{\mu e}^s+\delta_{\text{CP}})\sin^2\frac{\Delta m_{31}^2L}{4E} \\
 & -2|\epsilon_{\mu e}^s|s_{13}s_{23}\sin(\phi_{\mu e}^s+\delta_{\text{CP}})\sin\frac{\Delta m_{31}^2L}{2E} \\
 & -4|\epsilon_{\mu e}^d|s_{13}c_{2\times 23}s_{23}\cos(\phi_{\mu e}^d+\delta_{\text{CP}})\sin^2\frac{\Delta m_{31}^2L}{4E} \\
 & -2|\epsilon_{\mu e}^d|s_{13}s_{23}\sin(\phi_{\mu e}^d+\delta_{\text{CP}})\sin\frac{\Delta m_{31}^2L}{2E} \\
 & +4|\epsilon_{\tau e}^d|s_{13}s_{2\times 23}s_{23}\cos(\phi_{\tau e}^d+\delta_{\text{CP}})\sin^2\frac{\Delta m_{31}^2L}{4E} \\
 & -|\epsilon_{\mu e}^s|\frac{\Delta m_{21}^2}{\Delta m_{31}^2}s_{2\times 12}c_{23}\sin\phi_{\mu e}^s\frac{\Delta m_{31}^2L}{2E} \\
 & +2|\epsilon_{\mu e}^d|\frac{\Delta m_{21}^2}{\Delta m_{31}^2}s_{2\times 12}s_{23}^2c_{23}\cos\phi_{\mu e}^d\frac{\Delta m_{31}^2L}{4E}\sin\frac{\Delta m_{31}^2L}{2E} \\
 & -|\epsilon_{\mu e}^d|\frac{\Delta m_{21}^2}{\Delta m_{31}^2}s_{2\times 12}c_{23}\sin\phi_{\mu e}^d\frac{\Delta m_{31}^2L}{2E}\cdot\left[1-2s_{23}^2\sin^2\frac{\Delta m_{31}^2L}{2E}\right] \\
 & +2|\epsilon_{\tau e}^d|\frac{\Delta m_{21}^2}{\Delta m_{31}^2}s_{2\times 12}s_{23}c_{23}^2\cos\phi_{\mu e}^d\frac{\Delta m_{31}^2L}{4E}\sin\frac{\Delta m_{31}^2L}{2E} \\
 & +2|\epsilon_{\tau e}^d|\frac{\Delta m_{21}^2}{\Delta m_{31}^2}s_{2\times 12}s_{23}c_{23}^2\sin\phi_{\mu e}^d\frac{\Delta m_{31}^2L}{2E}\sin^2\frac{\Delta m_{31}^2L}{4E} \\
 & +\mathcal{O}\left(\left[\frac{\Delta m_{21}^2}{\Delta m_{31}^2}\right]^3\right)+\mathcal{O}\left(\left[\frac{\Delta m_{21}^2}{\Delta m_{31}^2}\right]^2s_{13}\right)+\mathcal{O}\left(\frac{\Delta m_{21}^2}{\Delta m_{31}^2}s_{13}^2\right) \\
 & +\mathcal{O}(s_{13}^3)+\mathcal{O}\left(\varepsilon\left[\frac{\Delta m_{21}^2}{\Delta m_{31}^2}\right]^2\right)+\mathcal{O}\left(\varepsilon\tilde{s}_{13}\frac{\Delta m_{21}^2}{\Delta m_{31}^2}\right)+\mathcal{O}(\varepsilon s_{13}^2)+\mathcal{O}(\varepsilon^2).
 \end{aligned} \tag{C.4}$$

The corresponding expression for the near detector is

$$P(\nu_\mu^s \rightarrow \nu_e^d)^{\text{ND}} = |\varepsilon_{\mu e}^s|^2 + |\varepsilon_{\mu e}^d|^2 + 2|\varepsilon_{\mu e}^s||\varepsilon_{\mu e}^d|\cos(\phi_{\mu e}^s - \phi_{\mu e}^d) + \mathcal{O}\left(\frac{\Delta m_{31}^2L}{4E}\right) + \mathcal{O}(\varepsilon^3). \tag{C.5}$$

If also matter effects are included, one obtains

$$\begin{aligned}
 P(\nu_\mu^s \rightarrow \nu_e^d)^{\text{mat}} &= 4\tilde{s}_{13}^2s_{23}^2\sin^2\frac{(\Delta m_{31}^2 - a_{\text{CC}})L}{4E} \\
 &+ \left(\frac{\Delta m_{21}^2}{\Delta m_{31}^2}\right)^2c_{23}^2s_{2\times 12}^2\left(\frac{\Delta m_{31}^2}{a_{\text{CC}}}\right)^2\sin^2\frac{a_{\text{CC}}L}{4E} \\
 &- \frac{\Delta m_{21}^2}{\Delta m_{31}^2}\tilde{s}_{13}s_{2\times 12}s_{2\times 23}\cos\delta_{\text{CP}}\frac{\Delta m_{31}^2}{a_{\text{CC}}}\left[\sin^2\frac{a_{\text{CC}}L}{4E} - \sin^2\frac{\Delta m_{31}^2L}{4E} + \sin^2\frac{(\Delta m_{31}^2 - a_{\text{CC}})L}{4E}\right] \\
 &- \frac{1}{2}\frac{\Delta m_{21}^2}{\Delta m_{31}^2}\tilde{s}_{13}s_{2\times 12}s_{2\times 23}\sin\delta_{\text{CP}}\frac{\Delta m_{31}^2}{a_{\text{CC}}}\left[\sin\frac{a_{\text{CC}}L}{2E} - \sin\frac{\Delta m_{31}^2L}{2E} + \sin\frac{(\Delta m_{31}^2 - a_{\text{CC}})L}{2E}\right]
 \end{aligned}$$

$$\begin{aligned}
 & -4|\epsilon_{\mu e}^s|\tilde{s}_{13}s_{23}\cos(\phi_{\mu e}^s+\delta_{\text{CP}})\sin^2\frac{(\Delta m_{31}^2-a_{\text{CC}})L}{4E} \\
 & -2|\epsilon_{\mu e}^s|\tilde{s}_{13}s_{23}\sin(\phi_{\mu e}^s+\delta_{\text{CP}})\sin\frac{(\Delta m_{31}^2-a_{\text{CC}})L}{2E} \\
 & +4|\epsilon_{\mu e}^d|\tilde{s}_{13}s_{23}\cos(\phi_{\mu e}^d+\delta_{\text{CP}})\left[c_{23}^2\sin^2\frac{a_{\text{CC}}L}{4E}-c_{23}^2\sin^2\frac{\Delta m_{31}^2L}{4E}\right. \\
 & \quad \left.+s_{23}^2\sin^2\frac{(\Delta m_{31}^2-a_{\text{CC}})L}{4E}\right] \\
 & +2|\epsilon_{\mu e}^d|\tilde{s}_{13}s_{23}\sin(\phi_{\mu e}^d+\delta_{\text{CP}})\left[c_{23}^2\sin\frac{a_{\text{CC}}L}{2E}-c_{23}^2\sin\frac{\Delta m_{31}^2L}{2E}-s_{23}^2\sin\frac{(\Delta m_{31}^2-a_{\text{CC}})L}{2E}\right] \\
 & -4|\epsilon_{\tau e}^d|\tilde{s}_{13}s_{23}^2c_{23}\cos(\phi_{\tau e}^d+\delta_{\text{CP}})\left[\sin^2\frac{a_{\text{CC}}L}{4E}-\sin^2\frac{\Delta m_{31}^2L}{4E}-\sin^2\frac{(\Delta m_{31}^2-a_{\text{CC}})L}{4E}\right] \\
 & -2|\epsilon_{\tau e}^d|\tilde{s}_{13}s_{23}^2c_{23}\sin(\phi_{\tau e}^d+\delta_{\text{CP}})\left[\sin\frac{a_{\text{CC}}L}{2E}-\sin\frac{\Delta m_{31}^2L}{2E}+\sin\frac{(\Delta m_{31}^2-a_{\text{CC}})L}{2E}\right] \\
 & -4|\epsilon_{e\mu}^m|\tilde{s}_{13}s_{23}c_{23}^2\cos(\phi_{e\mu}^m+\delta_{\text{CP}})\left[\sin^2\frac{a_{\text{CC}}L}{4E}-\sin^2\frac{\Delta m_{31}^2L}{4E}+\sin^2\frac{(\Delta m_{31}^2-a_{\text{CC}})L}{4E}\right] \\
 & -2|\epsilon_{e\mu}^m|\tilde{s}_{13}s_{23}c_{23}^2\sin(\phi_{e\mu}^m+\delta_{\text{CP}})\left[\sin\frac{a_{\text{CC}}L}{2E}-\sin\frac{\Delta m_{31}^2L}{2E}+\sin\frac{(\Delta m_{31}^2-a_{\text{CC}})L}{2E}\right] \\
 & +8|\epsilon_{e\mu}^m|\tilde{s}_{13}s_{23}^3\cos(\phi_{e\mu}^m+\delta_{\text{CP}})\frac{a_{\text{CC}}}{\Delta m_{31}^2-a_{\text{CC}}}\sin^2\frac{(\Delta m_{31}^2-a_{\text{CC}})L}{4E} \\
 & +4|\epsilon_{e\tau}^m|\tilde{s}_{13}s_{23}^2c_{23}\cos(\phi_{e\tau}^m+\delta_{\text{CP}})\left[\sin^2\frac{a_{\text{CC}}L}{4E}-\sin^2\frac{\Delta m_{31}^2L}{4E}+\sin^2\frac{(\Delta m_{31}^2-a_{\text{CC}})L}{4E}\right] \\
 & +2|\epsilon_{e\tau}^m|\tilde{s}_{13}s_{23}^2c_{23}\sin(\phi_{e\tau}^m+\delta_{\text{CP}})\left[\sin\frac{a_{\text{CC}}L}{2E}-\sin\frac{\Delta m_{31}^2L}{2E}+\sin\frac{(\Delta m_{31}^2-a_{\text{CC}})L}{2E}\right] \\
 & +8|\epsilon_{e\tau}^m|\tilde{s}_{13}s_{23}^2c_{23}\cos(\phi_{e\tau}^m+\delta_{\text{CP}})\frac{a_{\text{CC}}}{\Delta m_{31}^2-a_{\text{CC}}}\sin^2\frac{(\Delta m_{31}^2-a_{\text{CC}})L}{4E} \\
 & +2|\epsilon_{\mu e}^s|\frac{\Delta m_{21}^2}{\Delta m_{31}^2}s_{2\times 12}c_{23}\cos\phi_{\mu e}^s\frac{\Delta m_{31}^2}{a_{\text{CC}}}\sin^2\frac{a_{\text{CC}}L}{4E} \\
 & -|\epsilon_{\mu e}^s|\frac{\Delta m_{21}^2}{\Delta m_{31}^2}s_{2\times 12}c_{23}\sin\phi_{\mu e}^s\frac{\Delta m_{31}^2}{a_{\text{CC}}}\sin\frac{a_{\text{CC}}L}{2E} \\
 & -2|\epsilon_{\mu e}^d|\frac{\Delta m_{21}^2}{\Delta m_{31}^2}s_{2\times 12}c_{23}\cos\phi_{\mu e}^d\frac{\Delta m_{31}^2}{a_{\text{CC}}}\left[c_{23}^2\sin^2\frac{a_{\text{CC}}L}{4E}-s_{23}^2\sin^2\frac{\Delta m_{31}^2L}{4E}\right. \\
 & \quad \left.+s_{23}^2\sin^2\frac{(\Delta m_{31}^2-a_{\text{CC}})L}{4E}\right] \\
 & -|\epsilon_{\mu e}^d|\frac{\Delta m_{21}^2}{\Delta m_{31}^2}s_{2\times 12}c_{23}\sin\phi_{\mu e}^d\frac{\Delta m_{31}^2}{a_{\text{CC}}}\left[c_{23}^2\sin\frac{a_{\text{CC}}L}{2E}+s_{23}^2\sin\frac{\Delta m_{31}^2L}{2E}\right. \\
 & \quad \left.-s_{23}^2\sin\frac{(\Delta m_{31}^2-a_{\text{CC}})L}{2E}\right]
 \end{aligned}$$

$$\begin{aligned}
 & + 2|\epsilon_{\tau e}^d| \frac{\Delta m_{21}^2}{\Delta m_{31}^2} s_{2 \times 12} s_{23} c_{23}^2 \cos \phi_{\tau e}^d \frac{\Delta m_{31}^2}{a_{CC}} \left[\sin^2 \frac{a_{CC} L}{4E} + \sin^2 \frac{\Delta m_{31}^2 L}{4E} \right. \\
 & \quad \left. - \sin^2 \frac{(\Delta m_{31}^2 - a_{CC}) L}{4E} \right] \\
 & + |\epsilon_{\tau e}^d| \frac{\Delta m_{21}^2}{\Delta m_{31}^2} s_{2 \times 12} s_{23} c_{23}^2 \sin \phi_{\tau e}^d \frac{\Delta m_{31}^2}{a_{CC}} \left[\sin \frac{a_{CC} L}{2E} - \sin \frac{\Delta m_{31}^2 L}{2E} \right. \\
 & \quad \left. + \sin \frac{(\Delta m_{31}^2 - a_{CC}) L}{2E} \right] \\
 & + 4|\epsilon_{e\mu}^m| \frac{\Delta m_{21}^2}{\Delta m_{31}^2} s_{2 \times 12} c_{23}^3 \cos \phi_{e\mu}^m \frac{\Delta m_{31}^2}{a_{CC}} \sin^2 \frac{a_{CC} L}{4E} \\
 & - 2|\epsilon_{e\mu}^m| \frac{\Delta m_{21}^2}{\Delta m_{31}^2} s_{2 \times 12} s_{23}^2 c_{23} \cos \phi_{e\mu}^m \frac{\Delta m_{31}^2}{\Delta m_{31}^2 - a_{CC}} \left[\sin^2 \frac{a_{CC} L}{4E} - \sin^2 \frac{\Delta m_{31}^2 L}{4E} \right. \\
 & \quad \left. + \sin^2 \frac{(\Delta m_{31}^2 - a_{CC}) L}{4E} \right] \\
 & + |\epsilon_{e\mu}^m| \frac{\Delta m_{21}^2}{\Delta m_{31}^2} s_{2 \times 12} s_{23}^2 c_{23} \sin \phi_{e\mu}^m \frac{\Delta m_{31}^2}{\Delta m_{31}^2 - a_{CC}} \left[\sin \frac{a_{CC} L}{2E} - \sin \frac{\Delta m_{31}^2 L}{2E} \right. \\
 & \quad \left. + \sin \frac{(\Delta m_{31}^2 - a_{CC}) L}{2E} \right] \\
 & - 4|\epsilon_{e\tau}^m| \frac{\Delta m_{21}^2}{\Delta m_{31}^2} s_{2 \times 12} s_{23} c_{23}^2 \cos \phi_{e\tau}^m \frac{\Delta m_{31}^2}{a_{CC}} \sin^2 \frac{a_{CC} L}{4E} \\
 & - 2|\epsilon_{e\tau}^m| \frac{\Delta m_{21}^2}{\Delta m_{31}^2} s_{2 \times 12} s_{23} c_{23}^2 \cos \phi_{e\tau}^m \frac{\Delta m_{31}^2}{\Delta m_{31}^2 - a_{CC}} \left[\sin^2 \frac{a_{CC} L}{4E} - \sin^2 \frac{\Delta m_{31}^2 L}{4E} \right. \\
 & \quad \left. + \sin^2 \frac{(\Delta m_{31}^2 - a_{CC}) L}{4E} \right] \\
 & + |\epsilon_{e\tau}^m| \frac{\Delta m_{21}^2}{\Delta m_{31}^2} s_{2 \times 12} s_{23} c_{23}^2 \sin \phi_{e\tau}^m \frac{\Delta m_{31}^2}{\Delta m_{31}^2 - a_{CC}} \left[\sin \frac{a_{CC} L}{2E} - \sin \frac{\Delta m_{31}^2 L}{2E} \right. \\
 & \quad \left. + \sin \frac{(\Delta m_{31}^2 - a_{CC}) L}{2E} \right] \\
 & + \mathcal{O}\left(\left[\frac{\Delta m_{21}^2}{\Delta m_{31}^2}\right]^3\right) + \mathcal{O}\left(\left[\frac{\Delta m_{21}^2}{\Delta m_{31}^2}\right]^2 s_{13}\right) + \mathcal{O}\left(\frac{\Delta m_{21}^2}{\Delta m_{31}^2} s_{13}^2\right) + \mathcal{O}(s_{13}^3) \\
 & + \mathcal{O}\left(\varepsilon \left[\frac{\Delta m_{21}^2}{\Delta m_{31}^2}\right]^2\right) + \mathcal{O}\left(\varepsilon s_{13} \frac{\Delta m_{21}^2}{\Delta m_{31}^2}\right) + \mathcal{O}(\varepsilon s_{13}^2) + \mathcal{O}(\varepsilon^2). \tag{C.6}
 \end{aligned}$$

The expression for the time-reversed channel $\nu_e \rightarrow \nu_\mu$ (the golden neutrino factory channel), is obtained by making the replacements $\delta_{CP} \rightarrow -\delta_{CP}$ and $\phi_{\alpha\beta}^{s,m,d} \rightarrow -\phi_{\alpha\beta}^{s,m,d}$ [208, 209].

C.3 The $\nu_\mu \rightarrow \nu_\mu$ channel

For the $\nu_\mu \rightarrow \nu_\mu$ survival probability, one finds in vacuum

$$\begin{aligned}
 P(\nu_\mu^s \rightarrow \nu_\mu^d)^{\text{vac}} = & 1 - s_{2 \times 23}^2 \sin^2 \frac{\Delta m_{31}^2 L}{4E} \\
 & + 2|\epsilon_{\mu\mu}^s| \cos \phi_{\mu\mu}^s + 2|\epsilon_{\mu\mu}^d| \cos \phi_{\mu\mu}^d \\
 & - [2|\epsilon_{\mu\mu}^s| \cos \phi_{\mu\mu}^s + 2|\epsilon_{\mu\mu}^d| \cos \phi_{\mu\mu}^d] s_{2 \times 23}^2 \sin^2 \frac{\Delta m_{31}^2 L}{4E} \\
 & - 2 \left(|\epsilon_{\mu\tau}^s| \cos \phi_{\mu\tau}^s + |\epsilon_{\tau\mu}^d| \cos \phi_{\tau\mu}^d \right) c_{2 \times 23} s_{2 \times 23} \sin^2 \frac{\Delta m_{31}^2 L}{4E} \\
 & + \left(|\epsilon_{\mu\tau}^s| \sin \phi_{\mu\tau}^s + |\epsilon_{\tau\mu}^d| \sin \phi_{\tau\mu}^d \right) s_{2 \times 23} \sin \frac{\Delta m_{31}^2 L}{2E} \\
 & + \mathcal{O}\left(\frac{\Delta m_{21}^2}{\Delta m_{31}^2}\right) + \mathcal{O}(s_{13}) + \mathcal{O}(\varepsilon^2), \tag{C.7}
 \end{aligned}$$

and in matter

$$\begin{aligned}
 P(\nu_\mu^s \rightarrow \nu_\mu^d)^{\text{mat}} = & 1 - s_{2 \times 23}^2 \sin^2 \frac{\Delta m_{31}^2 L}{4E} \\
 & + 2|\epsilon_{\mu\mu}^s| \cos \phi_{\mu\mu}^s + 2|\epsilon_{\mu\mu}^d| \cos \phi_{\mu\mu}^d \\
 & - [2|\epsilon_{\mu\mu}^s| \cos \phi_{\mu\mu}^s + 2|\epsilon_{\mu\mu}^d| \cos \phi_{\mu\mu}^d] s_{2 \times 23}^2 \sin^2 \frac{\Delta m_{31}^2 L}{4E} \\
 & - 2 \left(|\epsilon_{\mu\tau}^s| \cos \phi_{\mu\tau}^s + |\epsilon_{\tau\mu}^d| \cos \phi_{\tau\mu}^d \right) c_{2 \times 23} s_{2 \times 23} \sin^2 \frac{\Delta m_{31}^2 L}{4E} \\
 & + \left(|\epsilon_{\mu\tau}^s| \sin \phi_{\mu\tau}^s + |\epsilon_{\tau\mu}^d| \sin \phi_{\tau\mu}^d \right) s_{2 \times 23} \sin \frac{\Delta m_{31}^2 L}{2E} \\
 & - |\epsilon_{\mu\tau}^m| \left[s_{2 \times 23}^3 \cos \phi_{\mu\tau}^m \frac{a_{\text{CC}} L}{2E} \sin \frac{\Delta m_{31}^2 L}{2E} + 4s_{2 \times 23} c_{2 \times 23}^2 \cos \phi_{\mu\tau}^m \frac{a_{\text{CC}}}{\Delta m_{31}^2} \sin^2 \frac{\Delta m_{31}^2 L}{4E} \right] \\
 & + \frac{1}{2} |\epsilon_{\mu\mu}^m| \left[s_{2 \times 23}^2 c_{2 \times 23} \frac{a_{\text{CC}} L}{2E} \sin \frac{\Delta m_{31}^2 L}{2E} - 4s_{2 \times 23}^2 c_{2 \times 23} \frac{a_{\text{CC}}}{\Delta m_{31}^2} \sin^2 \frac{\Delta m_{31}^2 L}{4E} \right] \\
 & - \frac{1}{2} |\epsilon_{\tau\tau}^m| \left[s_{2 \times 23}^2 c_{2 \times 23} \frac{a_{\text{CC}} L}{2E} \sin \frac{\Delta m_{31}^2 L}{2E} - 4s_{2 \times 23}^2 c_{2 \times 23} \frac{a_{\text{CC}}}{\Delta m_{31}^2} \sin^2 \frac{\Delta m_{31}^2 L}{4E} \right] \\
 & + \mathcal{O}\left(\frac{\Delta m_{21}^2}{\Delta m_{31}^2}\right) + \mathcal{O}(s_{13}) + \mathcal{O}(\varepsilon^2). \tag{C.8}
 \end{aligned}$$

To obtain the oscillation probabilities for the CP conjugates of the above equations, one has to make the replacements $\delta_{\text{CP}} \rightarrow -\delta_{\text{CP}}$, $\phi_{\alpha\beta}^{s,m,d} \rightarrow -\phi_{\alpha\beta}^{s,m,d}$ and $a_{\text{CC}} \rightarrow -a_{\text{CC}}$.

List of Figures

2.1	Results of a global fit of the neutrino oscillation parameters.	17
3.1	Feynman diagram for Mössbauer neutrinos.	35
3.2	Integration contours in the complex E plane, used in the evaluation of (3.76).	44
3.3	Integration contours in the complex p_0 plane, used in the evaluation of (3.97).	52
4.1	Impact of ε^s and ε^d on reactor neutrino experiments.	67
4.2	Impact of ε^s and ε^d on superbeam experiments.	68
4.3	Impact of ε^m on superbeam experiments.	69
4.4	NSI discovery reaches of Double Chooz, T2K, and of a combined analysis.	75
4.5	Examples for NSI-induced offsets and discrepancies in θ_{13} -fits.	78
4.6	Impact of $(V - A)(V - A)$ type CC NSI (fulfilling $\varepsilon_{\alpha\beta}^s = (\varepsilon_{\beta\alpha}^d)^*$) on the θ_{13} fits in T2K and Double Chooz.	80
4.7	Impact of arbitrary CC NSI (ε^s and ε^d treated as independent matrices) on the θ_{13} fits in T2K and Double Chooz.	81
4.8	Impact of non-standard matter effects proportional to $\varepsilon_{e\tau}^m$ on the θ_{13} fits in T2K, Double Chooz, NO ν A and DC-200.	82
4.9	Impact of combinations of several NSI effects on the θ_{13} fits in T2K, Double Chooz, NO ν A and DC-200.	83
4.10	Impact of ε^m on a neutrino factory.	85
4.11	NSI sensitivity of a neutrino factory as a function of E_μ	89
4.12	Baseline optimisation for a neutrino factory with respect to standard oscillation performance indicators.	90
4.13	Baseline optimisation for a neutrino factory with respect to the NSI sensitivities.	92
4.14	Summary of the neutrino factory performance with and without NSI.	95

List of Tables

3.1	The oscillation, coherence, localisation and resonance terms obtained for Mössbauer neutrinos in different theoretical approaches.	57
4.1	Current 90% C.L. bounds on non-standard matter effects.	65
4.2	Classification of non-standard interactions according to their expected impact on reactor and superbeam experiments.	71
4.3	Classification of non-standard interactions according to their expected impact on a neutrino factory.	84
4.4	Summary of the sensitivity of a neutrino factory to standard and non-standard observables.	94
A.1	Classification of the states appearing in a Mössbauer neutrino experiment.	102
B.1	Classification of NSI operators with arbitrary Lorentz structure according to their relevance in future experiments.	114

Bibliography

- [1] S. L. Glashow, *Interactions: A journey through the mind of a particle physicist and the matter of this world*, Warner Books, 1988.
- [2] E. Waxman, *Neutrino astrophysics: A new tool for exploring the universe*, Science **315** (2007), 63–65, [astro-ph/0701168](#).
- [3] Super-Kamiokande, Y. Fukuda et al., *Evidence for oscillation of atmospheric neutrinos*, Phys. Rev. Lett. **81** (1998), 1562–1567, [hep-ex/9807003](#).
- [4] Super-Kamiokande, Y. Ashie et al., *Evidence for an oscillatory signature in atmospheric neutrino oscillation*, Phys. Rev. Lett. **93** (2004), 101801, [hep-ex/0404034](#).
- [5] Super-Kamiokande, Y. Ashie et al., *A measurement of atmospheric neutrino oscillation parameters by Super-Kamiokande I*, Phys. Rev. **D71** (2005), 112005, [hep-ex/0501064](#).
- [6] Soudan-2, W. W. M. Allison et al., *Neutrino oscillation effects in Soudan-2 upward-stopping muons*, Phys. Rev. **D72** (2005), 052005, [hep-ex/0507068](#).
- [7] MACRO, M. Ambrosio et al., *Measurements of atmospheric muon neutrino oscillations, global analysis of the data collected with MACRO detector*, Eur. Phys. J. **C36** (2004), 323–339.
- [8] R. Davis, *A review of the Homestake solar neutrino experiment*, Prog. Part. Nucl. Phys. **32** (1994), 13–32.
- [9] SNO, Q. R. Ahmad et al., *Direct evidence for neutrino flavor transformation from neutral-current interactions in the Sudbury Neutrino Observatory*, Phys. Rev. Lett. **89** (2002), 011301, [nucl-ex/0204008](#).
- [10] Super-Kamiokande, J. P. Cravens et al., *Solar neutrino measurements in Super-Kamiokande-II*, Phys. Rev. **D78** (2008), 032002, [0803.4312](#).
- [11] KamLAND, K. Eguchi et al., *First results from KamLAND: Evidence for reactor anti- neutrino disappearance*, Phys. Rev. Lett. **90** (2003), 021802, [hep-ex/0212021](#).
- [12] KamLAND, T. Araki et al., *Measurement of neutrino oscillation with KamLAND: Evidence of spectral distortion*, Phys. Rev. Lett. **94** (2005), 081801, [hep-ex/0406035](#).

- [13] K2K, E. Aliu et al., *Evidence for muon neutrino oscillation in an accelerator- based experiment*, Phys. Rev. Lett. **94** (2005), 081802, [hep-ex/0411038](#).
- [14] MINOS, D. G. Michael et al., *Observation of muon neutrino disappearance with the MINOS detectors and the NuMI neutrino beam*, Phys. Rev. Lett. **97** (2006), 191801, [hep-ex/0607088](#).
- [15] R. N. Mohapatra et al., *Theory of neutrinos: A white paper*, Rept. Prog. Phys. **70** (2007), 1757–1867, [hep-ph/0510213](#).
- [16] M. Beuthe, *Oscillations of neutrinos and mesons in quantum field theory*, Phys. Rept. **375** (2003), 105–218, [hep-ph/0109119](#).
- [17] R. N. Mohapatra and A. Y. Smirnov, *Neutrino mass and new physics*, Ann. Rev. Nucl. Part. Sci. **56** (2006), 569–628, [hep-ph/0603118](#).
- [18] C. H. Albright and M.-C. Chen, *Model predictions for neutrino oscillation parameters*, Phys. Rev. **D74** (2006), 113006, [hep-ph/0608137](#).
- [19] ISS Physics Working Group, A. Bandyopadhyay et al., *Physics at a future neutrino factory and super-beam facility*, (2007), 0710.4947.
- [20] H.-T. Janka, K. Langanke, A. Marek, G. Martinez-Pinedo, and B. Mueller, *Theory of core-collapse supernovae*, Phys. Rept. **442** (2007), 38–74, [astro-ph/0612072](#).
- [21] S. Hannestad, *Neutrinos in cosmology*, New J. Phys. **6** (2004), 108, [hep-ph/0404239](#).
- [22] T.-P. Cheng and L.-F. Li, *Gauge theory of elementary particle physics*, Clarendon Press, 1984.
- [23] E. K. Akhmedov, *Neutrino physics*, (1999), [hep-ph/0001264](#).
- [24] R. G. Winter, *Neutrino oscillation kinematics*, Lett. Nuovo Cim. **30** (1981), 101–104.
- [25] C. Giunti, C. W. Kim, and U. W. Lee, *When do neutrinos really oscillate?: Quantum mechanics of neutrino oscillations*, Phys. Rev. **D44** (1991), 3635–3640.
- [26] C. Giunti and C. W. Kim, *Quantum mechanics of neutrino oscillations*, Found. Phys. Lett. **14** (2001), 213–229, [hep-ph/0011074](#).
- [27] C. Giunti, *Energy and momentum of oscillating neutrinos*, Mod. Phys. Lett. **A16** (2001), 2363, [hep-ph/0104148](#).
- [28] C. Giunti, *Coherence and wave packets in neutrino oscillations*, Found. Phys. Lett. **17** (2004), 103–124, [hep-ph/0302026](#).

- [29] E. K. Akhmedov, J. Kopp, and M. Lindner, *On application of the time-energy uncertainty relation to Mössbauer neutrino experiments*, (2008), 0803.1424.
- [30] C. Giunti, C. W. Kim, and U. W. Lee, *Coherence of neutrino oscillations in vacuum and matter in the wave packet treatment*, Phys. Lett. **B274** (1992), 87–94.
- [31] K. Kiers, S. Nussinov, and N. Weiss, *Coherence effects in neutrino oscillations*, Phys. Rev. **D53** (1996), 537–547, hep-ph/9506271.
- [32] C. Giunti and C. W. Kim, *Coherence of neutrino oscillations in the wave packet approach*, Phys. Rev. **D58** (1998), 017301, hep-ph/9711363.
- [33] C. Giunti, *The phase of neutrino oscillations*, Physica Scripta **67** (2003), 29, hep-ph/0202063.
- [34] R. Jacob and R. G. Sachs, *Mass and lifetime of unstable particles*, Phys. Rev. **121** (1961), no. 1, 350–356.
- [35] R. G. Sachs, *Interference phenomena of neutral K mesons*, Annals of Physics **22** (1963), 239–262.
- [36] C. Giunti, C. W. Kim, J. A. Lee, and U. W. Lee, *On the treatment of neutrino oscillations without resort to weak eigenstates*, Phys. Rev. **D48** (1993), 4310–4317, hep-ph/9305276.
- [37] J. Rich, *The quantum mechanics of neutrino oscillations*, Phys. Rev. **D48** (1993), 4318–4325.
- [38] W. Grimus and P. Stockinger, *Real oscillations of virtual neutrinos*, Phys. Rev. **D54** (1996), 3414–3419, hep-ph/9603430.
- [39] W. Grimus, P. Stockinger, and S. Mohanty, *The field-theoretical approach to coherence in neutrino oscillations*, Phys. Rev. **D59** (1999), 013011, hep-ph/9807442.
- [40] W. Grimus, S. Mohanty, and P. Stockinger, *Neutrino oscillations and the effect of the finite lifetime of the neutrino source*, Phys. Rev. **D61** (2000), 033001, hep-ph/9904285.
- [41] C. Y. Cardall, *Coherence of neutrino flavor mixing in quantum field theory*, Phys. Rev. **D61** (2000), 073006, hep-ph/9909332.
- [42] M. Beuthe, *Towards a unique formula for neutrino oscillations in vacuum*, Phys. Rev. **D66** (2002), 013003, hep-ph/0202068.
- [43] L. Wolfenstein, *Neutrino oscillations in matter*, Phys. Rev. **D17** (1978), 2369.
- [44] S. P. Mikheyev and A. Y. Smirnov, *Resonance enhancement of oscillations in matter and solar neutrino spectroscopy*, Sov. J. Nucl. Phys. **42** (1985), 913–917.

- [45] S. P. Mikheyev and A. Y. Smirnov, *Resonant amplification of neutrino oscillations in matter and solar neutrino spectroscopy*, Nuovo Cim. **C9** (1986), 17–26.
- [46] B. T. Cleveland et al., *Measurement of the solar electron neutrino flux with the Homestake chlorine detector*, Astrophys. J. **496** (1998), 505–526.
- [47] SAGE, J. N. Abdurashitov et al., *Measurement of the solar neutrino capture rate by the Russian-American gallium solar neutrino experiment during one half of the 22-year cycle of solar activity*, J. Exp. Theor. Phys. **95** (2002), 181–193, astro-ph/0204245.
- [48] GALLEX, W. Hampel et al., *GALLEX solar neutrino observations: Results for GALLEX IV*, Phys. Lett. **B447** (1999), 127–133.
- [49] GNO, M. Altmann et al., *GNO solar neutrino observations: Results for GNO I*, Phys. Lett. **B490** (2000), 16–26, hep-ex/0006034.
- [50] The KamLAND Collaboration, *Precision measurement of neutrino oscillation parameters with KamLAND*, (2008), arXiv:0801.4589 [hep-ex].
- [51] CHOOZ, M. Apollonio et al., *Search for neutrino oscillations on a long baseline at the CHOOZ nuclear power station*, Eur. Phys. J. **C27** (2003), 331–374, hep-ex/0301017.
- [52] K2K, M. H. Ahn et al., *Indications of neutrino oscillation in a 250-km long- baseline experiment*, Phys. Rev. Lett. **90** (2003), 041801, hep-ex/0212007.
- [53] K2K, M. H. Ahn et al., *Measurement of neutrino oscillation by the K2K experiment*, Phys. Rev. **D74** (2006), 072003, hep-ex/0606032.
- [54] MINOS, P. Adamson et al., *Measurement of neutrino oscillations with the MINOS detectors in the NuMI beam*, Phys. Rev. Lett. **101** (2008), 131802, 0806.2237.
- [55] M. Maltoni, T. Schwetz, M. A. Tortola, and J. W. F. Valle, *Status of global fits to neutrino oscillations*, New J. Phys. **6** (2004), 122, hep-ph/0405172.
- [56] V. M. Lobashev et al., *Direct search for mass of neutrino and anomaly in the tritium beta-spectrum*, Phys. Lett. **B460** (1999), 227–235.
- [57] C. Kraus et al., *Final results from phase II of the Mainz neutrino mass search in tritium beta decay*, Eur. Phys. J. **C40** (2005), 447–468, hep-ex/0412056.
- [58] G. L. Fogli et al., *Observables sensitive to absolute neutrino masses (Addendum)*, Phys. Rev. **D78** (2008), 033010, 0805.2517.
- [59] Y. Y. Y. Wong, *Neutrinos in cosmology*, AIP Conf. Proc. **972** (2008), 427–435.

-
- [60] H. V. Klapdor-Kleingrothaus et al., *Latest results from the Heidelberg-Moscow double-beta- decay experiment*, Eur. Phys. J. **A12** (2001), 147–154, [hep-ph/0103062](#).
- [61] S. Davidson, C. Pena-Garay, N. Rius, and A. Santamaria, *Present and future bounds on non-standard neutrino interactions*, JHEP **03** (2003), 011, [hep-ph/0302093](#).
- [62] M. C. Gonzalez-Garcia and M. Maltoni, *Phenomenology with massive neutrinos*, Phys. Rept. **460** (2008), 1–129, [0704.1800](#).
- [63] M. Maltoni, *New interactions: past and future experiments*, J. Phys. Conf. Ser. **136** (2008), 022024, [0810.3517](#).
- [64] M. C. Gonzalez-Garcia and M. Maltoni, *Status of oscillation plus decay of atmospheric and long-baseline neutrinos*, Phys. Lett. **B663** (2008), 405–409, [0802.3699](#).
- [65] Y. Farzan, T. Schwetz, and A. Y. Smirnov, *Reconciling results of LSND, Mini-BooNE and other experiments with soft decoherence*, JHEP **07** (2008), 067, [0805.2098](#).
- [66] M. Maltoni and T. Schwetz, *Sterile neutrino oscillations after first MiniBooNE results*, Phys. Rev. **D76** (2007), 093005, [0705.0107](#).
- [67] Double Chooz, F. Ardellier et al., *Double chooz: A search for the neutrino mixing angle θ_{13}* , (2006), [hep-ex/0606025](#).
- [68] Daya Bay, X. Guo et al., *A precision measurement of the neutrino mixing angle θ_{13} using reactor antineutrinos at Daya Bay*, (2007), [hep-ex/0701029](#).
- [69] T2K, K. Nishikawa et al., *Tokai-to-Kamioka (T2K) long baseline neutrino oscillation experiment proposal*, (2006).
- [70] NOvA, D. S. Ayres et al., *NOvA proposal to build a 30-kiloton off-axis detector to study neutrino oscillations in the Fermilab NuMI beamline*, (2004), [hep-ex/0503053](#).
- [71] P. Zucchelli, *A novel concept for a $\bar{\nu}_e/\nu_e$ neutrino factory: The beta beam*, Phys. Lett. **B532** (2002), 166–172.
- [72] P. Huber, M. Lindner, M. Rolinec, and W. Winter, *Physics and optimization of beta-beams: From low to very high gamma*, Phys. Rev. **D73** (2006), 053002, [hep-ph/0506237](#).
- [73] S. Geer, *Neutrino beams from muon storage rings: Characteristics and physics potential*, Phys. Rev. **D57** (1998), 6989–6997, [hep-ph/9712290](#).

- [74] A. De Rujula, M. B. Gavela, and P. Hernandez, *Neutrino oscillation physics with a neutrino factory*, Nucl. Phys. **B547** (1999), 21–38, [hep-ph/9811390](#).
- [75] A. Cervera et al., *Golden measurements at a neutrino factory*, Nucl. Phys. **B579** (2000), 17–55, [hep-ph/0002108](#).
- [76] Website of the *International Design Study for the Neutrino factory*, <http://www.hep.ph.ic.ac.uk/ids/>.
- [77] H. Minakata and H. Nunokawa, *Exploring neutrino mixing with low energy super-beams*, JHEP **10** (2001), 001, [hep-ph/0108085](#).
- [78] J. Burguet-Castell, M. B. Gavela, J. J. Gomez-Cadenas, P. Hernandez, and O. Mena, *On the measurement of leptonic CP violation*, Nucl. Phys. **B608** (2001), 301–318, [hep-ph/0103258](#).
- [79] G. L. Fogli and E. Lisi, *Tests of three-flavor mixing in long-baseline neutrino oscillation experiments*, Phys. Rev. **D54** (1996), 3667–3670, [hep-ph/9604415](#).
- [80] V. Barger, D. Marfatia, and K. Whisnant, *Breaking eight-fold degeneracies in neutrino CP violation, mixing, and mass hierarchy*, Phys. Rev. **D65** (2002), 073023, [hep-ph/0112119](#).
- [81] P. Huber, M. Lindner, M. Rolinec, and W. Winter, *Optimization of a neutrino factory oscillation experiment*, Phys. Rev. **D74** (2006), 073003, [hep-ph/0606119](#).
- [82] W. M. Visscher, *Neutrino detection by resonance absorption in crystals at low temperatures*, Phys. Rev. **116** (1959), no. 6, 1581–1582.
- [83] Mössbauer, Rudolf L., *Kernresonanzfluoreszenz von Gammastrahlung in Ir¹⁹¹*, Z. Phys. **151** (1958), 124.
- [84] W. P. Kells, *Resonant neutrino activation and neutrino oscillations*, AIP Conf. Proc. **99** (1983), 272–281.
- [85] W. P. Kells and J. P. Schiffer, *Possibility of observing recoilless resonant neutrino absorption*, Phys. Rev. **C28** (1983), 2162–2164.
- [86] J. N. Bahcall, *Theory of bound-state beta decay*, Phys. Rev. **124** (1961), no. 2, 495–499.
- [87] L. A. Mikaelyan, V. G. Tsinoev, and A. A. Borovoi, *Induced capture of orbital electron*, Yad. Fiz. **6** (1967), no. 2, 349–352.
- [88] R. S. Raghavan, *Recoilless resonant capture of antineutrinos*, (2005), [hep-ph/0511191](#).
- [89] R. S. Raghavan, *Recoilless resonant capture of antineutrinos from tritium decay*, (2006), [hep-ph/0601079](#).

- [90] R. S. Raghavan, *Hypersharp neutrino lines*, (2008), 0805.4155.
- [91] R. S. Raghavan, *Hypersharp resonant capture of anti-neutrinos*, (2008), 0806.0839.
- [92] W. Potzel, *Recoilless resonant capture of antineutrinos: Basic questions and some ideas*, Phys. Scripta **T127** (2006), 85–88.
- [93] R. Coussement, G. S’heeren, M. Van Den Bergh, and P. Boolchand, *Nuclear resonant absorption in long-lived isomeric transitions*, Phys. Rev. B **45** (1992), no. 17, 9755–9758.
- [94] S. M. Bilenky, F. von Feilitzsch, and W. Potzel, *Recoilless resonant neutrino capture and basics of neutrino oscillations*, J. Phys. **G34** (2007), 987, hep-ph/0611285.
- [95] S. M. Bilenky, *Recoilless resonance absorption of tritium antineutrinos and time-energy uncertainty relation*, (2007), arXiv:0708.0260 [hep-ph].
- [96] S. M. Bilenky, F. von Feilitzsch, and W. Potzel, *Time-energy uncertainty relations for neutrino oscillation and Mössbauer neutrino experiment*, J. Phys. **G35** (2008), 095003, 0803.0527.
- [97] S. M. Bilenky, F. von Feilitzsch, and W. Potzel, *Different schemes of neutrino oscillations in Mössbauer neutrino experiment*, (2008), 0804.3409.
- [98] E. K. Akhmedov, J. Kopp, and M. Lindner, *Oscillations of Mössbauer neutrinos*, JHEP **05** (2008), 005, 0802.2513.
- [99] G. C. Abell and D. F. Cowgill, *Low-temperature ^3He NMR studies in aged palladium tritide*, Phys. Rev. B **44** (1991), no. 9, 4178–4184.
- [100] W. Potzel, *Recoilless resonant emission and detection of electron antineutrinos*, in *Proceedings of the XXIIIrd International Conference on Neutrino Physics and Astrophysics*, 2008.
- [101] M. J. Puska and R. M. Nieminen, *Theory of hydrogen and helium impurities in metals*, Phys. Rev. B **29** (1984), no. 10, 5382–5397.
- [102] H. Frauenfelder, *The Mössbauer effect*, W. A. Benjamin Inc., New York, 1962.
- [103] W. Potzel, private communication.
- [104] H. Minakata and S. Uchinami, *Recoilless resonant absorption of monochromatic neutrino beam for measuring Δm_{31}^2 and θ_{13}* , New J. Phys. **8** (2006), 143, hep-ph/0602046.
- [105] R. V. Pound and G. A. Rebka, *Apparent weight of photons*, Phys. Rev. Lett. **4** (1960), no. 7, 337–341.

- [106] B. Kayser, *On the quantum mechanics of neutrino oscillation*, Phys. Rev. **D24** (1981), 110.
- [107] C. Giunti, *Neutrino wave packets in quantum field theory*, JHEP **11** (2002), 017, hep-ph/0205014.
- [108] H. J. Lipkin, *Quantum mechanics: New approaches to selected topics*, North Holland, Amsterdam, 1973.
- [109] D. H. Perkins, *Introduction to high energy physics*, fourth ed., Cambridge University Press, 2000.
- [110] B. Povh, K. Rith, C. Scholz, and F. Zetsche, *Teilchen und Kerne*, sixth ed., Springer, 2004.
- [111] F. Schwabl, *Quantum mechanics*, Springer, 2007.
- [112] F. Schwabl, *Advanced quantum mechanics*, Springer, 2005.
- [113] R. Coussement, M. van den Bergh, G. S'heeren, and P. Boolchand, *Mössbauer absorption on ^{109m}Ag , fake or reality?*, Hyperfine Int. **71** (1992), no. 1–4, 1487–1490.
- [114] J. Odeurs, *Homogeneous line broadening in long-lived nuclear states*, Phys. Rev. B **52** (1995), no. 9, 6166–6169.
- [115] B. Balko, I. W. Kay, J. Nicoll, J. D. Silk, and G. Herling, *Inhomogeneous and homogeneous broadening effects on nuclear resonance experiments*, Hyperfine Int. **107** (1997), 283.
- [116] J. Odeurs and R. Coussement, *Models for homogeneous line broadening in long-lived nuclear states*, Hyperfine Int. **107** (1997), no. 1–4, 299–306.
- [117] P. Meystre and M. Sargent, *Elements of quantum optics; 4th ed.*, Springer, Berlin, 2007.
- [118] R. B. Firestone and V. S. Shirley, *Table of isotopes*, 8th ed., Wiley-Interscience, 1998.
- [119] V. Weisskopf and E. P. Wigner, *Berechnung der natürlichen Linienbreite auf Grund der Diracschen Lichttheorie*, Z. Phys. **63** (1930), 54–73.
- [120] V. Weisskopf and E. Wigner, *Über die natürliche Linienbreite in der Strahlung des harmonischen Oszillators*, Z. Phys. **65** (1930), 18–29.
- [121] C. Cohen-Tannoudji, B. Diu, and F. Laloe, *Quantum mechanics*, vol. 2, Wiley-Interscience, 1977.

-
- [122] P. Meystre, M. O. Scully, and H. Walther, *Transient line narrowing: A laser spectroscopic technique yielding resolution beyond the natural line width*, Optics Communications **33** (1980), no. 2, 153–157.
- [123] A. G. Cohen, S. L. Glashow, and Z. Ligeti, *Disentangling Neutrino Oscillations*, (2008), 0810.4602.
- [124] A. Messiah, *Quantum mechanics*, vol. 1, North Holland, Amsterdam, July 1964.
- [125] J. W. F. Valle, *Resonant oscillations of massless neutrinos in matter*, Phys. Lett. **B199** (1987), 432.
- [126] M. M. Guzzo, A. Masiero, and S. T. Petcov, *On the MSW effect with massless neutrinos and no mixing in the vacuum*, Phys. Lett. **B260** (1991), 154–160.
- [127] E. Roulet, *Mikheyev-Smirnov-Wolfenstein effect with flavor-changing neutrino interactions*, Phys. Rev. **D44** (1991), R935–R938.
- [128] Y. Grossman, *Nonstandard neutrino interactions and neutrino oscillation experiments*, Phys. Lett. **B359** (1995), 141–147, hep-ph/9507344.
- [129] S. Bergmann, Y. Grossman, and E. Nardi, *Neutrino propagation in matter with general interactions*, Phys. Rev. **D60** (1999), 093008, hep-ph/9903517.
- [130] M. Blennow, T. Ohlsson, and W. Winter, *Non-standard Hamiltonian effects on neutrino oscillations*, Eur. Phys. J. **C49** (2007), 1023–1039, hep-ph/0508175.
- [131] A. de Gouvea and J. Jenkins, *A survey of lepton number violation via effective operators*, Phys. Rev. **D77** (2008), 013008, 0708.1344.
- [132] A. De Gouvea, G. F. Giudice, A. Strumia, and K. Tobe, *Phenomenological implications of neutrinos in extra dimensions*, Nucl. Phys. **B623** (2002), 395–420, hep-ph/0107156.
- [133] T. Ota and J. Sato, *Signature of the minimal supersymmetric standard model with right-handed neutrinos in long baseline experiments*, Phys. Rev. **D71** (2005), 096004, hep-ph/0502124.
- [134] M. Honda, Y. Kao, N. Okamura, A. Pronin, and T. Takeuchi, *The effect of topcolor assisted technicolor, and other models, on neutrino oscillation*, (0400), arXiv:0704.0369 [hep-ph].
- [135] M. Honda, Y. Kao, N. Okamura, A. Pronin, and T. Takeuchi, *Constraints on new physics from long baseline neutrino oscillation experiments*, (2007), arXiv:0707.4545 [hep-ph].
- [136] M. B. Gavela, D. Hernandez, T. Ota, and W. Winter, *Large gauge invariant non-standard neutrino interactions*, (2008), 0809.3451.

- [137] S. Antusch, J. P. Baumann, and E. Fernandez-Martinez, *Non-standard neutrino interactions with matter from physics beyond the standard model*, (2008), 0807.1003.
- [138] M. Malinsky, T. Ohlsson, and H. Zhang, *Non-standard neutrino interactions from a triplet seesaw model*, (2008), 0811.3346.
- [139] S. Bergmann, M. M. Guzzo, P. C. de Holanda, P. I. Krastev, and H. Nunokawa, *Status of the solution to the solar neutrino problem based on non-standard neutrino interactions*, Phys. Rev. **D62** (2000), 073001, hep-ph/0004049.
- [140] Z. Berezhiani, R. S. Raghavan, and A. Rossi, *Probing non-standard couplings of neutrinos at the Borexino detector*, Nucl. Phys. **B638** (2002), 62–80, hep-ph/0111138.
- [141] A. Friedland, C. Lunardini, and C. Pena-Garay, *Solar neutrinos as probes of neutrino–matter interactions*, Phys. Lett. **B594** (2004), 347, hep-ph/0402266.
- [142] O. G. Miranda, M. A. Tortola, and J. W. F. Valle, *Are solar neutrino oscillations robust?*, JHEP **10** (2006), 008, hep-ph/0406280.
- [143] A. Bolanos, O. G. Miranda, A. Palazzo, M. A. Tortola, and J. W. F. Valle, *Probing non-standard neutrino-electron interactions with solar and reactor neutrinos*, (2008), 0812.4417.
- [144] T. Ohlsson and H. Zhang, *Non-standard interaction effects at reactor neutrino experiments*, (2008), 0809.4835.
- [145] M. C. Gonzalez-Garcia et al., *Atmospheric neutrino observations and flavor changing interactions*, Phys. Rev. Lett. **82** (1999), 3202–3205, hep-ph/9809531.
- [146] S. Bergmann, Y. Grossman, and D. M. Pierce, *Can lepton flavor violating interactions explain the atmospheric neutrino problem?*, Phys. Rev. **D61** (2000), 053005, hep-ph/9909390.
- [147] N. Fornengo, M. Maltoni, R. T. Bayo, and J. W. F. Valle, *Probing neutrino non-standard interactions with atmospheric neutrino data*, Phys. Rev. **D65** (2001), 013010, hep-ph/0108043.
- [148] M. C. Gonzalez-Garcia and M. Maltoni, *Atmospheric neutrino oscillations and new physics*, Phys. Rev. **D70** (2004), 033010, hep-ph/0404085.
- [149] A. Friedland, C. Lunardini, and M. Maltoni, *Atmospheric neutrinos as probes of neutrino matter interactions*, Phys. Rev. **D70** (2004), 111301, hep-ph/0408264.
- [150] A. Friedland and C. Lunardini, *A test of tau neutrino interactions with atmospheric neutrinos and K2K*, Phys. Rev. **D72** (2005), 053009, hep-ph/0506143.

-
- [151] S. Bergmann and Y. Grossman, *Can lepton flavor violating interactions explain the LSND results?*, Phys. Rev. **D59** (1999), 093005, hep-ph/9809524.
- [152] T. Ota, J. Sato, and N.-a. Yamashita, *Oscillation enhanced search for new interaction with neutrinos*, Phys. Rev. **D65** (2002), 093015, hep-ph/0112329.
- [153] T. Ota and J. Sato, *Can ICARUS and OPERA give information on a new physics?*, Phys. Lett. **B545** (2002), 367–372, hep-ph/0202145.
- [154] N. Kitazawa, H. Sugiyama, and O. Yasuda, *Will MINOS see new physics?*, (2006), hep-ph/0606013.
- [155] A. Friedland and C. Lunardini, *Two modes of searching for new neutrino interactions at MINOS*, Phys. Rev. **D74** (2006), 033012, hep-ph/0606101.
- [156] M. Blennow, T. Ohlsson, and J. Skrotzki, *Effects of non-standard interactions in the MINOS experiment*, Phys. Lett. **B660** (2008), 522–528, hep-ph/0702059.
- [157] J. Kopp, M. Lindner, T. Ota, and J. Sato, *Non-standard neutrino interactions in reactor and superbeam experiments*, Phys. Rev. **D77** (2008), 013007, 0708.0152.
- [158] N. C. Ribeiro et al., *Probing nonstandard neutrino physics by two identical detectors with different baselines*, Phys. Rev. **D77** (2008), 073007, 0712.4314.
- [159] A. Bueno, M. Campanelli, M. Laveder, J. Rico, and A. Rubbia, *The flavor of neutrinos in muon decays at a neutrino factory and the LSND puzzle*, JHEP **06** (2001), 032, hep-ph/0010308.
- [160] M. C. Gonzalez-Garcia, Y. Grossman, A. Gusso, and Y. Nir, *New CP violation in neutrino oscillations*, Phys. Rev. **D64** (2001), 096006, hep-ph/0105159.
- [161] P. Huber and J. W. F. Valle, *Non-standard interactions: Atmospheric versus neutrino factory experiments*, Phys. Lett. **B523** (2001), 151–160, hep-ph/0108193.
- [162] A. M. Gago, M. M. Guzzo, H. Nunokawa, W. J. C. Teves, and R. Zukanovich Funchal, *Probing flavor changing neutrino interactions using neutrino beams from a muon storage ring*, Phys. Rev. **D64** (2001), 073003, hep-ph/0105196.
- [163] P. Huber, T. Schwetz, and J. W. F. Valle, *Confusing non-standard neutrino interactions with oscillations at a neutrino factory*, Phys. Rev. **D66** (2002), 013006, hep-ph/0202048.
- [164] M. Campanelli and A. Romanino, *Effects of new physics in neutrino oscillations in matter*, Phys. Rev. **D66** (2002), 113001, hep-ph/0207350.
- [165] J. Kopp, M. Lindner, and T. Ota, *Discovery reach for non-standard interactions in a neutrino factory*, Phys. Rev. **D76** (2007), 013001, hep-ph/0702269.

- [166] N. C. Ribeiro, H. Minakata, H. Nunokawa, S. Uchinami, and R. Zukanovich-Funchal, *Probing non-standard neutrino interactions with neutrino factories*, JHEP **12** (2007), 002, 0709.1980.
- [167] J. Kopp, T. Ota, and W. Winter, *Neutrino factory optimization for non-standard interactions*, Phys. Rev. **D78** (2008), 053007, 0804.2261.
- [168] W. Winter, *Testing non-standard CP violation in neutrino propagation*, (2008), 0808.3583.
- [169] A. Donini, K.-i. Fuki, J. Lopez-Pavon, D. Meloni, and O. Yasuda, *The discovery channel at the neutrino factory: $\nu_\mu \rightarrow \nu_\tau$ pointing to sterile neutrinos*, (2008), 0812.3703.
- [170] R. Adhikari, S. K. Agarwalla, and A. Raychaudhuri, *Can R-parity violating supersymmetry be seen in long baseline beta-beam experiments?*, Phys. Lett. **B642** (2006), 111–118, hep-ph/0608034.
- [171] G. L. Fogli, E. Lisi, A. Mirizzi, and D. Montanino, *Revisiting nonstandard interaction effects on supernova neutrino flavor oscillations*, Phys. Rev. **D66** (2002), 013009, hep-ph/0202269.
- [172] A. Esteban-Pretel, R. Tomas, and J. W. F. Valle, *Probing non-standard neutrino interactions with supernova neutrinos*, Phys. Rev. **D76** (2007), 053001, arXiv:0704.0032 [hep-ph].
- [173] G. Mangano et al., *Effects of non-standard neutrino electron interactions on relic neutrino decoupling*, Nucl. Phys. **B756** (2006), 100–116, hep-ph/0607267.
- [174] M. Blennow and D. Meloni, *Non-standard interaction effects on astrophysical neutrino fluxes*, (2009), 0901.2110.
- [175] Z. Berezhiani and A. Rossi, *Limits on the non-standard interactions of neutrinos from e^+e^- colliders*, Phys. Lett. **B535** (2002), 207–218, hep-ph/0111137.
- [176] J. Barranco, O. G. Miranda, C. A. Moura, and J. W. F. Valle, *Constraining non-standard interactions in $\nu_e e$ or $\bar{\nu}_e e$ scattering*, Phys. Rev. **D73** (2006), 113001, hep-ph/0512195.
- [177] J. Barranco, O. G. Miranda, and T. I. Rashba, *Low energy neutrino experiments sensitivity to physics beyond the standard model*, Phys. Rev. **D76** (2007), 073008, hep-ph/0702175.
- [178] J. Barranco, O. G. Miranda, and T. I. Rashba, *Probing new physics with coherent neutrino scattering off nuclei*, JHEP **12** (2005), 021, hep-ph/0508299.
- [179] P. Huber, T. Schwetz, and J. W. F. Valle, *How sensitive is a neutrino factory to the angle θ_{13} ?*, Phys. Rev. Lett. **88** (2002), 101804, hep-ph/0111224.

-
- [180] T. Kikuchi, H. Minakata, and S. Uchinami, *Perturbation theory of neutrino oscillation with nonstandard neutrino interactions*, (2008), 0809.3312.
- [181] P. Huber, M. Lindner, and W. Winter, *Simulation of long-baseline neutrino oscillation experiments with GLoBES*, Comput. Phys. Commun. **167** (2005), 195, hep-ph/0407333.
- [182] P. Huber, J. Kopp, M. Lindner, M. Rolinec, and W. Winter, *New features in the simulation of neutrino oscillation experiments with GLoBES 3.0*, Comput. Phys. Commun. **177** (2007), 432–438, hep-ph/0701187.
- [183] J. Kopp, *Efficient numerical diagonalization of hermitian 3×3 matrices*, Int. J. Mod. Phys. **C19** (2008), 523–548, physics/0610206, Erratum ibid. **C19** (2008) 845.
- [184] P. Huber, M. Lindner, and W. Winter, *Superbeams versus neutrino factories*, Nucl. Phys. **B645** (2002), 3–48, hep-ph/0204352.
- [185] Y. Itow et al., *The JHF-Kamioka neutrino project*, (2001), hep-ex/0106019.
- [186] M. Ishitsuka, T. Kajita, H. Minakata, and H. Nunokawa, *Resolving neutrino mass hierarchy and CP degeneracy by two identical detectors with different baselines*, Phys. Rev. **D72** (2005), 033003, hep-ph/0504026.
- [187] M. D. Messier, *Evidence for neutrino mass from observations of atmospheric neutrinos with Super-Kamiokande*, Ph.D. thesis, Boston University, 1999, UMI-99-23965.
- [188] E. A. Paschos and J. Y. Yu, *Neutrino interactions in oscillation experiments*, Phys. Rev. **D65** (2002), 033002, hep-ph/0107261.
- [189] T. Yang and S. Wojcicki, *Study of physics sensitivity of ν_μ disappearance in a totally active version of NO ν A detector*, (2004), Off-Axis-Note-SIM-30.
- [190] P. Huber, J. Kopp, M. Lindner, M. Rolinec, and W. Winter, *From Double Chooz to Triple Chooz: Neutrino physics at the Chooz reactor complex*, JHEP **05** (2006), 072, hep-ph/0601266.
- [191] P. Vogel and J. F. Beacom, *The angular distribution of the neutron inverse beta decay, $\bar{\nu}_e + p \rightarrow e^+ + n$* , Phys. Rev. **D60** (1999), 053003, hep-ph/9903554.
- [192] P. Huber and W. Winter, *Neutrino factories and the “magic” baseline*, Phys. Rev. **D68** (2003), 037301, hep-ph/0301257.
- [193] D. Autiero et al., *The synergy of the golden and silver channels at the neutrino factory*, Eur. Phys. J. **C33** (2004), 243–260, hep-ph/0305185.

- [194] OPERA, M. Guler et al., *OPERA: An appearance experiment to search for $\nu_\mu \rightarrow \nu_\tau$ oscillations in the CNGS beam. Experimental proposal*, (2000), CERN-SPSC-2000-028.
- [195] A. M. Dziewonski and D. L. Anderson, *Preliminary reference Earth model*, Phys. Earth Planet. Interiors **25** (1981), 297–356.
- [196] R. J. Geller and T. Hara, *Geophysical aspects of very long baseline neutrino experiments*, Nucl. Instrum. Meth. **A503** (2001), 187–191, [hep-ph/0111342](#).
- [197] T. Ohlsson and W. Winter, *The role of matter density uncertainties in the analysis of future neutrino factory experiments*, Phys. Rev. **D68** (2003), 073007, [hep-ph/0307178](#).
- [198] W. Winter, *Probing the absolute density of the Earth’s core using a vertical neutrino beam*, Phys. Rev. **D72** (2005), 037302, [hep-ph/0502097](#).
- [199] H. Minakata and S. Uchinami, *On in situ determination of Earth matter density in neutrino factory*, Phys. Rev. **D75** (2007), 073013, [hep-ph/0612002](#).
- [200] R. Gandhi and W. Winter, *Physics with a very long neutrino factory baseline*, Phys. Rev. **D75** (2007), 053002, [hep-ph/0612158](#).
- [201] V. Barger, S. Geer, and K. Whisnant, *Neutral currents and tests of three-neutrino unitarity in long-baseline experiments*, New J. Phys. **6** (2004), 135, [hep-ph/0407140](#).
- [202] N. Severijns, M. Beck, and O. Naviliat-Cuncic, *Tests of the standard electroweak model in beta decay*, Rev. Mod. Phys. **78** (2006), 991–1040, [nucl-ex/0605029](#).
- [203] P. Herczeg, *A note on limits on new interactions from the $(\pi \rightarrow e\nu)/(\pi \rightarrow \mu\nu)$ branching ratio*, Phys. Rev. **D52** (1995), 3949–3957.
- [204] A. I. Vainshtein, V. I. Zakharov, and M. A. Shifman, *A possible mechanism for the $\Delta T = 1/2$ rule in nonleptonic decays of strange particles*, JETP Lett. **22** (1975), 55–56.
- [205] W. Fetscher, *Helicity of the ν_μ in π^+ decay: A comment on the measurement of $p_\mu \xi_{\bar{\rho}}^\delta$ in muon decay*, Phys. Lett. **B140** (1984), 117–118.
- [206] Particle Data Group, C. Amsler et al., *Review of particle physics*, Phys. Lett. **B667** (2008), 1.
- [207] C. A. Gagliardi, R. E. Tribble, and N. J. Williams, *Global analysis of muon decay measurements*, Phys. Rev. **D72** (2005), 073002, [hep-ph/0509069](#).
- [208] E. K. Akhmedov, R. Johansson, M. Lindner, T. Ohlsson, and T. Schwetz, *Series expansions for three-flavor neutrino oscillation probabilities in matter*, JHEP **04** (2004), 078, [hep-ph/0402175](#).

- [209] E. K. Akhmedov, P. Huber, M. Lindner, and T. Ohlsson, *T violation in neutrino oscillations in matter*, Nucl. Phys. **B608** (2001), 394–422, hep-ph/0105029.

